

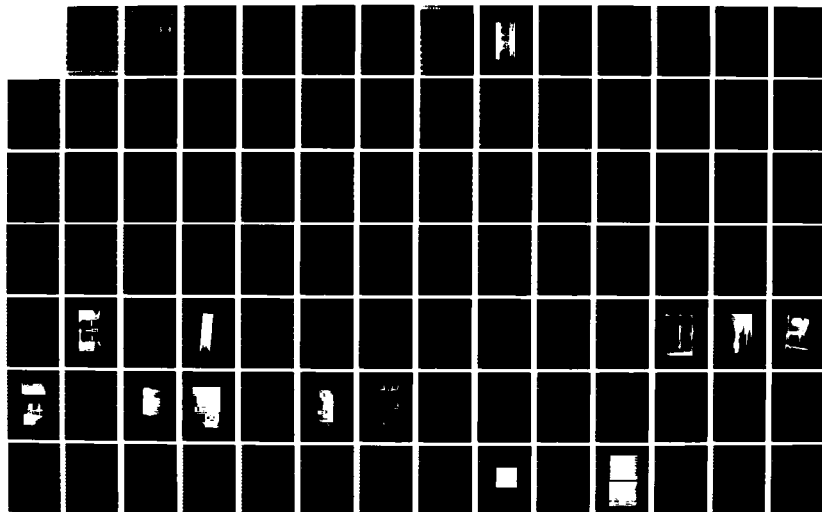
AD-A175 017

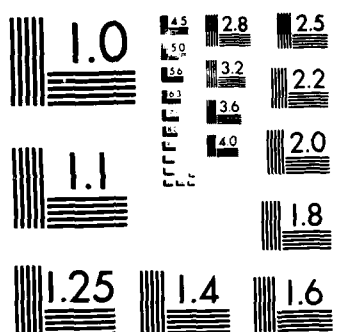
RESEARCH ON DAMAGE MODELS FOR CONTINUOUS FIBER
COMPOSITES(U) TEXAS A AND M UNIV COLLEGE STATION
MECHANICS AND MATERIALS CE D H ALLEN ET AL FEB 86
NN-5023-86-5 AFOSR-TR-86-2077 AFOSR-84-0067 F/G 11/4

1/4

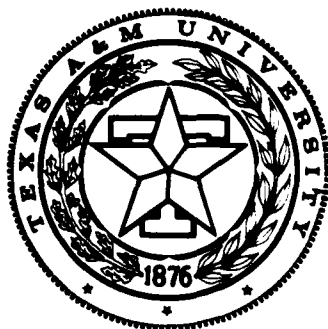
UNCLASSIFIED

NL





MICROCOPY RESOLUTION TEST CHART
NATIONAL BUREAU OF STANDARDS 1963-A



**Mechanics and Materials Center
TEXAS A&M UNIVERSITY
College Station, Texas**

AFOSR-TR. 86-2077

Dec - 9 Apr 86
 Dec - 9 Apr 86

RESEARCH ON DAMAGE MODELS FOR CONTINUOUS FIBER COMPOSITES

Annual Technical Report

by

D.H. Allen

and

C.E. Harris

Aerospace Engineering Department
Texas A&M University

to the

Air Force Office of Scientific Research
Office of Aerospace Research
United States Air Force

Approved for public release;
distribution unlimited.

AD-A175 017

33-1110

MM 5023-86-5

Grant No. AFOSR-84-0067
February 1986

86 12 00 00 00

REPORT DOCUMENTATION PAGE

1a. REPORT SECURITY CLASSIFICATION Unclassified			1b. RESTRICTIVE MARKINGS		
2a. SECURITY CLASSIFICATION AUTHORITY			3. DISTRIBUTION/AVAILABILITY OF REPORT Approved for public release, distribution unlimited		
2b. DECLASSIFICATION/DOWNGRADING SCHEDULE			4. PERFORMING ORGANIZATION REPORT NUMBER(S)		
5. MONITORING ORGANIZATION REPORT NUMBER(S) AFOSR-TR-86-2077			6a. NAME OF PERFORMING ORGANIZATION Aerospace Engineering Dept.		
6b. OFFICE SYMBOL (If applicable)			7a. NAME OF MONITORING ORGANIZATION Air Force Office of Scientific Research		
6c. ADDRESS (City, State and ZIP Code) Texas A&M University College Station, Texas 77843			7b. ADDRESS (City, State and ZIP Code) Bolling AFB Washington, D.C. 20332 - 6448		
8a. NAME OF FUNDING SPONSORING ORGANIZATION AFOSR		8b. OFFICE SYMBOL (If applicable) NA		9. PROCUREMENT INSTRUMENT IDENTIFICATION NUMBER Grant No. AFOSR-84-0067	
8c. ADDRESS (City, State and ZIP Code) Bolling AFB DC 20332-6448		10. SOURCE OF FUNDING NOS.			
		PROGRAM ELEMENT NO. 61102F		PROJECT NO. 2302	
				TASK NO. B2	
				WORK UNIT NO.	
11. TITLE (Include Security Classification) Research on Damage Models for Continuous Fiber Composites					
12. PERSONAL AUTHOR(S) D.H. Allen and C.E. Harris					
13a. TYPE OF REPORT Annual		13b. TIME COVERED FROM Feb '85 TO Feb '86		14. DATE OF REPORT (Yr., Mo., Day) February 1986	
15. PAGE COUNT					
16. SUPPLEMENTARY NOTATION					
17. COSATI CODES			18. SUBJECT TERMS (Continue on reverse if necessary and identify by block number)		
FIELD	GROUP	SUB. GR.	composites damage laminate analysis, failure		
			finite element methods, internal state variables, plasticity.		
19. ABSTRACT (Continue on reverse if necessary and identify by block number)					
<p>Continuous fiber composite laminates are known to undergo a substantial amount of complex load-induced damage which can adversely affect component performance. [N]. Therefore, it is desirable to develop new models capable of accounting for the effect of damage on materials properties.</p> <p>This report documents research completed during the second year of a three year effort under AFOSR grant no. AFOSR-84-0067 and originally detailed under Texas A&M Research Foundation proposal no. RF-84-34 and dated October 1983. The objective of this research is to develop an accurate damage model for predicting strength and stiffness of continuous fiber composite media subjected to fatigue or monotonic loading and to verify this model with experimental results obtained from composite specimens of selected geometry and makeup to be described herein.</p>					
20. DISTRIBUTION/AVAILABILITY OF ABSTRACT UNCLASSIFIED/UNLIMITED <input checked="" type="checkbox"/> SAME AS RPT <input type="checkbox"/> DTIC USERS <input type="checkbox"/>			21. ABSTRACT SECURITY CLASSIFICATION Unclassified		
22a. NAME OF RESPONSIBLE INDIVIDUAL J M Hercules, USIA			22b. TELEPHONE NUMBER (Include Area Code) (202) 767-4935		22c. OFFICE SYMBOL NA

RESEARCH ON DAMAGE MODELS
FOR CONTINUOUS FIBER COMPOSITES

Annual Technical Report

Submitted by

D.H. Allen

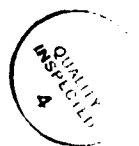
and

C.E. Harris

Aerospace Engineering Department
Texas A&M University

to the

Air Force Office of Scientific Research
Office of Aerospace Research
United States Air Force



Accession For	
NTIS CRA&I	<input checked="checked" type="checkbox"/>
DTIC TAB	<input type="checkbox"/>
Unannounced	<input type="checkbox"/>
Justification	
By	
Distribution /	
Availability Codes	
Dist	Avail and/or Special
A-1	

TABLE OF CONTENTS

	Page
1. INTRODUCTION	1
1.1 Summary	1
1.2 Statement of Work	1
2. RESEARCH COMPLETED TO DATE	1
2.1 Summary of Completed Research	1
2.2 Experimental Investigation of Damage Mechanisms in Graphite/Epoxy Laminates	2
2.3 Relationship Between Fracture Mechanics and Matrix Crack Damage	4
2.4 Modelling Axial Stiffness Loss Due to Matrix Cracks	8
2.5 Modelling Out-of-Plane Stiffness Loss Due to Curved Cracks	8
2.6 Experimental and Theoretical Characterization of Interply Delamination	12
2.7 References	14
3. PUBLICATIONS LIST	15
4. PROFESSIONAL PERSONNEL INFORMATION	16
4.1 Faculty Research Assignments	16
4.2 Additional Staff and Students	16
5. INTERACTIONS	17
5.1 Papers Presented	17
5.2 Research Related Travel and Consultative Functions	17
6. APPENDIX - INTERIM TECHNICAL REPORTS	
6.1 An Investigation of Damage Accumulation in Graphite/Epoxy Laminates	
6.2 A Thermomechanical Constitutive Theory for Elastic Composites with Distributed Damage Part I: Theoretical Development	
6.3 A Thermomechanical Constitutive Theory for Elastic Composites with Distributed Damage Part II: Application to Matrix Cracking in Laminated Composites	
6.4 An Experimental and Analytical Treatment of the Mechanics of Damage in Laminated Composites	
6.5 Characterization of Stiffness Loss in Crossply Laminates with Curved Matrix Cracks	
6.6 A Damage Model for Continuous Fiber Composite Laminates with Matrix Cracks and Interlaminar Delamination	

1.0 INTRODUCTION

1.1 Summary

Continuous fiber composite laminates are known to undergo a substantial amount of complex load-induced damage which can adversely affect component performance [1]. Therefore, it is desirable to develop new models capable of accounting for the effect of damage on material properties.

This report documents research completed during the second year of a three year effort under AFOSR grant no. AFOSR-84-0067 and originally detailed under Texas A&M Research Foundation proposal no. RF-84-34 and dated October 1983. The objective of this research is to develop an accurate damage model for predicting strength and stiffness of continuous fiber composite media subjected to fatigue or monotonic loading and to verify this model with experimental results obtained from composite specimens of selected geometry and makeup to be described herein.

1.2 Statement of Work

The following is a brief summary of work to be performed under the present grant:

- 1) develop constitutive equations relating stresses to strains and damage internal state variables (ISV) which may be used in a stress gradient field;
- 2) develop ISV growth laws as a function of load history for matrix cracking, interlaminar fracture, etc.;
- 3) develop finite element algorithms capable of evaluating ply properties in damaged components.
- 4) perform experiments on components with selected stacking sequences in order to verify the model.

2.0 RESEARCH COMPLETED TO DATE

2.1 Summary of Completed Research

The following research has been completed during the second year:

- 1) an experimental investigation of damage mechanisms in graphite/epoxy laminates (Appendix 6.1);
- 2) the theoretical relationship between fracture mechanics and matrix crack damage (Appendix 6.3); and
- 3) a theoretical and experimental investigation of curved matrix cracks in crossply laminates (Appendix 6.4).

In addition, the following research is well underway at the end of the second year:

- 1) damage modelling of curved cracks in crossply laminates (Appendix 6.5);
- 2) experimental characterization of interply delaminations;
- 3) damage modelling of interply delamination (Appendix 6.6); and
- 4) a study of model accuracy in a stress gradient field.

2.2 Experimental Investigation of Damage Mechanisms in Graphite/Epoxy Laminates

A literature survey during the first year of research [1] indicated that no experimental data were currently available in the open literature which reported all of the data necessary to characterize the damage model developed under this grant. It was therefore necessary to initiate an experimental effort as part of the current research. This research has thus far resulted in one M.S. Thesis (Appendix 6.1). The results of this experimental effort are briefly reviewed in this section.

It was decided that the model should be first applied for a single damage mode. The damage mode of interest is matrix cracking. Matrix cracks are cracks in any ply that run parallel to fibers in the matrix material. This damage mode occurs in all practical continuous fiber composite structures. This phenomenon was investigated experimentally in seven different laminates subjected to quasi-static, stepwise loading. All the laminates were cross-ply laminates, consisting of 0° plies (fibers in the principle load direction) and 90° plies. This type of laminate was chosen to promote the growth of matrix cracks and to suppress other damage modes. A comprehensive data base is essential not only to develop the present model but to insure that the experimental results are useful for future research needs. Primary attention was placed on identifying the mechanisms of initiation and growth of matrix cracks. Secondary emphasis was placed on observing the effect of cracking on material response.

A qualitative analysis was made to determine the significance of the damage events observed. These included crack density, stiffness reduction, crack shapes, development of crack surface area, and residual strain. An effort was made to interpret the effects of stress level, specimen thickness, geometry, and stacking sequence on damage formation.

In this experimental program, two distinct types of transverse cracks were observed (See Fig. 1.). Typical transverse cracks formed at regular intervals along the length of the specimen and generally spanned the 90° layer perpendicular to the laminate plane. The accepted explanation for this widely observed phenomenon is the concept of shear lag. This type of transverse crack was termed a "straight crack." The second type of crack had many features that indicated that it possessed a totally different growth mechanism. The most obvious of these features was the incidence angle to the plane of the laminate at which the crack initially propagated. This crack was termed an "angle crack." Several important observations of this phenomenon are enumerated as follows:

1. The angle always formed in conjunction with a straight crack. An angle crack did not form as an isolated, independent crack.

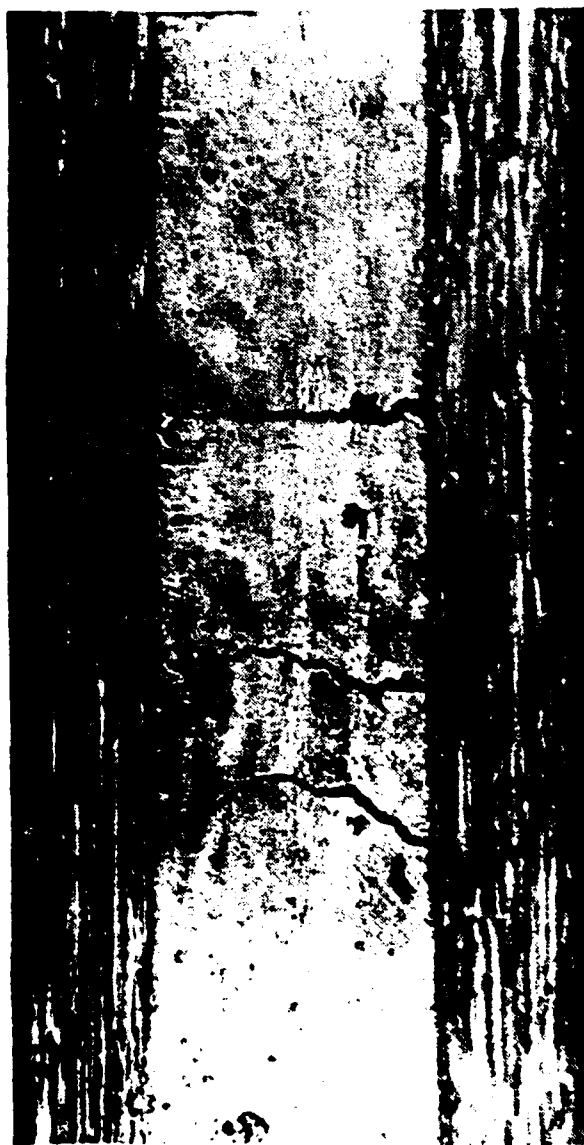


FIG. 1. Edge replica of $[0_2/90_2]_S$ laminate showing nested curved cracks

2. The crack was always oriented toward the straight crack.
3. The angle crack formed within a characteristic distance from a straight crack or another angle crack. This distance was found to be less than or equal to the thickness of the 90° ply group.
4. The proportion of angled cracks to straight cracks increased with an increase in the 90° ply thickness.
5. Two angle cracks at opposite interfaces would commonly intersect at the midplane to form a "curved crack."
6. The acoustic emission of an angle crack was audibly different from that of a straight crack.
7. Upon unloading, a number of angled cracks could be seen in intermediate stages of growth. This was not the case with straight cracks.

Two damage phenomena were found to be associated with the cracks. Edge delaminations formed as bands across the width of the specimens. In each case, the delamination propagated along the angle crack interface. Longitudinal splits formed over the delamination areas with one end of the split terminating at the angle crack interface.

Several observations were made concerning laminate response. A laminate with alternating 0° and 90° plies developed less stiffness loss than a similar laminate with the 90° plies grouped together (See Fig. 2.). Possible causes are the difference in 90° constraint and the difference in crack opening displacement. Another observation was that the strain at which first ply failure occurred was inversely related to the number of 90° plies grouped together.

2.3 Relationship Between Fracture Mechanics and Matrix Crack Damage

In order to demonstrate the potential of the model to predict degraded stiffness components, a specialized form of the constitutive model was developed for the case of transverse matrix cracks in 90° layers of cross-ply laminates. For this special case, only one component of the internal state variable (ISV) tensor must be specified. Specific values of the ISV corresponding to various amounts of matrix crack damage can be determined by using fracture mechanics to relate the ISV to the strain energy release rate for crack extension during load-up. The relationship between the ISV and the matrix crack strain energy release rate is developed in the following discussion (Complete details are given in Appendix 6.3).

The local energy due to cracking, u_L^c , is related to the ISV for matrix cracks as follows [See Appendix 6.2]:

$$u_L^c = I_{22}^1 \epsilon_2 \alpha_2^1, \quad (1)$$

where I_{22}^1 is a material constant, ϵ_2 is the strain in the 90° layer perpendicular to the fibers and α_2 is the ISV for straight-through matrix

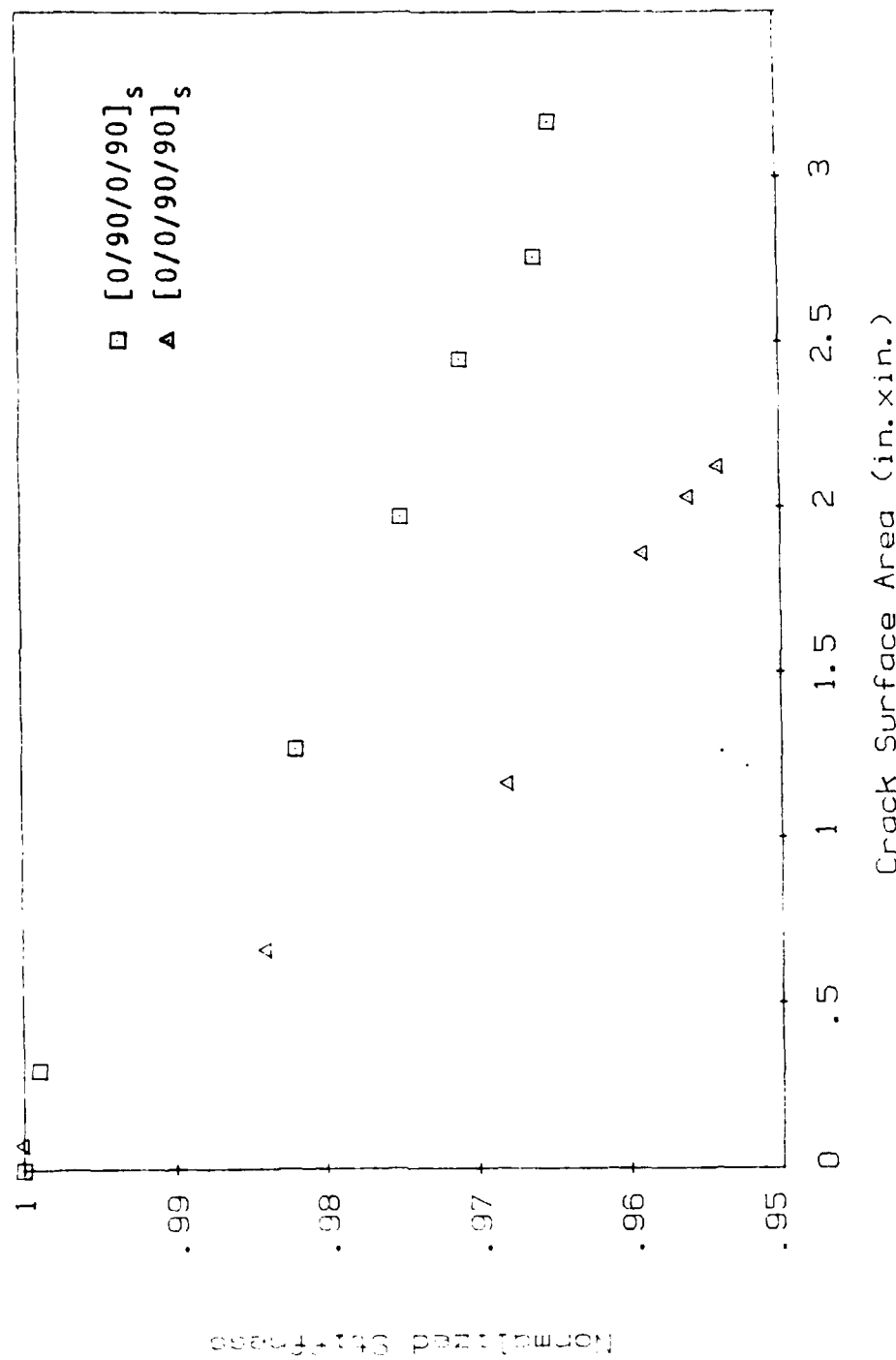


Fig. 2. Relationship between crack surface area and stiffness reduction for the [0₂/90₂]_s and [0/90/0/90]_s laminates

cracks in 90° layers. Also, the local energy due to matrix crack growth is related to the strain energy release rate, G , by

$$d_L^c = -\frac{1}{V_L} \int_0^{S_2} G dS_2, \quad (2)$$

where S_2 is the matrix crack surface area and V_L is the local volume. By equating these two expressions we obtain the following relationship between the ISV and G for crack extension during load-up:

$$\alpha_2^1 \Big|_{\text{load-up}} = -\frac{1}{V_L \epsilon_2 I_{22}^1} \int_0^{S_2} G dS_2. \quad (3)$$

For a matrix crack extending completely through the thickness of a 90° layer, the strain energy release rate is defined as

$$G = -\frac{1}{B} \frac{\partial U}{\partial a}, \quad (4)$$

where B is the thickness of the 90° layer and U is the strain energy in the 90° layer. It can be shown that equation (4) reduces to the following expression for a crack growing in the presence of existing cracks:

$$G = B [U_0 f(S/B)] \quad (5)$$

where U_0 is the strain energy density in the 90° layer in the absence of cracks and $f(S/B)$ is a function that depends on the crack spacing, S , and the layer thickness. Assuming linear elastic behavior of the 90° layer in the absence of cracks, the strain energy density is given by

$$U_0 = \frac{1}{2} E_{22} \epsilon_2^2 \quad (6)$$

where E_{22} is the initial undamaged modulus of the 90° layer transverse to the fibers. Because of the complexity of the interaction between cracks, the function $f(S/B)$ was determined from experimental tests of cross-ply laminates. The experimentally based expression for $f(S/B)$ together with equations (3), (5) and (6) are used to specify the value of the ISV as a function of matrix crack surface area during load-up.

Although it is possible for matrix crack surface area to increase during unloading, in the current development this effect is assumed to be negligible. Therefore, on unloading α_2 depends only on the crack-closure displacement and would go to zero on complete crack closure. Assuming that

the crack-closure displacement is linear with strain and the matrix crack surface area is constant, on unloading the ISV is expressed as

$$\alpha_2^1 \Big|_{\text{unloading}} = c \epsilon_2, \quad (7)$$

where c is a constant and depends only on the matrix crack damage state.

Considering a tensile test with a load and unloading cycle, at the instant of load reversal the expressions for the ISV for load-up and unloading must be equal. Therefore, by equating equations (3) and (7) at the same value of strain yields a relationship between the unloading constant, c , the strain energy release rate and the associated damage state. This relationship is given by

$$c = B \frac{1}{2V_L} \frac{E_{22}}{I_{22}^1} \int_0^{S_2} f(S/B) dS_2. \quad (8)$$

Since the local volume for matrix crack damage is the thickness of 1 ply multiplied by the length and width of the specimen over which the damage state is determined, the thickness to volume ratio in equation (8) is given by

$$\frac{B}{V_L} = n, \quad (9)$$

where n is the number of consecutive 90° layers and the damage is specified over a 1.0" width and 1.0" length. Equation (8) reduces to

$$c = \frac{1}{2} n \frac{E_{22}}{I_{22}^1} \int_0^{S_2} f(S/B) dS_2. \quad (10)$$

It has been previously shown that the effective stiffness of a laminate is related to the partial derivative of the ISV with respect to strain. Using equation (7) above, gives

$$\frac{\alpha_2^1}{\epsilon_2} = c, \quad (11)$$

which is a constant during unloading. Therefore, equations (10) and (11) are used to predict the effective axial stiffness (E_x) of cross-ply laminates as a function of the matrix crack damage state.

2.4 Modelling Axial Stiffness Loss Due to Matrix Cracks

As described in detail in Appendix 6.3, equation (11) may be utilized to predict stiffness loss in crossply laminates with matrix cracks. By using standard laminate analysis techniques, the following reduced stiffness equations may be derived:

$$S'_{im} = \sum_{k=1}^n (\bar{C}_{ij})_k t_k + \sum_{k=1}^n \sum_{j=1}^9 (\bar{I}_{ij})_k (z_k - z_{k-1}) (\partial \bar{\alpha}_j / \partial \epsilon_m^0)_k, \quad (12)$$

where S'_{im} are the components of the effective laminate stiffness, n is the number of plies, and overbars denote quantities measured in laminate coordinates.

Equations (12) were utilized to predict the damage dependent reduced axial stiffness of several crossply laminates. The reduced stiffnesses were compared to experimental results obtained for graphite/epoxy coupons composed of Hercules AS4/3502. A typical result is shown in Fig. 3. The model appears to be accurate in predicting stiffness loss for the crossply laminates considered herein. Further results are contained in Appendix 6.3.

2.5. Modelling Out-of-Plane Stiffness Loss Due to Curved Cracks

In Section 2.2 experimental evidence was reviewed which indicated that curved matrix cracks can occur in significant quantities in crossply laminates. As a measure of the capability of the model to predict stiffness loss components other than the axial stiffness, it was decided to use the model to predict out-of-plane stiffness loss due to the curved cracks. Although this research is still underway at this time, the theoretical procedure has been completed. The procedure will be briefly reviewed here. Further details are given in Appendix 6.5.

Consider now a local volume element with n_c cracks as shown in Fig. 4. Equations (1) may be written in the following^c form:

$$\alpha_{ij}^1 = \frac{1}{twL} \sum_{k=1}^{n_c} \int_{S_{2k}^1} u_i n_j dS, \quad (13)$$

where matrix cracking is designated by the superscript 1. Now define

$$\alpha_{ij}^{1k} = \frac{1}{twL} \int_{S_{2k}^1} u_i n_j dS, \quad (14)$$

so that equation (5) may be written

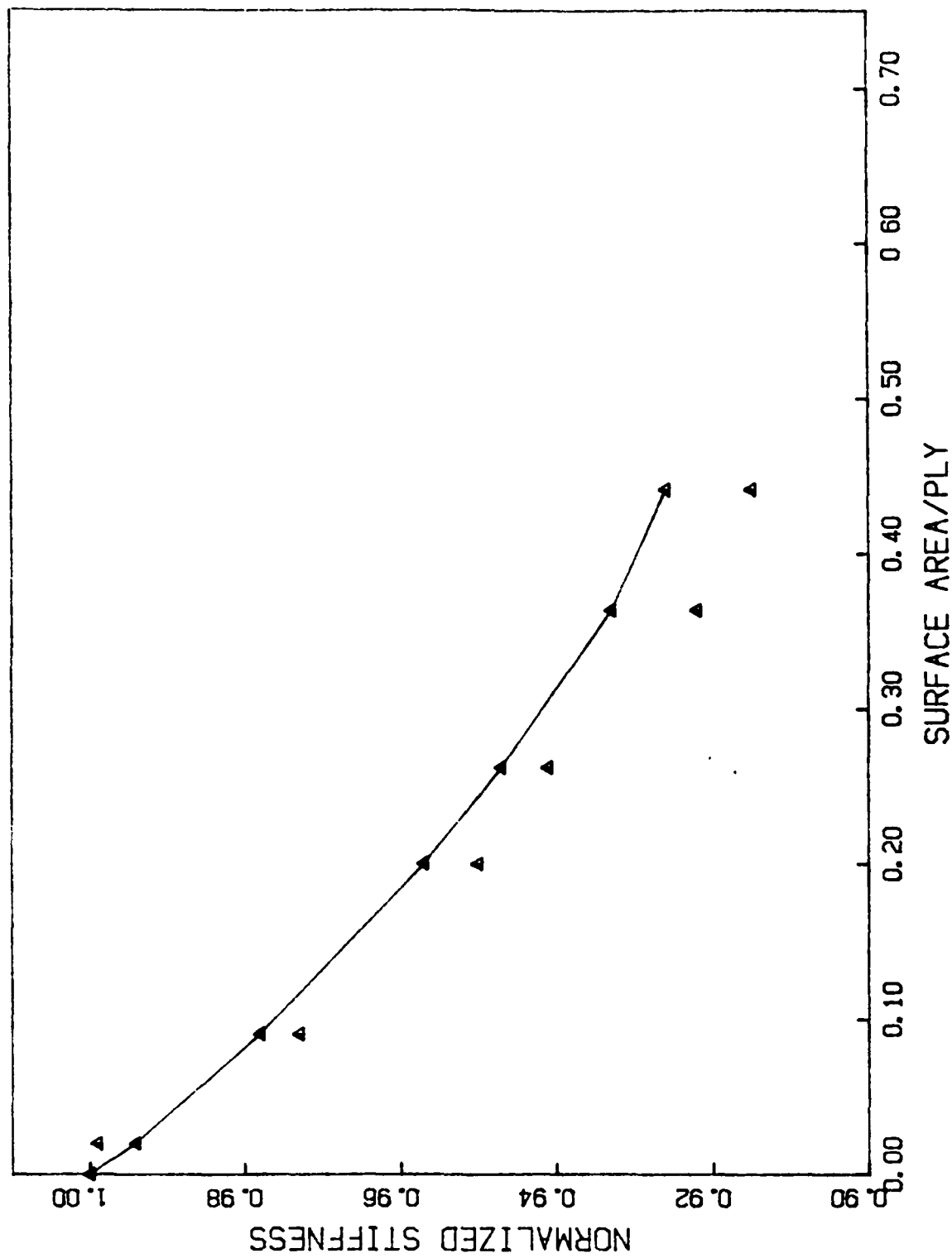


Fig. 3. Model vs. Experiment for $[0,90_2]_s$ Laminate

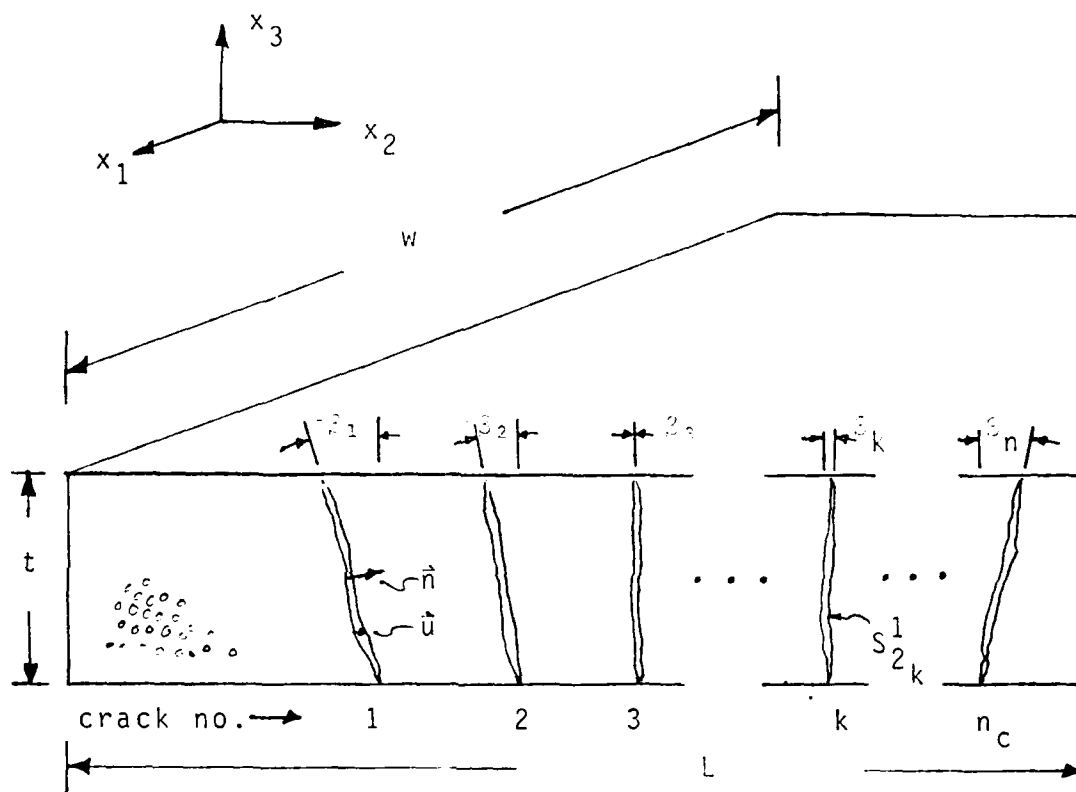


Fig. 4. Description of Curved Crack Geometry in a Single Crossply

$$\alpha_{ij}^1 = \sum_{k=1}^{n_c} \alpha_{ij}^{1k} \quad . \quad (15)$$

Now, since α_{ij}^1 is a second order tensor,

$$\alpha_{ij}^1 = \sum_{k=1}^{n_c} a_{ip}^k a_{jq}^k \alpha_{p'q'}^{1k} \quad , \quad (16)$$

where a_{ip}^k are the direction cosines relating the coordinates of the k th crack to the laminate coordinates. Differentiating (16) with respect to the midplane strain components gives

$$\frac{\partial \alpha_{ij}^1}{\partial \epsilon_{mn}} = \sum_{k=1}^{n_c} a_{ip}^k a_{jq}^k \frac{\partial \alpha_{p'q'}^{1k}}{\partial \epsilon_{mn}} \quad . \quad (17)$$

Transforming to the coordinates of the crack gives

$$\begin{aligned} \frac{\partial \alpha_{ij}^1}{\partial \epsilon_{mn}} &= \sum_{k=1}^{n_c} a_{ip}^k a_{jq}^k \frac{\partial \alpha_{p'q'}^{1k}}{\partial \epsilon_{r's'}^k} \frac{\partial \epsilon_{r's'}^k}{\partial \epsilon_{mn}} \\ &= \sum_{k=1}^{n_c} a_{ip}^k a_{jq}^k a_{mn}^k a_{ns}^k \frac{\partial \alpha_{p'q'}^{1k}}{\partial \epsilon_{r's'}^k} \quad . \quad (18) \end{aligned}$$

However, since it is assumed that $\partial \alpha_{22}^1 / \partial \epsilon_{22}$ is the only non-zero component, the above reduces to

$$\frac{\partial \alpha_{ij}^1}{\partial \epsilon_{mn}} = \sum_{k=1}^{n_c} a_{i2}^k a_{j2}^k a_{m2}^k a_{n2}^k \frac{\partial \alpha_{2'2'}^1}{\partial \epsilon_{2'2'}^1} \quad . \quad (19)$$

The above equations may be utilized to obtain the last term in reduced stiffness equations (4), where it is assumed that $\partial \alpha_{2'2'}^1 / \partial \epsilon_{2'2'}^1$ is independent of crack orientation and is obtained from $[0,90,0]$ experimental data [2].

An experimental study of matrix crack damage revealed that the curved cracks formed after the straight cracks and followed a repeatable pattern of location and orientation relative to the straight cracks. For a $[0,90_2]$ laminate the average location of the curved crack relative to the straight crack was approximately two ply thicknesses away. Furthermore, it was found that the curved cracks were never an isolated phenomenon. Therefore, it was postulated that the growth mechanism for curved cracks is driven by the stress state resulting from the formation of the straight crack. The cracks were found to exhibit slow stable crack growth behavior through the thickness unlike the brittle fracture behavior of the straight cracks. An analytical investigation of the curved crack phenomenon was performed using a finite element model of a crossply laminate with straight cracks. The analytical results for a $[0,90_2]$ indicated that the principal stress and strain undergo significant rotation as well as attaining a maximum value at approximately one ply thickness away from the cracks (see Fig. 5.), thus substantiating the postulated growth mechanisms. Growth mechanisms for both types of cracks were experimentally related to the number of consecutive 90° plies, the ratio of 0° to 90° plies, and the applied stress level. Further details of this study are given in Appendix 6.4.

2.6 Modelling Axial Stiffness Loss Due to Interlaminar Delamination

As described in detail in Appendix 6.6 the axial stiffness loss in crossply laminates with both matrix cracks and interlaminar delaminations is given by

$$S'_x = A_{11} - \sum_{k=1}^n (\bar{C}_{11})_k t_k \left(\frac{\partial \alpha^m}{\partial \epsilon_x} \right)_k - A_{13} \frac{\partial \alpha_3^D}{\partial \epsilon_x}, \quad (20)$$

where A_{11} is the undamaged axial stiffness, the second term denotes the axial stiffness loss due to matrix cracking, where α^m represents the ISV for matrix cracking, and the last term corresponds to the stiffness loss due to interlaminar delamination, where α_3^D represents the ISV for delamination. In deriving equation (20) a different local volume must be used for obtaining the locally averaged ISV for interlaminar delamination than for matrix cracks. Here the entire laminate is treated as the local volume. For interlaminar delamination there are only three nonzero components of the tensor valued ISV. However, for predicting axial stiffness only α_3^D is of interest.

The ISV for interlaminar delamination is related to the surface area following a similar procedure for matrix cracking. Incorporating fracture mechanics and thermodynamics gives

$$\alpha_3^D = \frac{-h}{V_L A_{13} \epsilon_x} \int_0^{S_2^D} G_D \, dS, \quad (21)$$

where h is the total ply thickness, V_L is the local volume, S_2^D is the damage surface area, and G_D is the energy release rate associated with

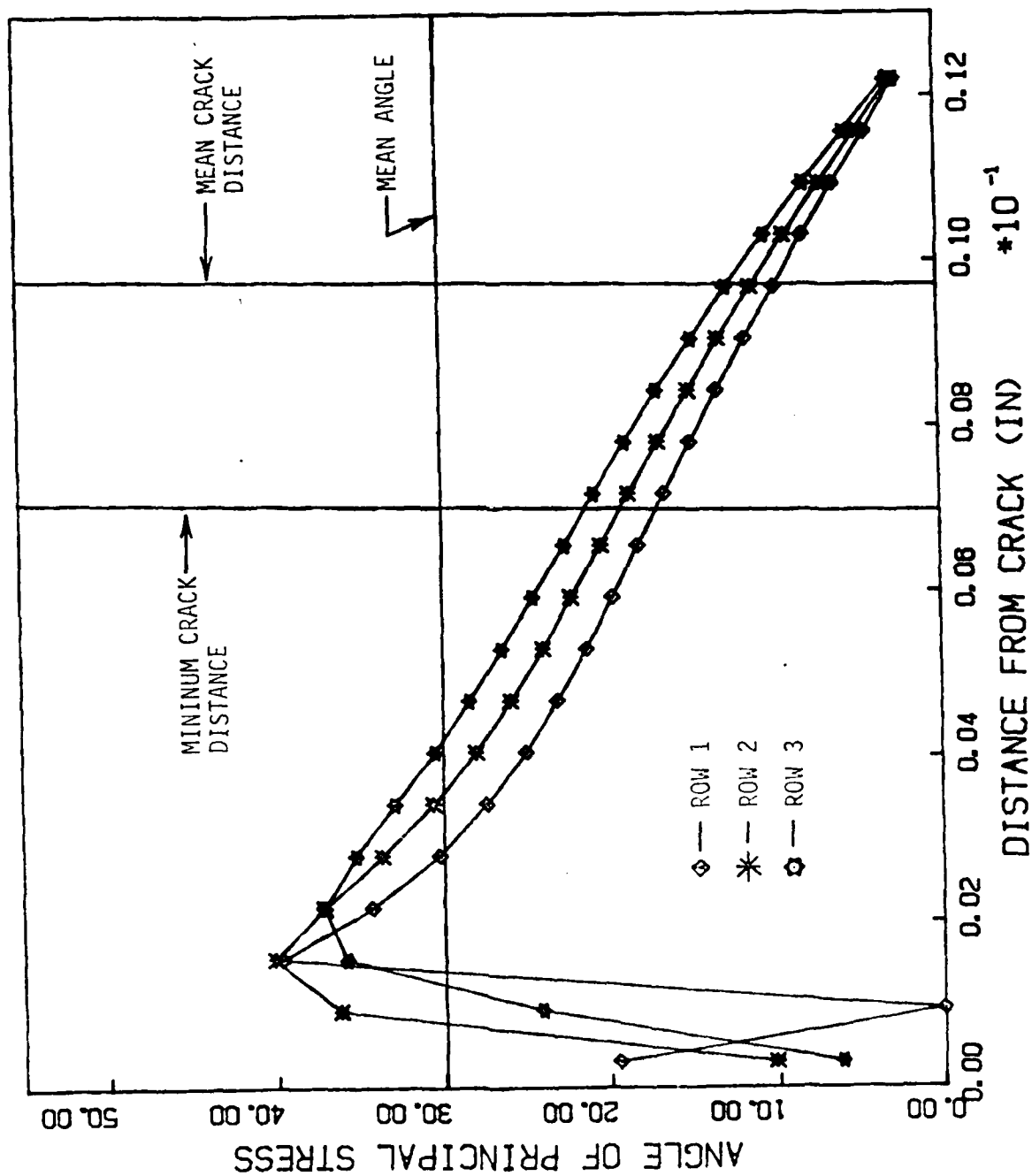


Fig. 5. Variation in the Principal Stress Angle Near the $0^\circ/90^\circ$ Interface.

interlaminar delamination. Again, because of the complexity G_D is determined experimentally from the strain energy in the body as follows:

$$G_D = -V_L \epsilon_x^2 \frac{\partial E_x}{\partial S^D} \quad . \quad (22)$$

Once the energy release rate is characterized equation (20) can be used for model predictions of axial stiffness loss.

2.7 References

- [1] Groves, S.E., and Allen, D.H., "A Survey of Damage in Continuous Fiber Composites," Texas A&M University Mechanics and Materials Center, MM-5023-84-6, March 1984.

3. PUBLICATION LIST

3.1 Submitted for Publication

1. "A Thermomechanical Constitutive Theory for Elastic Composites with Distributed Damage, Part I - Theoretical Development," by D.H. Allen, S.E. Groves, R.A. Schapery, and C.E. Harris (Appendix 6.2), submitted to Mechanics of Materials.

2. "A Thermomechanical Constitutive Theory for Elastic Composites with Distributed Damage, Part II - Application to Matrix Cracking in Laminated Composites," by D.H. Allen, C.E. Harris, S.E. Groves, and R.A. Schapery, (Appendix 6.3), submitted to Mechanics of Materials.

3. "An Experimental and Analytical Treatment of the Mechanics of Damage in Laminated Composites," by S.E. Groves, D.H. Allen, C.E. Harris, A.L. Highsmith, and R.G. Norvell (Appendix 6.4), submitted to Experimental Mechanics.

3.2 To Be Submitted for Publication

1. "Characterization of Stiffness Loss in Crossply Laminates with Curved Matrix Cracks," by D.H. Allen, C.E. Harris, and S.E. Groves (Appendix 6.5), to be submitted to ASTM for inclusion in the STP for the United States/Japan Symposium on Composite Materials, Japan, June 1986.

2. "A Damage Model for Continuous Fiber Composite Laminates with Matrix Cracks and Interlaminar Delaminations," by S.E. Groves, D.H. Allen, C.E. Harris, and I. Georgiou (Appendix 6.6), to be submitted to ASTM for inclusion in the STP for the Symposium on Composite Materials Testing and Design: 8th Symposium, Charleston, SC. April 1986.

4.0 PROFESSIONAL PERSONNEL INFORMATION

4.1 Faculty Research Assignments

1. Dr. D.H. Allen (Co-principal Investigator) - overall program coordination; development of stiffness relationships; construction of ISV growth laws; mechanical testing.

2. Dr. C.E. Harris (Co-Principal Investigator) - overall experimental coordination; mechanical testing; nondestructive evaluation; stiffness modelling; fracture mechanics.

4.2 Additional Staff

1. Mr. S. E. Groves (Lecturer, Research Assistant, and Ph.D. Candidate) - ISV growth laws; laminate analysis; finite element modelling; mechanical testing.

2. Mr. I. Georgiou (Research Assistant and M.S. Candidate) - mechanical testing; nondestructive evaluation; ISV growth laws.

3. Mr. B. Harbert (Lab Technician) - experimental lab support.

4. Mr. C. Fredericksen (Lab Technician) - experimental lab support.

5. Mrs. C. Rice (Secretary) - secretarial support.

5. INTERACTIONS

5.1 Papers Presented

5.1.1 Presented Under This Grant

1. D.H. Allen, "Modelling of Stiffness Reduction Due to Matrix Cracks in Graphite/Epoxy Laminates," Society of Engineering Science 22nd Annual Meeting, State College, PA, October 1985.

2. S.E. Groves, "Experimental/Analytical Correlation of Damage Accumulation in Laminated Composites," Society of Engineering Science 22nd Annual Meeting, State College, PA, October 1985.

5.1.2 Related Research Presentations

1. D.H. Allen and W.E. Haisler, "Predicted Temperature Field in a Thermomechanically Heated Viscoplastic Space Truss Structure," 26th SDM Conference, Orlando, April, 1985 (also presented at the 3rd Forum on Large Space Structures, Texas A&M University, July 1985).

2. C.E. Harris, D.H. Morris, and C.C. Poe, Jr., "The Fracture Behavior of Filament Wound Cylinders with Surface Flaws," 26th SDM Conference, Orlando, April 1985.

3. C.E. Harris and D.H. Morris, "Fracture of Thick Laminated Composites," Spring Conference of the Society for Experimental Mechanics, Las Vegas, June 1985.

4. D.H. Allen, C.E. Harris, E.W. Nottorf, and G. Wren, "A Fractographic Study of Damage Mechanisms in Short-Fiber Metal Matrix Composites," ASTM Symposium on Fractography of Modern Engineering Materials, Nashville, November, 1985. (also presented at the 22nd SES Conference, Penn State, October 1985).

5. C.E. Harris and D.H. Morris, "A Fractographic Investigation of the Influence of Stacking Sequence on the Strength of Notched Laminated Composites," ASTM Symposium on Fractography of Modern Engineering Materials, Nashville, November 1985

6. APPENDIX - INTERIM TECHNICAL REPORTS

APPENDIX 6.1

AN INVESTIGATION OF DAMAGE ACCUMULATION
IN GRAPHITE/EPOXY LAMINATES

A Thesis

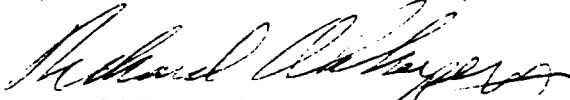
by


ROBERT GERALD NORVELL

Approved as to style and content by:



David H. Allen
(Co-Chair of Committee)

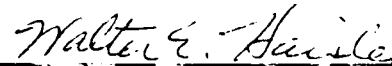

Richard A. Schapery
(Co-Chair of Committee)



Charles E. Harris
(Member)



Vikram K. Kinra
(Member)



Walter E. Haisler
(Head of Department)

August 1985

AN INVESTIGATION OF DAMAGE ACCUMULATION IN
GRAPHITE/EPOXY LAMINATES

A Thesis

by

ROBERT GERALD NORVELL

Submitted to the Graduate College of
Texas A&M University
in partial fulfillment of the requirements for the degree of
MASTER OF SCIENCE

August 1985

Major Subject: Aerospace Engineering

ABSTRACT

An Investigation of Damage Accumulation in
Graphite/Epoxy Laminates. (August 1985)

Robert Gerald Norvell, B.S., Texas A&M University

Co-Chairs of Advisory Committee: Dr. David H. Allen
Dr. Richard A. Schapery

The objective of this investigation has been to identify the mechanisms of initiation and growth of matrix cracks in graphite/epoxy laminates and to identify the effect of matrix cracking on material response. An extensive experimental data base was produced for use in the development of a damage model and for model verification.

An as yet unreported form of transverse cracking has been observed. Two distinct forms of transverse cracks were found, each clearly having its own mechanisms of initiation and growth. Subsequent damage modes associated with transverse cracks, such as longitudinal splitting and delamination, also developed separate forms corresponding to the transverse crack variations.

ACKNOWLEDGEMENTS

I would like to extend my sincere appreciation to all the members of my advisory committee for their help and guidance. I would like to thank Dr. Allen and Dr. Schapery for allowing me the responsibility to use my discretion in pursuing this research. I would like to thank Dr. Kinra for his keen interest in my work and Dr. Harris for his expertise and guidance during this experimental investigation.

My appreciation is extended to Dr. Donald Parker of the Insitute for Solid State Electronics and Dr. Robert W. Nottorf of DuPont for their assistance with X-ray radiography.

My thanks go to P.K. Imbrie and George James for their help with the data acquisition system and to Greg Eden for his assistance with graphics and for his long friendship. I would also like to thank Mr. Carl Frederickson for his valuable assistance with electronic equipment.

I am especially grateful to my wife, Kelly, for her encouragement and understanding.

I also wish to thank the Air Force Office of Scientific Research for their financial support that allowed me to continue my education.

TABLE OF CONTENTS

	Page
ABSTRACT	iii
ACKNOWLEDGEMENT	iv
TABLE OF CONTENTS	v
LIST OF TABLES	vii
LIST OF FIGURES	viii
INTRODUCTION	1
LITERATURE SURVEY	4
EXPERIMENTAL TECHNIQUE	11
Laminate Selection	11
Specimen Fabrication	12
Edge Replication	23
X-ray Radiography	25
Mechanical Testing	36
Determination of Stiffness	45
Measurement of Residual Strain	46
Measurement of Surface Area	49
RESULTS AND DISCUSSION	51
Overview of Results	51
Type A $[0/90_s]_s$	79
Type B $[0/90_s]_s$	86
Type C $[0/90_2]_s$	90
Type D $[0/90]_s$	95
Type E $[0_2/90_2]_s$	98
Type F $[0/90/0]_s$	100

TABLE OF CONTENTS (cont.)

Type G [0/90/0/90] _s	104
Laminate Comparisons	106
CONCLUSIONS	114
REFERENCES	117
VITA	120

LIST OF TABLES

Table		Page
1	Laminate Types Tested	13
2	Material Properties for Hercules AS4/3502 . . .	14
3	Post-cure Resin Content	17
4	Laminate Ultimate Properties	53
5	Stress and Strain at First Ply Failure (FPF) .	55
6	Crack Angle and Length Distribution in Specimen A-4, $[0/90_4]_s$, 98% F_{tu}	88
7	Crack Angle and Length Distribution in Specimen B-5, $[0/90_3]_s$, 94% F_{tu}	92
8	Crack Angle and Length Distribution in Specimen C-8, $[0/90_2]_s$, 91% F_{tu}	96
9	Crack Angle and Length Distribution in Specimen E-9, $[0_2/90_2]_s$, 94% F_{tu}	101
10	Comparison of Total Crack Density and Straight Crack Density	113

LIST OF FIGURES

Figure		Page
1	AS4/3502 graphite/epoxy cure cycle	16
2	Schematic of test specimen types	20
3	V-notched aluminum extensometer mounting tab .	21
4	Extensometer mounting arrangement	22
5	Typical edge replica of a [0/90] _s laminate showing transverse cracks in the 90° plies . .	24
6	Arrangement used to make an X-ray radiograph, showing geometric factors which affect resolution	28
7	Loading fixture for the application of X-ray enhancing agent and X-ray exposure	32
8	Detail of trough used to accelerate infiltration of enhancing agent	33
9	X-ray tube head (source) with 3-axis positioning	34
10	Load frame and X-ray source with and without shielding	35
11	X-ray radiograph showing transverse cracks, longitudinal splits, and delaminations	37
12	Testing set-up with load frame, computer data acquisition system, analog plotter, and microfiche reader	38
13	Technique used to calibrate extensometers . . .	40
14	Specimen in testing machine with longitudinal and transverse extensometers mounted	41
15	The effect of relaxing grips on the strain rate	47
16	Loop formed in stress-strain curve during load reversal	48

LIST OF FIGURES (cont.)

Figure		Page
17	Specimen coordinate system	52
18	Edge replica of a typical straight crack in a $[0_2/90_2]_s$ laminate	57
19	Edge replicas of angle cracks; (a) partial crack, (b) curved crack	59
20	Detail of a radiograph showing the difference between straight and angle cracks .	60
21	Coordinate system used to document crack angles	61
22	Edge replica of $[0_2/90_2]_s$ laminate showing nested curved cracks	63
23	Edge replica of a $[0/90_4]_s$ laminate showing crack groups or families	64
24	Microphotograph of delamination propagating from an angle crack at the $0^\circ/90^\circ$ interface of a $[0/90_4]_s$ laminate	66
25	Crack development by type for $[0_2/90_2]_s$ laminate	68
26	Edge replica of $[0/90_4]_s$ laminate showing development of a curved ^s crack, $63\% F_{tu}$	70
27	Edge replica of $[0/90_4]_s$ laminate showing development of a curved ^s crack, $69\% F_{tu}$	71
28	Edge replica of $[0/90_4]_s$ laminate showing development of a curved ^s crack, $81\% F_{tu}$	72
29	Edge replica of $[0/90_4]_s$ laminate showing development of a curved ^s crack, $94\% F_{tu}$	73
30	Edge replica of two intersecting partial cracks	74
31	Lengthwise fracture of transverse fibers . . .	76

LIST OF FIGURES (cont.)

Figure		Page
32	Fiber fracture in 0° ply near transverse crack	77
33	Example of crack branching from transverse crack at 0°/90° interface	78
34	X-ray radiographs for a progressively loaded [0/90 _s] laminate (dark rectangles are aluminum extensometer mounting tabs)	80
35	Crack development by type for [0/90 _s] laminate	82
36	Edge replica of [0/90 _s] laminate with delaminations growing from both curved cracks .	83
37.	Stiffness reduction for a [0/90 _s] laminate . .	85
38.	Measured stiffness loss as a function of crack surface area for a [0/90 _s] laminate . .	87
39	X-ray radiographs for a progressively loaded [0/90 _s] laminate	89
40	Crack development by type for [0/90 _s] laminate	91
41	X-ray radiographs for a progressively loaded [0/90 ₂] _s laminate	93
42	Crack development by type for [0/90 ₂] _s laminate	94
43	X-ray radiographs for a progressively loaded [0/90] _s laminate	97
44	X-ray radiographs for a progressively loaded [0 ₂ /90 ₂] _s laminate	99
45	Edge replica of a [0/90/0] _s laminate	102
46	Crack development for a [0/90/0] _s laminate . .	103
47	Typical edge replica of a [0/90/0/90] _s laminate	105

LIST OF FIGURES (cont.)

Figure		Page
48	Conceptual representation of the through-the-thickness variation of the normal stress in the $[0_2/90_2]_s$ and $[0/90/0/90]_s$ laminates . .	107
49	Comparison of stiffness reduction for three similar laminates	108
50	Comparison of generated crack surface area for the $[0/90/0/90]_s$ and $[0_2/90_2]_s$ laminates .	110
51	Relationship between crack surface area and stiffness reduction for the $[0_2/90_2]_s$ and $[0/90/0/90]_s$ laminates	111

INTRODUCTION

The advantages of composite materials for use in aerospace vehicles are numerous. Properties such as high strength-to-weight ratio and reduced part count make composite laminates desirable replacements for metallic structures. However, most applications have been restricted to non-critical structures because of a lack of understanding of the behavior of composite laminates as their ultimate strength is approached. This problem arises due to the complex microstructure of the composite which lends itself to complicated forms of damage. Damage is defined as any fracture process. Unlike metals, composite laminates are subject to an array of possible damage modes. One damage mode may interact with another damage mode or may contribute to the growth of new modes. All this leads to a very complex damage state which is dependent on stacking sequence. Because of the major differences in damage growth between composites and metals, linear elastic fracture mechanics of non-interacting cracks and other standard analytical methods have failed when applied to composites. To maximize the use of composites, it is of utmost importance to understand the mechanisms of damage and to develop models to predict strength reduction and changes in material

This thesis follows the style and format of the Journal of Composite Materials.

properties due to these mechanisms.

The research described here represents the experimental portion of a damage model for fibrous composites currently being developed at Texas A&M University [1,2]. The objective of this research has been to identify the parameters controlling damage accumulation in laminated composites. The damage mode of interest is matrix cracking. Matrix cracks are cracks in any ply that run parallel to fibers in the matrix material. This damage mode occurs in all practical continuous fiber composite structures. This phenomenon has been investigated experimentally in seven different laminates subjected to quasi-static, stepwise loading. All the laminates are cross-ply laminates, consisting of 0° plies (fibers in the principle load direction) and 90° plies. This type of laminate has been chosen to promote the growth of matrix cracks and to suppress other damage modes. A comprehensive data base is essential not only to develop the present model but to insure that the experimental results are useful for future research needs. Primary attention has been placed on identifying the mechanisms of initiation and growth of matrix cracks. Secondary emphasis has been placed on observing the effect of cracking on material response.

A qualitative analysis has been made to determine the significance of the damage events observed. These include

crack density, stiffness reduction, crack shapes, development of crack surface area, and residual strain. An effort has been made to interpret the effects of stress level, specimen thickness, geometry, and stacking sequence on damage formation.

LITERATURE SURVEY

Current literature concerning damage growth mechanisms and damage accumulation in advanced fibrous composites is extensive and diverse. Works concerning matrix cracking, both analytical and experimental, are discussed in the following paragraphs.

One of the earliest investigations of matrix cracking was reported by Vasilév, et al. [3] in which a closed form solution was derived for simplified governing equations for a $[0/90]_s$ laminate with a transverse crack in the 90° plies subjected to a load in the 0° direction. This analysis predicts distributions of the two in-plane normal stresses and the interlaminar shear stress as a function of distance from the crack in both the 0° and 90° plies.

Tsai and Hahn [4,5] developed a simplified elasticity model of a cracked 90° ply within a laminate which was used to predict matrix crack spacing and the overall stress-strain behavior of a $[0/90]_s$ glass/epoxy laminate. Their model involved a gradual failure mode, employing a secant modulus which is reduced through a parameter representing the degree of degradation occurring in the 90° plies as a function of the applied stress when subjected to uniaxial tension. This is significantly different from the method proposed by Jones [6] in which the entire lamina stiffness matrix is set to zero with the onset of

cracking.

Kim & Hahn [7] have shown the importance of environmental conditioning on composite laminates. They investigated the effect of residual stress on the onset of matrix cracking which they refer to as first ply-failure (FPF). Variation of residual stresses was accomplished by moisture absorption. They noted that in fiber dominated laminates (containing 0° fibers) the absorbed moisture increases both the FPF stress and the ultimate tensile strength. Herakovich and coworkers [8] investigated the characteristics of thermally induced transverse cracks in graphite/epoxy cross-ply and quasi-isotropic laminates, both experimentally and analytically. The state of stress in the vicinity of a transverse crack and the influence of transverse cracking on the laminate coefficient of thermal expansion was predicted using a generalized plane strain finite element analysis and a modified shear lag analysis.

Garrett and Bailey [9] investigated the thickness effect of 90° plies in cross-ply laminates. Using specimens of glass fibers and polyester resin, they varied the transverse ply thickness between .75 mm and 3 mm. They observed that for a given strain, a higher crack density occurred as the number of transverse layers decreased. Cracks were seen on the edge of the specimen running at 45° to the main transverse cracks. These cracks formed at high strains and failure occurred soon thereafter. No

attempt was made to explain these angled cracks. A simple theory was advanced to predict the crack spacing for a given applied stress and transverse ply thickness when longitudinal and transverse plies are elastically bonded. This theory is based on earlier work by Aveston and Kelly [10].

Flaggs and Kural [11] reported experimental work in which they investigated the uniaxial tensile loads at which transverse cracking initiated in the 90° laminae of $[\pm\theta/90_n]_s$ T300/934 laminates. The transverse strengths of the 90° laminae corresponding to these loads were then calculated based upon lamination theory predictions including effects of residual thermal stresses. The stress at which transverse cracking initiated was found to be a function of both laminae thickness and the orientation of adjacent $\pm\theta$ laminae.

A.S.D. Wang and coworkers [12-16] analyzed the growth mechanisms of transverse cracking and delamination with the application of linear elastic fracture mechanics and finite element calculations of the strain energy release rate. A series of graphite/epoxy laminates in the form of $[\pm 25/90_n]_s$, $n=1/2, 1, 2, 3, 4, 6, 8$, were examined both analytically and experimentally. To predict transverse crack spacing, the strain energy release rate associated with the formation of a single transverse crack in the 90° ply was calculated using a crack closure method. They

then postulated that saturation spacing is that spacing at which the strain energy release rate associated with the formation of a second crack is equal to that associated with the formation of the first crack. They assumed that the values of critical strain energy release rate associated with transverse fracture and interply delamination were the same. Their experimental results showed that transverse cracks did not occur for $n=1/2$ and $n=1$ laminates until the onset of delamination. For $n=2$ and greater, the transverse crack density increased with 90° ply thickness.

Reifsnider [17] developed a one-dimensional shear-lag model which can approximate normal stress in the load direction in the various plies of a laminate. He contends that shear deformations in any given ply are restricted to a thin area in the region of ply interfaces. In the model, this thin region is assumed to transfer all the loads between plies through shear. The model predicts the longitudinal stress field in the region of a transverse crack, and with a critical stress criterion, the model predicts the crack spacing in the laminate.

Talug [18] formulated a finite difference solution to determine how transverse cracking in off-axis plies affects the stiffness of the overall laminate. This technique yields a full-field solution where all six stress components are determined throughout the laminate in the

presence of a crack. With this information, the distance from the crack over which the stresses are redistributed to reach laminate analysis values can be determined. Also, the out of plane stresses, which may initiate delaminations, are determined.

Reifsnider, et al. [19,20] introduced the concept of a "characteristic damage state (CDS)," a condition in which a saturation of matrix cracking is ultimately achieved in both static and cyclic loading and for which a characteristic spacing of cracks is observed. The CDS is said to be independent of load history, and depends only upon the material, geometry, and stacking sequence. From a mechanics standpoint, Reifsnider and Masters [21] propose the CDS has the same significance as the single crack for homogeneous materials with regard to the well-defined physical state from which the fracture event develops. They also point out that the CDS is different in that the final fracture does not occur by the further development of that state as with the single crack situation. Bader, et al. [22] also reported on the formation of a characteristic spacing of transverse cracks in angle-ply laminates. Highsmith and Reifsnider [23] have examined changes in stiffness due to matrix cracks. They proposed a model for treating the problem analytically wherein elements of the lamina stiffness tensor are systematically reduced in relation to crack density and the laminate stiffness is

then determined from a laminated plate theory.

Kelly [24] investigated transverse cracking and included the effects of curing stress. He hypothesized the existence of longitudinal splits caused by a mismatch in Poisson's ratio between plies. He suggested that the splitting would be complete when a saturation of transverse cracking occurred. Laws, Dvorak, and Hejazi [25] developed constitutive equations for fibrous composites which contain groups of longitudinal slits. They investigated the case in which the cracks and fiber diameter were of similar size and the special case of small diameter fibers and large cracks. The overall elastic moduli and compliance components of the cracked composite were obtained using a variation of the self-consistent method.

Stinchcomb, et al. [26] studied the effects of ply constraint on damage development in composite materials. They determined that through-the-thickness constraints control the pattern and spacing of cracks which in turn determines the state of stress and state of strength in the damaged laminate. They also determined that constraint situations that produce greatest static strength do not minimize the extent of damage that develops during loading. Likewise, minimum damage situations do not correspond to maximum strength cases.

Nuismer et al. [27-28] introduced a continuum theory

for the constitutive behavior of a damaged composite ply. A model of the growth of a matrix crack in a 90° ply subjected to transverse tension was developed and incorporated into the theory. This model is based on fracture mechanics and an approximate stress analysis. The model predictions indicate that, after damage begins, the ply constitutive behavior is laminate dependent.

Internal state variable theories have been recently incorporated into cumulative damage models. These models are based on the notion that one or more internal state variables can be used to describe the state of damage within a composite laminate. These variables may be scalar, vector, or tensor valued. Talreja [29] proposes that damage be modeled by a set of independent vector fields based on continuum mechanics. The variables would be proportional to the crack density, crack surface area, and a shape parameter. Allen, et al. [1,2] propose a model using tensor valued internal state variables reflected through the local constitutive equations. A set of local functions describing the energy of cracking is suggested for characterizing the damage variable. The local variables are globally averaged over the entire laminate so that the effects of damage are averaged over a local volume element.

EXPERIMENTAL TECHNIQUE

Laminate Selection

The principle objective of this investigation was to observe the effects of matrix cracking on the stiffness of a laminate. The second objective was to glean as much information as possible about the damage mechanisms of matrix cracking. To meet these objectives, several factors were considered in selection of laminates to be studied. Laminate sequences that included 90° plies were an obvious choice since matrix cracking is the predominant form of damage in this lay-up. To this end, cross-ply laminates consisting of only 0° and 90° plies were desirable. Another consideration was to preclude other damage modes. The last consideration was to use a realistic material system. In this case, a graphite/epoxy system was desired.

In graphite/epoxy systems, the ratio of longitudinal modulus to transverse modulus (E_1/E_2) is very large as compared to a glass/epoxy system. The load carried by 90° plies is small, and even with total degradation of the 90° layers, the decrease in modulus is small. For example, a $[0/90]_s$ laminate would have a stiffness loss of about 6 percent. This might suggest that a $\pm\theta^\circ$ combination might be substituted for the 0° plies to decrease the fiber dominance. Unfortunately this greatly increases the

tensile interlaminar stresses and, thus, the tendency for delamination. With this in mind, the decision was made to use the laminates with only 0° and 90° combinations.

Seven laminates were chosen for this investigation. These are listed in Table 1. The laminate types are identified by letter designations. The $[0/90_n]_s$ series was used to investigate the effect of the thickness of the 90° layer on laminate response and damage growth. The $[0/90]_s$ and $[0_2/90_2]_s$ laminates were included for scaling comparison. The $[0/90/0]_s$ and $[0/90/0/90]_s$ were studied for the effect of 0° ply constraint on crack growth in the 90° plies. There were numerous other points of comparison for this laminate group.

Two other laminates were tested. A $[0_s]_t$ (Type Z) laminate and a $[90_s]_t$ (Type N) laminate were used to determine laminate properties.

Specimen Fabrication

The material used throughout this investigation was AS4/3502 graphite/epoxy manufactured by Hercules Corp. The material was supplied as a preimpregnated tape in 12 inch wide rolls. The material was stored at 0°F until ready to be used. Table 2 lists the various properties of the material. Laminates of 12 inch by 12 inch size were fabricated locally using an air cavity, heated platen press with a microprocessor to control heating and cooling

Table 1. Laminate Types Tested

TYPE	LAY-UP	SUCCESSIVE 90° PLIES	PERCENTAGE 90° PLIES
A	$[0/90_4]_s$	8	80
B	$[0/90_3]_s$	6	75
C	$[0/90_2]_s$	4	66
D	$[0/90]_s$	2	50
E	$[0_2/90_2]_s$	4	50
F	$[0/90/0]_s$	1	33
G	$[0/90/0/90]_s$	2/1	50

Table 2. Material Properties for Hercules AS4/3502

Lamina Properties

Longitudinal Modulus, E_{11}	$21.0 \times 10^6 \pm 2.0\%$	psi
Transverse Modulus, E_{22}	$1.39 \times 10^6 \pm 2.1\%$	psi
Shear Modulus, G_{12}^1	$.694 \times 10^6$	psi
Poisson's Ratio ν_{12}	$.3.10 \pm 3.7\%$	
	$\nu_{21} .030 \pm 35.0\%$	
Longitudinal Strength, F_{tu_1}	$326000 \pm 3.5\%$	psi
Transverse Strength, F_{tu_2}	$11085 \pm 9.8\%$	psi
Long. Failure Strain, ϵ_{tu_1}	$.0144 \pm 4.6\%$	in/in
Tran. Failure Strain, ϵ_{tu_2}	$.00773 \pm 6.7\%$	in/in

Prepreg Properties

Fiber Areal Weight ²	164 g/m^2
Fiber Volume Fraction ²	$.58 \pm .03$
Resin Content, % by weight ²	35 ± 3

¹Theoretical²Hercules Inc. Specifications

rates, vacuum and cavity pressure. The laminates were cured following the cure cycle in Figure 1. Each stacked laminate was weighed before and after the curing cycle. In this way the amount of resin bled from the plate was monitored. This information, in conjunction with resin density and resin content, was used to calculate the fiber volume fraction after cure. These data are presented in Table 3. By placing a .025 inch thick sheet of milled teflon on each side of the stacked laminate before curing, a fine matte finish was left on the surface of the laminate. In this way the cross-hatch pattern of peel-ply or bleed cloth was avoided. Likewise, the wrinkles or air tracks sometimes left by teflon release film were also avoided. This was important so as not to create stress concentrations or patterns on the X-ray exposures. Each laminated plate was inspected by visual observation for general condition and surface anomalies, and by ultrasonic C-Scan for voids, inclusions, and delaminations.

A typical specimen was identified by its laminate type and the position it was cut from the laminated plate. For example, specimen C-3 was the third specimen cut from the $[0/90_2]_3$ laminate.

Specimens were cut from the plate using a Micro-Matic Precision Slicing and Dicing Machine. The blade was a 6 inch diameter, .05 inch thick, diamond-edge cut-off wheel. The wheel was operated at 2850 rpm with a feed rate of 1.3

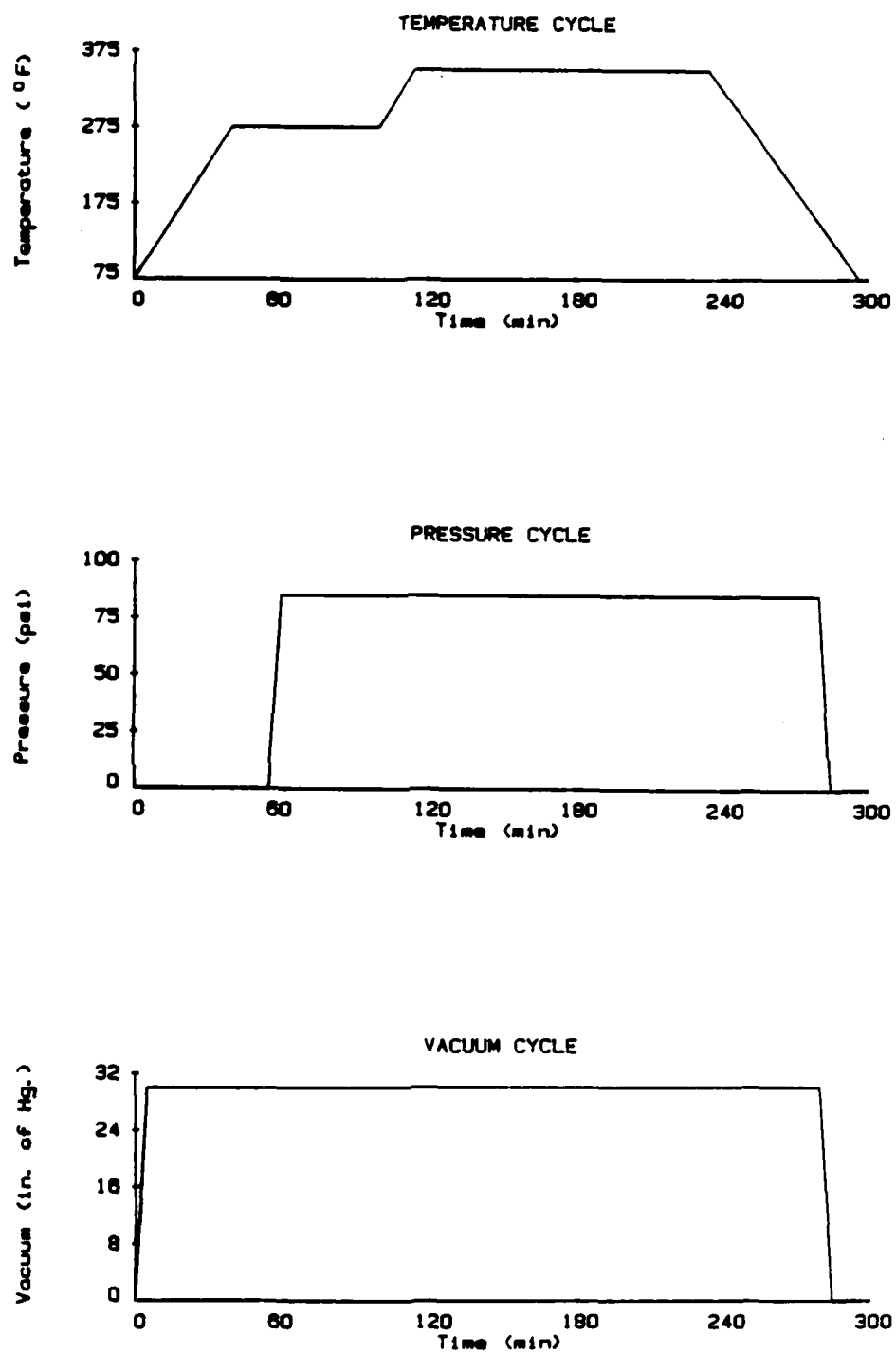


Figure 1. AS4/3502 graphite/epoxy cure cycle

Table 3. Post-cure Resin Content

TYPE	LAMINATE WEIGHT g, UNCURED	LAMINATE WEIGHT g, CURED	RESIN LOST g	RESIN CONTENT, % WT.
A	208.9	182.3	26.6	24.6
B	165.3	144.4	20.9	24.7
C	122.0	110.7	18.8	27.5
D	81.8	74.6	7.2	27.8
E	165.2	145.4	18.8	25.9
F	123.1	108.9	14.2	25.6

Nominal resin content by weight, uncured : $34.2 \pm 1.6\%$

in/min and was cooled with ethylene glycol. The nominal dimensions for all specimens were 1 inch in width and 11 inches in length. Width measurements were made with a dial caliper at three locations in the one inch gage length and averaged. Thickness measurements were made with a .0001 inch resolution micrometer at nine locations in the one inch gage length and averaged.

The 0° unidirectional specimens were provided with 2 inch end tabs made from woven cross-ply glass/epoxy material. Strips of tabbing material were tapered at 15° and bonded to the laminated plate with film adhesive manufactured by 3-M Corporation before cutting the specimens. This adhesive required 1 hour of cure time at 250°F. Because these unidirectional specimens are subjected to extremely high loads, tabs were used to prevent the wedge action grips from digging into the graphite/epoxy and to reduce the grip effect. None of the other specimens had end tabs. However the ends of the specimens (approximately 2 in.) were coated with a layer of MS 907 two-part epoxy manufactured by Miller-Stephenson Chemical Company. This epoxy remains fairly ductile after cure, resists chipping, and bonds well with the graphite/epoxy. The epoxy coating was lightly sanded to a uniform thickness. 320 grit emery cloth was placed between the grips and the specimen during loading to improve the gripping friction. The epoxy layer and emery cloth serve to pro-

protect the specimen from the wear due to the coarse diamond serration of the grips. The two specimen types are shown schematically in Figure 2.

Displacement measurements were made for all tests by means of an extensometer. The extensometer, used to measure longitudinal displacement, had a 1 inch gage length and was attached to the center portion of the specimen. The knife edges of the extensometer sat in narrow, V-shaped channels machined into aluminum tabs (Figure 3). The tabs were bonded to the specimen using RTV silicone adhesive manufactured by General Electric Corp. The extensometer mounting arrangement is shown in Figure 4.

To prepare the specimens for edge replication (an NDE technique to be described) the edges of all the specimens were polished. Each specimen was polished first with 5.0 micron aluminum oxide slurry on a felt polishing cloth. Approximately 400 strokes on each edge were used. Then each was polished with 1 micron slurry in a similar fashion. Approximately 200 strokes were needed. To check polishing quality, the specimens were periodically examined under a 100x power microscope.

During preparation and prior to being tested, the specimens were stored at room temperature in an airtight chamber containing desiccant in order to minimize environmental effects.

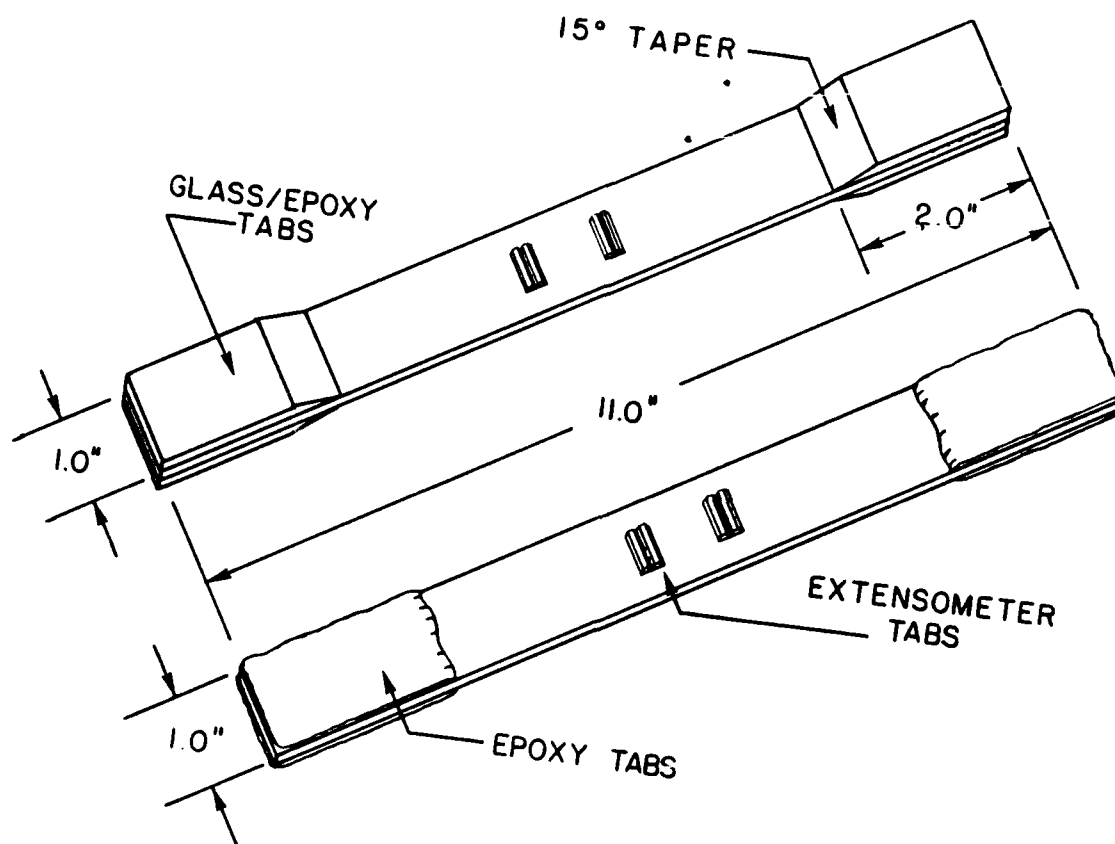


Figure 2. Schematic of test specimen types

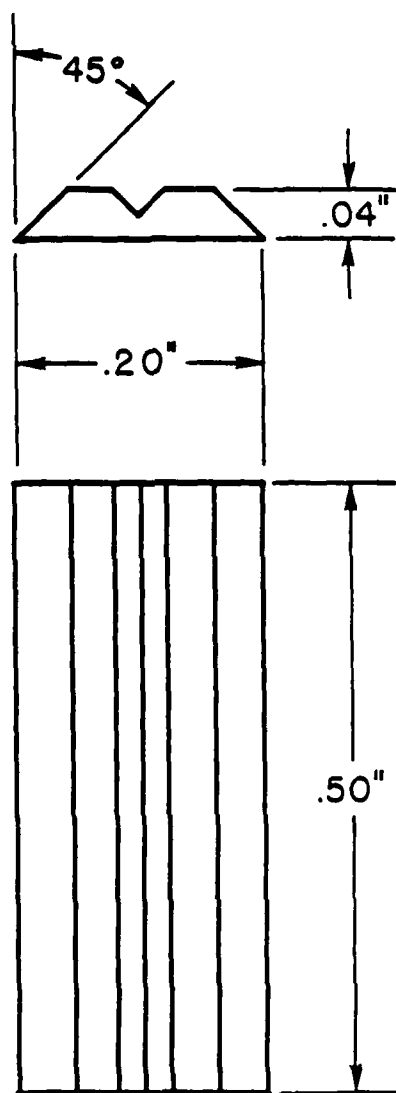


Figure 3. V-notched aluminum extensometer mounting tab

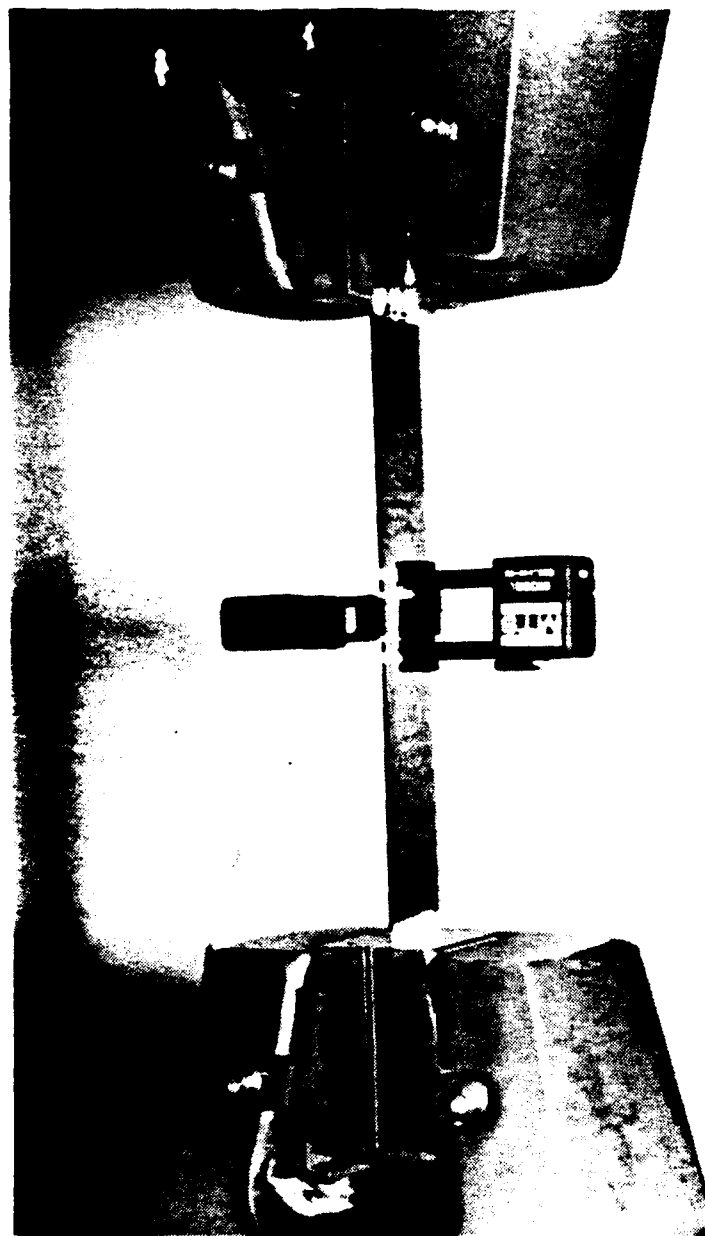


Figure 4. Extensometer mounting arrangement

Edge Replication

Surface replication is a technique used to duplicate the surface topography of a material onto another medium. The technique was originally developed and used in metallography, and was extended to use with composites by Stalnaker and Stinchcomb [30]. Replicas are produced by pressing cellulose acetate tape softened by exposure to acetone to the edge of the composite specimen. After the acetone evaporates and the acetate hardens, a permanent record of the surface features is obtained. This method provides details of the damage state at the edge of the laminate and, when taken at various times during loading, records the history of damage development. In particular, details such as number, spacing, shape, and location of transverse cracks, and delaminations that manifest themselves at the edge are readily observable. An example is shown in Figure 5.

The quality of the details that could be seen on an edge replica was greatly increased when the edge was polished as described previously. Details were further improved by making the replica while the specimen was still under load. This served to open the cracks to allow better penetration of the softened acetate. After a load step, the specimen was reloaded to a modest fraction of the previous load and a replica was made. To produce a



Figure 5. Typical edge replica of a $[0/90]_3$ laminate showing transverse cracks in the 90° plies

replica, strips of acetate were taped to an appropriately sized long slender block with a smooth surface. The block was held lengthwise against the specimen in the load frame, tilted away from the specimen slightly, and a small stream of acetone was allowed to run the length of the tape. This was quickly repeated as the block tilted lengthwise in the other direction. This technique facilitated an even coverage of acetate tape by acetone. The block was held firmly in place for approximately one minute. When the tape was removed, its quality was checked in a 25x power microfiche reader before proceeding with the next load step. With experience, it is possible to place two replicas side by side on one strip of tape, one replica of each side of the specimen. When viewed in the microfiche reader, one can easily ascertain the continuity of a transverse crack from one edge of the specimen to the other.

To prevent the excess acetone from running down the specimen and softening the epoxy tab coatings, an "apron" of masking tape was placed at the bottom of the specimen before making an edge replica. The cellulose acetate used was No. 11340 Replicating Tape manufactured by Ernest F. Fullam, Inc.

X-ray Radiography

X-ray Radiography is becoming a common technique in

the investigation of damage in advanced composites. This method of non-destructive evaluation provides an image of the internal structure of a material. The image is produced on film as the material under examination selectively absorbs or transmits the radiation. A variation in radiation absorption in a composite material can be caused by the presence of voids, cracks, delaminations, and inherent flaws. It is obvious that this can be an important tool in damage characterization.

A problem arises in that the components of a graphite/ epoxy material system are organic, and thus their absorptivity of radiation is only slightly different from the surrounding air. As a consequence, an X-ray opaque substance, or enhancing agent, must be applied to the composite to distinguish a damaged region from an undamaged region. When the enhancing agent is introduced into damaged regions, the resulting X-ray image, or film exposure, shows these regions distinctly.

A candidate for an enhancing agent must contain some type of "heavy" element such as iodine, zinc, lead, or barium. Several enhancing agents are used both in research and in industry; tetrabromethane (TBE), diiodobutane (DIB), diiodomethane, and zinc iodide are examples. All of these are considered toxic to humans except zinc iodide. Rummel and coworkers [31] found that a zinc iodide solution was comparable to the other enhancing

agents in both penetration into a composite material and its opacity to X-rays. They also found no influence of the zinc iodide on the mechanical response of a graphite/epoxy material system.

Several investigators have suggested a working solution consisting of 60 grams of zinc iodide, 10 ml of water, 10 ml of isopropyl alcohol, and 10 ml of Kodak "Photo-Flo 600." This solution was used for all radiographs in this investigation. The zinc iodide was obtained from Fisher Scientific Company. The Photo-Flo acts as a wetting agent, reducing surface tension of the solution when applied to a crack. It can be obtained from most photographic supply outlets.

In X-ray radiography, it is important to achieve as high a resolution as possible to increase the detail of the damage seen in a radiograph. One cause of decreased resolution is the penumbra effect. In the case of visible light, the penumbra is the area of partial illumination between a perfect shadow and full light. Figure 6 shows a schematic of the arrangement used to make a radiograph; where a denotes the size of the anode, or source of X-rays, l is the distance from the ^{anode} ~~object~~ to the ^{object} ~~film~~, d is the distance from the object to the film, c is the arc length between two intersecting X-ray beams, and θ is the angle between those beams. To maximize the resolution one must minimize the arc length c . This can be accomplished

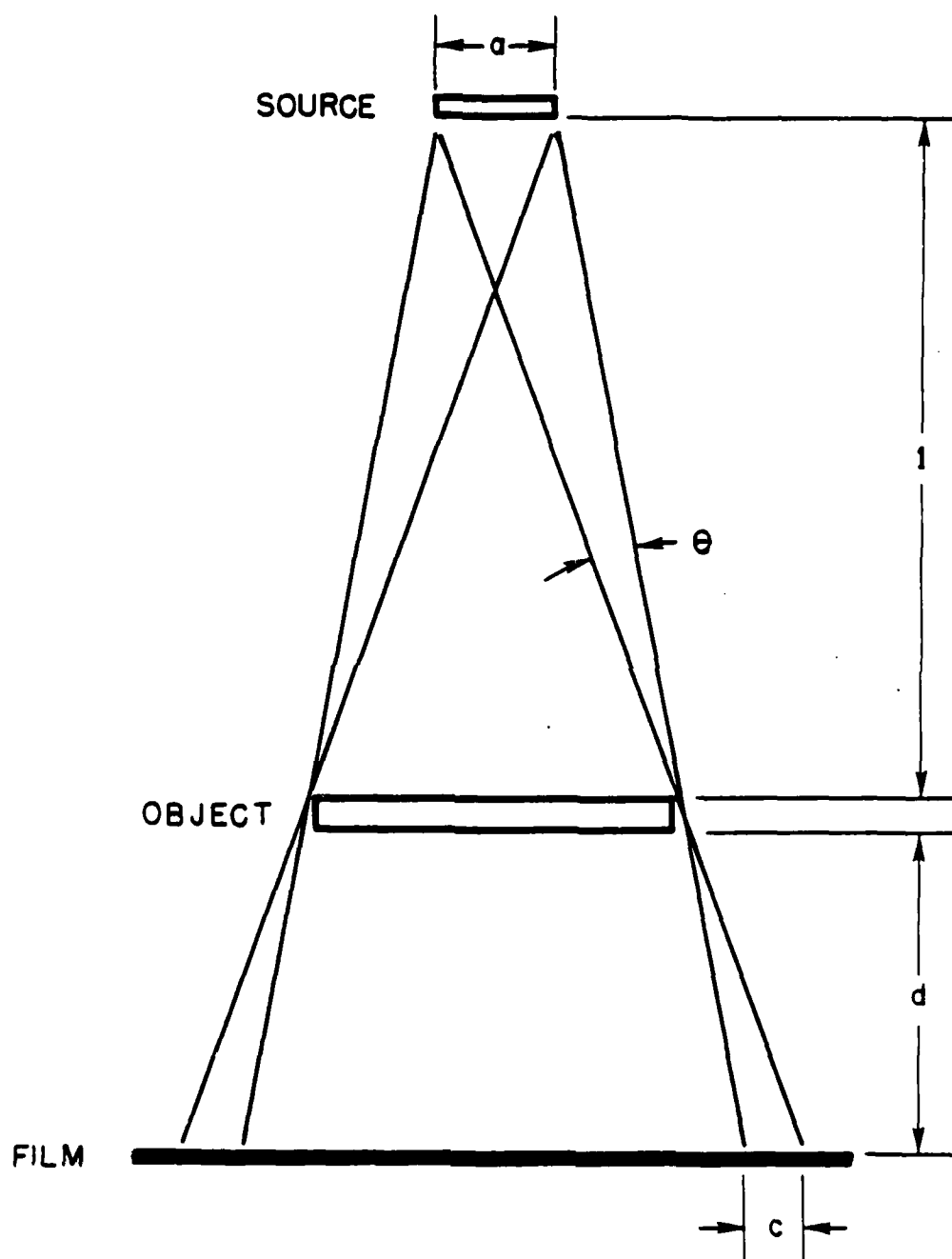


Figure 6. Arrangement used to make an X-ray radiograph, showing geometric factors which affect resolution

by simply moving the film as close as possible to the object, i.e. decrease d . This does not eliminate the problem altogether because the object still has a finite depth. Another method is to increase the source-to-object distance. This decreases the angle θ . A third method to reduce the penumbra effect is to use a small source, thereby decreasing both a and θ .

There are other nongeometric means to increase resolution. In an X-ray exposure, one can only discern details as small as the grain on the film. By using a fine-grained film, more detailed features can be seen. Another means to increase resolution is to use a film with high emulsion contrast. Scattered radiation which may fog an exposure can be reduced by using a collimator or diaphragm to limit the exposed radiographic field.

The voltage which operates the X-ray tube head, measured in kilovolts (kVp), determines the intensity or "speed" of the X-ray radiation. High kVp creates "hard" or intense X-rays while low kVp produces "soft" X-rays. If an exposure is made at a kVp that is too high, the rays pass through the object unhindered. The film, when developed, will be totally exposed as if no object was in the path of the X-rays. If the operating kVp is too low, no X-rays penetrate the object, and therefore no internal damage will be seen at all. The proper kVp setting depends on the absorptivity of the object material. When

a proper voltage is found, the developed film should be black in the area surrounding the object, gray in the area covered by the object, and white in the damaged areas that have enhancing agent present. In this way the voltage controls the contrast of the radiograph. Another factor that controls the quality of the image is the time of the exposure. This determines the "number" of X-rays that pass through the object. The correct time of exposure is dependent on the operating voltage and the source distance to the object. The time of exposure is related to the square of the distance. If the distance to the object is doubled, an identical exposure can be made by increasing the time of exposure by a factor of four.

The X-ray unit used was a Phillips Model K 140 Be with a 140 kVp range and Beryllium window. The nominal film-to-source distance was 37 inches. A lead bronze diaphragm with a radiographic field of 4 inches by 19 inches was used. The tube current was 2 mA with a .6 mm by .6 mm focal spot.

The zinc iodide solution was introduced to the damaged areas through the edge of the specimen. The infiltration of the zinc iodide can be accelerated by putting the specimen under a tensile load. Loading the specimen reopens the matrix cracks and provides a capillary path for the solution to travel to other damage forms. This loading was accomplished with a small load frame incorporating

Instron grips rated for 5000 pounds (Figure 7). Load was applied by turning a nut which drew a threaded shaft connected to a grip through a hollow shaft. The specimen was placed in the load frame with the edge upward and loaded to approximately 300 pounds. Two strips of silicone rubber were clamped to each face of the specimen approximately $1/4$ inch beyond the edge. Silicone grease compound from General Electric was placed between the strips at each end of the specimen to form a trough. The zinc iodide solution was injected into this trough and allowed to remain for 15 minutes as gravity assisted the infiltration (Figure 8). This procedure was repeated for the other edge of the specimen. The residual solution was then removed and the specimen edges and surfaces were cleaned with methyl ethyl ketone.

All X-ray exposures were made while the specimens were still under load in the small load frame. The tube head was mounted on an optical stand with three axis control for exact positioning of the tube head (Figure 9). The frame and X-ray tube head were completely enclosed in a lead shield during operation (Figure 10). The optimum operating voltage for the laminates used was found to be 30 kVp. The film used was Kodak Industrex M-type, double emulsion, high resolution film. Exposure times were 30 seconds for 4 ply laminates and 40 seconds for 10 ply laminates. An example of the details visible in an X-ray

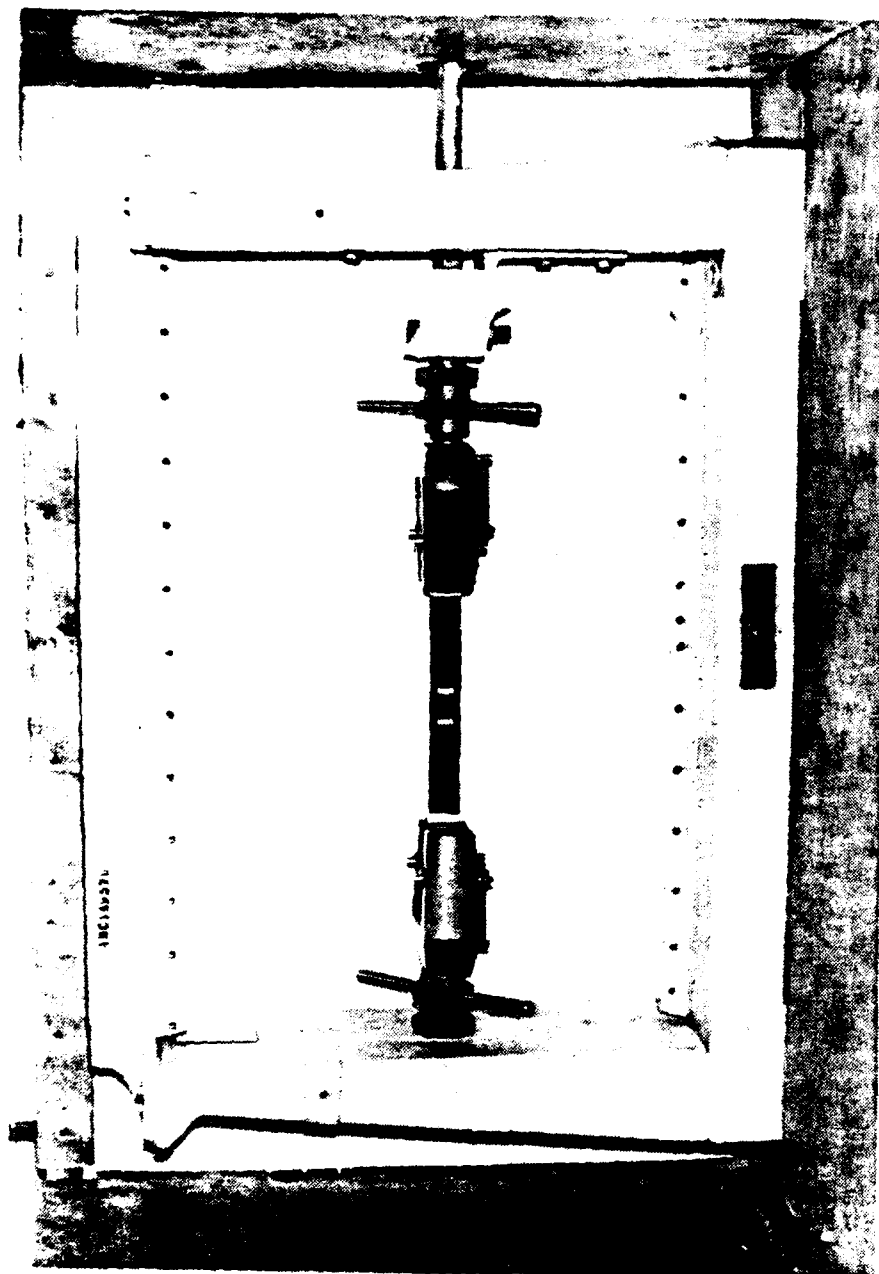


Figure 7. Loading fixture for the application of X-ray enhancing agent and X-ray exposure



Figure 8. Detail of trough used to accelerate infiltration of enhancing agent



Figure 9. X-ray tube head (source) with
3-axis positioning

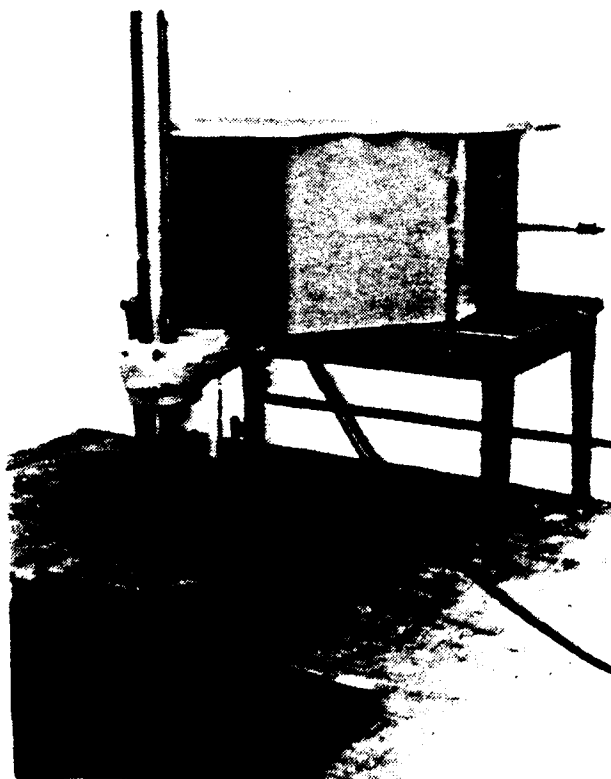


Figure 10. Load frame and X-ray source with and without shielding

radiograph are shown in Figure 11.

Mechanical Testing

Mechanical testing was conducted in the Materials Characterization Laboratory, Department of Aerospace Engineering, Texas A&M University. Figure 12 shows the array of equipment used in this investigation. All tests were performed on a mechanical screw-driven Instron 1125 Universal Testing System with wedge action grips. Tests were run at a constant cross-head speed of .05 inches per minute as recommended in ASTM Standard 3039-76. Extensometers were used to measure both longitudinal and transverse displacement. These extensometers were manufactured by Material Testing System, Inc. (MTS). An MTS 632.11B-20 extensometer with a one inch gage length was used to measure the longitudinal displacement. This extensometer was seated on the specimen in the aluminum grooved tabs described previously. It was held in place by elastic bands. An MTS 632.11C-20 extensometer (metric) was used to measure the transverse displacement. The flat sides of the knife blades were placed against the edges of the specimen. An elastic band placed around the "legs" of the extensometer kept the blades in compression against the specimen edges. Another elastic band was used to position the extensometer on the the specimen. Cardboard spacers were used to increase the gage length of the transverse

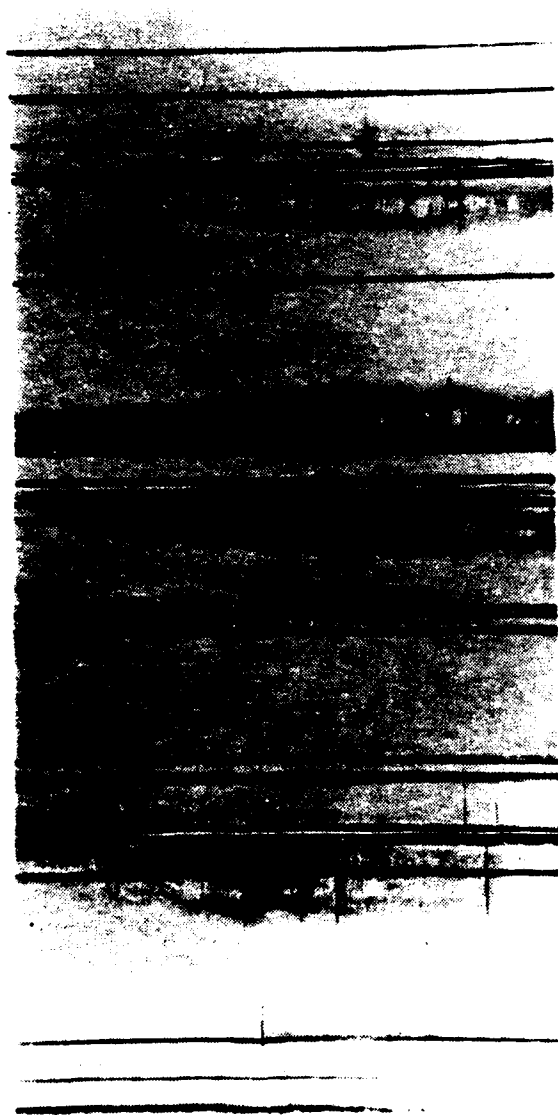


Figure 11. X-ray radiograph showing transverse cracks, longitudinal splits, and delaminations

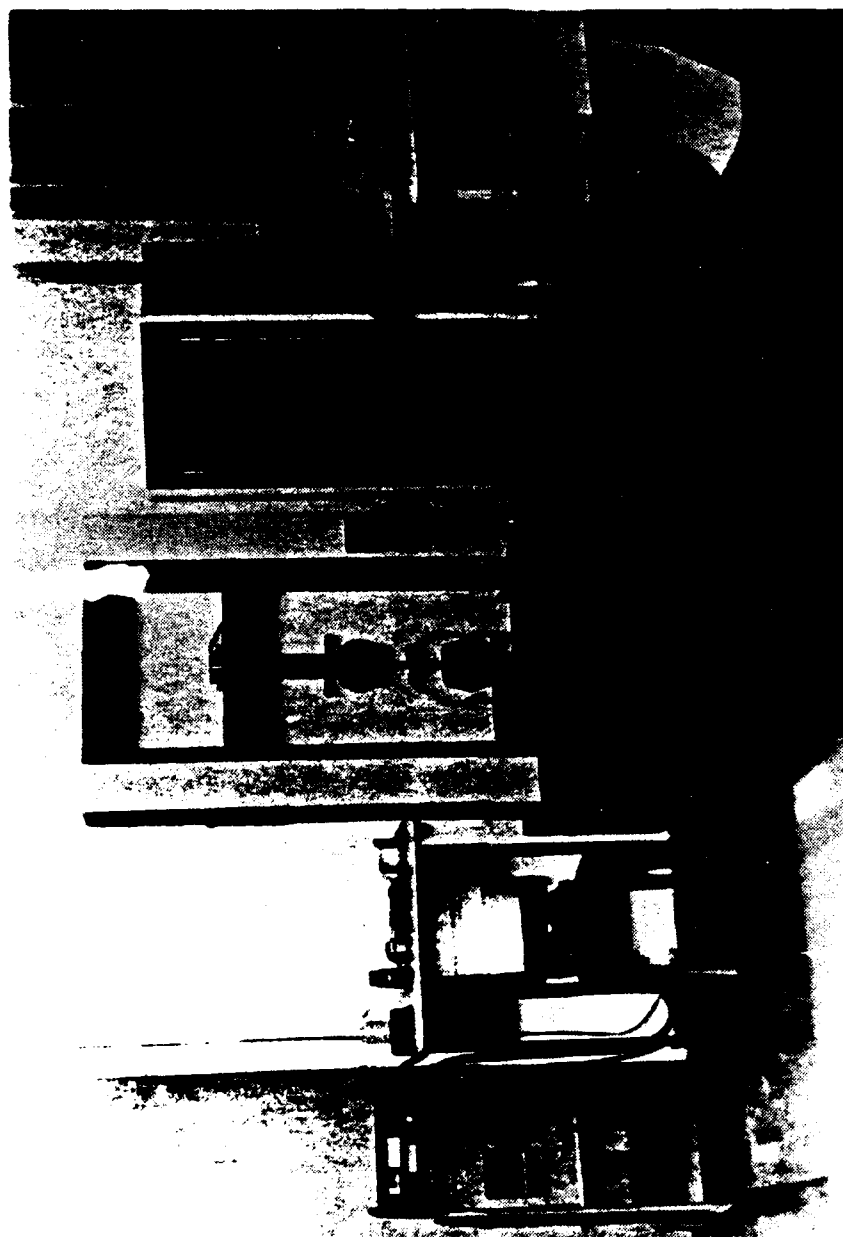


Figure 12. Testing set-up with load frame, computer data acquisition system, analog plotter, and microfiche reader

extensometer so that the zero point or center of the response range of the device would be used when mounted. The extensometers were calibrated just prior to mounting for each load step (Figure 13). The extensometers were mounted on opposite sides at the center portion of the specimen (Figure 14).

The monitoring of stiffness degradation was a major point of interest in this investigation. For this reason, it was imperative to insure the accuracy of the stiffness measurement. Load measurement is easily accomplished with a load cell and is subject to few error possibilities. The most common methods of measuring strain are through the use of resistance strain gages and extensometers. There are advantages in both techniques. Strain gages are permanently fixed to the specimen surface while extensometers are not. Depending on the mounting technique, extensometers may slip during loading. Strain gages are sensitive only to the material beneath the gage. In a metal, the deformation field is continuous even down to the microscopic level. A statistically representative volume of the material is several orders of magnitude smaller than the size of the strain gage. Of course, this kind of deformation would be best measured by resistance strain gages. In a composite laminate, the size of the a single local damage phenomenon, such as a transverse crack, can be on the same order of magnitude as the size

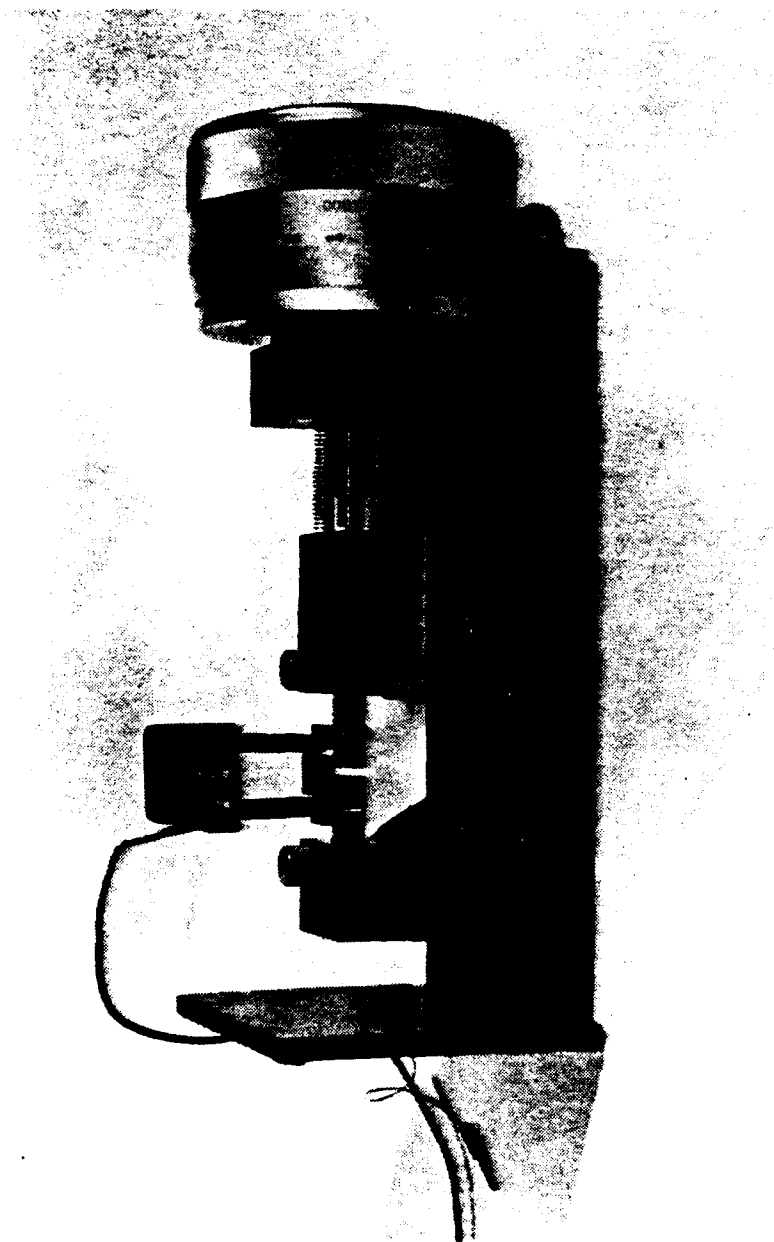


Figure 13. Technique used to calibrate extensometers

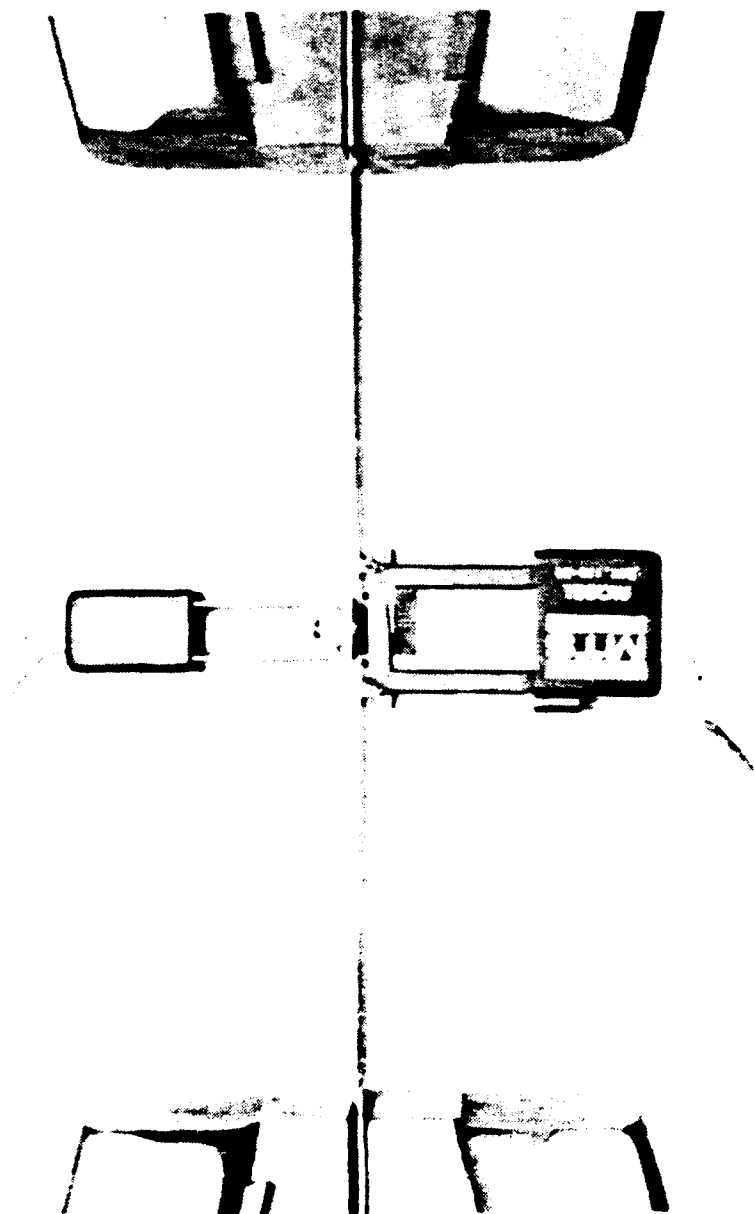


Figure 14. Specimen in testing machine with longitudinal and transverse extensometers mounted

of a strain gage. This could lead to a misinterpretation of the total response of the material system. Extensometers, on the other hand, integrate the material response over a comparatively large gage length. Extensometer measurements are more indicative of the total specimen response. For this reason extensometers were used exclusively.

The response of the extensometers was amplified by a signal conditioner manufactured in-house. The load cell response was processed by the conditioner built into the Instron controller. The longitudinal displacement and the load signals were monitored continuously and recorded on an analog X-Y plotter.

A digital data acquisition system was used to record four channels of data for each test. The signals that were recorded were the load, longitudinal displacement, transverse displacement, and time. The computer was a DEC PDP 11/23 Plus manufactured by Digital Equipment Corporation. The A-to-D conversion board was manufactured by the ADAC Corporation. The test parameters entered into the acquisition program were the calibration factors for the load cell and extensometers, the specimen dimensions, cross-head rate, and the rate at which data points were recorded. After data reduction, any two of the following test outputs could be plotted against one another: stress, longitudinal strain, transverse strain, Poisson's ratio,

and time. Since the tests were run at constant cross-head speed, this capability was needed to determine stress and strain rates for each test. The digitized information was plotted on a Hewlett-Packard 7470A plotter.

The Instron wedge action grips had the capability to test two inch wide specimens. These were used instead of one inch wide grips to prevent a loss of gripping effect at the edges of the one inch wide specimens. Aluminum templates were used to keep the specimen centered in the grips. Once a specimen was placed in the lower fixed grip with a template, it was aligned with the grip insert face with a level and the grip was tightened. A steel straight edge was used to align the upper grip insert face with its lower counterpart.

Three types of tests were conducted for each laminate group. In the first type of test, two specimens of each laminate were tested by monotonically loading to failure. The specimen was fully instrumented with longitudinal and transverse extensometers. The first audible acoustic emission was recorded and any significant patterns in the emissions were noted. This test supplied information on first ply failure, ultimate strength, ultimate strains, and modulus for an undamaged laminate. This information set the framework for the following tests.

In the second type of test, a single specimen from each laminate was repeatedly loaded and unloaded, each

succeeding load step greater than the previous one. Only load and longitudinal strain were measured. An edge replica was taken over the center 4 inches of the specimen after each load step when the extensometer was removed. At no time was the specimen removed from the grips. The number of load steps performed were typically between 8 and 12 steps. This test indicated the crack patterns and modulus changes to expect in further testing.

The last set of tests involved a procedure similar to the one described above, except that an X-ray radiograph was made upon unloading from each step. Of course this necessitated the removal of the specimen from the grips also. In most cases, the longitudinal and transverse strains were monitored. The load level to which a specimen was taken was based on the amount of audible damage that could be heard when loading a specimen. The object of this was to develop a consistent increase in damage (i.e. transverse cracks) for each load step.

Care was taken to avoid holding a specimen at extreme loads where cracking occurs spontaneously without the addition of load. Attempting to make an edge replica at this peak load would further complicate this situation. Once a test had reached a desired load level, it was immediately returned to zero load at the same cross-head rate as loading. The extensometer was then removed and the specimen was reloaded, typically to 300 pounds. Edge

replicas were made of the full seven inches between the grips, on both edges of the specimen.

Determination of Stiffness

As mentioned before, an important aspect to this investigation was to monitor stiffness degradation. For the step-wise loading test, stiffness was measured only on the unloading part of the test. In this way, the stiffness reflected the effects of damage accumulation during that particular load step.

A least-squares linear curve fit was used to determine the stiffness. A computer program was created to do the numerical fit to the digitized data. The fit was made between specified high and low load values.

All laminate types tended to have a stress-strain curve that was concave up. As a consequence, a stiffness calculated from the least-squares fit was dependent on the specified load levels. A systematic method of deriving the stiffness was needed.

From preliminary tests, it was found that a typical one inch wide 0° lamina could carry an ultimate load of approximately 1500 pounds. Because all the laminates in this investigation were fiber dominated, this information was useful in determining the ultimate load of each of the laminates. For example, the failure load of a $[0_2/90_2]_S$ laminate was approximately 6000 pounds. It was found that

the first indication of damage occurred at about half of this estimated ultimate load for all the laminates. This made a convenient high load for the least-squares calculation and was used in all cases for the determination of stiffness.

Since the tests were conducted at a fixed cross-head rate, the stress or strain rates were not necessarily constant. Figure 15 shows an example of this. When a test was initiated or neared complete unloading, the stress and strain rates were affected as the pressure of the grip wedges eased. The low load for the least-squares fit was chosen to avoid this condition.

Measurement of Residual Strain

One of the goals of this investigation was to monitor residual strain after each load step. This proved to be anomalous. When a specimen was pulled to the desired load, it was immediately unloaded. At this point the stress-strain curve would sometimes "loop" back on itself. That is, the strain signal would decrease sharply, while the load signal decreased only slightly. This is illustrated in Figure 16. This phenomenon was not consistent from test to test. Since the residual strain upon unloading was very small, it was of the same order of magnitude as this loop. An inertial effect, backlash in the drive train, or movement of the extensometer may be explanations

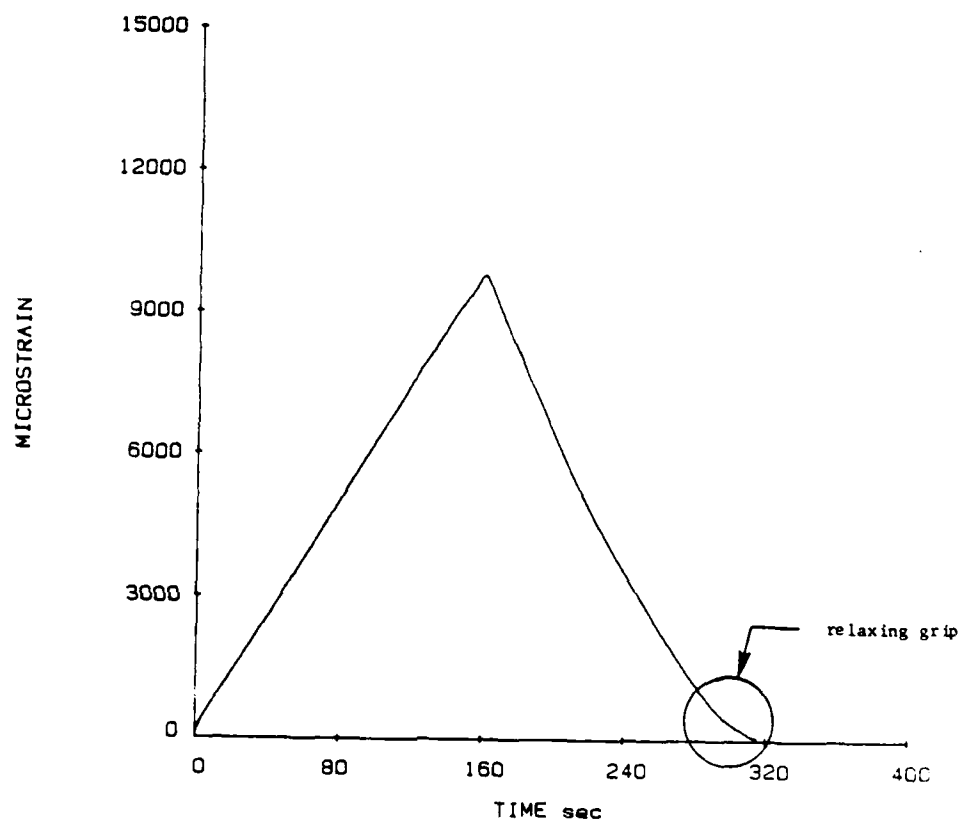


Figure 15. The effect of relaxing grips on the strain rate

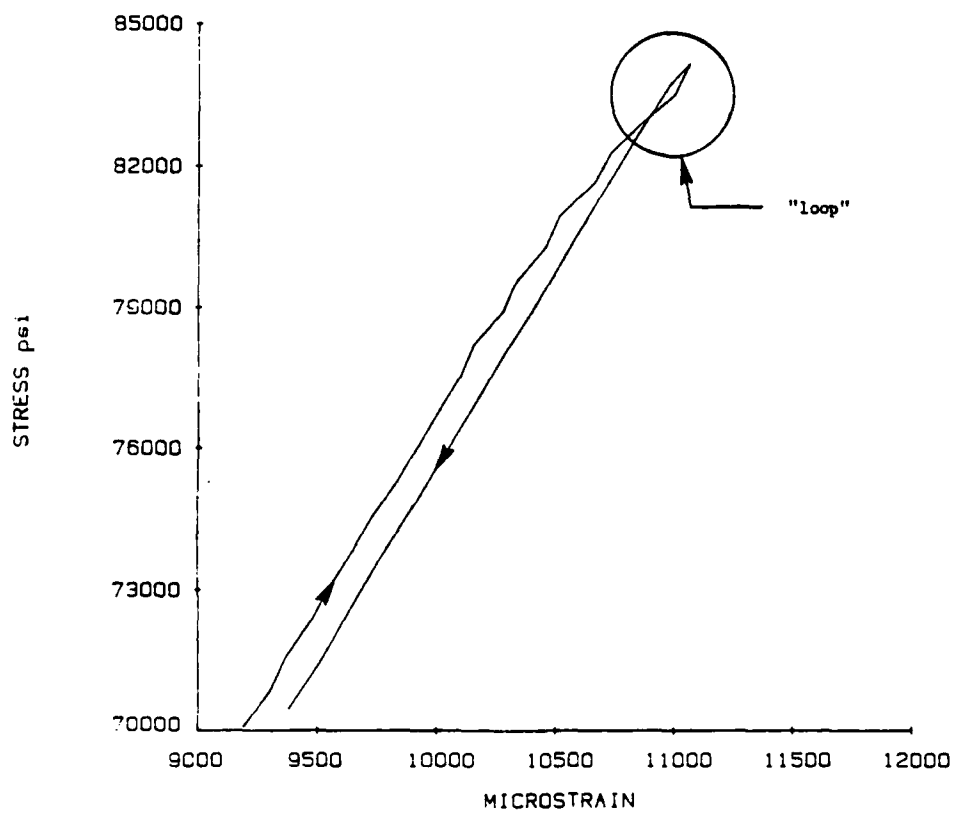


Figure 16. Loop formed in stress-strain curve during load reversal

for this occurrence.

Measurement of Surface Area

Another objective of this investigation was to quantitatively determine the surface area produced during damage accumulation. Previous research concentrated on determining the number of cracks produced during loading and the resulting crack density (number of cracks per unit length). This quantity would then be compared to the stiffness loss of the laminate. A simple modification was made to this procedure to obtain surface area. This was done by taking the product of the number of cracks, the width of the specimen, the thickness of the 90° group, and a factor of 2 (for each face of a crack).

Preliminary tests indicated that many transverse cracks did not grow selfsimilarly. From the inspection of edge replicas, it was found that many cracks had irregular shapes and curvatures, and in some incidences the cracks did not propagate through the full thickness of the transverse ply groups. X-ray radiographs indicated that some cracks did not span the full width of the specimen. It would seem that an incomplete crack would not have the same impact on the response of the laminate as would a full crack. Simply counting it as just another crack and using the aforementioned procedure could be misleading.

To avoid this misrepresentation, crack surface area

measurements were made on a crack by crack basis. In this way compensation could be made for incomplete cracks and crack curvature. The basis for the area measurement was to determine crack length through the thickness of the laminate. Crack lengths were measured from edge replicas with a 100x power microscope. The eyepiece of the microscope incorporated a calibrated 100 division scale. At the magnification used, there were 100 divisions per millimeter, or approximately 25 divisions per lamina thickness.

Crack lengths were measured on both sides of the specimen and then averaged. In this way changes in the length (through the thickness) across the width of the specimen could be accounted for. By doubling the length and multiplying by the width of the specimen, the crack surface area was approximated. Since a nondestructive technique was not available to measure the surface area directly, it was assumed that this would be a suitable approximation.

The angle at which cracks grew across the thickness of the specimen was also of interest. A video camera was attached to the microscope and the picture of the edge replica was displayed on a large video monitor. Angles could be measured accurately using a large homemade protractor.

RESULTS AND DISCUSSION

The results are presented in three parts. First, a general overview of the test results is presented. Second, observations are presented for each laminate type. Third, important comparisons are made for similar laminates.

Overview of Results

As mentioned before, the tests in this investigation were designed to promote the growth of matrix cracks. In addition to matrix cracking, some other forms of damage did occur. These included delaminations, fiber breakage, fiber splitting, and transverse crack branching, depending on the laminate type.

A coordinate system shown in Figure 17 has been used to help describe the various damage phenomenon. The x- and y-axes define the lamina plane with the x-axis aligned with the longitudinal or loading direction. The z-axis is perpendicular to the lamina plane and goes from front surface to back surface.

A compilation of the ultimate strengths and ultimate strains of all the laminates tested is shown in Table 4. The data for unidirectional 0° and 90° laminates are included. All laminates had an ultimate strain less than that of the unidirectional 0° laminate due to the complex

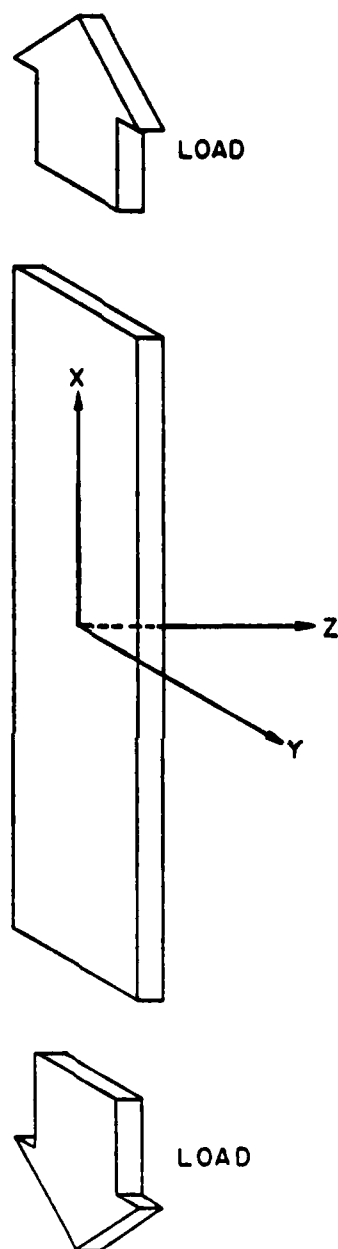


Figure 17. Specimen coordinate system

Table 4. Laminate Ultimate Properties

TYPE	LAY-UP	ULTIMATE STRENGTH (ksi)	ULTIMATE STRAIN %
Z	$[0_s]_s$	$326.0 \pm 11.$	$1.44 \pm .07$
N	$[90_s]_s$	11.1 ± 1.1	$.77 \pm .05$
A	$[0/90_s]_s$	51.2 ± 3.0	$1.22 \pm .12$
B	$[0/90_s]_s$	74.3 ± 1.1	$1.33 \pm .09$
C	$[0/90_2]_s$	106.9 ± 1.4	$1.41 \pm .03$
D	$[0/90]_s$	150.3 ± 6.5	$1.32 \pm .07$
E	$[0_2/90_2]_s$	159.9 ± 6.0	$1.38 \pm .05$
F	$[0/90/0]_s$	181.7 ± 9.8	$1.32 \pm .08$
G	$[0/90/0/90]_s$	165.9 ± 8.6	$1.40 \pm .11$

localized stress states associated with various damage modes present in the transverse layers. The $[0/90_4]_S$ (Type A) had the lowest ultimate strain due to extensive damage formation. The transverse crack development was irregularly spaced and delamination was widespread. No consistent pattern could be found for the remaining laminates and further comparison of the laminates with respect to ultimate strain was inconclusive.

During each test of an undamaged specimen, the load at the first audible acoustic emission was recorded. Table 5 lists this information for each laminate type. For comparison, the ultimate strength and strain data for a unidirectional 90° laminate is included in the table. The first "pop" was assumed to be the formation of the first transverse crack. This was termed as the first ply failure (FPF). This, of course, is a misnomer since the ply is able to carry a load along the remainder of its length. In general, the strain at FPF was inversely related to the number of 90° plies in a group. This is easily seen in laminates types A through D. The $[0/90_2]_S$ and $[0_2/90_2]_S$ laminates both had four 90° layers and had very nearly the same FPF strain. With the large group of 90° plies, the additional constraint of the 0° plies in the $[0_2/90_2]_S$ laminate had little effect. The constraining effect is evident in the $[0/90/0]_S$ laminate. The FPF strain is almost the same as the ultimate strain of a

Table 5. Stress and Strain at First Ply Failure (FPF)

TYPE	LAY-UP	FPF STRENGTH (ksi)	FPF STRAIN %
N	$[90_6]_s$	11.1 ± 1.1	$.77 \pm .05$
A	$[0/90_4]_s$	14.5 ± 3.8	$.30 \pm .08$
B	$[0/90_3]_s$	19.0 ± 1.1	$.31 \pm .01$
C	$[0/90_2]_s$	44.1 ± 8.0	$.55 \pm .09$
D	$[0/90]_s$	72.9 ± 7.7	$.63 \pm .09$
E	$[0_2/90_2]_s$	64.4 ± 6.5	$.56 \pm .06$
F	$[0/90/0]_s$	101.4 ± 5.6	$.74 \pm .03$
G	$[0/90/0/90]_s$	77.9 ± 2.2	$.69 \pm .02$

unidirectional 90° laminate.

As described previously, a matrix crack is a crack that runs parallel to the fibers in any ply. A transverse crack is a matrix crack in a ply whose fibers are not oriented in a principal loading direction. This was the predominant mode of damage, as should be expected for cross-ply laminates. Of significant importance was the observation of two different types of transverse cracks. These will be referred to as "straight" cracks and "angle" cracks. A description follows.

Figure 18 shows a typical transverse crack in a group of 90° plies. As a rule, this type of crack was continuous across the width of a specimen and grew in a self-similar manner through the thickness of the 90° plies. As seen in an edge replica, the crack generally passed around fibers in its path and extended into the resin rich region at the 0°/90° ply interfaces. The crack extended from interface to interface, nearly perpendicular to the plane of the laminae. It rarely deviated from this course more than 3 or 4 fiber diameters. When the front surface of the specimen was viewed in an X-ray radiograph, the transverse crack appeared as a sharp, well defined line running across the specimen width from edge to edge. A transverse crack of this type was labeled as a "straight crack." This type of crack was found in all cross-ply laminates and was the exclusive type found in laminates

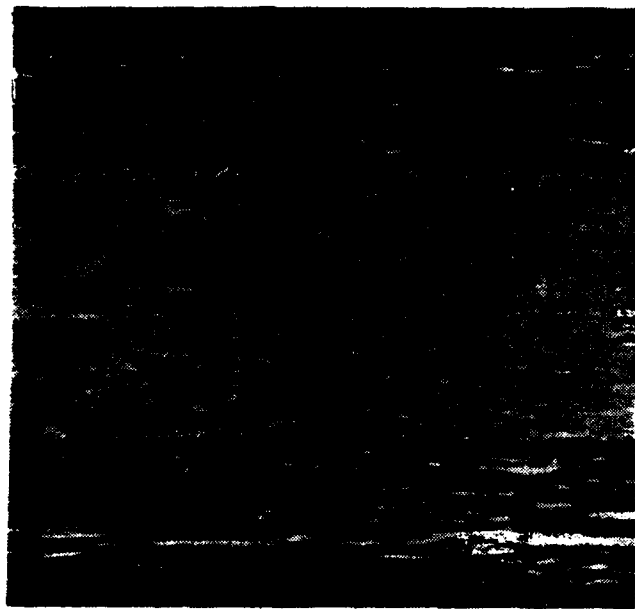


Figure 18. Edge replica of a typical straight crack in a $[0_2/90_2]_s$ laminate

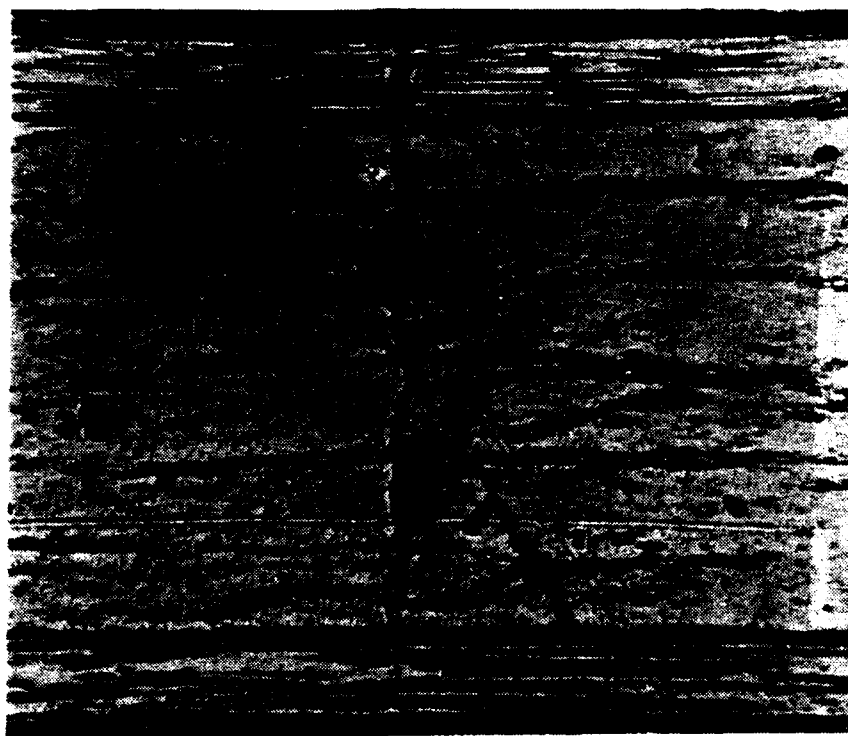
that had groups of 90° plies of less than two.

The second kind of transverse crack was called an "angle" crack. Several features distinguished this type of crack from a straight crack. The most obvious of these is its shape as seen on an edge replica. As the name implies, the crack propagates at an angle to the straight crack from a $0^\circ/90^\circ$ interface. One form of the angle crack is a partial crack which does not span the full thickness of a group of 90° plies. A "curved" crack is an extension of the angle crack in which cracks from the two interfaces meet at some point in the interior of the 90° group. An example of a partial crack (a) and a curved crack (b) are shown in Figure 19.

When viewed closely in an X-ray radiograph, an angle crack can be easily distinguished from a straight crack. When the crack is tilted in relation to the X-ray beam it presents a greater projected area but is less effective in absorbing the radiation. As a result, the angle crack appears as a fuzzy band traversing the specimen while a straight crack appears as a sharp fine line (Figure 20).

Figure 21 establishes a coordinate system to describe the angle crack phenomenon. As seen from the edge, the specimen is laying on its front surface and a straight crack is parallel to the z-axis and is assigned an angle of 0° . Rotation clockwise from the z-axis is positive and counterclockwise is negative. All crack angles are

(a)



(b)

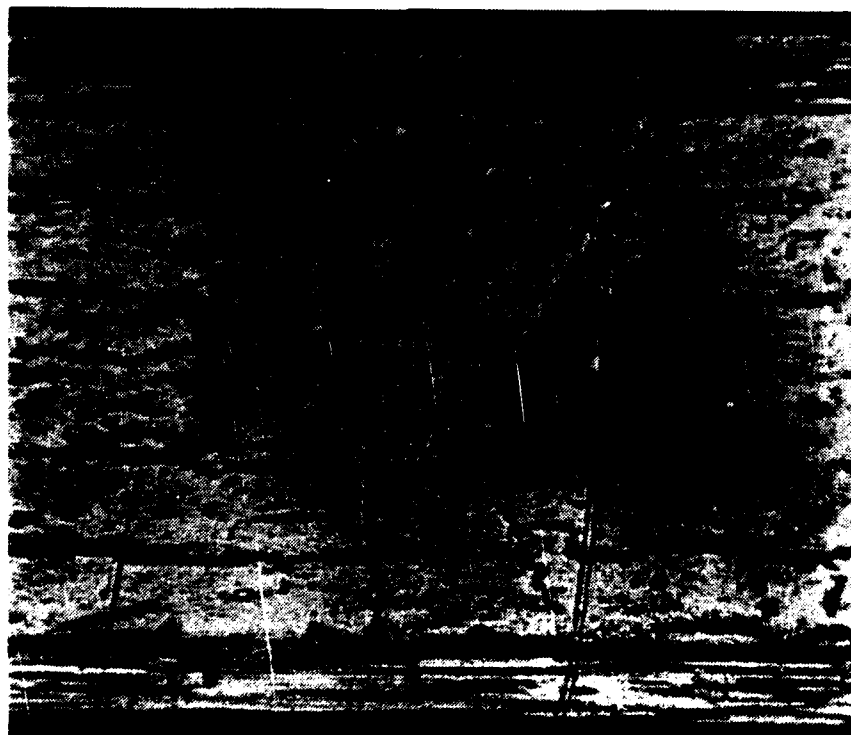
 $\phi = 0.007''$ $\phi_{max} = 0.016''$

Figure 19. Edge replicas of angle cracks;
(a) partial crack, (b) curved crack

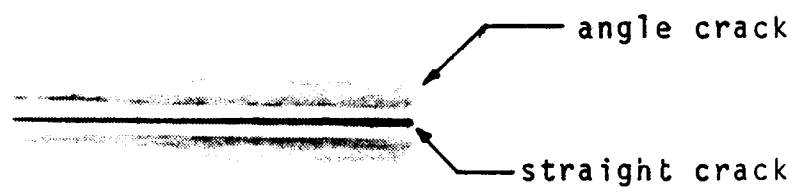


Figure 20. Detail of a radiograph showing the difference between straight and angle cracks

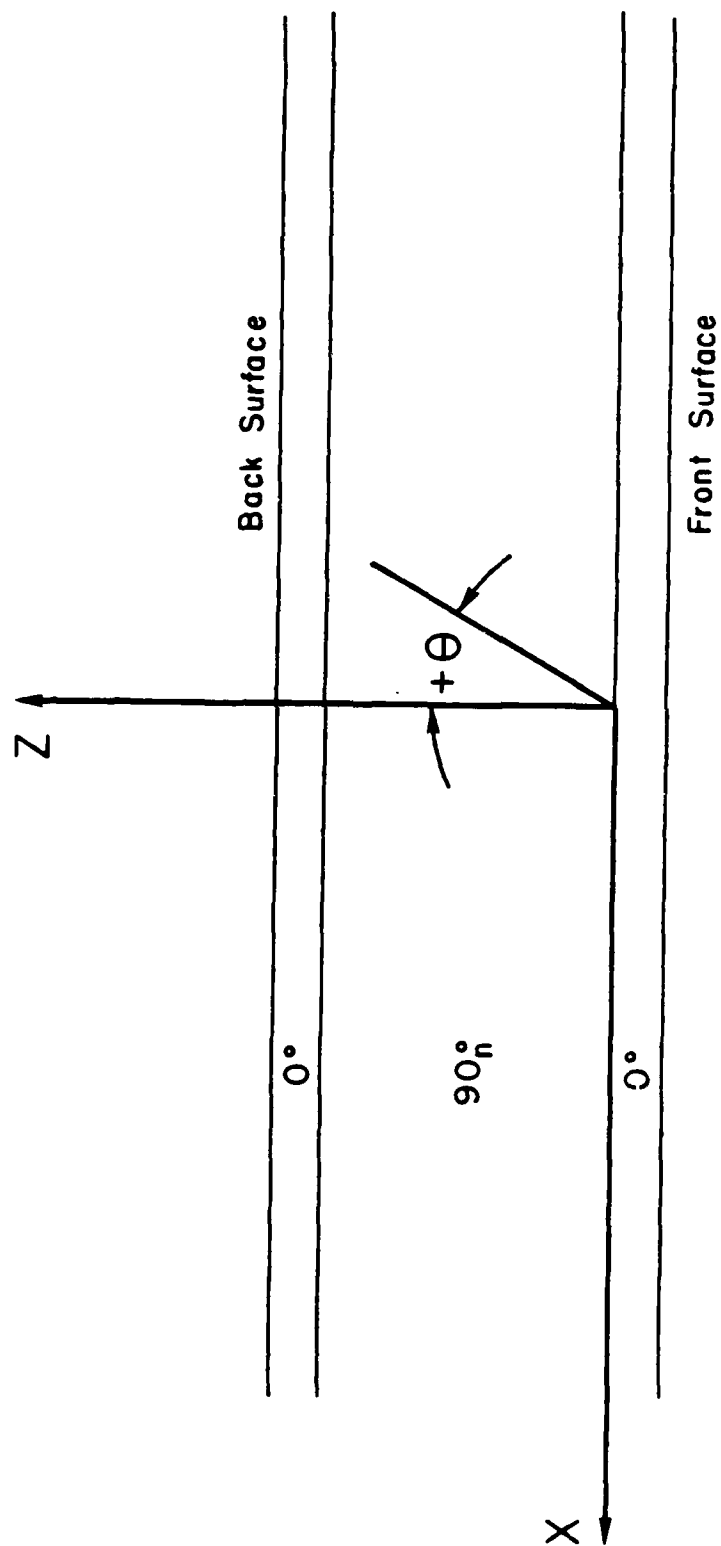


Figure 21. Coordinate system used to document crack angles

between -90° and $+90^\circ$. The curved crack could grow from 4 to 30 fiber diameters in the x-direction, depending on the initial angle and the thickness of the 90° layer. A single ply thickness has between 18 and 22 fiber diameters through the thickness.

Another characteristic of the angle crack is its proximity to a straight crack. There was not a single incidence of a curved or partial crack forming as an isolated crack. They always formed relatively close to a straight crack or another angle crack. From observation, it was found that the following rule applied. The ratio of the thickness of the 90° layer to the distance between two cracks was generally less than 1.0 for a straight and curved crack. However, the ratio was usually greater than 1.5 between two straight cracks or two groups of cracks.

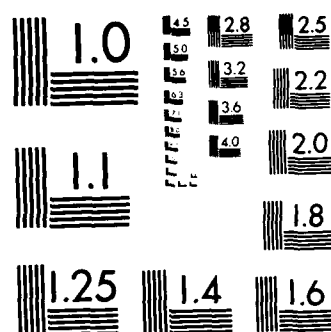
As can be seen in Figure 19, these cracks also grow toward the straight crack. In the case of a curved crack, the convex side always faced toward the straight crack. It was not uncommon for several curved cracks to nest together; all associated with one straight crack (Figure 22). This observation prompts the definition of a "crack family." A crack family is a group consisting of two or more cracks, where one and only one can be considered a straight crack. Figure 23 shows an example of several of these groups.

RESEARCH ON DAMAGE MODELS FOR CONTINUOUS FIBER
COMPOSITES(U) TEXAS A AND M UNIV COLLEGE STATION
MECHANICS AND MATERIALS CE D H ALLEN ET AL FEB 86

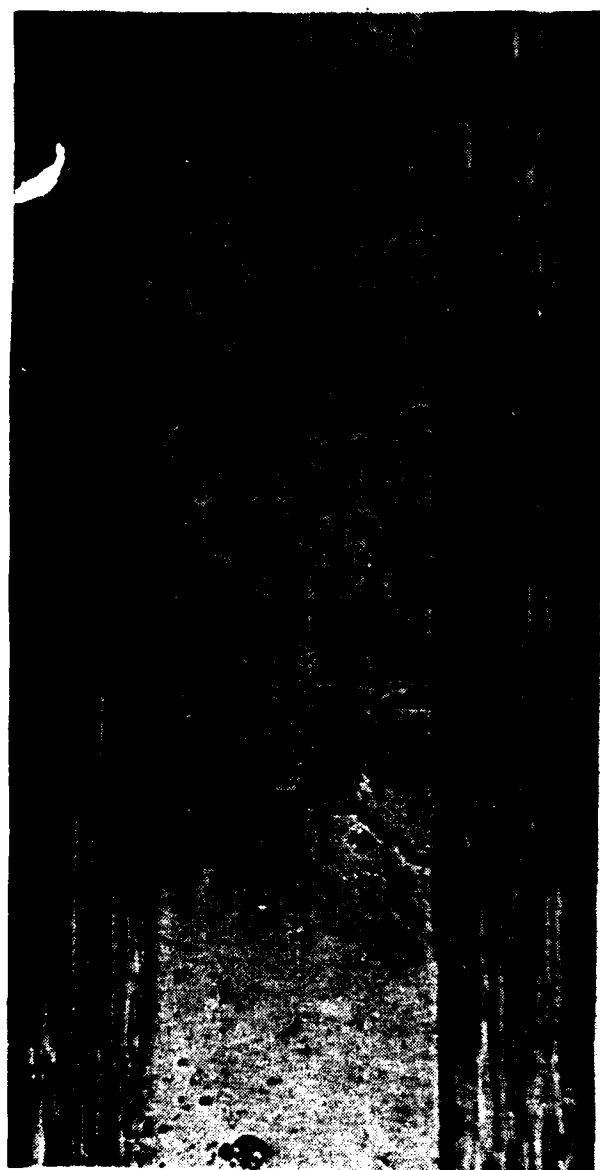
NI

UNCLASSIFIED

MM-5023-86-5 AFOSR-TR-86-2077 AFOSR-84-0067 F/G 11/4



MICROCOPY RESOLUTION TEST CHART
NATIONAL BUREAU OF STANDARDS-1963-A



$d_{min} \approx 0.0086''$

Figure 22. Edge replica of $[0_2/90_2]_3$ laminate showing nested curved cracks



Figure 23. Edge replica of a $[0/90_s]$ laminate showing crack groups or families

In the $[0/90_2]_s$ and $[0/90_3]_s$ laminates, some delamination at the $0^\circ/90^\circ$ interface did occur. The delaminations propagated from the point where an angle crack met the 0° ply (Figure 24). A delamination was never observed to originate from a straight crack.

The process by which the transverse crack density (number of cracks per unit length) increases has been explained as a shear-lag effect. That is, after an initial transverse crack forms, the stress field in the surrounding area is relieved. Moving away from the crack in the load direction, the load carried by 0° plies is redistributed into the 90° layers through shear. The stress field then approaches that of an undamaged laminate at some finite distance from the crack. At this point another crack may form. This explanation does not account for the formation of angle cracks near straight cracks. Obviously another damage mechanism is driving the growth of these cracks.

By comparing two laminates with similar geometry but different damage modes, some possible explanations can be attempted. Laminate theory predicts that a $[0/90]_s$ and $[0_2/90_2]_s$ will have identical mechanical behavior. One is a scaled version of the other. In reality, the larger laminate developed a complex pattern of curved, partial, and straight cracks, while the thinner laminate developed a dense, evenly spaced pattern of straight cracks. Some



Figure 24. Microphotograph of delamination propagating from an angle crack at the $0^\circ/90^\circ$ interface of a $[0/90,]_s$ laminate

alteration of the stress field must be involved in the scaling process. By examining the factors which are not scaled, an explanation may be found. Several features do not change from one laminate to another. Fiber diameter and ply thickness remain the same. The resin rich region at a $0^\circ/90^\circ$ is also nearly the same. Recent work [23] indicates that the resin rich area is responsible for most of the load transfer from the 0° plies to the 90° plies. When the laminate is scaled up, the constant thickness resin rich region must transmit a correspondingly larger load. This coupled with a stress concentration near a straight transverse crack could possibly cause initiation of an angled crack.

Figure 25 demonstrates the relationship between the number of straight and curved cracks with increasing stress for a $[0_2/90_2]_S$ laminate. As expected, the total number of cracks increased with each additional increase in stress. Initially, the only cracks present are straight. Curved cracks begin forming at higher levels of stress. Note that as the ultimate stress is approached, the straight cracks practically cease to form while the curved cracks are actively increasing. The saturation of straight cracks may correspond to a characteristic damage state. In some specimens it appears that the straight cracks have a consistent and regular spacing.

The belief that the typical straight transverse crack

SPECIMEN E-9 [0/0/90/90]_s

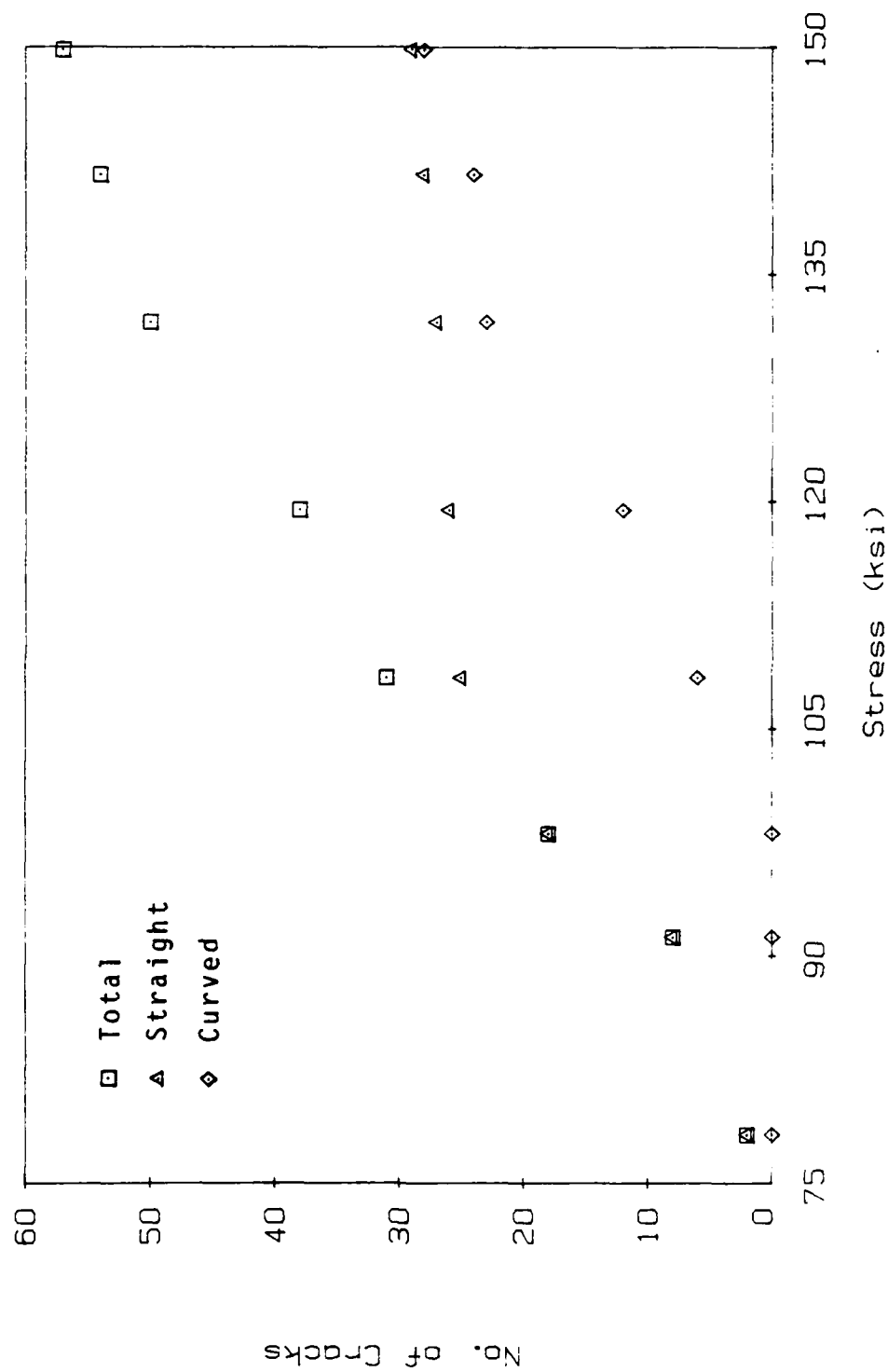


Figure 25. Crack development by type for [0₂/90₂]_s laminate

propagates in a rapid, unstable fashion is widely accepted. This is supported by the fact that a partially formed crack is rarely found. In laminates with large groups of 90° plies, the formation of a transverse crack in the extensometer gage length causes a clear discontinuity in the stress-strain curve. This phenomenon would support the idea of unstable crack growth. The clear, distinct pop that is heard when the crack forms would also indicate an almost instantaneous crack propagation.

This is not the case with angle cracks. At stress levels where angle cracks form, the familiar popping sound becomes less distinct and begins to sound more like a tear than a pop. This phenomenon, along with the observation of partial cracks, indicates that the fracture process is considerably slower.

Although it is not clear at what point a straight crack initiates, this is not the case for an angle crack. The evidence presented indicates that the angle crack initiates at the $0^\circ/90^\circ$ interface. Figures 26 through 29 are a sequence of edge replicas at increasing load levels. The curved crack is formed by the merging of two partial cracks growing from opposite ply interfaces. Figure 30 shows the result of two partial cracks "overshooting" one another. A partial crack from one interface has intercepted a partial crack growing from the opposite interface at a point behind the original crack tip.

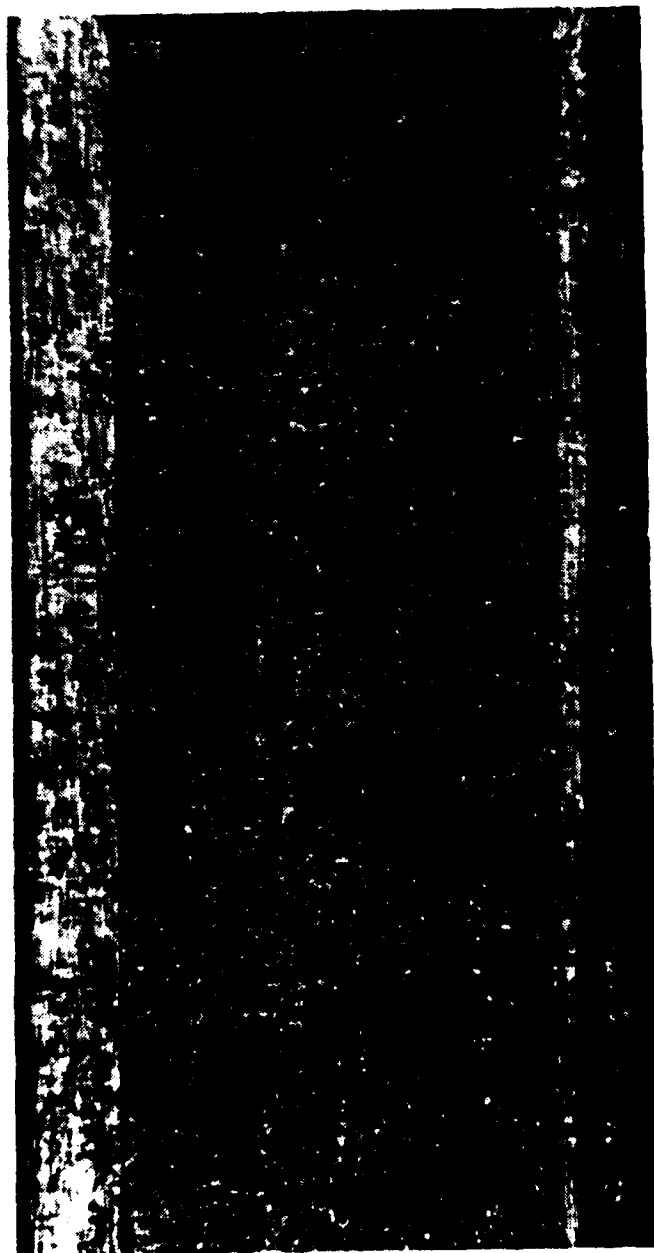


Figure 26. Edge replica of $[0/90,]_s$ laminate showing development of a curved crack, $63\% F_{tu}$

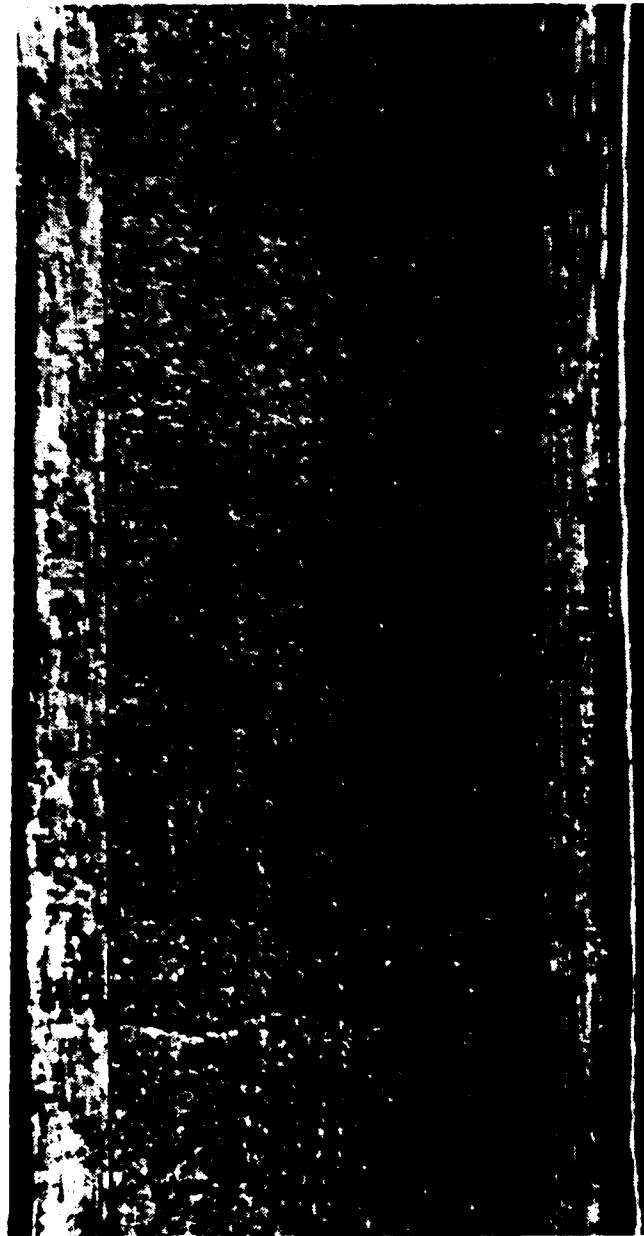
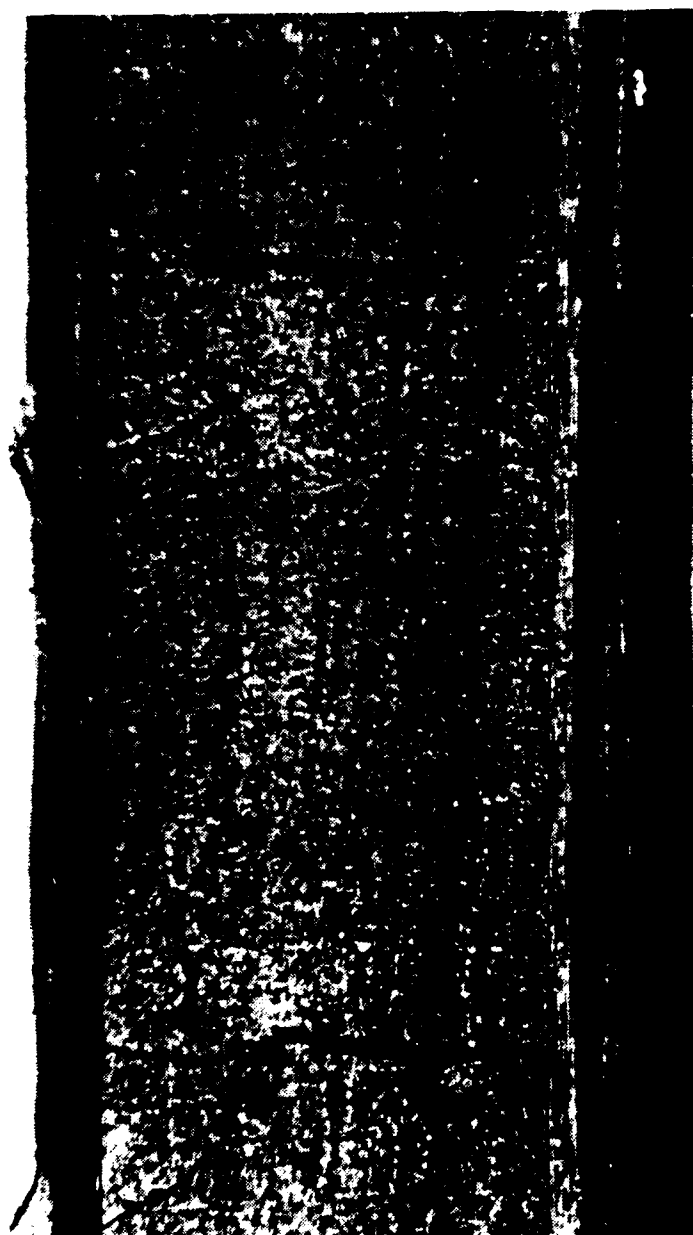


Figure 27. Edge replica of $[0/90_s]$ laminate showing development of a curved crack, $69\% F_{tu}$



$d = 0.0061"$

Figure 28. Edge replica of $[0/90_3]$ laminate showing development of a curved crack, 81% F_{tu}

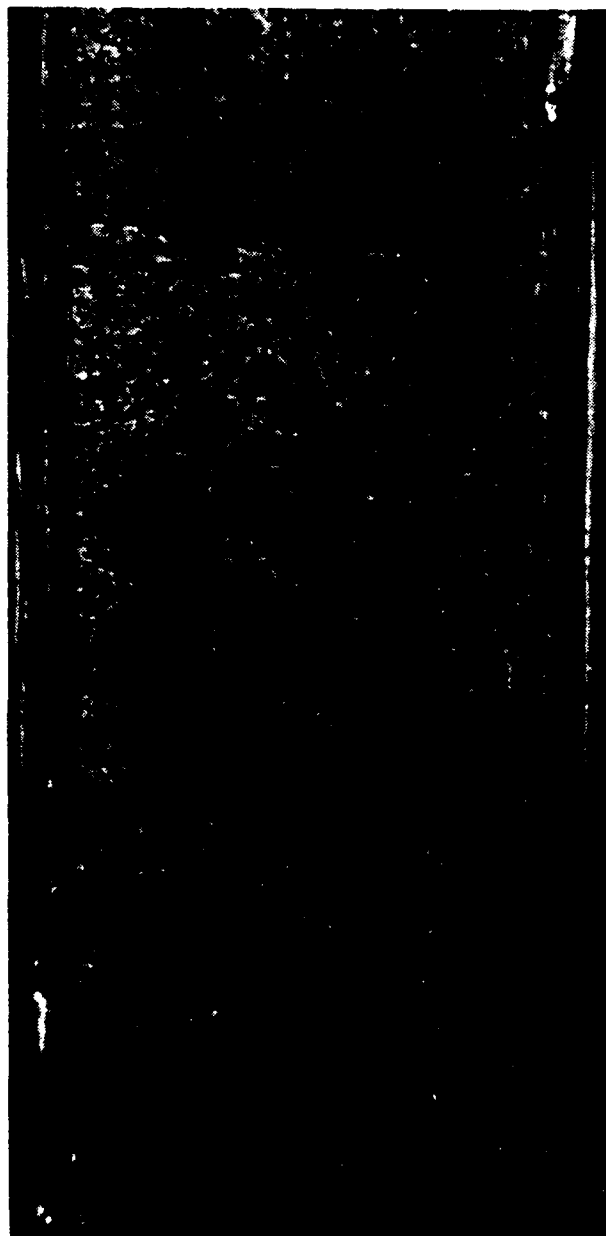
$d = 0.0053''$ 

Figure 29. Edge replica of $[0/90,]_s$ laminate showing development of a curved crack, 94% F_{tu}

 $d = 6.0063$

Figure 30. Edge replica of two intersecting partial cracks

Several other forms of minor damage were observed. In some instances, a transverse crack would fracture a fiber lengthwise rather than propagate in the matrix around the fiber. Figure 31 shows an example of this. Sectioning along the specimen length might reveal the extent of fiber splitting. Fiber fracture could sometimes be seen at the edge of the specimen in the 0° plies. These breaks were typically near the $0^\circ/90^\circ$ interface and adjacent to termination point of straight transverse cracks. The fiber breaks were not generally associated with angle cracks. Figure 32 shows a detail of a typical fiber break zone. This phenomenon was not monitored closely and the effect on stiffness measurements is not known. Obviously, another destructive evaluation technique, may be used to find the extent of fiber fracture across the width of the specimens. Fiber breaks and fiber splits were found in all the laminates tested.

In the $[0/90_2]_3$ and $[0_2/90_2]_3$ laminates, a different type of crack pattern was observed on the edges of the specimens. This phenomenon was termed "crack branching." An example is shown in Figure 33. This occurred at the point where a transverse crack met the $0^\circ/90^\circ$ interface and was in the laminate plane. The branches grew from both angle cracks and straight cracks. Branches were seen at the crack tip of every transverse crack. These branches appeared to be delaminations; although, a close

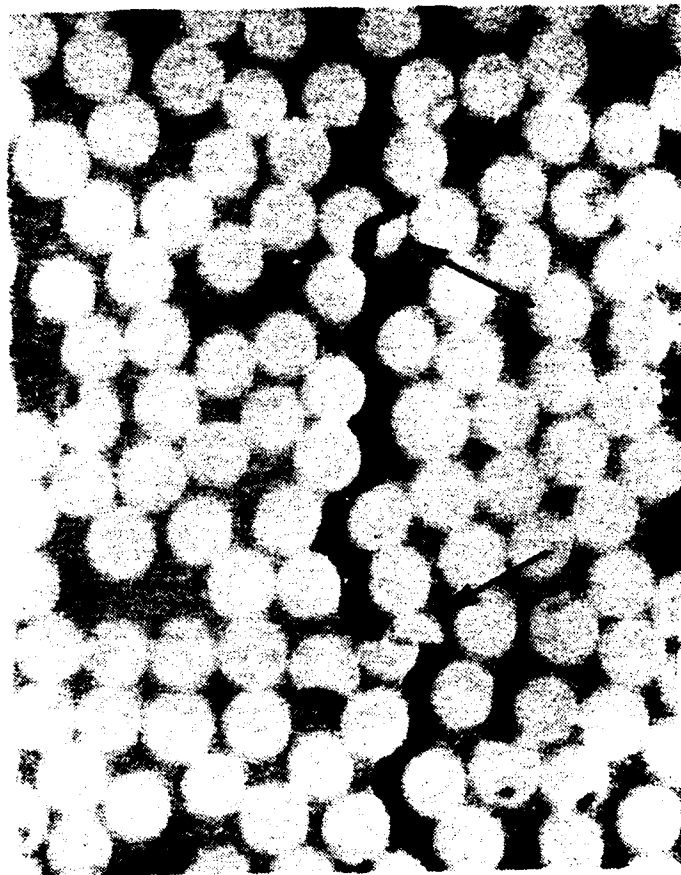


Figure 31. Lengthwise fracture of transverse fibers

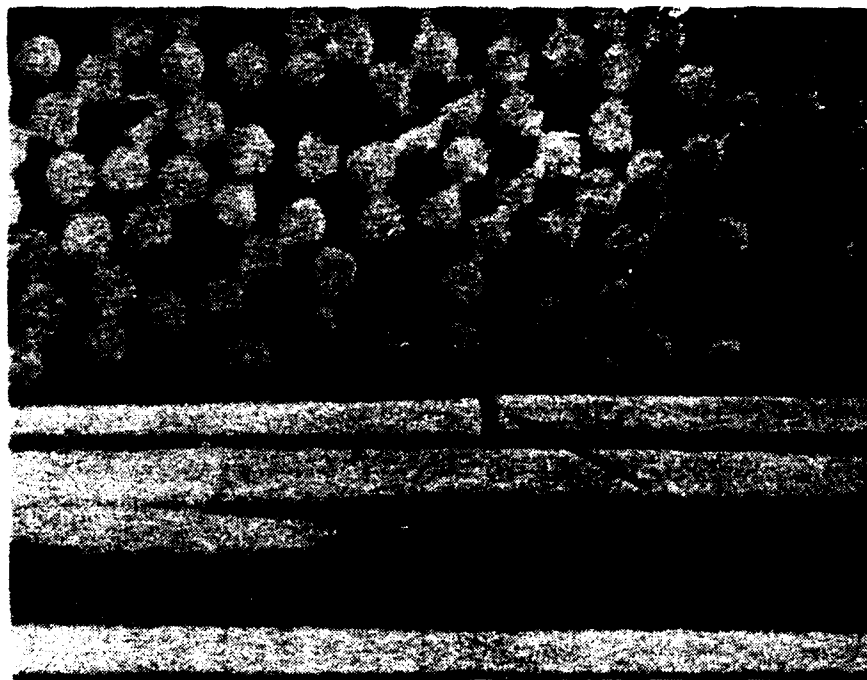


Figure 32. Fiber fracture in 0° ply near transverse crack



Figure 33. Example of crack branching from transverse crack at 0°/90° interface

inspection of the radiograph revealed no evidence of delaminations. Unlike a delamination, which develops as a separate form of damage, these branches formed as an integral part of the transverse cracks. The crack opening, as seen at the edge, is less than half that of the transverse crack. Because nothing can be seen in the radiograph, the distance that these branches extend into the width of the specimen is unknown. It is possible that this form of damage is restricted to the edge. Longitudinal sectioning of the specimen may further explain these cracks.

Type A [0/90_s]

This laminate type had the largest grouping of 90° plies. As a result, a very complex damage pattern developed. Although the damage mode of interest was matrix cracking, the chief form of damage which developed was delamination. The X-ray radiographs in Figure 34 show the incremental growth of the damage. Straight cracks, angle cracks, longitudinal splits, and delaminations can all be seen in these radiographs.

Initial transverse cracking was sporadic. No pattern in the spacing developed. In most cases, the crack pattern which developed in the gage length beneath the extensometer was not representative of the damage elsewhere in the specimen.

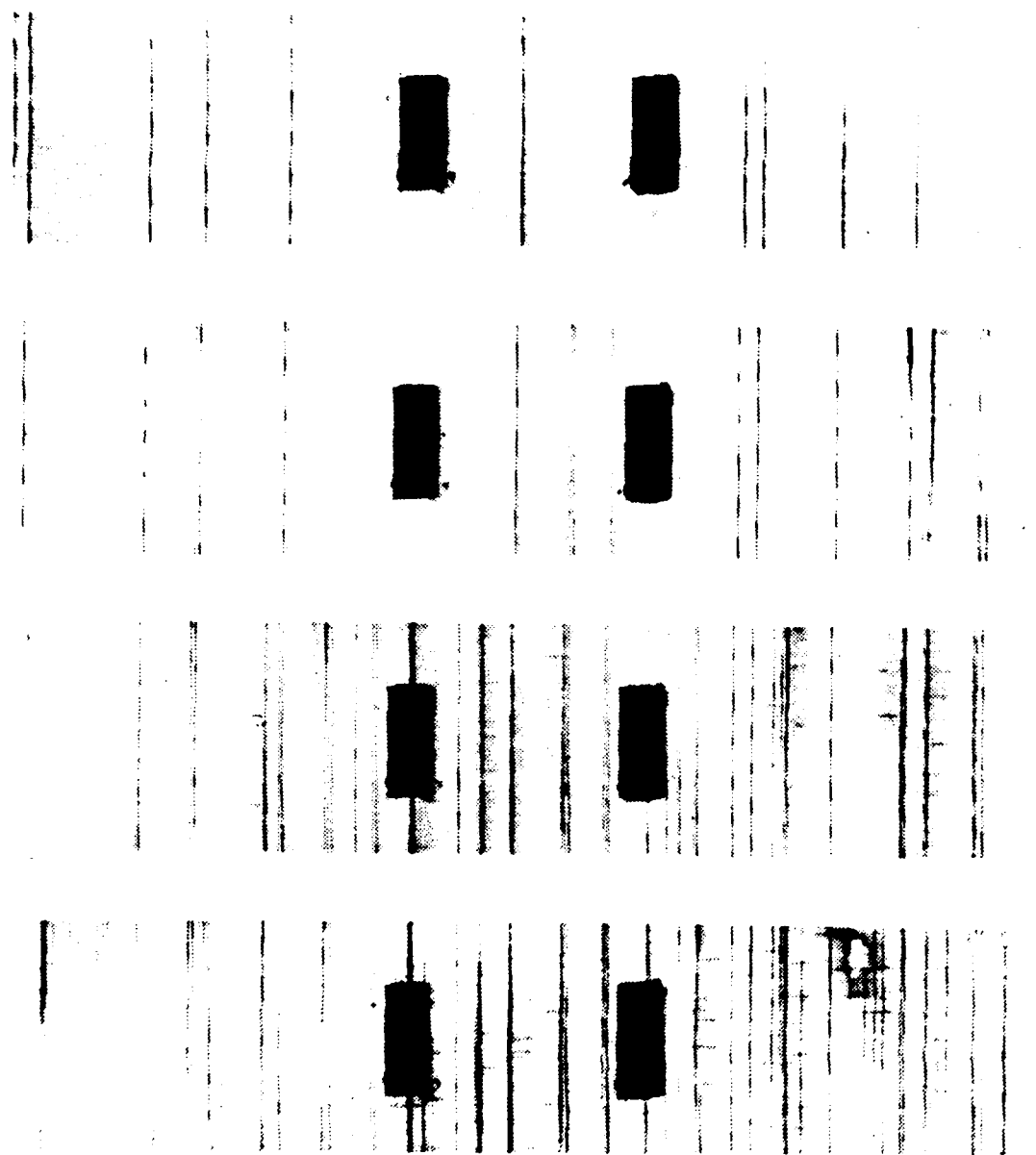


Figure 34. X-ray radiographs for a progressively loaded $[0/90_4]_s$ laminate (dark rectangles are aluminum extensometer mounting tabs)

This laminate was susceptible to angle cracks. Straight cracks stopped forming at a relatively low stress level and a rapid increase in angle cracks followed. The cracks were counted at each loadstep and the number of cracks formed were plotted against their respective stress levels. Figure 35 shows that the angle cracks far outnumber the straight cracks, near failure. Large groups of angle cracks developed throughout the specimen.

Delaminations grew readily in this laminate. A delamination originated at the free edge and propagated along the length and width in the plane of the laminate. A delamination formed at the edge soon after an angle crack formed. The delaminations then propagated as narrow bands across the width of the specimen. These bands can easily be seen in Figure 34. A typical delamination originated at the edge of the specimen and at the tip of angle crack. The cause of the delaminations is not clear. The possible causes could be interlaminar stress at the edge or the localized stress field at the matrix crack tip. The direction of growth along the length of the specimen was always away from the angle crack group. An example is shown in Figure 36.

The last radiograph in Figure 34 indicates the widespread delaminations in this laminate. A radiograph does not show the depth at which the delaminations are located. In fact, the delaminations generally form in an alternat-

SPECIMEN A-10 [0/90/90/90/90]_s

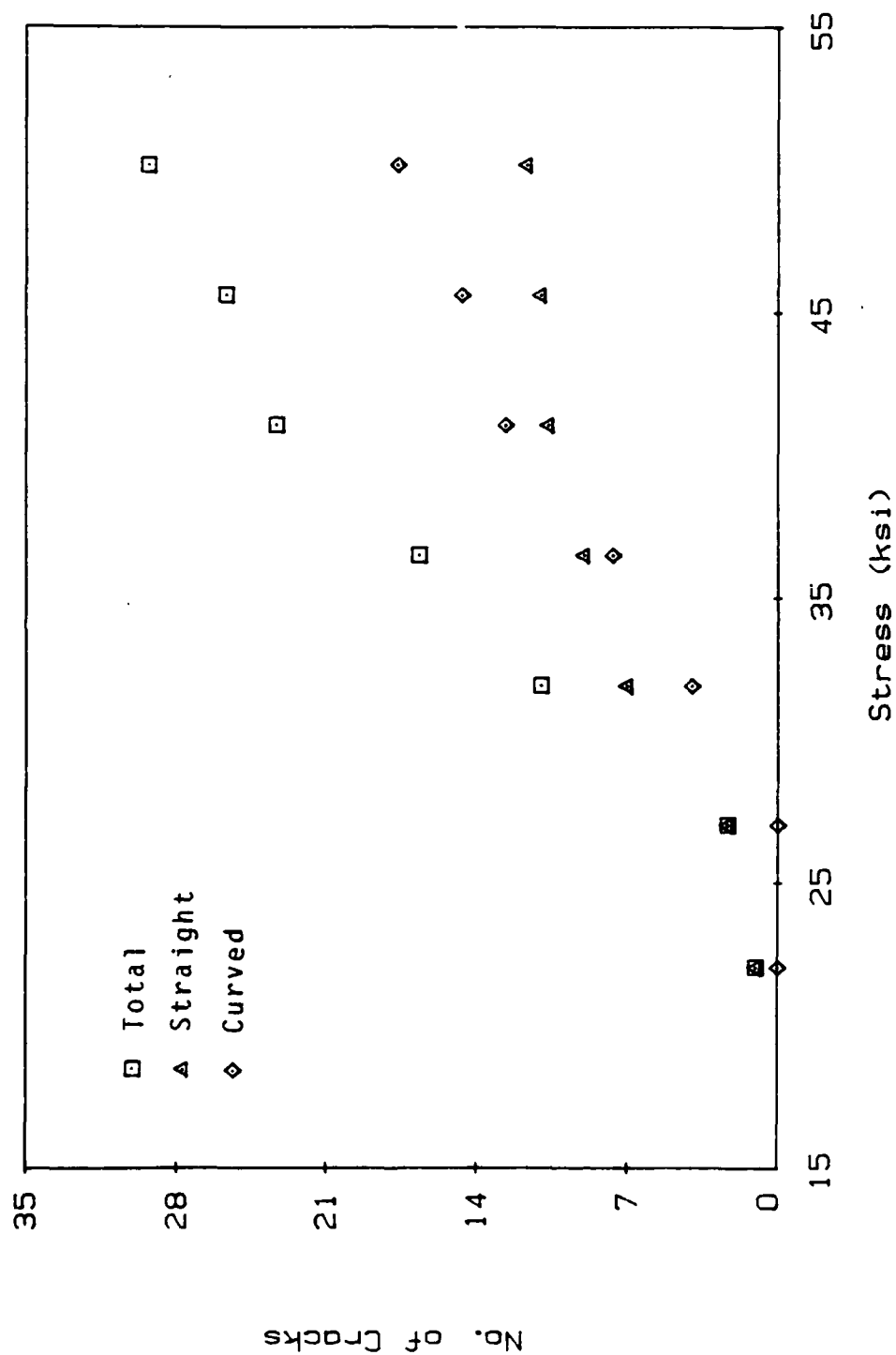


Figure 35. Crack development by type for [0/90_s]_s laminate

$$d_1 = 0.0084''$$
$$d_2 = 0.0116''$$

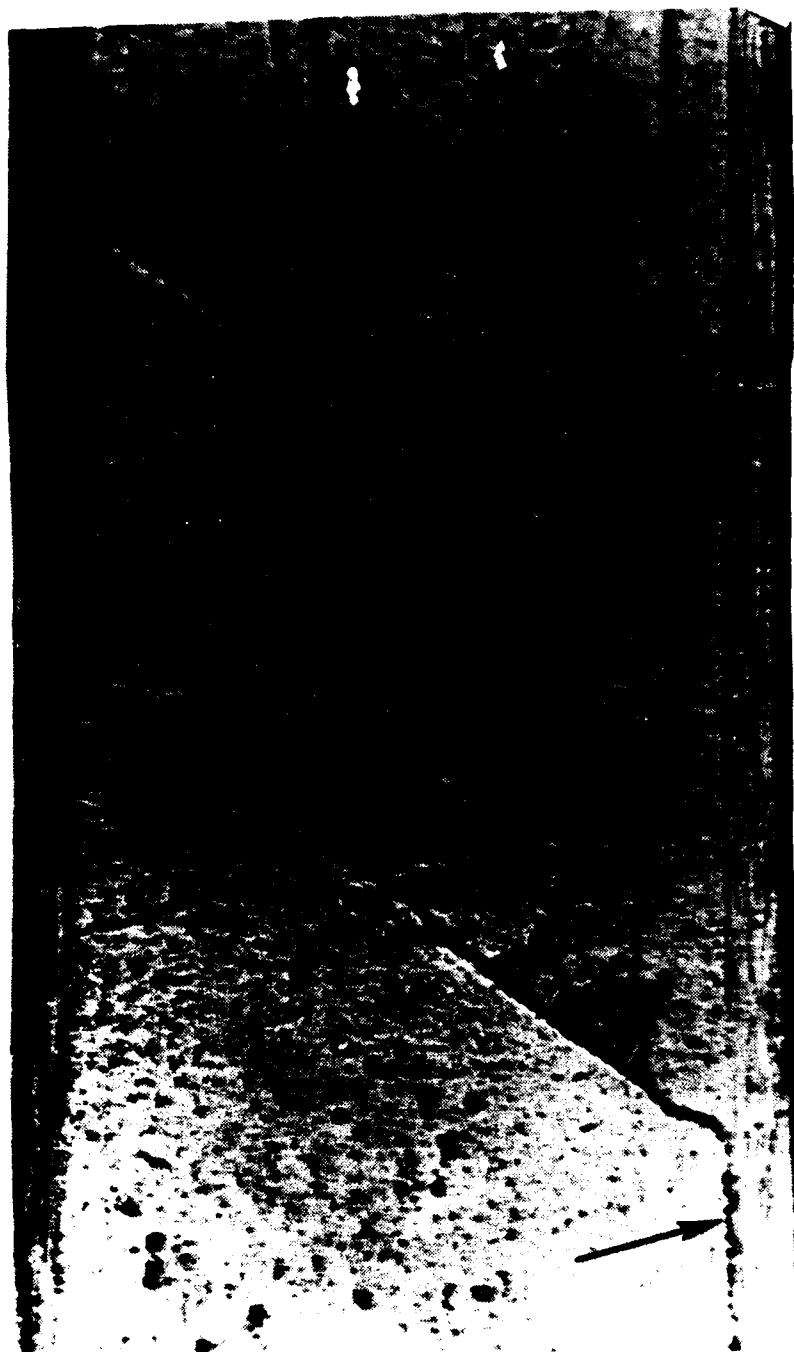


Figure 36. Edge replica of $[0/90_4]_s$ laminate with delaminations growing from both curved cracks

ing pattern along the length of the specimen. What appears to be side by side delaminations in the radiograph are actually at opposite $0^{\circ}/90^{\circ}$ interfaces. This pattern was verified by examining the edge replica.

Longitudinal splits also formed throughout this laminate. These splits were found only in areas of delaminations. No split was seen crossing a transverse crack in an adjacent ply except when a transverse crack formed after the split. A split appeared in the 0° ply over a delamination area and did not extend beyond this boundary. No split was seen without an accompanying delamination zone. Sufficient evidence was not found to conclude that the delaminations initiated at the intersection of a transverse crack and a longitudinal split. There is, however, evidence that some longitudinal splits formed after the growth of a delamination zone. Figure 34 shows the formation of a split over an already existing delamination. In this case, the delaminations may drive the growth of the longitudinal splits.

Just prior to ultimate failure, this laminate incurred as much as a 15% reduction in stiffness. This reduction was a result of all the damage modes described above. Figure 37 graphically represents the stiffness reduction as a function of stress level. The sharp decrease in the stiffness occurred at the stress at which delaminations appeared.

SPECIMEN A-4 [0/90/90/90/90]_s

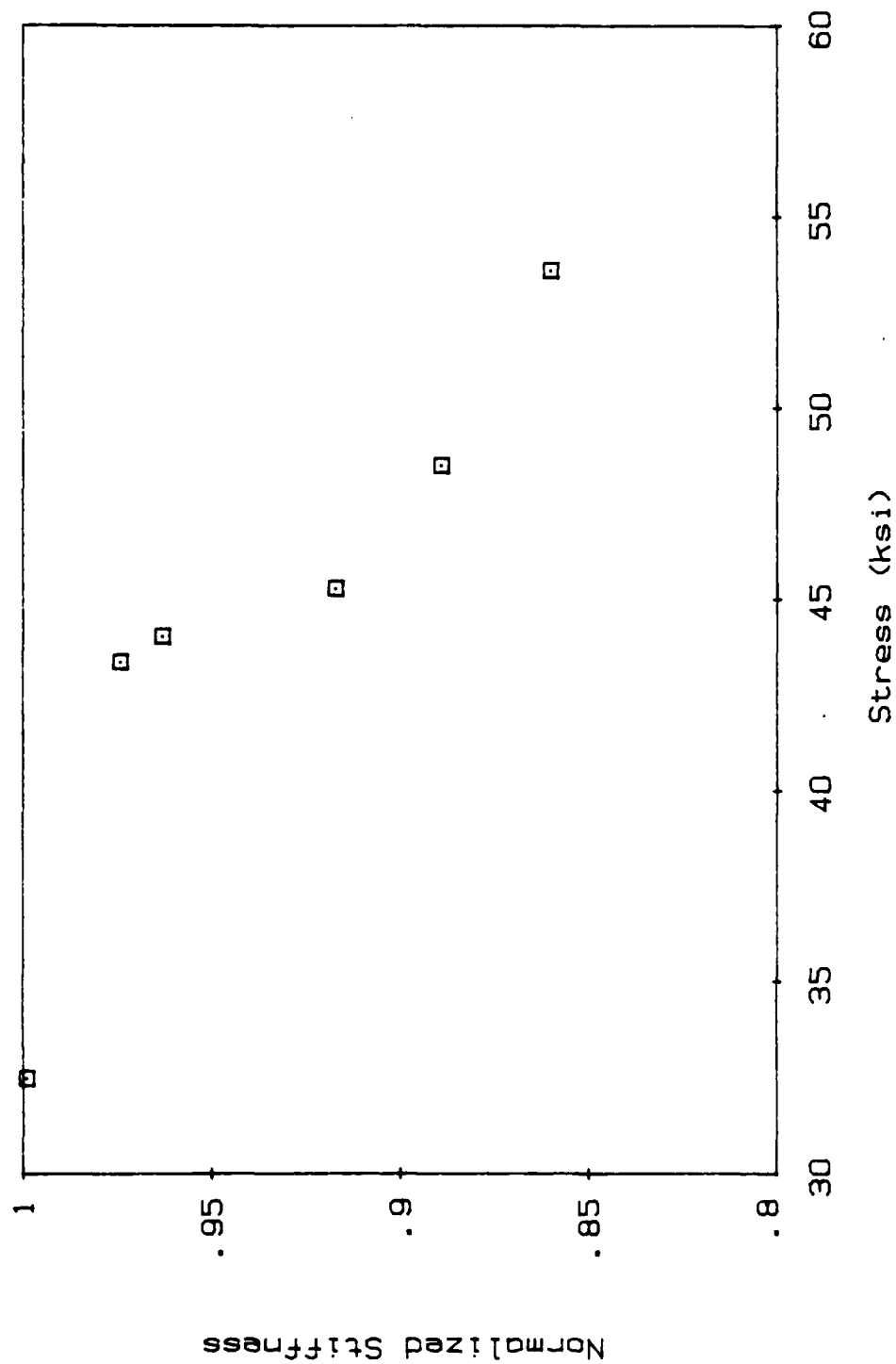


Figure 37. Stiffness reduction for a [0/90₄]_s laminate

Since the measurement of crack surface area was performed only for matrix cracks, a correlation between the total surface area (including delaminations) and the stiffness reduction was not made. Figure 38 does show this correlation prior to the formation of delaminations in the gage length. The crack lengths and angles at which the transverse cracks grew are listed in Table 6.

Type B [0/90₃]_s

Like the previously described laminate, the [0/90₃]_s also developed some edge delaminations, although not on such a large scale. Typically three or four edge delaminations appeared within the full length of the specimen. The series of radiographs in Figure 39 shows the progression of damage with increased load. As was the case with the [0/90₃] laminate, the damage in the gage length was not necessarily representative of damage growth elsewhere in the laminate.

This laminate developed some longitudinal splits in areas other than over delamination zones. These splits were found in groups of three to five, along individual transverse cracks. These splits were limited in size to approximately .025 inches long. Unlike the longitudinal splits associated with edge delaminations, these splits could be found bisecting single straight transverse cracks, rather than just growing from one side of a curved

SPECIMEN A-10 [0/90/90/90/90]_s

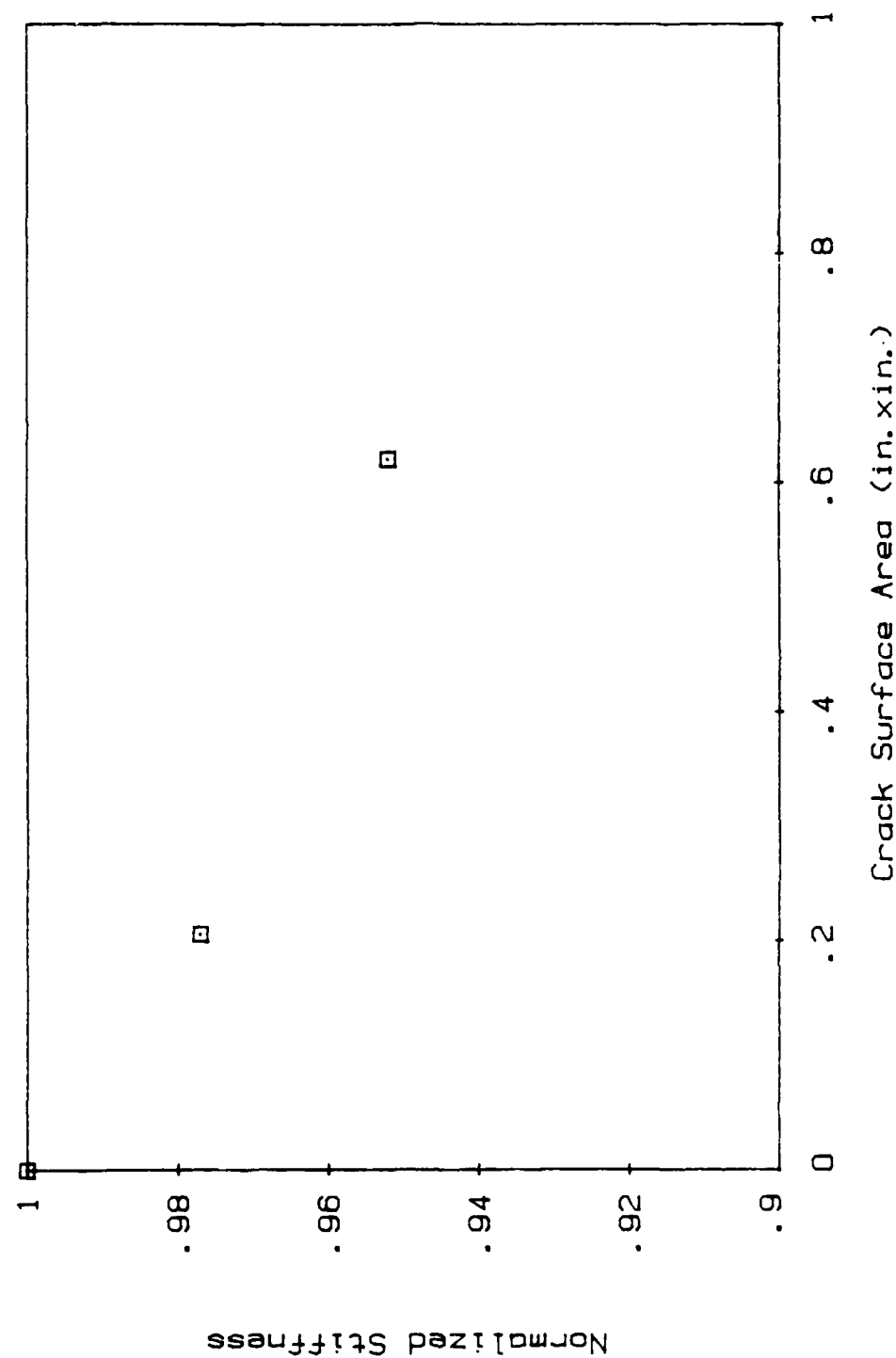


Figure 38. Measured stiffness loss as a function of crack surface area for a [0/90₄]_s laminate

Table 6. Crack Angle and Length Distribution in
Specimen A-4, $[0/90_4]_s$, 98% F_{tu}

Length of cracks (L) in inches ¹										
Angle $\pm\theta$	1st ply	2nd ply	3rd ply	4th ply	5th ply	6th ply	7th ply	8th ply	$\cos\theta$ x L	$\sin\theta$ x L
0	.0132	.0155	.0163	.0240	.0211	.0123	.0126	.0112	.1262	.0
5	.0022	.0022	.0	.0	.0	.0	.0	.0	.0044	.0004
10	.0	.0	.0	.0	.0024	.0045	.0022	.0022	.0111	.0020
15	.0	.0	.0	.0	.0	.0	.0	.0	.0	.0
20	.0	.0	.0049	.0024	.0	.0026	.0024	.0049	.0162	.0059
25	.0	.0	.0	.0	.0	.0028	.0028	.0028	.0076	.0035
30	.0106	.0055	.0053	.0053	.0051	.0051	.0051	.0051	.0408	.0236
35	.0057	.0057	.0047	.0	.0	.0027	.0027	.0	.0176	.0123
40	.0083	.0124	.0081	.0053	.0028	.0028	.0065	.0077	.0413	.0346
45	.0	.0	.0	.0	.0	.0	.0	.0	.0	.0
Total Length	.0400	.0413	.0393	.0370	.0314	.0328	.0343	.0339	.2652	.0823

Area Generated by Transverse Cracking

$$\text{Area} = 2 \times L \times W \quad (W = 1.005 \text{ in.})$$

Total area of all transverse cracks 0.5830 in.²

Projected area perpendicular to laminate plane . . . 0.5331 in.²

Projected area parrallel with laminate plane 0.1654 in.²

¹Each entry is the total length of all cracks
in the gage length at the specified angle.

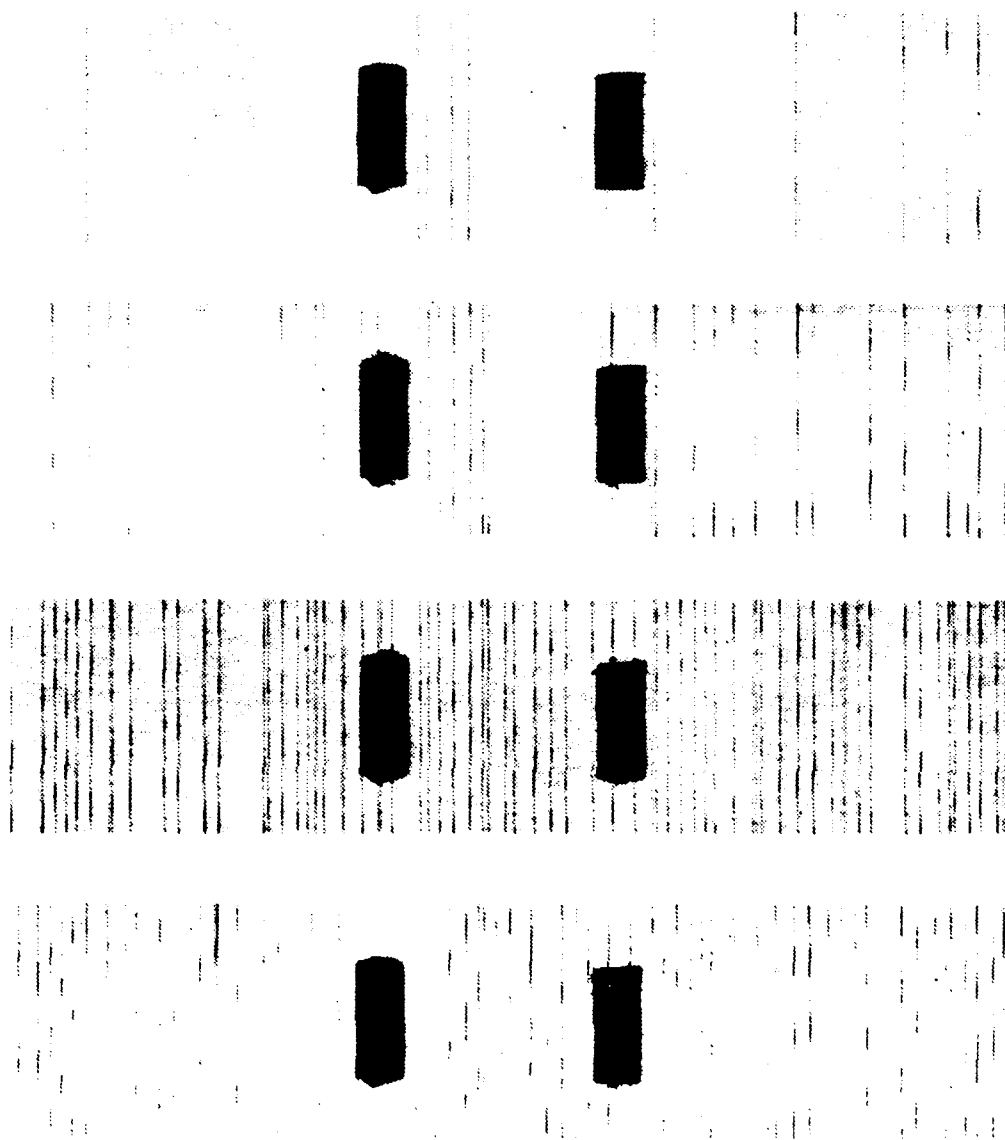


Figure 39. X-ray radiographs for a progressively loaded $[0/90,]_s$ laminate

transverse crack.

A few cases of interlaminar delaminations were found at the intersection of longitudinal splits and transverse cracks. An interlaminar delamination is one which develops in the interior of a laminate with no connection with the free edge. These were extremely small compared to the size of the edge delaminations. Angle cracks constituted more than half of the total number of cracks formed at failure. Figure 40 shows that the straight cracks formed at a steady rate, while curved cracks began forming very rapidly at a higher stress level. Table 7 numerically documents the crack pattern for comparison to stiffness reduction.

Type C [0/90₂]₃

No delaminations or longitudinal splits were generated in this laminate. The transverse cracking pattern was very similar to the [0/90₃]₃ laminate, although the crack spacing was slightly more dense and angle cracks were not as predominant. The radiographs in Figure 41 show the progression of damage with each load step. There seemed to be a more even distribution of transverse cracking along the length of the specimen. Figure 42 shows that at 95% of the ultimate strength, approximately half of the transverse cracks are straight cracks. In this laminate there appears to be a more clearly defined point

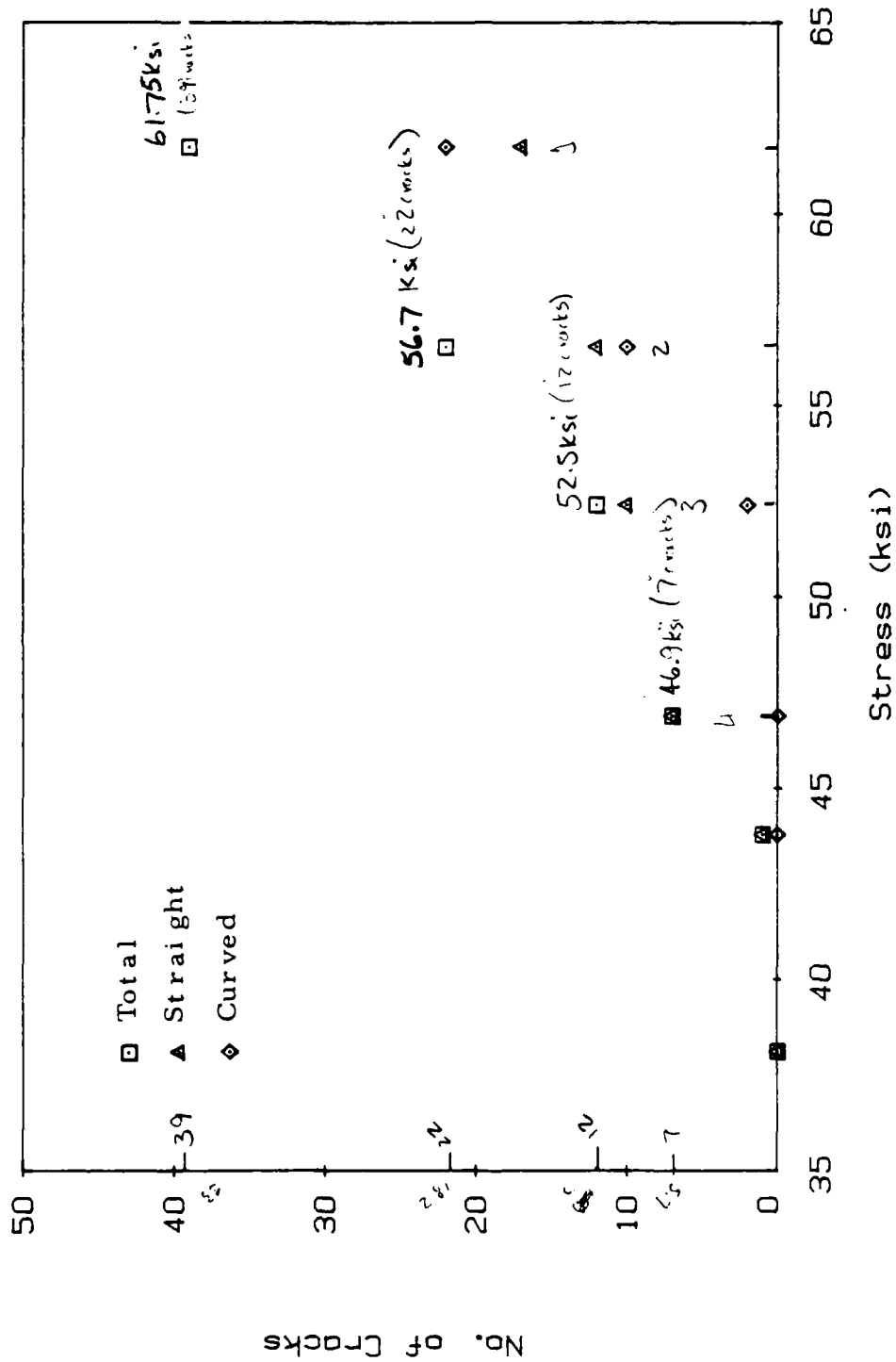


Figure 40. Crack development by type for $[0/90]_s$ laminate

Table 7. Crack Angle and Length Distribution in
Specimen B-5, $[0/90_3]_s$, 94% F_{tu}

Length of cracks (L) in inches ¹								
Angle θ	1st ply	2nd ply	3rd ply	4th ply	5th ply	6th ply	$\cos\theta$ x L	$\cos\theta$ x L
-45	.0	.0	.0	.0	.0	.0	.0	
-40	.0	.0	.0	.0	.0	.0	.0	
-35	.0014	.0	.0	.0010	.0061	.0061	.0120	.0083
-30	.0030	.0	.0	.0	.0029	.0055	.0099	.0057
-25	.0	.0	.0	.0028	.0	.0	.0025	.0012
-20	.0	.0	.0	.0034	.0	.0	.0032	.0012
-15	.0	.0	.0028	.0028	.0028	.0028	.0108	.0029
-10	.0	.0	.0	.0	.0	.0	.0	.0
-5	.0	.0	.0	.0	.0	.0	.0	.0
0	.0884	.0915	.0829	.0825	.0886	.0819	.5158	.0
5	.0	.0	.0	.0	.0	.0	.0	.0
10	.0	.0	.0055	.0	.0028	.0	.0082	.0014
15	.0	.0	.0	.0	.0	.0	.0	.0
20	.0	.0	.0026	.0028	.0028	.0028	.0103	.0038
25	.0	.0	.0	.0	.0	.0	.0	.0
30	.0	.0	.0	.0	.0	.0	.0	.0
35	.0030	.0	.0	.0	.0	.0	.0025	.0017
40	.0	.0	.0	.0	.0	.0	.0	.0
45	.0030	.0	.0	.0	.0	.0	.0	.0
Total	.0948	.0915	.0938	.0953	.1060	.991	.5752	.0262
Length								

Area Generated by Transverse Cracking

$$\text{Area} = 2 \times L \times W \quad (W = 1.005 \text{ in.})$$

Total area of all transverse cracks 1.1662 in.²
 Projected area perpendicular to laminate plane . . . 1.1562 in.²
 Projected area parrallel with laminate plane 0.0527 in.²

¹Each entry is the total length of all cracks
in the gage length at the specified angle.

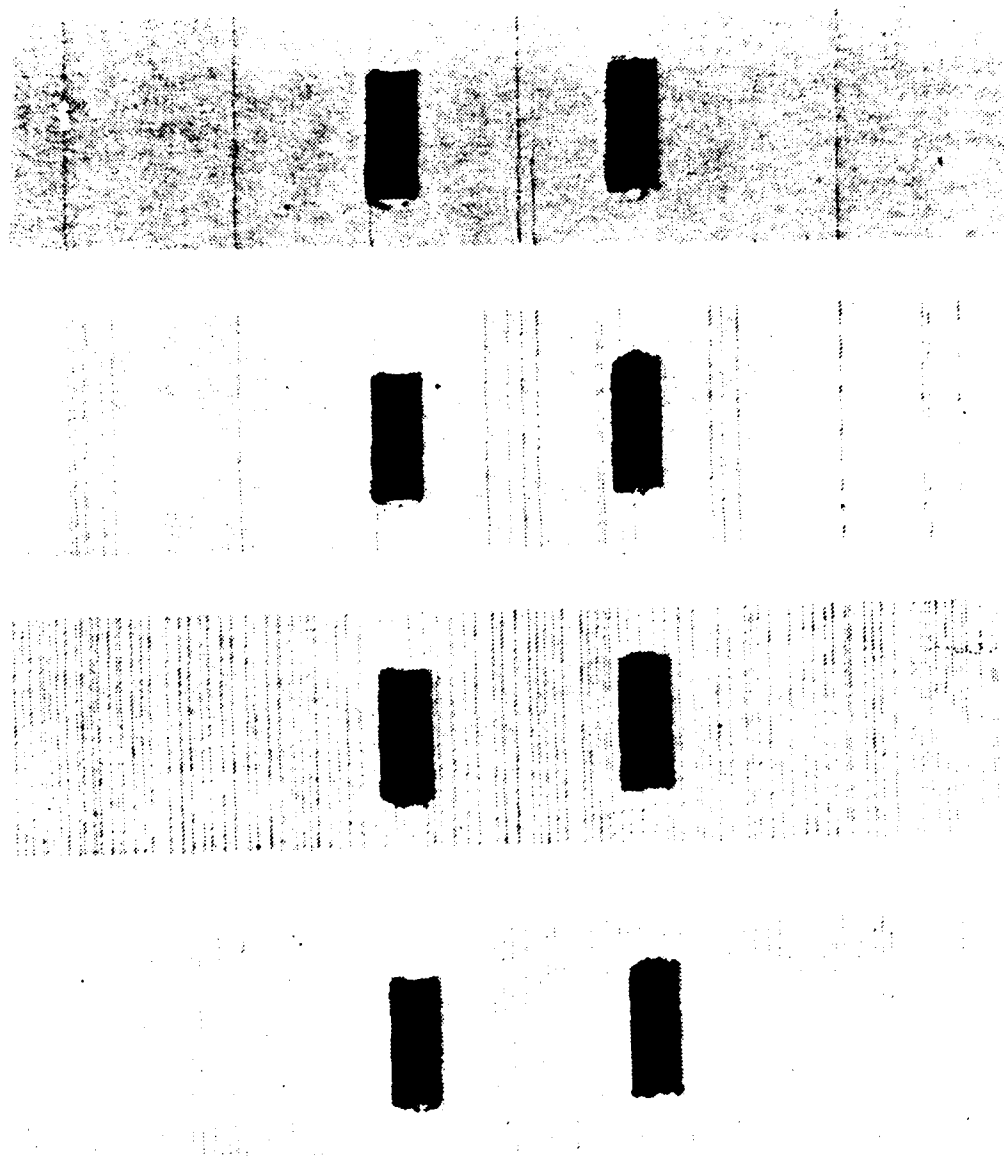
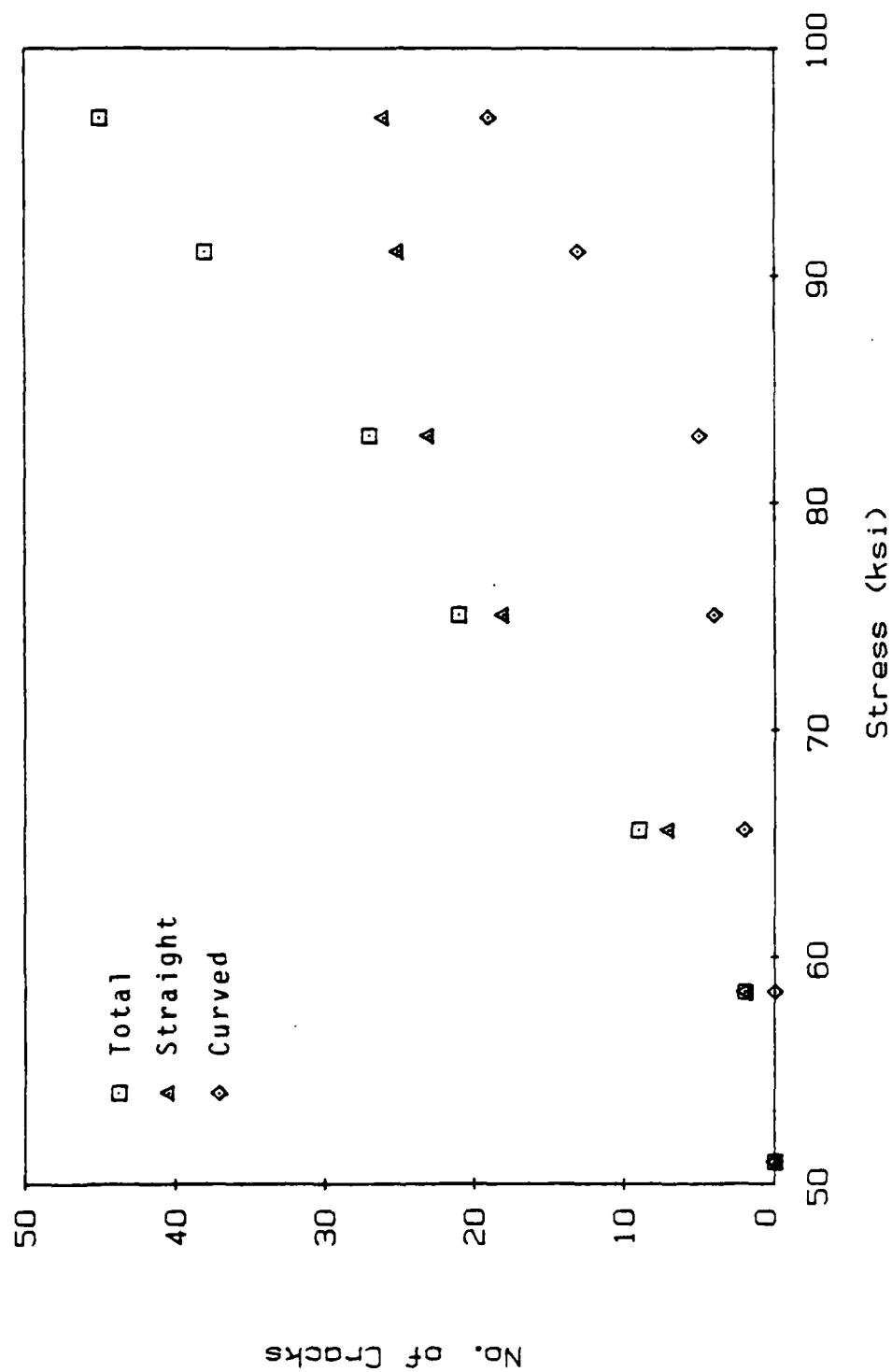


Figure 41. X-ray radiographs for a progressively loaded $[0/90_2]_s$ laminate

SPECIMEN C-8 [0/90/90]_sFigure 42. Crack development by type for [0/90₂]_s laminate

at which straight cracks saturate and curved cracks begin. This laminate showed a transverse crack density of 48 crack per inch at 92% of the ultimate stress. Typically very few of these cracks would be partial cracks. Table 8 was used to determine the surface area generated by transverse cracks.

If the curved and partial cracks were ignored, the straight cracks appeared to show a consistent, even spacing. This would correspond to the saturation of straight cracks seen in Figure 42. This might be considered a characteristic damage state with approximately 29 cracks per inch.

Type D [0/90]_s

This laminate was the most difficult to test. Because it had only four plies, it was susceptible to various gripping and alignment problems. The total stiffness loss at ultimate failure was only three percent.

This laminate developed a very consistent transverse crack spacing. The radiographs in Figure 43 show the evenly distributed crack spacing during each load step. At 93% of the ultimate stress the crack density was about 45 cracks per inch. The spacing averaged .022 inches between transverse cracks. No curved cracks were seen until the last load step, at which time one or two were found. These cracks were located less than .01 inches

Table 8. Crack Angle and Length Distribution in
Specimen C-8, $[0/90_2]_s$, 91% F_{tu}

Length of cracks (L) in inches ¹										
Angle θ	RIGHT EDGE				LEFT EDGE				$\cos\theta$ x L	$\sin\theta$ x L
	1st ply	2nd ply	3rd ply	4th ply	1st ply	2nd ply	3rd ply	4th ply		
-45	.0	.0	.0	.0	.0	.0	.0	.0	.0	.0
-40	.0	.0	.0	.0	.0	.0	.0	.0059	.0022	.0019
-35	.0	.0	.0	.0	.0	.0	.0	.0	.0	.0
-30	.0053	.0053	.0	.0	.0	.0	.0055	.0057	.0094	.0055
-25	.0051	.0051	.0051	.0055	.0047	.0108	.0051	.0051	.0211	.0098
-20	.0053	.0053	.0053	.0102	.0053	.0104	.0110	.0104	.0297	.0108
-15	.0049	.0049	.0102	.0152	.0157	.0	.0053	.0104	.0322	.0086
-10	.0108	.0	.0096	.0098	.0	.0100	.0209	.0010	.0306	.0054
-5	.0	.0	.0	.0098	.0047	.0148	.0049	.0098	.0219	.0019
0	.1116	.1384	.1577	.1209	.1429	.1504	.1384	.1343	.5473	.0
5	.0281	.0248	.0100	.0189	.0	.0	.0047	.0047	.0454	.0040
10	.0102	.0	.0047	.0150	.0051	.0051	.0	.0	.0197	.0035
15	.0	.0049	.0102	.0047	.0051	.0	.0047	.0047	.0120	.0032
20	.0055	.0055	.0049	.0	.0	.0	.0	.0	.0075	.0027
25	.0104	.0211	.0	.0	.0102	.0051	.0110	.0047	.0283	.0132
30	.0161	.0075	.0	.0047	.0114	.0077	.0	.0059	.0231	.0133
35	.0057	.0	.0	.0	.0	.0	.0	.0	.0023	.0016
40	.0059	.0	.0	.0	.0059	.0	.0	.0	.0045	.0038
45	.0	.0	.0	.0	.0	.0	.0	.0	.0	.0
Total	.2262	.2228	.2179	.2148	.2112	.2144	.2116	.2118	.8372	.0892

Length

Area Generated by Transverse Cracking

$$\text{Area} = 2 \times L \times W \quad (W = 1.004 \text{ in.})$$

Total area of all transverse cracks 1.7376 in.²Projected area perpendicular to laminate plane . . . 1.6811 in.²Projected area parallel with laminate plane 1.791 in.²

¹Each entry is the total length of all cracks
in the gage length at the specified angle.

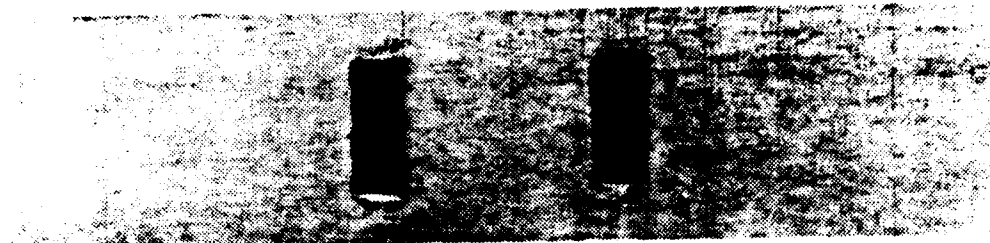


Figure 43. X-ray radiographs for a progressively loaded $[0/90]_s$ laminate

from a straight crack.

Type E $[0_2/90_2]_3$

The most notable phenomenon during the testing of this laminate was the formation of longitudinal splits. These were of a different form than those found in the $[0/90_2]_3$ (Type A) and $[0/90_3]_3$ (Type B) laminates. The splits were very prominent, typically running the full length of the 7 inch gage length (Figure 44). Unfortunately, all of the splits had at least one end within the grip, so the effect of the grip on the formation of the splits is uncertain. This laminate was the only one to exhibit this damage form. The reason this occurs in the $[0_2/90_2]_3$ laminate and not in the $[0/90_2]_3$ is not clear. This laminate was the only one tested with more than one 0° ply on the outside surface. It is possible that the residual thermal stress state in this laminate may be responsible for the long splits. No delaminations formed at the intersection of the splits and transverse cracks as expected. One would expect delaminations to form if the laminate were subjected to cyclic loading.

The splits began forming at approximately 70% of the ultimate load. With the growth of the longitudinal splits, a distinct tearing sound could be heard (as compared to the "pop" of a transverse crack). This implies that the growth of the crack is relatively slow and

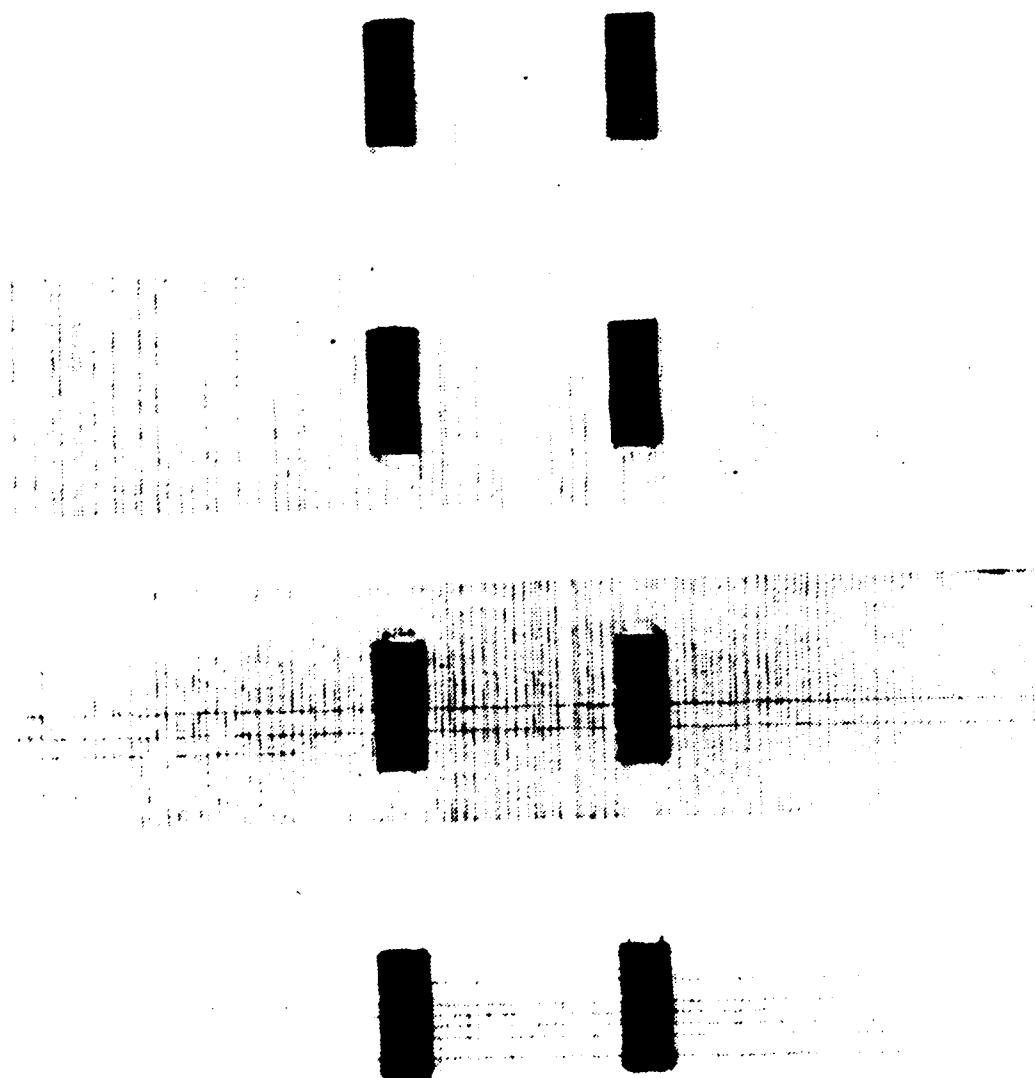


Figure 44. X-ray radiographs for a progressively loaded $[0_2/90_2]_s$ laminate

stable.

At approximately 95% of the failure strength, almost half of the cracks formed could be considered either curved or partial cracks. Figure 25 is a graphic representation of the formation of all the cracks. Notice that the formation of straight cracks has nearly ceased at about 70% of the ultimate strength, while the number of curved cracks is rapidly increased from 75% to failure. Partial and curved cracks were counted together. The number of longitudinal splits formed is also plotted. Table 9 was used to determine the crack surface area from the measured length and angle of cracks in an edge replica of a one inch gage section.

Type F [0/90/0]_s

This laminate was tested to determine the behavior of a single isolated 90° ply. An edge replica with typical transverse cracks is shown in Figure 45. At about 95% of the ultimate load, this laminate developed a transverse crack density of 65 cracks per inch. Figure 46 indicates that the cracks did not reach a saturation level before ultimate failure. Some crack branching was seen in the edge replicas, but since the crack opening was so slight, these were very difficult to see.

Prior to failure the [0/90/0]_s laminate had a stiffness loss of about 3%. This is almost identical to

Table 9. Crack Angle and Length Distribution in
Specimen E-9, $[0_2/90_2]_s$, 92% F_{tu}

Length of cracks (L) in inches¹

Angle θ	RIGHT EDGE				LEFT EDGE				$\cos\theta$ x L	$\sin\theta$ x L
	1st ply	2nd ply	3rd ply	4th ply	1st ply	2nd ply	3rd ply	4th ply		
-45	.0112	.0023	.0	.0	.0	.0	.0	.0	.0048	.0048
-40	.0	.0071	.0	.0	.0128	.0063	.0	.0	.0100	.0084
-35	.0171	.0	.0053	.0053	.0	.0	.0049	.0049	.0154	.0108
-30	.0222	.0153	.0053	.0104	.0329	.0122	.0	.0057	.0450	.0260
-25	.0098	.0	.0049	.0	.0049	.0	.0049	.0157	.0183	.0086
-20	.0057	.0	.0055	.0200	.0	.0047	.0045	.0094	.0235	.0086
-15	.0	.0051	.0141	.0053	.0106	.0152	.0	.0053	.0269	.0072
-10	.0100	.0102	.0198	.0049	.0150	.0148	.0138	.0148	.0509	.0090
-5	.0051	.0076	.0289	.0236	.0049	.0142	.0	.0	.0430	.0037
0	.1118	.1441	.1396	.1404	.1270	.1443	.1783	.1400	.5628	.0000
5	.0289	.0238	.0047	.0	.0094	.0230	.0090	.0142	.0564	.0049
10	.0194	.0149	.0051	.0	.0148	.0098	.0148	.0047	.0412	.0073
15	.0	.0145	.0051	.0	.0205	.0	.0045	.0096	.0263	.0070
20	.0145	.0055	.0165	.0110	.0102	.0	.0049	.0049	.0318	.0116
25	.0206	.0102	.0047	.0102	.0	.0057	.0	.0114	.0285	.0133
30	.0	.0	.0	.0059	.0055	.0112	.0106	.0185	.0224	.0130
35	.0	.0	.0	.0116	.0	.0	.0	.0	.0047	.0033
40	.0	.0	.0	.0106	.0169	.0039	.0	.0	.0120	.0100
45	.0	.0	.0	.0	.0	.0	.0	.0	.0000	.0000
Total	.2763	.2626	.2595	.2592	.2854	.2653	.2502	.2591	1.0239	.1575

Length

Area Generated by Transverse Cracking

$$\text{Area} = 2 \times L \times W \quad (W = 1.002 \text{ in.})$$

Total area of all transverse cracks 2.1218 in.²

Projected area perpendicular to laminate plane . . . 2.0519 in.²

Projected area parallel with laminate plane3156 in.²

¹Each entry is the total length of all cracks
in the gage length at the specified angle.

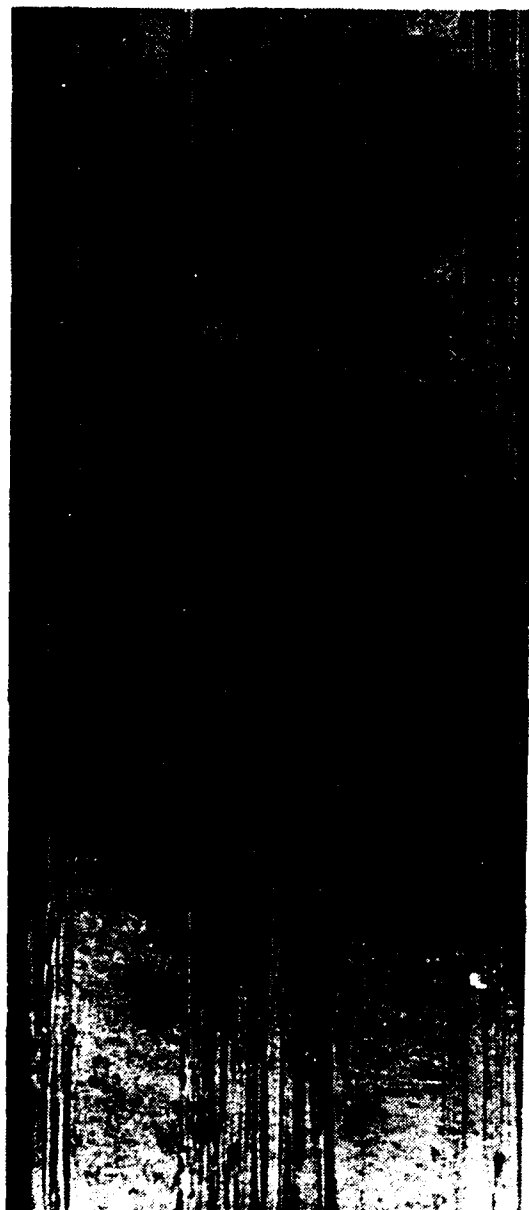


Figure 45. Edge replica of a $[0/90/0]_s$ laminate

SPECIMEN F-4 [0/90/0]_s

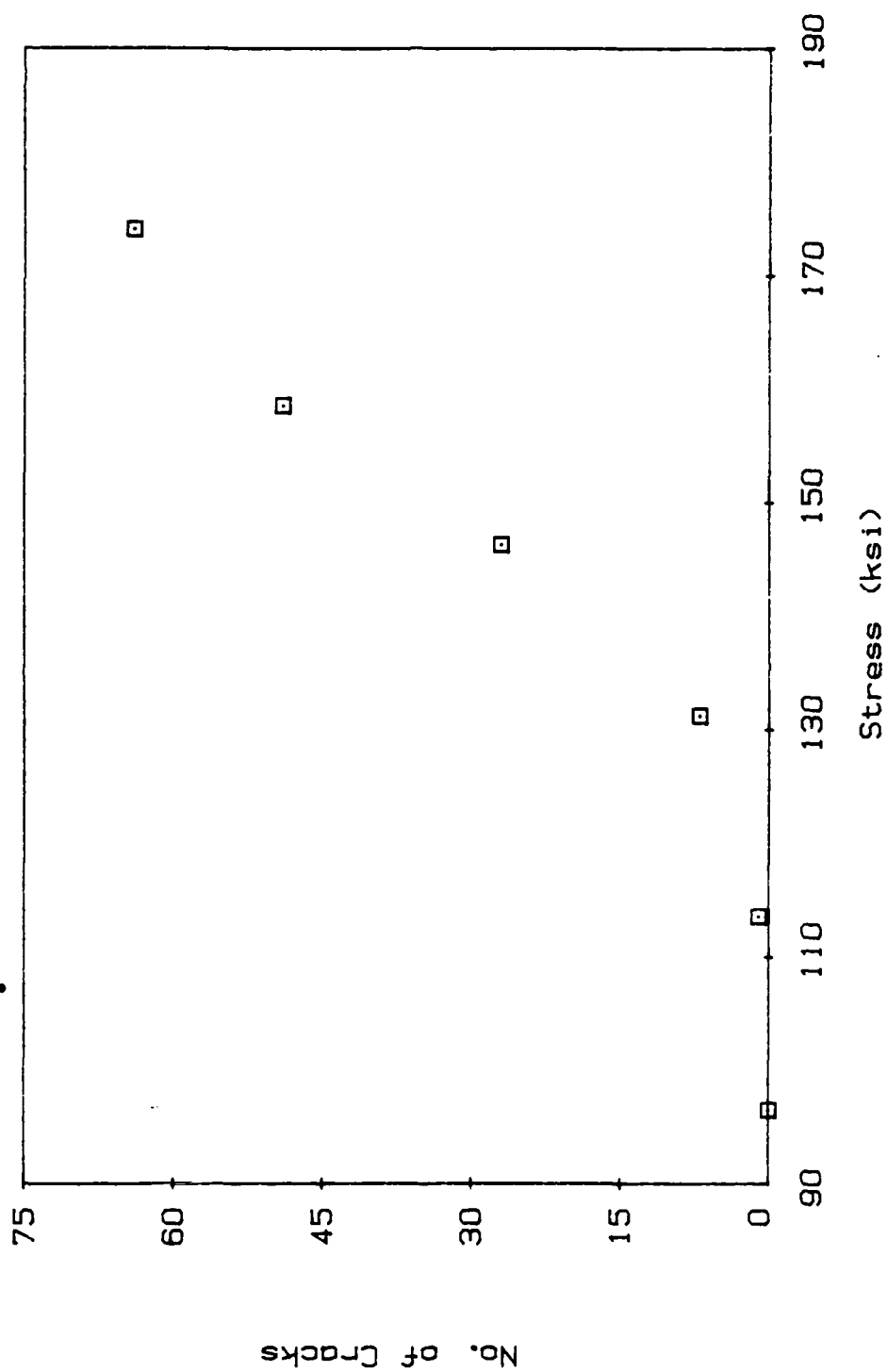


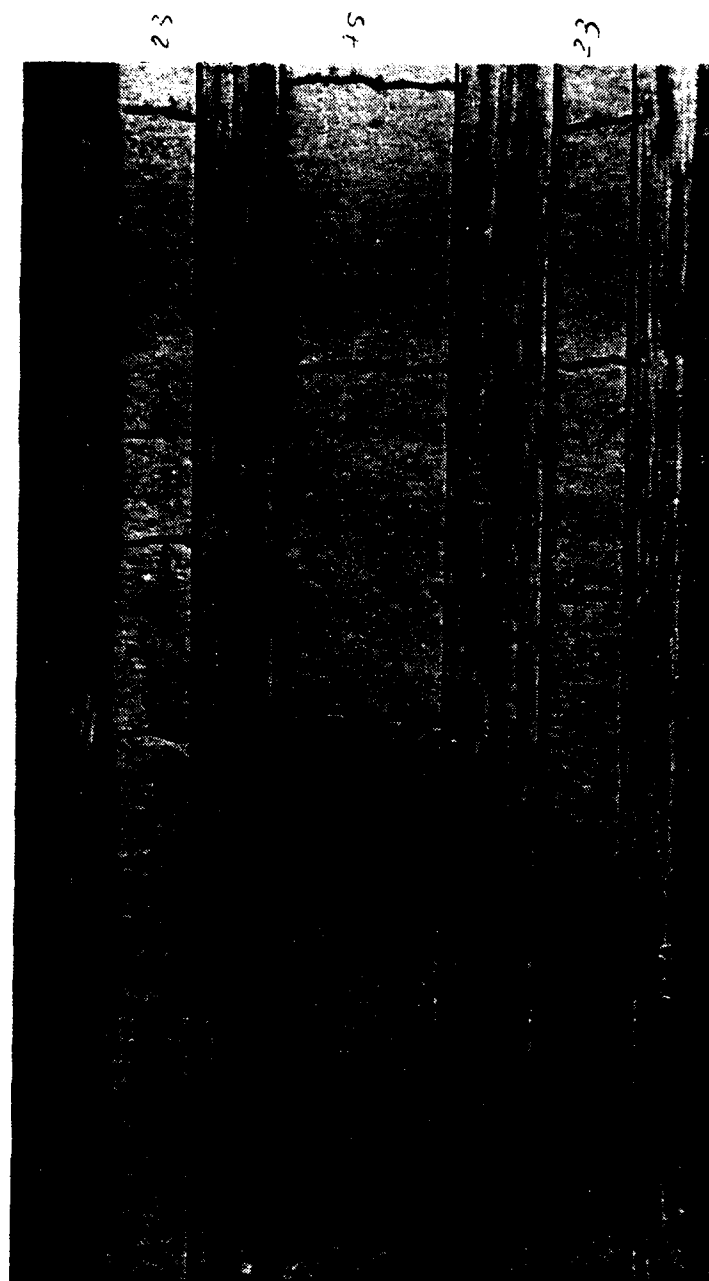
Figure 46. Crack development for a [0/90/0]_s laminate

the stiffness loss in the $[0/90]_s$ even though it has a lower percentage of 0° plies. This may have happened because the $[0/90/0]_s$ laminate generated a third more crack surface area than the $[0/90]_s$ laminate, thus making up for the original difference in stiffness.

Type G $[0/90/0/90]_s$

This laminate was the most representative of an aerospace structure of all the laminates. Typical composite applications usually have alternating orientations in adjacent lamina, except when unusual structural properties are needed.

Figure 47 shows a typical edge replica of this laminate. At 95% of the ultimate load, each single 90° ply had between 95 and 100 transverse cracks per inch. The double 90° layer had about 60 cracks per inch. These densities are higher than both the $[0/90/0]_s$ laminate (single 90°) and the $[0/90]_s$ laminate (double layer). This indicates that a saturation level had not been reached in these two laminates. This probably occurred because the $[0/90/0/90]_s$ laminate was able to carry a disproportionately larger load than the two other laminates. The ratio of ultimate load to number of 0° plies for the $[0/90/0/90]_s$ laminate was about 1750 pounds per ply. This ratio was about 1450 pounds per ply for the other two laminates.



d_1 0.0066"
 d_2 0.0063"
 d_3 0.0070" 0.0070"
 d_4 0.0074"
 d_5 0.0078"
 d_6 0.0046"
 d_7 0.0057"

Figure 47. Typical edge replica of a $[0/90/0/90]_s$ laminate

The ability of the $[0/90/0/90]_s$ laminate to have such a high ultimate strength must be due the alternating stacking sequence. Consider a $[0_2/90_2]_s$ cross-ply laminate whose only damage mode prior to failure is transverse cracking. Rupture of a 0° ply (and total failure) probably occurs where a transverse crack in a 90° contacts the 0° ply. This rupture would be caused by a stress riser at the crack tip. A qualitative representation of the through-the-thickness variation of the normal stress is shown in Figure 48a. The area under the curve represents the load carried by the laminate. Now consider a $[0/90/0/90]_s$ subjected to the same load. The mechanical properties predicted by laminate theory are identical. Figure 48b shows transverse cracks in each of the three 90° plies lying in the same plane. In this laminate the load is redistributed at 6 interfaces rather than two. This means that the stress concentration at any interface will be smaller than in the first case, thus requiring additional load to develop a critical stress.

Laminate Comparisons

The stiffness losses of three laminates are compared in Figure 49. The three laminates have identical theoretical mechanical properties (ratio of 0° plies to 90° plies is 1). The $[0/90/0/90]_s$ and $[0_2/90_2]_s$ laminates have the same number of plies, but have different stacking

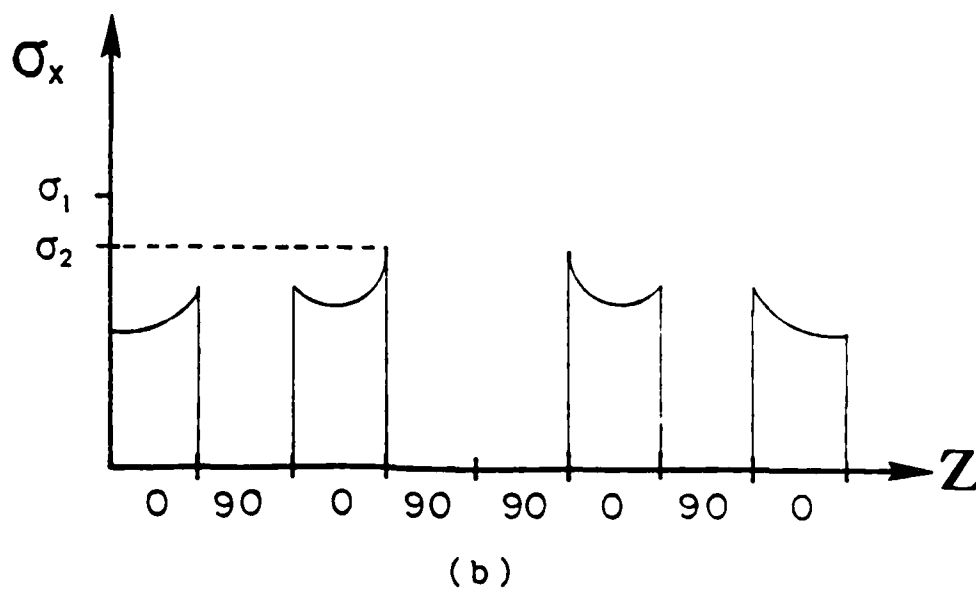
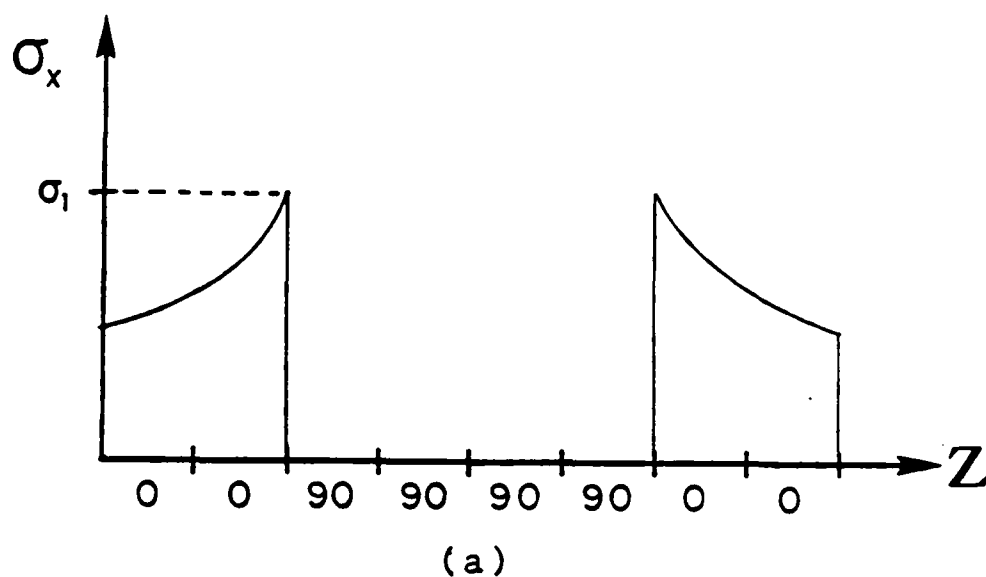


Figure 48. Conceptual representation of the through-the-thickness variation of the normal stress in the $[0_2/90_2]_s$ and $[0/90/0/90]_s$ laminates

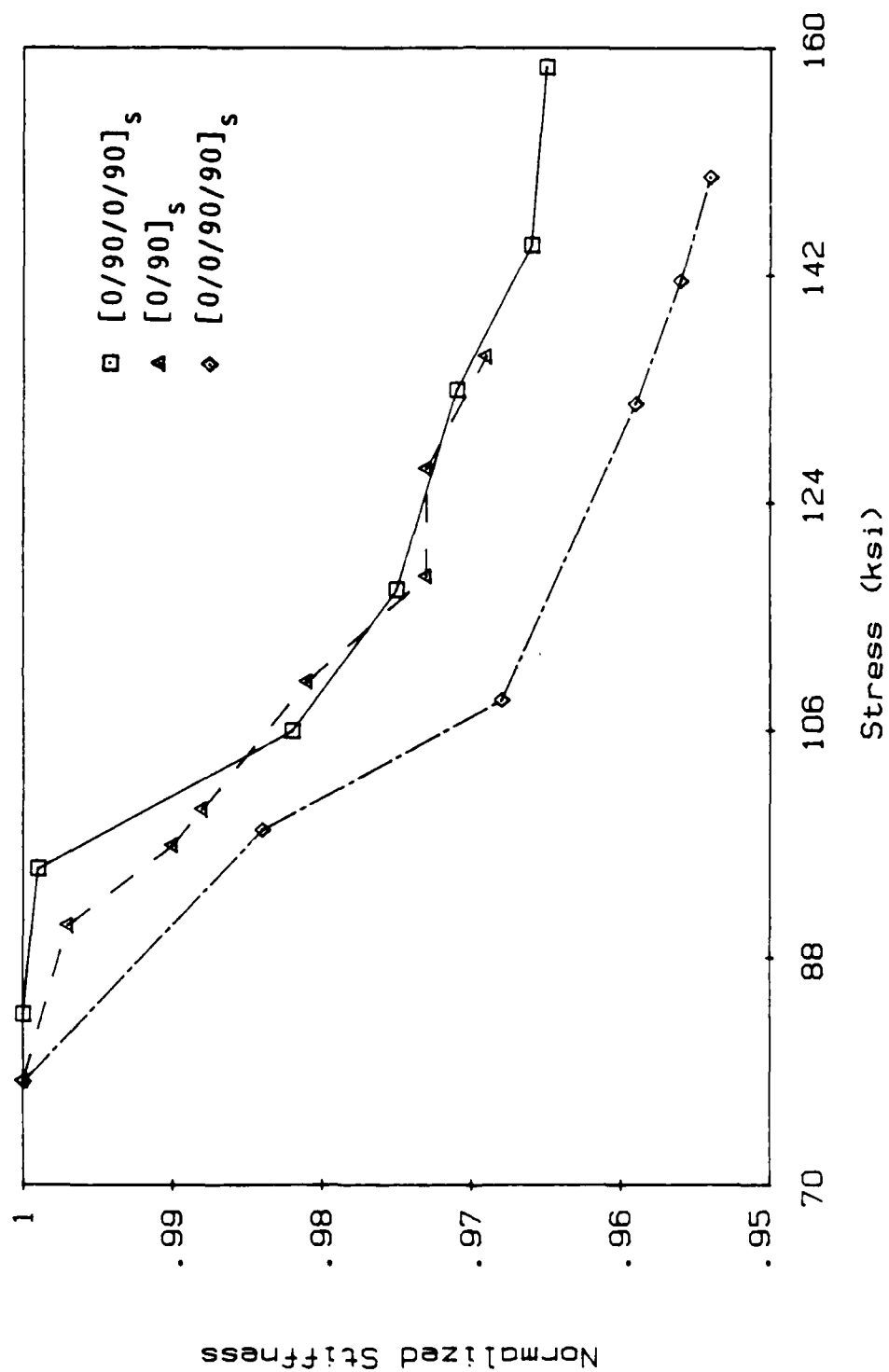


Figure 49. Comparison of stiffness reduction for three similar laminates

sequences. The $[0_2/90_2]_s$ and $[0/90]_s$ laminates have the same stacking sequence, but a different number of plies. The stiffness loss is plotted as a function of stress level. The difference between the $[0_2/90_2]_s$ and $[0/90/0/90]_s$ curves can be explained by the constraint conditions on the 90° plies. Although the $[0/90/0/90]_s$ has a greater crack surface area at all stresses (Figure 50), a larger portion of the load is shared by the 90° plies. The increased $0^\circ/90^\circ$ interface surface area allows a greater proportion of the load to be redistributed by shear into the transverse layers. This effectively makes the $[0/90/0/90]_s$ laminate stiffer at all stress levels. Figure 51 shows the correlation of crack surface area to stiffness loss. The large difference in behavior can be attributed to the 90° constraint effect which also affects the crack opening displacement in the transverse cracks.

The constraint conditions in the $[0/90]_s$ and $[0/90/0/90]_s$ laminates are very nearly the same. In fact, a $[0/90]_s$ type laminate makes up the core of the thicker laminate. The ratio of crack surface area to number of 90° plies at each stress level was compared for the two laminates, and it was found that the ratio was only slightly higher in the $[0/90/0/90]_s$ laminate. This can be attributed to the high crack density in the isolated 90° plies. All of these phenomenon support the observation that the two laminates develop nearly the same stiffness

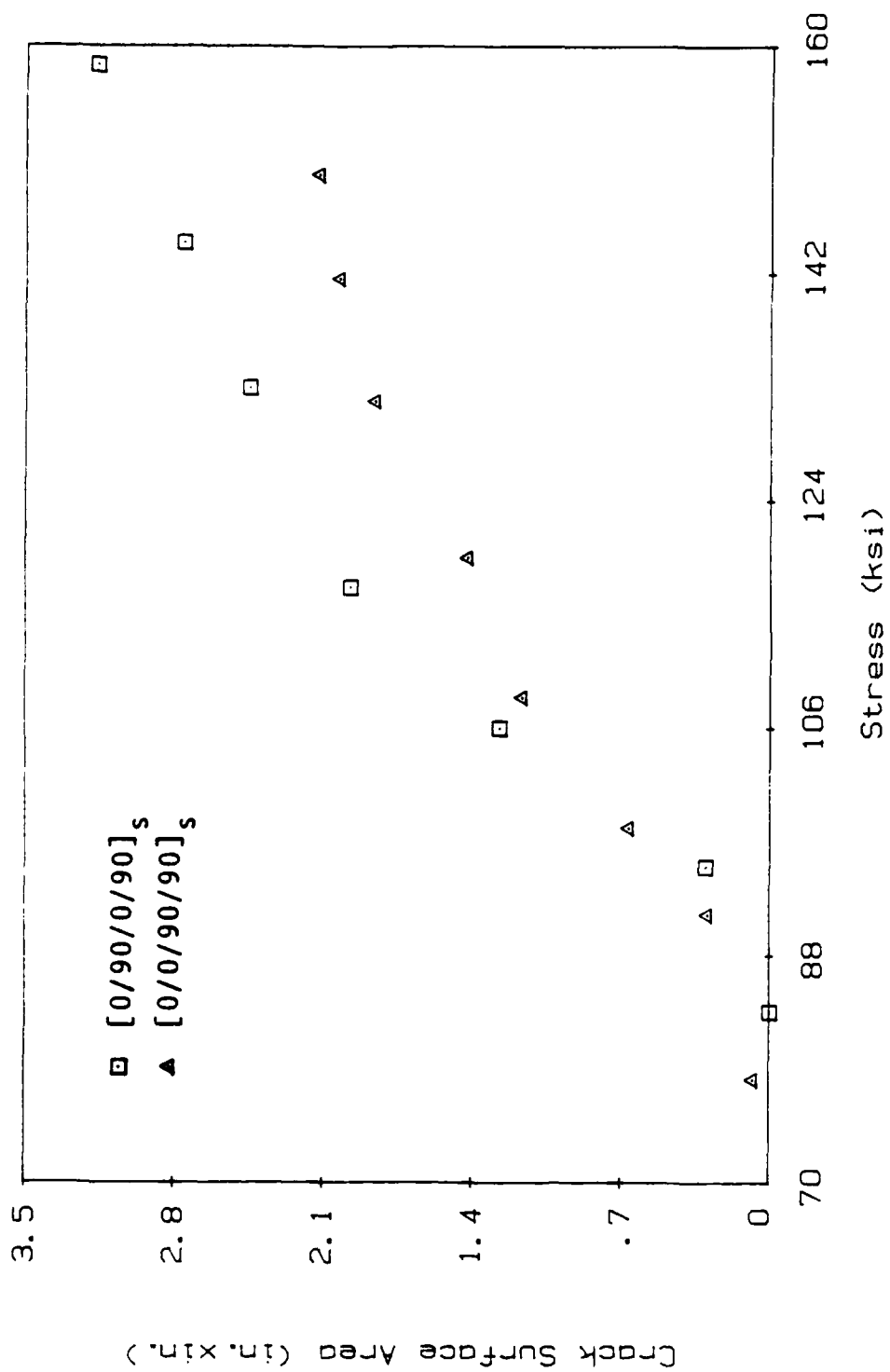


Figure 50. Comparison of generated crack surface area for the $[0/90/0/90]_s$ and $[0/0/90/90]_s$ laminates

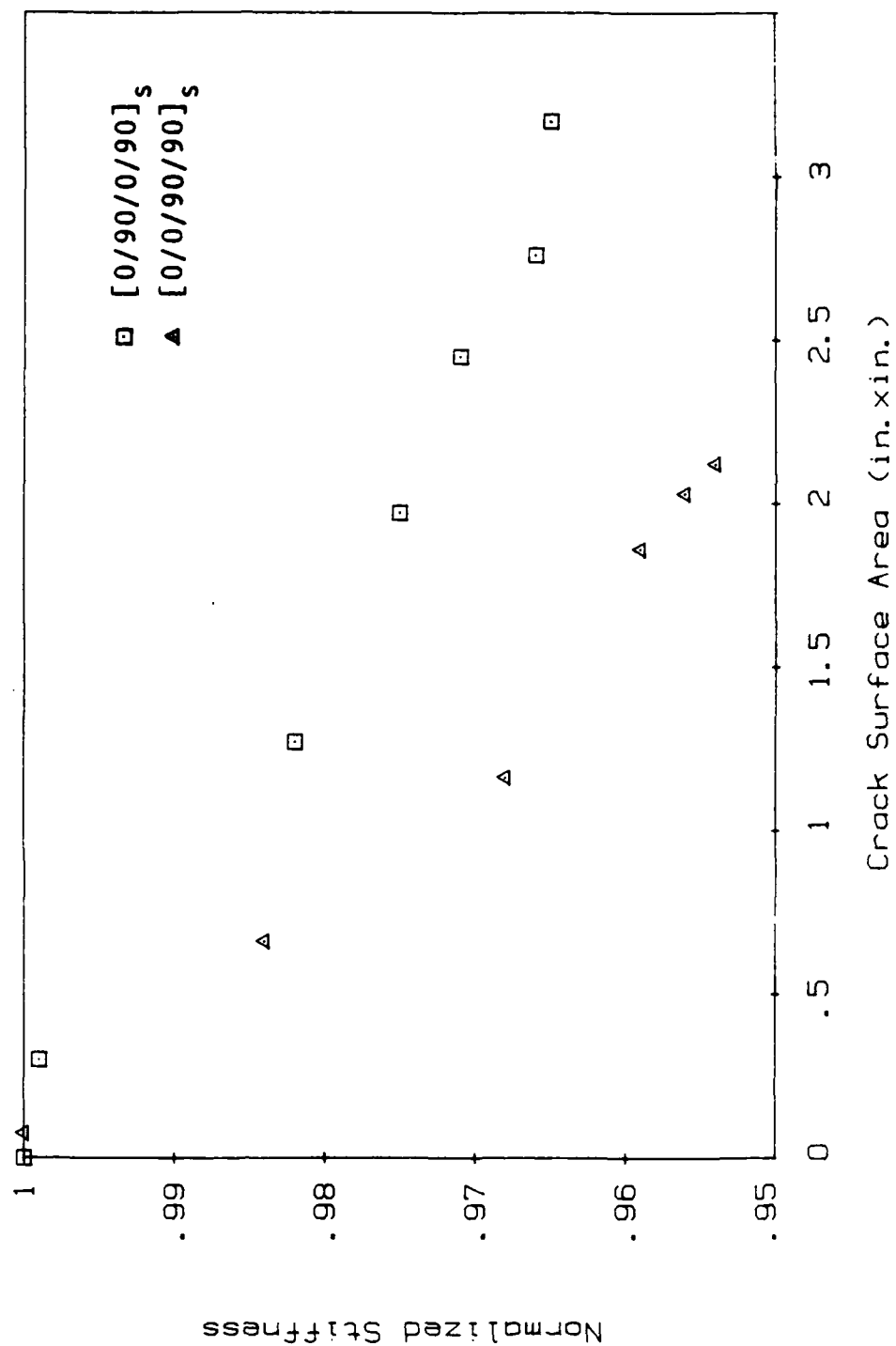


Figure 51. Relationship between crack surface area and stiffness reduction for the [0₂/90₂]_s and [0/90/0/90]_s laminates

loss with respect to stress level.

Laminates A through D were designed to observe the effects of 90° ply thickness on laminate response. All the laminates contained two 0° plies. The load at failure for this group was usually between 2600 and 3000 pounds. The damage development in each laminate has been described in detail in the previous section.

Several investigators [9,14,20,22] have studied the effect of 90° ply thickness. In every case, it was found that for a given strain, as the thickness of the 90° layer increased, the crack density decreased. In the AS4/3502 material system, this trend was obscured by the formation of curved and partial cracks.

Table 10 indicates the number of straight cracks observed just prior to ultimate failure for each laminate. The $[0/90/0]_s$ laminate can be considered to be two adjacent $[0/90/0]_t$ laminates. This assumption allows the comparison with the other laminates. The relationship between straight crack density and 90° ply thickness is obvious. When only straight cracks are considered, the familiar relationship is established. In each case the straight transverse cracks appear to approach a saturation crack density. No instance of curved crack saturation is observed.

Table 10. Comparison of Total Crack Density and
Straight Crack Density

TYPE	LAY-UP	TOTAL NO. OF CRACKS	NO. OF STRAIGHT CRACKS
A	$[0/90_4]_s$	32	10
B	$[0/90_3]_s$	38	18
C	$[0/90_2]_s$	45	30
D	$[0/90]_s$	45	43
F	$[0/90/0]_s$	63	63

CONCLUSIONS

The objective of this investigation has been to identify the mechanisms of initiation and growth of matrix cracks in a graphite/epoxy laminate and to identify the effect of matrix cracking on the material response. This information has been used in the development of a constitutive model based on internal state variable theory. The model currently utilizes an internal state variable based on the surface area generated by matrix cracking. The response of a laminate with an isolated 90° ply has been used as input for the model; and, the theoretical predictions of the model have been compared to the experimental results from several cross-ply laminates.

In this experimental program, two distinct types of transverse cracks were observed. Typical transverse cracks formed at regular intervals along the length of the specimen and generally spanned the 90° layer perpendicular to the laminate plane. The accepted explanation for this widely observed phenomenon is the concept of shear lag. This type of transverse crack was termed a "straight crack." The second type of crack had many features that indicated that it possessed a totally different growth mechanism. The most obvious of these features was the incidence angle to the plane of the laminate at which the crack initially propagated. This crack was termed an

"angle crack." Several important observations of this phenomenon are enumerated as following:

1. The angle crack always formed in conjunction with a straight crack. An angle crack did not form as an isolated, independent crack.
2. The crack was always oriented toward the straight crack.
3. The angle crack formed within a characteristic distance from a straight crack or another angle crack. This distance was found to be less than or equal to the thickness of the 90° ply group.
4. The proportion of angled cracks to straight cracks increased with an increase in the 90° ply thickness.
5. Two angle crack at opposite interfaces would commonly intersect at the midplane to form a "curved crack."
6. The acoustic emission of an angle crack was audibly different than that of a straight crack.
7. Upon unloading, a number of angled cracks could be seen in intermediate stages of growth. This was not the case with straight cracks.

Two damage phenomena were found to be associated with the cracks. Edge delaminations formed as bands across the

width of the specimens. In each case, the delamination propagated along the angle crack interface. Longitudinal splits formed over the delamination areas with one end of the split terminating at the angle crack interface.

Several observations were made concerning laminate response. A laminate with alternating 0° and 90° plies developed less stiffness loss than a similar laminate with the 90° plies grouped together. Possible causes are the difference in 90° constraint and the difference in crack opening displacement. Another observation was that the strain at which first ply failure occurred was inversely related to the number of 90° plies grouped together.

REFERENCES

1. D.H. Allen, S.E. Groves, and R.A. Schapery, "A Damage Model for Continuous Fiber Composites Part I: Theoretical Development," Mechanics and Materials Center, Texas A&M University, MM-5023-84-17, August 1984.
2. S.E. Groves, D.H. Allen, C.E. Harris, and R.A. Schapery, "A Damage Model for Continuous Fiber Composites Part II: Model Applications," Mechanics and Materials Center, Texas A&M University, MM-5023-84-18, February 1984.
3. V.V. Vasilev, A.A. Dudchenko, and A.N. Elpatevskii, "Analysis of the Tensile Deformation of Glass-Reinforced Plastics," Mekhanika Polimerov, No. 1 (1970), p.144.
4. H.T. Hahn and S.W. Tsai, "On The Behavior of Composite Laminates After Initial Failure," J. Composite Materials, Vol. 8 (1974), p. 288.
5. S.W. Tsai and H.T. Hahn, Inelastic Behavior of Composite Material, Vol. 13, American Society of Mechanical Engineers, Easton, Penn., 1975, p. 73.
6. R.M. Jones, Mechanics of Composite Materials, McGraw-Hill Book Co., New York, N.Y., 1975.
7. R.Y. Kim and H.T. Hahn, "Effect of Curing Stress on the First Ply-Failure in Composite Laminates," J. Composite Materials, Vol. 13 (1979) p.2.
8. D.S. Adams, D.E. Bowles, and C.T. Herakovich, "Characteristics of Thermally-induced Transverse Cracks in Graphite/Epoxy Composite Laminates," NASA Langley Research Center, NASA-TM-85429, 1983.
9. K.W. Garrett and J.E. Bailey, "Multiple Transverse Fracture In 90° Cross-ply Laminates of Glass Fibre-reinforced Polyester," J. Materials Science, Vol. 12 (1977), p. 157.
10. J. Aveston and A. Kelly, "Theory of Multiple Fracture of Fibrous Composites," J. Materials Science, Vol. 8 (1973), p. 255.

11. D.L. Flagg and M.H. Kural, "Experimental Determination of the In Situ Transverse Lamina Strength in Graphite/Epoxy Laminates," J. Composite Materials, Vol. 16 (1982), p.103.
12. A.S.D. Wang and G.E. Law, "Advanced Composites: Design and Application," National Bureau of Standards, NBS-SP-563 (1979), p. 255.
13. A.S.D. Wang and F.W. Crossman, "Initiation and Growth of Transverse Cracks and Edge Delamination in Composite Laminates: Part 1.," J. Composite Materials, Supplemental Vol. (1980), p. 76.
14. F.W. Crossman, W.J. Warren, A.S.D. Wang and G.E. Law Jr., "Initiation and Growth of Transverse Cracks and Edge Delamination in Composite Laminates: Part 2. Experimental Correlation," J. Composite Materials, Supplemental Vol. (1980), p.103.
15. A.S.D. Wang, "Growth Mechanisms of Transverse Cracks and Ply Delamination In Composite Laminates," Proc. 3rd. Int'l. Conf. on Comp. Matl., Paris, 1980, p. 170.
16. F.W. Crossman and A.S.D. Wang, "The Dependence of Transverse Cracking and Delamination On Ply Thickness In Graphite/Epoxy Laminates," ASTM STP-775, 1982, p. 118.
17. K.L. Reifsnider, "Some Fundamental Aspects of the Fatigue and Fracture Response of Composite Materials," Proc. 14th Annual Society of Engineering Science Meeting, Lehigh University, Nov. 14-16, 1977.
18. A. Talug, "Analysis of Stress Fields in Composite Laminates with Interior Cracks," Thesis, Doctor of Philosophy, College of Engineering, Virginia Polytechnic Institute and State University, September 1978.
19. K.L. Reifsnider, E.G. Henneke and W.W. Stinchcomb, "Defect-Property Relationships In Composite Materials," Air Force Materials Laboratory, AFML-TR-76-81, 1979.
20. K.L. Reifsnider and J.E. Masters, "Investigation of Characteristic Damage States In Composite Laminates," ASME Winter Annual Meeting, San Francisco, Calif., 1978.

21. J.E. Masters and K.L. Reifsnider, "An Investigation of Cumulative Damage Development In Quasi-Isotropic Graphite/Epoxy Laminates," ASTM STP-775, 1982, p. 40.
22. W.G. Bader, J.E. Bailey, A. Parvizi, and P.T. Curtis, "The Mechanisms of Initiation and Development of Damage In Multi-Axial Fiber-reinforced Plastic Laminates," Mechanical Behavior of Materials: Proc. 3rd. Int'l. Conf., Vol. 3, 1979, p. 227.
23. A.L. Highsmith and K.L. Reifsnider, "Stiffness-Reduction Mechanisms In Composite Laminates," ASTM STP-775, 1982, p. 103.
24. A. Kelly, "Multiple Fracture of Laminates," Fracture of Composite Materials, G. Sih, ed., Sijthoff and Noordhoff, Alphen aan den Rijn, Netherlands 1978, p. 193.
25. N. Laws, G.J. Dvorak, and M. Hejazi, "Stiffness Changes in Unidirectional Composites Caused By Crack Systems," Cranfield Institute of Technology, England, ISBN-0902937-901, 1983.
26. W.W. Stinchcomb, K.L. Reifsnider, P. Yeung, and J. Masters, "Effect of Ply Constraint On Fatigue Damage Development In Composite Material Laminates," ASTM STP-723, 1981, p. 64.
27. R.J. Nuismer, "Predicting the Performance and Failure of Multidirectional Polymeric Composite Laminates: A Combined Micro-macro Approach," Proc. 3rd. Int'l. Conf. on Comp. Matl., Paris, 1980, p. 436.
28. R.J. Nuismer, "The Role of Matrix Cracking in the Continuum Constitutive Behavior of a Damaged Composite Ply," University of Utah, Rep. No. UTEC 82-052, 1982.
29. R. Talreja, "A Continuum Mechanics Characterization of Damage in Composite Materials," Proc. Royal Society London, 1981, p. 461.
30. D.O. Stalnaker and W.W. Stinchcomb, "Load History-Edge Damage Studies in Two Quasi-isotropic Graphite/Epoxy Laminates," ASTM STP-674, 1980, p. 620.
31. W.D. Rummel, T. Tedrow, and H.D. Brinkerhof, "Enhanced X-ray Stereoscopic NDE of Composite Materials," Martin/ Aerospace Denver, Air Force Wright Aeronautical Laboratories, AFWAL-TR-80-3053, 1980.

VITA

Robert Gerald Norvell was born February 16, 1961, in Biloxi, Mississippi, the son of Gail and Lt. Col. Robert T. Norvell. He graduated from Lackland Sr. High School, San Antonio, Texas, in May of 1979.

Gerry entered Texas A&M University in the Fall of 1979 and majored in Aerospace Engineering. He graduated cum laude in May 1983 with a Bachelor of Science Degree. He received his Master of Science Degree in Aerospace Engineering in August, 1985.

Gerry is employed as an Engineer at General Dynamics, Ft. Worth Division, in the Advanced Methods Group.

Mr. Norvell is married to Kelly Simmons Norvell.

Permanent Address: 8271 Lifford Place

Ft. Worth, Texas 76116

APPENDIX 6.2

unclassified

SECURITY CLASSIFICATION OF THIS PAGE

REPORT DOCUMENTATION PAGE				
1a. REPORT SECURITY CLASSIFICATION Unclassified		1b. RESTRICTIVE MARKINGS		
2a. SECURITY CLASSIFICATION AUTHORITY		3. DISTRIBUTION/AVAILABILITY OF REPORT Unlimited		
2b. DECLASSIFICATION/DOWNGRADING SCHEDULE				
4. PERFORMING ORGANIZATION REPORT NUMBER(S)		5. MONITORING ORGANIZATION REPORT NUMBER(S)		
6a. NAME OF PERFORMING ORGANIZATION Aerospace Engineering Dept.		6b. OFFICE SYMBOL (If applicable)		7a. NAME OF MONITORING ORGANIZATION Air Force Office of Scientific Research
6c. ADDRESS (City, State and ZIP Code) Texas A&M University College Station, Texas 77843		7b. ADDRESS (City, State and ZIP Code) Bolling AFB Washington, D.C. 20332		
8a. NAME OF FUNDING SPONSORING ORGANIZATION AFOSR		8b. OFFICE SYMBOL (If applicable)		9. PROCUREMENT INSTRUMENT IDENTIFICATION NUMBER Grant No. AFOSR-84-0067
8c. ADDRESS (City, State and ZIP Code) same		10. SOURCE OF FUNDING NOS.		
		PROGRAM ELEMENT NO.	PROJECT NO.	TASK NO.
11. TITLE (Include Security Classification) A Thermomechanical Constitutive Theory for...		WORK UNIT NO.		
12. PERSONAL AUTHOR(S) D.H. Allen, S.E. Groves, and C.E. Harris				
13a. TYPE OF REPORT Interim		13b. TIME COVERED FROM _____ TO _____		14. DATE OF REPORT (Yr., Mo., Day) October 1985
15. PAGE COUNT 33				
16. SUPPLEMENTARY NOTATION				
17. COSATI CODES			18. SUBJECT TERMS (Continue on reverse if necessary and identify by block number)	
FIELD	GROUP	SUB. GR.	composites damage laminate analysis	
			internal state variables continuum mechanics	
19. ABSTRACT (Continue on reverse if necessary and identify by block number)				
<p>A continuum mechanics approach is utilized herein to develop a model for predicting the thermomechanical constitution of elastic composites subjected to both monotonic and cyclic fatigue loading. In this model the damage is characterized by a set of second order tensor valued internal state variables representing locally averaged measures of specific damage states such as matrix cracks, fiber-matrix debonding, interlaminar cracking, or any other damage state. Locally averaged history dependent constitutive equations are posed utilizing constraints imposed from thermodynamics with internal state variables.</p> <p>In Part I the thermodynamics with internal state variables is constructed and it is shown that suitable definitions of the locally averaged field variables will lead to useful thermodynamic constraints on a local scale containing statistically homogeneous damage. Based on this result the Helmholtz free energy is then expanded in a Taylor series in terms of strain, temperature, and the internal state variables to obtain the stress-strain relation for composites with damage. In part II the three dimensional tensor equations developed in</p>				
20. DISTRIBUTION/AVAILABILITY OF ABSTRACT UNCLASSIFIED UNLIMITED <input checked="" type="checkbox"/> SAME AS RPT. <input type="checkbox"/> DTIC USERS <input type="checkbox"/>			21. ABSTRACT SECURITY CLASSIFICATION Unclassified	
22a. NAME OF RESPONSIBLE INDIVIDUAL Anthony K. Amos			22b. TELEPHONE NUMBER (Include Area Code) (202) 767-4937	22c. OFFICE SYMBOL

A THERMOMECHANICAL CONSTITUTIVE THEORY FOR ELASTIC
COMPOSITES WITH DISTRIBUTED DAMAGE

PART I: Theoretical Development

by

D.H. Allen

S.E. Groves

and

C.E. Harris

Aerospace Engineering Department
Texas A&M University
College Station, Texas 77843

A THERMOMECHANICAL CONSTITUTIVE THEORY FOR ELASTIC
COMPOSITES WITH DISTRIBUTED DAMAGE

PART I: Theoretical Development

by

D.H. Allen
S.E. Groves
C.E. Harris

ABSTRACT

A continuum mechanics approach is utilized herein to develop a model for predicting the thermomechanical constitution of elastic composites subjected to both monotonic and cyclic fatigue loading. In this model the damage is characterized by a set of second order tensor valued internal state variables representing locally averaged measures of specific damage states such as matrix cracks, fiber-matrix debonding, interlaminar cracking, or any other damage state. Locally averaged history dependent constitutive equations are posed utilizing constraints imposed from thermodynamics with internal state variables.

In Part I the thermodynamics with internal state variables is constructed and it is shown that suitable definitions of the locally averaged field variables will lead to useful thermodynamic constraints on a local scale containing statistically homogeneous damage. Based on this result the Helmholtz free energy is then expanded in a Taylor series in terms of strain, temperature, and the internal state variables to obtain the stress-strain relation for composites with damage. In Part II the three dimensional tensor equations developed in Part I are simplified using material symmetry constraints and are written in engineering notation. The resulting constitutive model is then cast into laminate equations and an example problem is solved and compared to experimental results.

It is concluded that although the model requires further development and extensive experimental verification it may be a useful tool in characterizing the thermomechanical constitutive behavior of continuous fiber composites with damage.

INTRODUCTION

Ultimate failure of composite structural components is preceded by a sequence of microstructural and macrostructural events such as microvoid growth, matrix cracking, fiber-matrix debonding, interlaminar cracking, edge delamination, and fiber fracture, which are all loosely termed damage. Considerable experimental research has been performed in the last decade detailing the growth of damage under both monotonic and cyclic loading conditions [1-7]. The significance of this damage lies in the fact that numerous global material properties such as stiffness, damping and residual strength may be substantially altered during the life of the component, as shown in Fig. 1 [8]. It has been found that the first phase of fatigue is typified by development of a characteristic damage state (CDS) [9] which is composed primarily of matrix cracking in off-axis plies. During the second phase of damage development the CDS contributes to fiber-matrix debonding, delamination, and fiber microbuckling. These phenomena in turn contribute to a tertiary damage phase in which edge delamination and fiber fracture lead to ultimate failure of the specimen [6].

Analytical modeling of the damage state appears to be only recently studied. The earliest attempts fall under the general heading of laminate analysis, in which various empirical schemes have been developed to discount ply properties in the presence of damage [10-12]. Axial stiffness reduction and stress distribution in the CDS have also been predicted using a one-dimensional shear lag concept [5]. Several researchers have obtained analytic solutions for effective moduli of elastic bodies with distributed cracks [13-17]. In the case where cracks are either aligned [15] or randomly oriented [13,14,16] the total crack surface area is found to cause a first order effect on the stiffness. These theoretical results apply only to elastic bodies with cracks of homogeneous and predetermined dimensions.

Fracture based concepts have recently been utilized to model damage development [18-21]. Although the first of these studies [18] contains a general theory which may be applied to fibrous composites, it has so far only been utilized for quasi-isotropic random particulate composites such as solid rocket propellant [9], and as such has not been applied to continuous fiber composites. Although the theory in the latter two [20,21] has not been utilized to predict reduction of off-axis stiffness components, it has been utilized to develop fatigue crack growth laws. Kachanov's modulus reduction technique [22] has also been applied to fibrous composites [23] and although promising results were obtained, the model was utilized in uniaxial form only.

A complex interactive experiment and analysis model (called a mechanistic model) has been proposed [8] for prediction of life of damaged composites. The mechanistic model appears to require numerous experimental results for each geometric layup in order to determine which damage mode results in failure.

Finally, extended forms of Miner's rule [24] have been proposed for life prediction [18,25]. However, they are based on simplified microphysical models at this time.

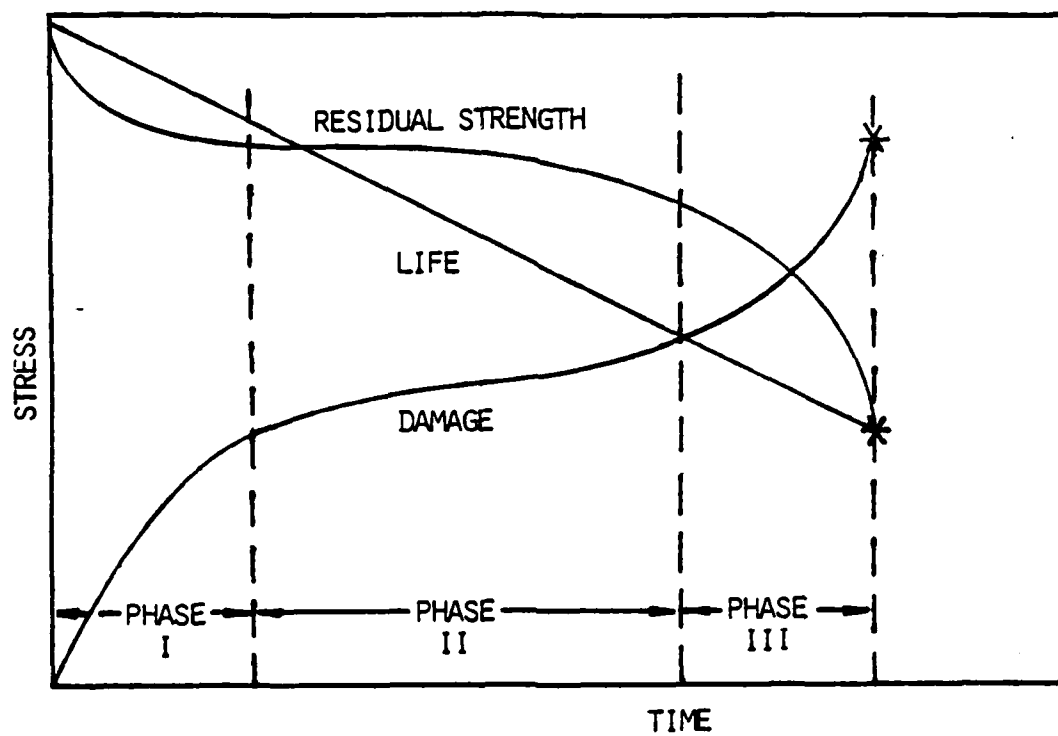


Fig. 1. Damage Accumulation in a Continuous Fiber Composite Subjected to Monotonic Load or Strain Controlled Cyclic Fatigue (from ref. 8).

The concept of damage as an internal state variable [26] has been previously utilized in continuum mechanics/thermodynamics based theories for crystalline and/or brittle materials [27-34], as well as for nonlinear viscoelastic materials [18]. A study has been made of the effect of vector-valued damage parameters on various compliance terms [35], and this methodology is currently undergoing further development [36, 37].

The research reviewed above indicates that although important progress has been made in characterizing damage in composites, substantial and continued research is warranted before several issues can be resolved.

In this paper an attempt will be made to assemble many of the concepts embodied in the research efforts mentioned briefly above and to utilize these concepts to develop a thermomechanical constitutive model for damage in composites which is rigorously based in continuum mechanics/thermodynamics and is generic with regard to material type, load spectrum, and specimen geometry.

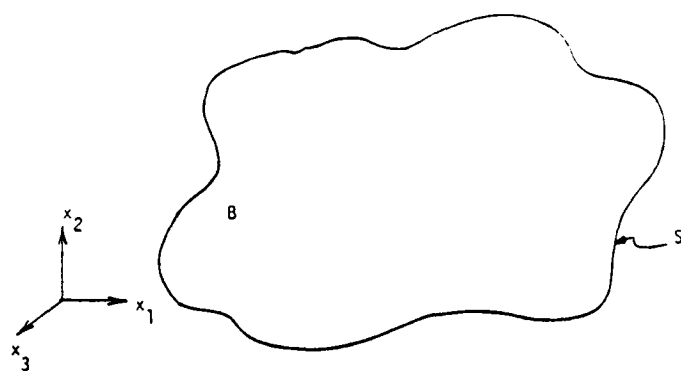
The model will utilize the concept of a local volume element with statistically homogeneous damage to construct constitutive equations relating stress, strain, and damage. Unlike current analytical methods, the local volume element will be modelled experimentally. The model will therefore not be restricted to linear elastic media with homogeneous elastic properties. Furthermore, the model will be applicable to cracks which are oriented and of heterogeneous and irregular size and shape. The effect of the cracks will be reflected through locally averaged quantities describing the kinematics of the cracks.

The output of the model will be a set of constitutive equations which apply on a scale that is small compared to the boundary value problem of interest. Therefore, it will be applicable to the analysis of bodies with stress gradients and heterogeneous damage states as long as the scale of the microcracks, voids, etc. is relatively small.

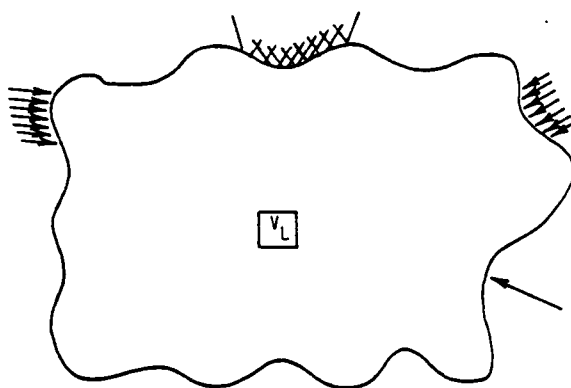
CHARACTERIZATION OF DAMAGE AS A SET OF INTERNAL STATE VARIABLES

Consider an initially unloaded and undamaged composite structural component, denoted B , as shown in Fig. 2a, where undamaged is defined here to mean that the body may be considered to be continuous (without cracks) on a scale several orders of magnitude smaller than the smallest external dimension of the component. Although cracks may exist in the initial state, their total surface area is assumed to be small compared to the external surface area of the component. Under this assumption the body is assumed to be simply connected and we call the initial bounding surface the external boundary S . Although the component is undamaged, there may exist local heterogeneity caused by processing and second phase materials including fibers, matrix tougheners and voids. In addition, the body may be subjected to some residual stress state due to processing, cool down, etc.

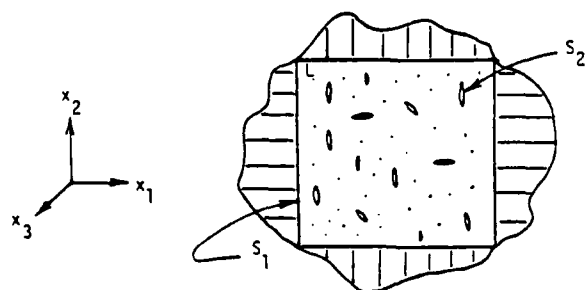
Now suppose that the component is subjected to some



(a)



(b)



(c)

Fig. 2. Structural Component Labelled B
 a) Undamaged State
 b) With Applied Tractions
 c) Local Volume Element

traction and/or deformation history, as shown in Fig. 2b. The specimen will undergo a thermodynamic process which will in general be in some measure irreversible. This irreversibility is introduced by the occurrence of such phenomena as material inelasticity (even in the absence of damage), fracture (both micro- and macroscale), friction (due to rubbing and/or slapping of fractured surfaces), temperature flux, and chemical change. While all of these phenomena can and do commonly occur in composites, in the present research it will be assumed that all irreversible phenomena of significance occur in small zones near crack surfaces. Outside these zones, the behavior will be considered to be elastic and therefore reversible under constant temperature conditions. All fracture events will be termed damage. Due to these fracture events, the body will necessarily become multiply connected, and all newly created surfaces not intersecting the external boundary will be termed internal boundaries. Because of the above assumptions the model may be limited to polymeric and ceramic matrix composites at temperatures well below the glass transition temperature T_g or melting temperature, where viscoelasticity in matrix materials is small. Metal matrix composites may have to be excluded due to complex post-yield behavior of the matrix.

While fracture involves changes in the boundary conditions governing a complex field problem, it is hypothesized that one may neglect boundary condition changes caused by creation and alteration of both internal and external surfaces created during fracture as long as the resulting damage in the specimen is statistically homogeneous on a local scale which is small compared to the scale of the body of interest. However, the total newly created surface area (which includes internal surfaces) may be large compared to the original external surface area. Under the condition of small scale statistical homogeneity all continuum based conservation laws are assumed to be valid on a global scale in the sense that all changes in the continuum problem resulting from internal damage are reflected only through alterations in constitutive behavior. Typical microstructural events which may qualify as damage are matrix cracking in lamina, fiber/matrix debonding, localized interlaminar delamination and fiber fracture. Large scale changes in the external surface such as edge delaminations, however, are treated as boundary effects which must be reflected in conservation laws via changes in the external boundary conditions rather than in constitutive equations [35,38].

THERMODYNAMICS OF MEDIA WITH DAMAGE

We now proceed to construct a concise model of the composite with damage. To do this, consider once again the structural component, denoted B in Fig. 2a. The body B is assumed to be of the scale of some appropriate boundary value problem of interest. Now consider some local element labelled V_L and with external surface faces S_1 arbitrarily chosen normal to a set of Cartesian coordinate axes (x_1, x_2, x_3) , as shown in Fig.

2c. The element V_L extracted from B and the newly created surfaces, denoted S_2 and with volume V_0 , are subjected to appropriate boundary conditions so that the element response is identical to that when it is in B. Furthermore, the volume of the element is defined to be V_L , which includes the volume of any initial voids. The scale of V_L is chosen so that its dimensions are small compared to the dimensions of B, but at the same time, the dimensions of V_L are large enough to guarantee statistical homogeneity of the material heterogeneities and defects in V_L even though the total surface area of defects may be of the same order of magnitude as S_1 [39]. Suppose furthermore that in the absence of defects or at constant damage state the material behavior is linearly thermoelastic. Now consider the local volume element V_L . For the case where tractions or displacements are applied uniformly to the external boundary of V_L , the average stresses and strains in V_L will be determinable from the external boundary tractions or displacements.

Although the damage process actually involves the conversion of strain energy to surface energy, the fact that the damage is reflected in the local constitutive equations rather than boundary conditions suggests that it be treated as a set of energy dissipative local state variables which are not discernible on the external boundary of the local element.

Review of Thermodynamic Constraints on Linear Thermoelastic Media

The following notation is adopted. Quantities without capitalized subscripts denote pointwise quantities. Those with subscripts L denote quantities which are averaged over the local element V_L . Finally, the subscript E denotes linear thermoelastic properties.

Under the conditions described in the previous section the pointwise Helmholtz free energy per unit volume h of the undamaged linear elastic medium may be expressed as a second order expansion in terms of strain ϵ_{ij} and temperature T as follows [40]:

$$h \equiv u - Ts = h(\epsilon_{ij}, T) = A + B_{ij}\epsilon_{ij} + \frac{1}{2}C_{ijkl}\epsilon_{ij}\epsilon_{kl} + D\Delta T + E_{ij}\epsilon_{ij}\Delta T + \frac{1}{2}F\Delta T^2, \quad (1)$$

where u and s are the internal energy and entropy per unit volume, respectively, and A , B_{ij} , C_{ijkl} , D , E_{ij} and F are material parameters which are independent of strain and temperature and $\Delta T \equiv T - T_R$, where T_R is the reference temperature at which the strains are zero at zero external loads. In addition, we assume here that all motions are associated with small deformations. Furthermore, inertial effects and electromagnetic coupling are assumed to be negligible.

Pointwise conservation laws appropriate to the body are as follows:

1) conservation of linear momentum

$$\sigma_{ji,j} = 0 \quad ; \quad (2)$$

where σ_{ij} is the work conjugate stress tensor to the strain tensor ϵ_{ij} and body forces are assumed to be negligible;

2) conservation of angular momentum (assuming body moments may be neglected)

$$\sigma_{ij} = \sigma_{ji} \quad ; \quad (3)$$

3) balance of energy

$$\dot{u} - \sigma_{ij} \dot{\epsilon}_{ij} + q_{j,j} = r \quad ; \quad (4)$$

where q_j are the components of the heat flux vector, and r is the heat source per unit volume. In addition, dots denote time differentiation and $_{,j} \equiv \partial/\partial x_j$;

4) the second law of thermodynamics

$$\dot{s} - \frac{r}{T} + (q_j/T)_{,j} \geq 0 \quad . \quad (5)$$

Furthermore,

$$\epsilon_{ij} \equiv \frac{1}{2}(u_{i,j} + u_{j,i}) \quad . \quad (6)$$

Constraints imposed by the second law of thermodynamics will result in [40]

$$s = s_E = - \frac{\partial h}{\partial T} E = - D - E_{ij} \epsilon_{ij} - F \Delta T \quad , \quad (7)$$

and

$$\sigma_{ij} = \sigma_{Eij} = \frac{\partial h}{\partial \epsilon_{ij}} E = B_{ij} + C_{ijkl} \epsilon_{kl} + E_{ij} \Delta T \quad , \quad (8)$$

where B_{ij} are interpreted as components of residual stresses at the reference temperature at which $\Delta T=0$, and [40]

$$q_i = -k_{ij}g_j, \quad (9)$$

where

$$g_j \equiv T_{,j}, \quad (10)$$

and k_{ij} is the thermal conductivity tensor.

Thermodynamic Constraints with Local Damage

It is our intention to construct locally averaged field equations which are similar in form to the pointwise field equations discussed above. In performing this averaging process the pointwise Helmholtz free energy described in equation (1) will undergo a natural modification to include the energy conversion due to crack formation.

Now consider the local element shown in Fig. 2c with traction boundary conditions on the external surface S_1 . In addition, the interior of V_L is assumed to be composed entirely of linear elastic material and cracks (which may include thin surface layers of damage). Integrating pointwise equations (1) through (6) over the local volume will result in

$$h_{EL} = A_L + B_{Lij}\epsilon_{Lij} + \frac{1}{2}C_{Lijkl}\epsilon_{Lij}\epsilon_{Lkl} + D_L\Delta T_L + E_{Lij}\epsilon_{Lij}\Delta T_L + \frac{1}{2}F_L\Delta T_L^2, \quad (11)$$

where A_L , B_{Lij} , C_{Lijkl} , D_L , E_{Lij} , and F_L are locally averaged material constants. Also,

$$\sigma_{Lji,j} = 0, \quad (12)$$

$$\sigma_{Lij} = \sigma_{Lji}, \quad (13)$$

$$\dot{u}'_L - \sigma_{Lij}\dot{\epsilon}_{Lij} + q_{Lj,j} = r_L, \quad (14)$$

and

$$\dot{s}_L - \frac{\dot{r}_L}{T_L} + (\frac{q_{Lj}}{T_L})_{,j} \geq 0, \quad (15)$$

where u'_L , called the effective local internal energy, is given by

$$\dot{u}'_L \equiv \dot{u}_{EL} + \dot{u}_L^C, \quad (16)$$

u_{EL} represents the internal energy of the equivalent uncracked body, given by

$$\dot{u}_{EL} \equiv \frac{1}{V_L} \int_{V_L} \dot{u} dV - \frac{1}{V_L} \int_{S_2} T_1^E \dot{u}_1 dS, \quad (17)$$

where T_1^E are called equivalent tractions, representing tractions in the uncracked body acting along fictitious crack faces, as described in detail in the appendix, and \dot{u}_L^C is the mechanical power output due to cracking, given by

$$\dot{u}_L^C \equiv - \frac{1}{V_L} \int_{S_2} T_1^C \dot{u}_1 dS, \quad (18)$$

where T_1^C are fictitious tractions applied to the crack faces which represent the difference between the actual crack face tractions and T_1^E . Furthermore, the locally averaged stress is given by

$$\sigma_{Lij} \equiv \frac{1}{V_L} \int_{V_L} \sigma_{ij} dV, \quad (19)$$

and the locally averaged strain is given by

$$\epsilon_{Lij} \equiv \frac{1}{V_L} \int_{S_1} \frac{1}{2} (u_i n_j + u_j n_i) dS, \quad (20)$$

Equations (11) through (15) are identical in form to equations (1) through (5), respectively. Further details on this similarity are given in the appendix.

On the basis of this similarity we now define the locally averaged Helmholtz free energy [18, 38]:

$$h_L \equiv u'_L - T_L s_L = u_{EL} - T_L s_L + u_L^C = h_{EL} + u_L^C, \quad (21)$$

where it can be seen from definition (17) that h_{EL} is the locally averaged elastic Helmholtz free energy for which residual damage is zero.

The similarity between the pointwise and local field equations leads to the conclusion that

$$s_L = - \frac{\partial h_L}{\partial \epsilon_L} \quad , \quad (22)$$

$$\sigma_{Lij} = \frac{\partial h_L}{\partial \epsilon_{Lij}} = \frac{\partial h_{EL}}{\partial \epsilon_{Lij}} + \frac{\partial u_L^c}{\partial \epsilon_{Lij}} \quad , \quad (23)$$

$$q_{Li} = - k_{Lij} g_{Lj} \quad , \quad (24)$$

and

$$g_{Lj} \equiv T_{L,j} \quad , \quad (25)$$

where

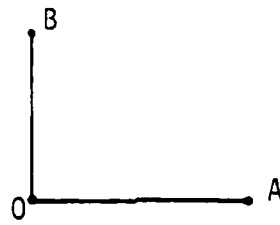
$$k_{Lik} \equiv \frac{1}{g_{Lk} V_L} \int_{V_L} k_{ij} g_j dV \quad , \quad (26)$$

Note the similarity between equations (7) through (10) and (22) through (25), respectively.

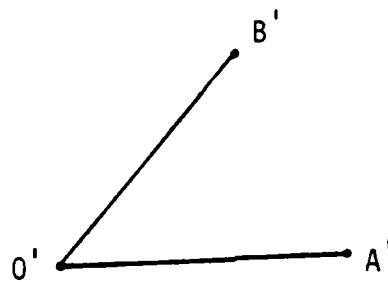
Equations (23) will serve as the basis for thermomechanical stress-strain relations in damaged composites. All damage will be reflected through the local energy due to cracking u_L^c . This term will be modelled with internal state variables characterizing the various damage modes.

Description of the Internal State

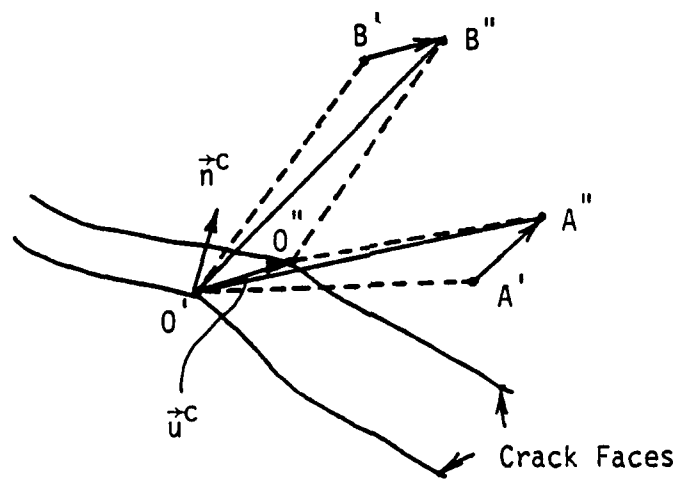
In order to describe the internal state, we first consider the kinematics of a typical point O with neighboring points A and B, as shown in Fig. 3. Before deformation lines OA and OB are orthogonal, as shown in (a). After deformation we imagine that lines joining O', A', and B' are as shown in (b), and just at the instant that deformation is completed, a crack forms normal to the plane of AOB through point O', as shown in (c). Furthermore, point O' becomes two material points O' and O'' on opposite crack faces and points A' and B' deform further to



(a)



(b)



(c)

Fig. 3 . Kinematics of the Damage Process

- a) Point "O" Prior to Deformation,
- b) Point "O" after Deformation and Prior to Fracture Process,
- c) Point "O" after Fracture.

points A" and B". It is assumed that all displacements, including displacement jumps across crack faces, are infinitesimal, so that strain gages attached at points O, A, and B record only the deformation A"O'B". However, the actual strain is associated with A"O"B". Therefore, it is essential to construct an internal state variable which will relate these two strain descriptions. We therefore construct the vectors \hat{u}^c connecting O' and O" and \hat{n}^c describing the normal to the crack face at O', as shown in (c). It should be noted that \hat{u}^c can be used to construct a pseudo-strain representing the difference in rotation and extension of lines A"O'B" and A"O"B".

Now recall that the mechanical power output during cracking is given by equation (18). We assume that at any point in time t_1 tractions T_i can be applied along the crack faces which will result in an energy equivalent to that produced by the damage process:

$$u_L^c(t_1) = - \frac{1}{V_L} \int_{S_2(t_1)} T_i u_i^c dS \quad (27)$$

The quantities T_i do not necessarily coincide with the terms in the integrand of (18) since the process is in some measure irreversible. However, we define them such that the total energies in equations (18) and (27) are equivalent. For convenience we will call them crack closure tractions, although they do not necessarily result in complete crack closure.

Guided by the fact that \hat{u}^c and \hat{n}^c describe the kinematics of the cracking process at point O, we now define the following second order tensor valued internal state variable:

$$\alpha_{ij} \equiv u_i^c n_j^c \Rightarrow [\alpha_{ij}] = \begin{bmatrix} u_1^c n_1^c & u_1^c n_2^c & u_1^c n_3^c \\ u_2^c n_1^c & u_2^c n_2^c & u_2^c n_3^c \\ u_3^c n_1^c & u_3^c n_2^c & u_3^c n_3^c \end{bmatrix} \quad (28)$$

The above description has been previously proposed by M. Kachanov[41]. Substituting the above into (27) and utilizing Cauchy's formula gives

$$u_L^c = \frac{1}{V_L} \int_{S_2} \sigma_{ij}^c \alpha_{ij} dS \quad (29)$$

where it should be pointed out that integration is performed with respect to undeformed coordinates.

Note that the components of \hat{u}^c can be recovered from (28) by using simple row multiplication on α_{ij} :

$$u_i^2 = u_{in_j}^c u_{in_j}^c \quad (\text{no sum on } i) \quad (30)$$

Similarly, \hat{n}^c can be recovered by using column multiplication on α_{ij} :

$$n_j^2 = \left(\frac{1}{u^c}\right)^2 u_{in_j}^c u_{in_j}^c \quad (\text{no sum on } j) \quad (31)$$

Therefore, although it would not be necessary to actually perform the operations described in equations (30) and (31), the normal and shear modes of crack displacement can be recovered from α_{ij} .

Note furthermore that α_{ij} is generally an asymmetric tensor, and that a symmetric alternative to equations (28) could not be utilized to recover normal and shear modes as described in (30) and (31). As an example, consider the following decomposition of (28) into symmetric and anti-symmetric components

$$\alpha_{ij} = \omega_{1ij} + \omega_{2ij} \quad (32)$$

where

$$\omega_{1ij} \equiv \frac{1}{2}(u_{in_j}^c + u_{jn_i}^c) \quad (33)$$

and

$$\omega_{2ij} \equiv \frac{1}{2}(u_{in_j}^c - u_{jn_i}^c) \quad (34)$$

In order for the anti-symmetric tensor ω_{2ij} to be zero, \hat{u}^c and \hat{n}^c must be parallel vectors, implying pure mode I fracture. In this case ω_{1ij} could be decomposed into a vector (in local coordinates), thus resulting in vector-valued internal state variables. For the case where the cracks in the local volume V_L are randomly oriented and of statistically homogeneous shape and size, the surface integral in equation (29) may be carried out over all cracks. However, if various groups of cracks in V_L are distinguished by markedly different crack normals \hat{n}^c or geometries, then it will be necessary to distinguish between the damage modes in order to retain the kinematic features of the damage process. Therefore, define the locally averaged internal state variable α_{Lij}^n for the n th damage mode as follows:

$$\alpha_{Lij}^n \equiv \frac{1}{V} \int_{S_2^n} u_{in_j}^c dS = \frac{1}{V} \int_{S_2^n} \alpha_{ij} dS \quad (35)$$

where

$$S_2 = \sum_{n=1}^N S_2^n, \quad (36)$$

and N is the number of damage modes. For a continuous fiber laminated composite, the modes might be represented by matrix cracks, interply delamination, fiber fracture, and fiber-matrix debond ($N=4$). For a quasi-isotropic chopped-fiber metal matrix composite, a single isotropic damage tensor might suffice for randomly oriented matrix cracking ($N=1$).

Therefore, if we define σ_{Lij}^{cn} to be the average crack closure stress for the n th damage mode such that

$$\sigma_{Lkl}^{cn} \alpha_{Lkl}^n \equiv \frac{1}{V} \int_{S_2} \sigma_{ij}^c \alpha_{ij}^n dS, \quad (37)$$

it follows from equations (29), (35), (36), and (37) that

$$u_L^c = \sigma_{Lij}^{cn} \alpha_{Lij}^n, \quad (38)$$

where we have assumed that repeated indices n imply summation over the range N . It is clear from the above discussion that the value of N must be sufficiently large to recover the essential physics of the damage process. In a mathematical sense, this implies that, whereas the mapping from α_{ij} to α_{Lij}^n is unique, the inverse should also be true in an approximate sense. However, there is no clearcut definition for the range N which will lead to an accurate description of the internal damage state. Due to the inclusion of crack opening displacements in the description of the internal state variables α_{Lij}^n , these quantities should not be interpreted strictly as "damage" parameters. Since cracks may actually close on unloading (without healing), α_{Lij}^n should be interpreted as damage parameters only during loadup. Note also that both u_i and n_j in equations (35) will be affected by crack interaction in the local volume.

As an example, consider the case of mode I opening of an elliptic crack. For this case, equation (35) will result in dependence of α_{Lij}^n on the volume of the inclusion. Although analytic models for linear elastic bodies with cracks result in response which is dependent on the surface area of cracks only [14-16], it should be pointed out that they also require the average crack diameter. This quantity is replaced herein by the crack opening displacement, which is proportional to the crack

diameter in a linear elastic body. Therefore, specifying the crack opening displacement is equivalent to specifying the crack diameter.

Now consider equation (38) in further detail. The kinetic quantities σ_{Lij}^{cn} may be interpreted as generalized stresses which are energy conjugates to the kinematic strain-like internal state variables α_{Lij}^n . We infer from this that there exists a constitutive relation between these variables of the form

$$\sigma_{Lij}^{cn} = \sigma_{Lij}^{cn}(\epsilon_{Lkl}, T_L, \alpha_{Lkl}^n) \quad , \quad (39)$$

which is history dependent via the explicit dependence on the internal state variables.

Therefore, substituting (39) into (38) will give

$$u_L^c(t_1) = \int_{-\infty}^{t_1} \dot{u}_L^c(t) dt = u_L^c(\epsilon_{Lkl}(t_1), T_L(t_1), \alpha_{Lkl}^n(t_1)) \quad . \quad (40)$$

It is now proposed that u_L^c be expanded in a Taylor series which is second order in each of the arguments in equation (40) as follows:

$$\begin{aligned} u_L^c = & G_{ij}^n \alpha_{Lij}^n + H_{ij}^n \alpha_{Lij}^n \Delta T_L + I_{ijkl}^n \epsilon_{Lij} \alpha_{Lkl}^n + J_{ijkl}^{n\zeta} \alpha_{Lij}^n \alpha_{Lkl}^{\zeta} \Delta T_L \\ & + L_{ijklmn}^{n\zeta} \epsilon_{Lij} \alpha_{Lkl}^n \alpha_{Lmn}^{\zeta} + \frac{1}{2} M_{ijklmn}^n \epsilon_{Lij} \epsilon_{Lkl} \alpha_{Lmn}^n \\ & + N_{ijkl}^n \epsilon_{Lij} \alpha_{Lkl}^n \Delta T_L + P_{ij}^n \alpha_{Lij}^n \Delta T_L^2 + \frac{1}{2} Q_{ijklmnpq}^{n\zeta} \epsilon_{Lij} \epsilon_{Lkl} \alpha_{Lmn}^n \alpha_{Lpq}^{\zeta} \\ & + R_{ijklmn}^{n\zeta} \epsilon_{Lij} \alpha_{Lkl}^n \alpha_{Lmn}^{\zeta} \Delta T_L + S_{ijkl}^{n\zeta} \alpha_{Lij}^n \alpha_{Lkl}^{\zeta} \Delta T_L^2 \\ & + T_{ijklmn}^n \epsilon_{Lij} \epsilon_{Lkl} \alpha_{Lkl}^n \Delta T_L + U_{ijkl}^n \epsilon_{Lij} \alpha_{Lkl}^n \Delta T_L^2 \\ & + V_{ijklmnop}^{n\zeta} \epsilon_{Lij} \epsilon_{Lkl} \alpha_{Lmn}^n \alpha_{Lop}^{\zeta} \Delta T_L + W_{ijklmn}^n \epsilon_{Lij} \epsilon_{Lkl} \alpha_{Lmn}^n \Delta T_L^2 \\ & + X_{ijklmn}^{n\zeta} \epsilon_{Lij} \alpha_{Lkl}^n \alpha_{Lmn}^{\zeta} \Delta T_L^2 + \frac{1}{2} Y_{ijklmn}^{n\zeta} \epsilon_{Lij} \alpha_{Lkl}^n \alpha_{Lmn}^{\zeta} \Delta T_L \\ & + Z_{ijklmnpq}^{n\zeta} \epsilon_{Lij} \epsilon_{Lkl} \alpha_{Lmn}^n \alpha_{Lpq}^{\zeta} \Delta T_L^2 \quad , \quad (41) \end{aligned}$$

where all terms are at least linear in α_{Lij}^n due to the fact

that u_L^c depends explicitly on damage, and $\Delta T_L \equiv T_L - T_R$. Thus, substituting (11) and (41) into equations (23) and neglecting higher order terms yields:

$$\sigma_{Lij} = B_{Lij} + E_{Lij} \Delta T_L + C_{Lijkl} \epsilon_{Lkl} + I_{ijkl}^n \alpha_{Lkl}^n \quad , \quad (42)$$

Equations (42) may be written in the following alternate form for isothermal conditions

$$\sigma_{Lij} = \sigma_{Lij}^R + C'_{Lijkl} \epsilon_{Lkl} \quad , \quad (43)$$

where

$$\sigma_{Lij}^R \equiv B_{Lij} \quad , \quad (44)$$

is the residual stress tensor; and

$$C'_{Lijkl} \epsilon_{Lkl} \equiv C_{Lijkl} \epsilon_{Lkl} + I_{Lijkl}^n \alpha_{Lkl}^n \quad , \quad (45)$$

defines the effective modulus tensor C'_{Lijkl} for any damage state. Note that although equations (43) are similar to Kachanov's model [22], the stiffness reduction is a first order effect of damage. Note also that the inclusion of higher order terms will result in damage dependent residual and thermal stresses, as well as nonlinear stiffness loss as a function of damage.

Equations (42) are the completed description of the stress-strain relationship. Note that these equations reduce to the standard linear thermoelastic equations in the absence of damage ($\alpha_{Lij}^n = 0$).

Damage Growth Laws

The model is completed with the construction of the damage growth laws, which may be described in the following differential equation form:

$$\dot{\alpha}_{Lij}^n = \Omega_{ij}^n(\epsilon_{Lkl}, \dot{\epsilon}_{Lkl}, T_L, \alpha_{Lkl}^n) \quad , \quad (46)$$

or equivalently, when α_{ij}^n are single valued functions of time,

$$\alpha_{Lij}^n(t_1) = \int_{-\infty}^{t_1} \Omega_{ij}^n(\epsilon_{Lkl}(t), T_L(t), \alpha_{Lkl}^u(t)) dt \quad (47)$$

Although the above equations are called "growth" laws they have the more general capability to model such phenomena as healing.

The precise nature of equations (47) is determinable only through a concise experimental program coupled with an understanding of the micromechanics of the medium. Indeed, these growth laws constitute the single most complex link in the model development.

In this section an example of a first generation growth law will be constructed for predicting damage up to the CDS in continuous fiber composites. Experimental evidence suggests that matrix cracks dominate development of the CDS [4-6]. Guided by this observation, a single damage tensor is considered in this section: α_{Lij}^1 representing matrix cracking.

In order to completely define equations (47), it is necessary to construct indicators of both the magnitude and direction of the damage tensor. In this first generation model it is assumed that the direction of the damage tensor is known a priori and does not vary as the damage state changes. Specifically, in a typical laminate, it is assumed that, for this simple example, in accordance with equation (35), the locally averaged resultants of \hat{u}^c and \hat{n}^c are normal to the fiber direction in each ply, as shown in Fig. 4. Thus, for example, in a 0° ply $\alpha_{L22}^1 \neq 0$, and all other components are zero, whereas in a 90° ply, $\alpha_{L11}^1 \neq 0$, and all other components are zero (in global coordinates). In Part II a somewhat more general case of the damage state for matrix cracking will be considered.

Under the above assumptions, the magnitude of the damage tensor is the sole repository for history dependence in each ply. Experimental evidence indicates that for matrix cracking in randomly oriented particulate composites [42] and matrix cracks in fibrous composites [20,21] the growth of damage surface area is related to the energy release rate G by

$$\frac{dS_2}{dN} \propto G^n \quad (48)$$

where S_2 represents crack area, N represents the number of cycles in a fatigue test, and n is some material parameter. Guided by these results, a similar law is constructed here. Equation (48) may be rewritten in the following form:

$$\frac{dS_2}{dt} = kG^n \frac{dN}{dt} \quad (49)$$

so that it follows that

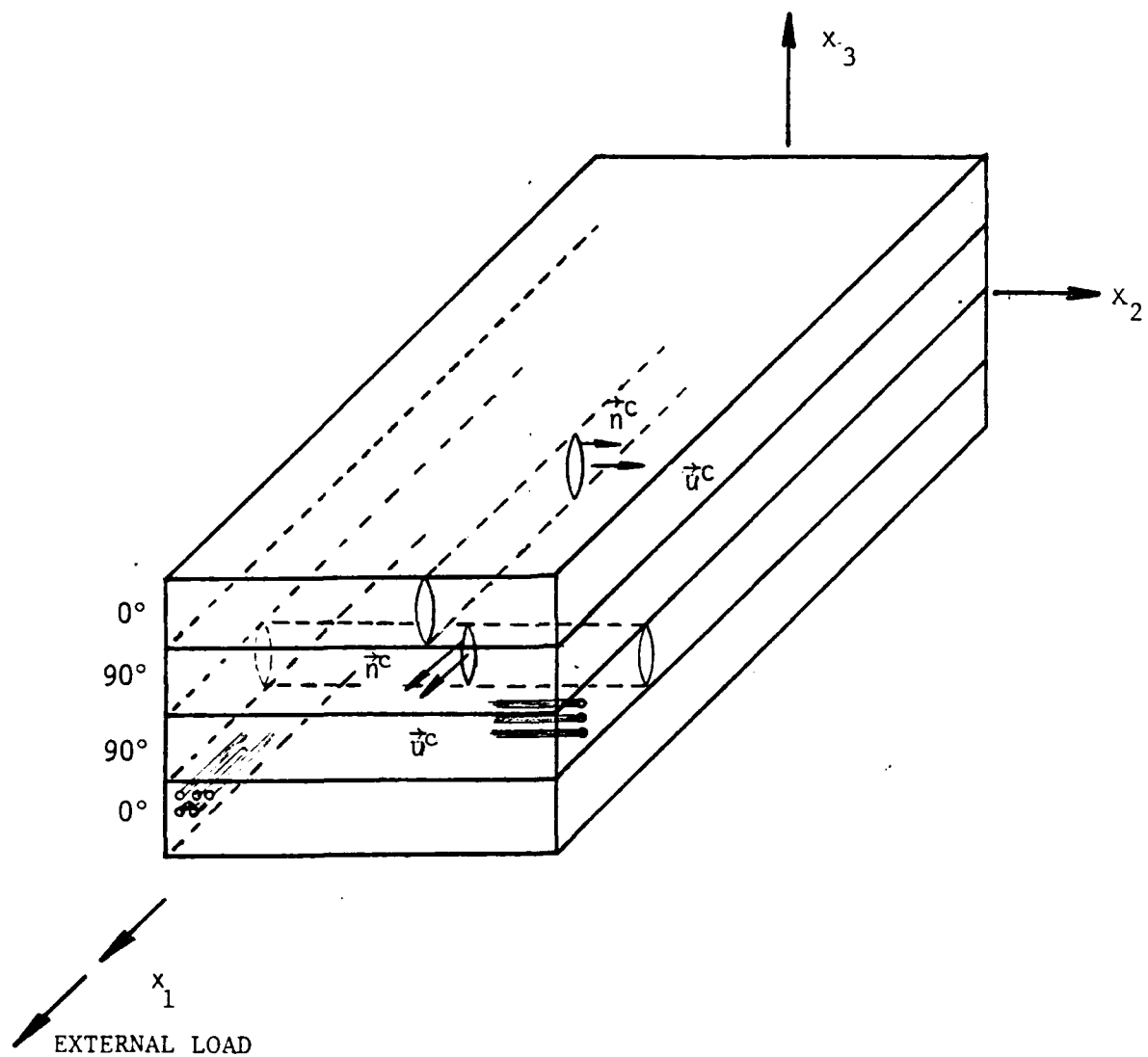


Fig. 4. Assumed Damage Vector Directions in a $[0,90]_s$ Laminate.

$$\dot{\alpha}_{L22}^1 = \frac{d\alpha_{L22}^1}{dS_2} \cdot \frac{dS_2}{dt} = \frac{d\alpha_{L22}^1}{dS_2} \cdot K G^n \cdot \frac{dN}{dt} \quad (50)$$

Assuming that the energy release rate is essentially mode I and therefore depends on the maximum normal strain, the damage growth law for matrix cracking is thus hypothesized to be of the form

$$\begin{aligned} \dot{\alpha}_{L22}^1 &= k_1 \left(\frac{\epsilon_n - \epsilon_{nmin}}{\alpha_{L22}^1} \right)^n \cdot \frac{d\epsilon_n}{dt} \text{ if } \epsilon_{nmin} < \epsilon_n, \text{ and} \\ \dot{\alpha}_{L22}^1 &= k_2 \epsilon_n \text{ if } \epsilon_{nmin} \geq \epsilon_n, \end{aligned} \quad (51)$$

where ϵ_n is the local normal strain component which is normal to the fibers. Furthermore, ϵ_{nmin} is the value of ϵ_n at which matrix cracking initiates. k_1 , k_2 , and n are experimentally determined material parameters which may depend on the initial damage state or on history dependent damage other than matrix cracks. The use of ϵ_n presupposes that the fracture mode is predominantly mode I in nature, which may not be the case in some complex layups. In these cases, mode II and mode III terms may be required. Note that all components of α_{Lij}^1 are zero except α_{L22}^1 , which is nonzero in the local ply coordinate system wherein the fibers are aligned parallel to the local x_1 axis.

Experimental evidence [43] indicates that in crossply laminates with multiple adjacent crossplies in sequence, it is not uncommon to observe matrix cracks which are curved rather than normal to the plane of the ply. For these cases it is necessary to carry components of α_{Lij}^1 in both the x_2 and x_3 coordinate directions. Although it is hypothesized that these components may perhaps be determinable from the orientation of the maximum normal strain ϵ_n , this issue is under further investigation by the authors.

Equations (51) complete the description of the damage model for the case of matrix cracking. Integration of these equations in time will lead to current values of the damage tensor which is input to constitutive equations (42). Fig. 5 shows a typical growth history for a specimen subjected to monotonically increasing deformation $u(L)$. It should be pointed out, however, that these equations may be extremely nonlinear and as such must in some cases be integrated numerically with stiff integration schemes [44].

CONCLUSION

Stress-strain relations have been developed herein which account for various forms of damage in continuous fiber composites. Furthermore, a damage growth law has been proposed for matrix cracking in fibrous composites. The model developed

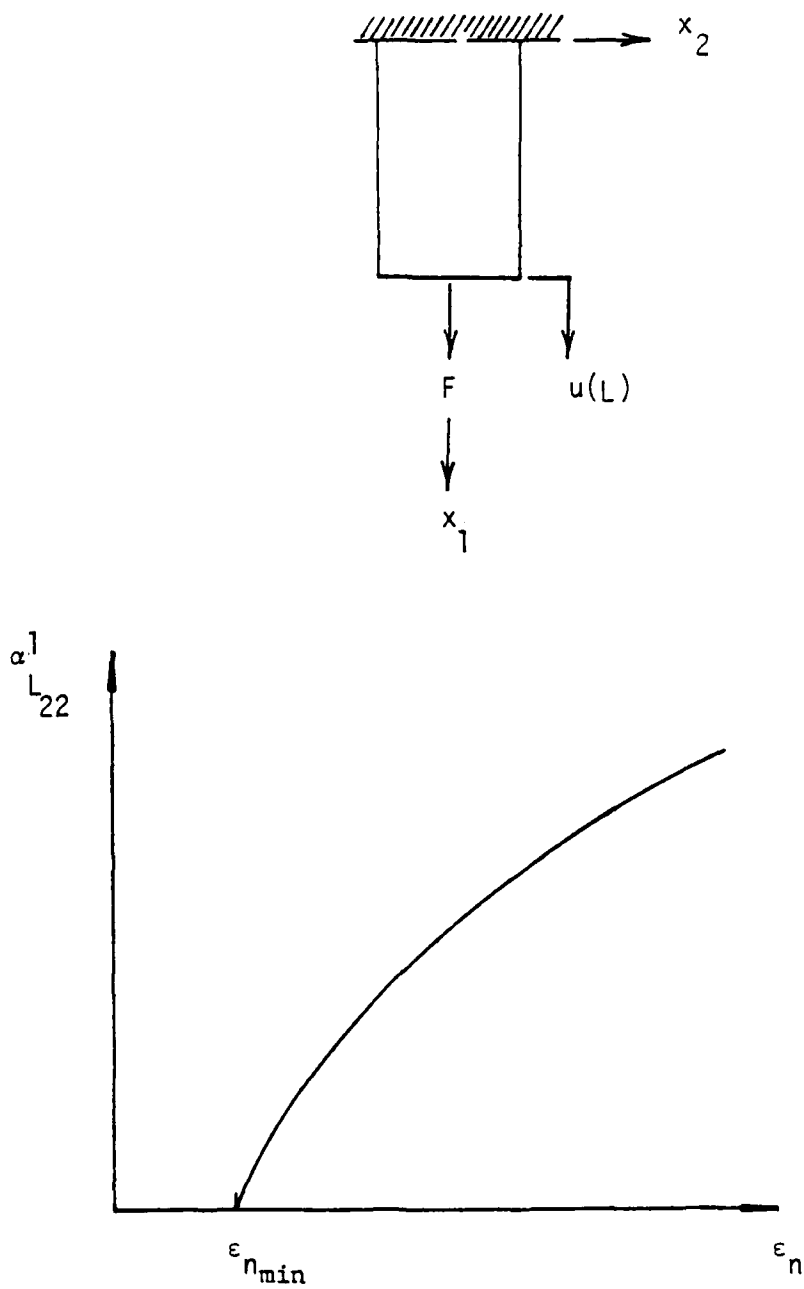


Fig. 5. Typical Growth of Damage in a Specimen with Matrix Cracks.

herein is thus a complete description necessary to characterize the thermomechanical constitution of a fibrous composite with matrix cracks (excluding failure).

The actual use of this model is complicated by the requirement for numerous experimentally determined quantities, as well as the necessity to determine locally based observable state variables by analytic methods. The construction of these parameters constitutes an entire separate research effort which is considered in Part II.

Finally, it should be pointed out that although an internal state variable growth law has been proposed herein only for matrix cracks, the model is in principle applicable to more complex damage states in laminated composites, and research is underway to consider other damage modes.

ACKNOWLEDGEMENT

The authors gratefully acknowledge the support for this research which was provided by the Air Force Office of Scientific Research under contract no. AFOSR-84-0067.

The authors wish to express thanks to Dr. R.A. Schapery of the Civil Engineering Department at Texas A&M University for his guidance on this research.

The authors also wish to express thanks to Dr. Ramesh Talreja of the Technical University of Denmark for his helpful discussions on damage mechanics.

REFERENCES

1. Stinchcomb, W.W., and Reifsnider, K.L., "Fatigue Damage Mechanisms in Composite Materials: A Review", Fatigue Mechanisms, Proc. of ASTM-NBS-NSF Symp., Kansas City, MO., May 1978, J.J. Fong, ed., ASTM STP 679, 1979; pp. 762-787.
2. Hahn, H.T., "Fatigue Behavior and Life Prediction of Composite Laminates", Composite Materials: Testing and Design (Fifth Conf.), ASTM STP 674, 1979; pp. 383-417.
3. Lehman, M.W., "An Investigation of Intra-Ply Microcrack Density Development in a Cross-Ply Laminate," Texas A&M University Mechanics and Materials Research Center, MM 3724-80-11, December, 1980.
4. Stinchcomb, W.W., Reifsnider, K.L., Yeung, P., and Masters, J., "Effect of Ply Constraint on Fatigue Damage Development in Composite Material Laminates," Fatigue of Fibrous Composite Materials, ASTM STP 723, 1981, pp. 65-84.
5. Highsmith, A.L., Stinchcomb, W.W., and Reifsnider, K.L., "Stiffness Reduction Resulting from Transverse Cracking in Fiber-Reinforced Composite Laminates," Virginia Polytechnic Institute and State University, VPI-E-81.33, November, 1981.
6. Reifsnider, K.L., and Jamison, R., "Fracture of Fatigue-Loaded Composite Laminates," Int. J. Fatigue, 1982, pp. 187-197.
7. Leichti, K.M., Masters, J.E., Ulman, D.A., and Lehman, M.W., "SEM/TEM Fractography of Composite Materials," AFWAL-TR-82-4035, September, 1982.
8. Ulman, D.A., "Cumulative Damage Model for Advanced Composite Materials," Semi-annual Report No. 3 (FZM-7070) and No. 4 (FZM-7106), Air Force Materials Laboratory, 1983.
9. Reifsnider, K.L., and Highsmith, A., "Characteristic Damage States: A New Approach to Representing Fatigue Damage in Composite Laminates," Materials, Experimentation, and Design in Fatigue, Westbury House, Surrey, England, pp. 246-260, 1981.
10. Hill, R., The Mathematical Theory of Plasticity, Oxford University Press, London, 1950.
11. Tsai, Stephen W., "Strength Theories of Filamentary Structures," in R.T. Schwartz and H.S. Schwartz (eds.), Fundamental Aspects of Fiber Reinforced Plastic Composites, Wiley Interscience, New York, 1968, pp. 3-11.
12. O'Brien, T.K., "An Evaluation of Stiffness Reduction as a Damage Parameter and Criterion for Fatigue Failure in Composite Materials," Ph.D. Dissertation, Virginia Polytechnic Institute and State University, October, 1978.

13. Budiansky, B. and O'Connell, R.J., "Elastic Moduli of a Cracked Body," Int. J. of Solids Structures, Vol. 12, 1981.
14. Horii, H. and Nemat-Nasser, S., "Overall Moduli of Solids with Microcracks: Load-Induced Anisotropy," J. Mech. & Phys. Solids, Vol. 31, No. 2, pp. 155-171, 1983.
15. Laws, N., Dvorak, G.J., and Hejazi, M., "Stiffness Changes in Unidirectional Composites Caused by Crack Systems," Mechanics of Materials, Vol. 2, 1983.
16. Margolin, L.G., "Elastic Moduli of a Cracked Body," Int. J. Fracture, Vol. 22, 1983.
17. Mura, T., Micromechanics of Defects in Solids, Martinus Nijhoff Publ., The Hague, Boston, 1982.
18. Schapery, R.A., "On Viscoelastic Deformation and Failure Behavior of Composite Materials with Distributed Flaws," Advances in Aerospace Structures and Materials, ASME AD-01, 1981, pp. 5-20.
19. Schapery, R.A., "Models for Damage Growth and Fracture in Nonlinear Viscoelastic Particulate Composites," Proc. 9th U.S. National Cong. Appl. Mech., August, 1982.
20. Chou, P.C., Wang, A.S.D., and Miller, H., "Cumulative Damage Model for Advanced Composite Materials," AFWAL-TR-82-4-83, September, 1982.
21. Wang, A.S.D., and Bucinell, R.B., "Cumulative Damage Model for Advanced Composite Materials," Interim Report No. 6, Feb. 1984.
22. Kachanov, L.M., "On the Creep Fracture Time," Izv. AN SSR, Otd. Tekhn. Nauk, No. 8, pp. 26-31, 1958 (in Russian).
23. Poursartrip, A., et al., "Damage Accumulation during Fatigue of Composites," Cambridge University (England) Dept. of Engineering, Nov. 1981, p. 29.
24. Miner, M.A., "Cumulative Damage in Fatigue," J. Appl. Mech., Vol. 12, 1945, p. 159.
25. Hashin, Z., and Rotem, A., "A Cumulative Damage Theory of Fatigue Failure," AFOSR-TR-77-0717, 1977.
26. Coleman, B.D., and Gurtin, M.E., "Thermodynamics with Internal State Variables," Journal of Chemical Physics, Vol. 47, pp. 597-613, 1967.
27. Lemaitre, J. and Chaboche, J.L., "Aspect Phenomenologique de la Rupture par Endommagement," Journal de Mecanique Appliquee, Vol. 2, 1978, pp. 317-365.

28. Bodner, S.R., "A Procedure for Including Damage in Constitutive Equations for Elastic-Viscoplastic Work-Hardening Materials," Physical Non-Linearities in Structural Analysis, Springer-Verlag, Berlin, 1981, pp. 21-28.
29. Krajcinovic, D., and Fonseka, G.U., "The Continuous Damage Theory of Brittle Materials-Part I - General Theory," J. Appl. Mech., Vol. 48, 1981, pp. 809-815.
30. Krajcinovic, D., "Continuum Damage Mechanics," Applied Mechanics Reviews, Vol. 37, No. 1, January 1984.
31. Krajcinovic, D., "Continuous Damage Mechanics Revisted: Basic Concepts and Definitions," To appear in Journal of Applied Mechanics, 1984.
32. Davidson, L., and Stevens, A.L., "Thermomechanical Constitution of Spalling Elastic Bodies," J. Appl. Phys., Vol. 44, No. 2, pp. 668-674, 1973.
33. Kratochvil, J., and Dillon, O.W., Jr., "Thermodynamics of Elastic-Plastic Materials as a Theory with Internal State Variables," J. of Applied Physics, Vol. 40, 1969, pp. 3207-3218.
34. Kratochvil, J. and Dillon, O.W., Jr., "Thermodynamics of Crystalline Elastic-Visco-Plastic Materials," J. of Applied Physics, Vol. 44, 1970, pp. 1470-1478.
35. Talreja, R., "A Continuum Mechanics Characterization of Damage in Composite Materials," Proc. R. Soc. London, Vol. 399A, 1985, pp. 195-216.
36. Talreja, R., "Residual Stiffness Properties of Cracked Composite Laminates," Danish Center for Applied Mathematics and Mechanics, The Technical University of Denmark, Report No. 277, Feb., 1984.
37. Talreja, R., "Transverse Cracking and Stiffness Reduction in Composite Laminates," Danish Center for Appl. Mathematics and Mechanics, The Technical University of Denmark, July, 1984.
38. Arenburg, R.T., "Analysis of the Effect of Matrix Degradation of Fatigue Behavior of a Graphite/Epoxy Laminate," Texas A&M Mechanics and Materials Center (M.S. Thesis), MM 3724-82-2, May, 1982.
39. Hashin, Z., "Analysis of Composites-A Survey," J. Appl. Mech., Vol. 50, pp. 481-505, 1983.
40. Coleman, B.D., and Noll, W., "The Thermodynamics of Elastic Materials with Heat Conduction and Viscosity," Archive for Rational Mechanics and Analysis, Vol. 13, p. 167, 1963.

41. Kachanov, M., "Continuum Model of Medium with Cracks," Journal of the Engineering Mechanics Division, ASCE, Vol. EM5, pp. 1039-1051, 1980.

42. Schapery, R.A. and Riggins, M., "Development of Cyclic Nonlinear Viscoelastic Constitutive Equations for Marine Sediment," MM 3168-82-4, Texas A&M University, May 1982.

43. Norvell, R.G., "An Investigation of Damage Accumulation in Graphite/Epoxy Laminates," Texas A&M University M.S. Thesis, August, 1985.

44. Gear, C.W., "The Automatic Integration of Stiff Ordinary Differential Equations," Information Processing, Vol. 1, 1969, pp. 187-193.

APPENDIX

Consider a local volume element with some damage state, where the crack faces are defined as traction free surfaces, as shown in Fig. A1 (a1). For convenience we show only one crack, although in actuality the damage must be statistically homogeneous in V_L . Now replace the actual cracks with fictitious cracks which are described by the bounding surface between elastic and inelastic response near cracks, as shown in (a2). We define this surface to be S_2 . In order to insure that the total mechanical states in the two systems are identical, the fictitious case must include tractions labelled T_i^F on S_2 .

Now suppose that V_L is subjected to boundary tractions on S_1 in the undamaged state as shown in (b1). We define an equivalent elastic problem in which the surface S_2 described in (a2) is cut from V_L and elastic tractions T_i^E are applied on S_2 so that the total mechanical states of systems (b1) and (b2) are equivalent.

The actual system of interest is described in (a1). However, for pragmatic reasons we wish to replace the actual system with a fictitious system with equivalent mechanical state. To do this, we first replace (a1) with (a2), which by definition has equivalent mechanical state. Next, we define a system equivalent to (a2), such that

$$T_i^C \equiv T_i^F - T_i^E \Rightarrow T_i^F = T_i^C + T_i^E \quad , \quad (A1)$$

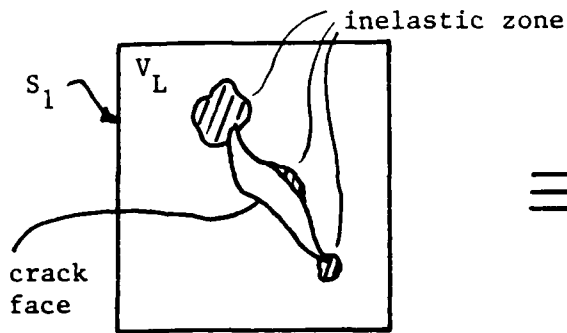
as shown in (c). Integrating the balance of energy (4) over the local volume and dividing through by the local volume results in

$$\frac{1}{V_L} \int_{V_L} \dot{u} dV - \frac{1}{V_L} \int_{V_L} \sigma_{ij} \dot{\epsilon}_{ij} dV + \frac{1}{V_L} \int_{V_L} q_{j,j} dV = \frac{1}{V_L} \int_{V_L} r dV \quad . \quad (A2)$$

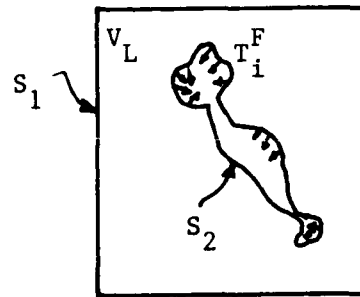
Now consider the second term in equation (A2). Recall that since σ_{ij} is a symmetric tensor

$$\sigma_{ij} \dot{\epsilon}_{ij} = \frac{1}{2} \sigma_{ij} (\dot{u}_{i,j} + \dot{u}_{j,i}) = \sigma_{ij} \dot{u}_{i,j} \quad . \quad (A3)$$

Thus, assuming that the stresses are negligible in V_C , the volume enclosed by S_2 , using the divergence theorem and substituting Cauchy's formula gives

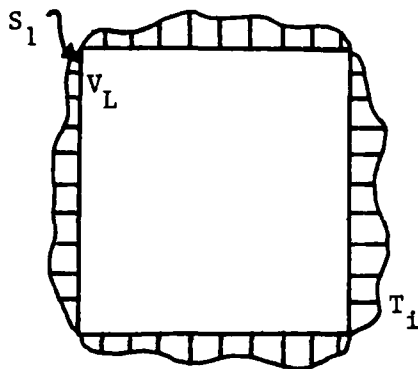


(a1) actual damage

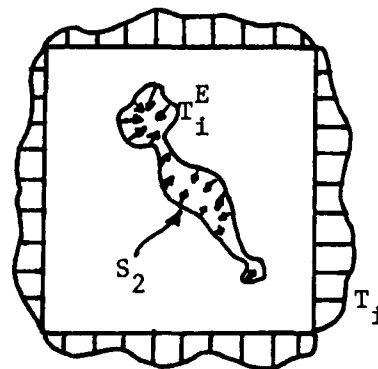


(a2) fictitious equivalent damage

(a) Replacement of actual crack with fictitious crack

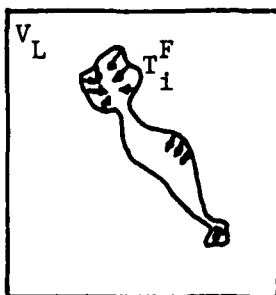


(b1) undamaged V_L

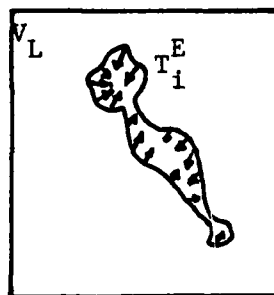


(b2) equivalent V_L with internal surfaces described in (a2)

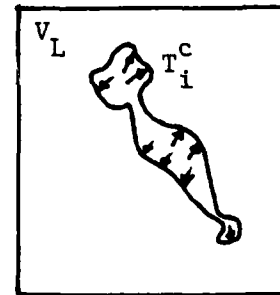
(b) V_L subjected to tractions without damage



(c1) same as (a2)



(c2) same as (b2)



(c3) effective tractions

Fig. A1. Description of Local Volume Element with Damage

$$\begin{aligned}
\frac{1}{V_L} \int_{V_L} \sigma_{ij} \dot{\epsilon}_{ij} dV &= \frac{1}{V_L} \int_{V_L - V_C} \sigma_{ij} \dot{u}_{i,j} dV = \frac{1}{V_L} \int_{S_1} T_i \dot{u}_i dS + \frac{1}{V_L} \int_{S_2} T_i^F \dot{u}_i dS \\
&= \frac{1}{V_L} \int_{S_1} T_i \dot{u}_i dS + \frac{1}{V_L} \int_{S_2} T_i^E \dot{u}_i dS + \frac{1}{V_L} \int_{S_2} T_i^C \dot{u}_i dS \quad , \quad (A4)
\end{aligned}$$

where n_i are the components of the unit outer normal vector to the surface $S = S_1 + S_2$. Now define

$$\dot{u}_L^C \equiv - \frac{1}{V_L} \int_{S_2} T_i^C \dot{u}_i dS \quad , \quad (A5)$$

which is the effective specific mechanical power output of the continuum due to the crack surface tractions. This term contains both the mechanical power due to crack extension as well as the mechanical power due to apparent stiffness loss caused by existing cracks. For the special case of a reversible process this is the time rate of change of surface energy release per unit local volume due to cracking in V_L . Furthermore, define

$$\epsilon_{Lij} \equiv \frac{1}{V_L} \int_{S_1} \frac{1}{2} (u_i n_j + u_j n_i) dS \quad , \quad (A6)$$

and

$$\sigma_{Lij} \equiv \frac{1}{V_L} \int_{S_1} \frac{1}{2} (\sigma_{im} n_m x_j + \sigma_{jm} n_m x_i) dS = \frac{1}{V_L} \int_{V_L} \sigma_{ij} dV \quad , \quad (A7)$$

Therefore, for the case of either spacially uniform surface tractions or displacements which are linear in coordinates on S_1 one readily obtains

$$\sigma_{Lij} \epsilon_{Lij} = \frac{1}{V_L} \int_{S_1} \sigma_{ij} \dot{u}_i n_j dS = \frac{1}{V_L} \int_{S_1} T_i \dot{u}_i dS \quad , \quad (A8)$$

Although it will be assumed in the remainder of this paper that the above conditions are satisfied, they need only be approximately true if V_L is statistically homogeneous. Thus,

equation (A4) becomes

$$\frac{1}{V_L} \int_{V_L} \sigma_{ij} \dot{\epsilon}_{ij} dV = \sigma_{Lij} \dot{\epsilon}_{Lij} + \frac{1}{V_L} \int_{S_2} T_i^E \dot{u}_i dS - \dot{u}_L^c \quad , \quad (A9)$$

Define also

$$q_{Li,j} \equiv \frac{1}{V_L} \int_{S_1} q_i n_j dS \quad , \quad (A10)$$

and

$$r_L \equiv \frac{1}{V_L} \int_{V_L} r dV \quad , \quad (A11)$$

Now define

$$\dot{u}_{EL} \equiv \frac{1}{V_L} \int_{V_L} \dot{u} dV - \frac{1}{V_L} \int_{S_2} T_i^E \dot{u}_i dS \quad , \quad (A12)$$

which can be seen from Fig. A1 (b) to be the equivalent internal energy rate that would be produced in the body without cracks. Note that u_{EL} is not path dependent since it represents elastic response. Substituting equations (A4), (A5), (A9), (A10), (A11), and (A12) into equation (A2) yields the following locally averaged balance of energy:

$$\dot{u}_{EL} + \dot{u}_L^c - \sigma_{Lij} \dot{\epsilon}_{Lij} + q_{Lj,j} = r_L \quad , \quad (A13)$$

We now define the effective internal energy u_L' (which may be path dependent) such that

$$\dot{u}_L' \equiv \dot{u}_{EL} + \dot{u}_L^c \quad , \quad (A14)$$

Substitution of (A14) into (A13) results in

$$\dot{u}_L' - \sigma_{Lij} \dot{\epsilon}_{Lij} + q_{Lj,j} = r_L \quad , \quad (A15)$$

which can be seen to be equivalent in form to energy balance law (4).

In order to construct a similar statement for entropy production inequality (5), first multiply through by T and then integrate over the local volume V_L and divide by this quantity to obtain

$$\frac{1}{V_L} \int_{V_L} \dot{s} T dV - \frac{1}{V_L} \int_{V_L} r dV + \frac{1}{V_L} \int_{V_L} T (q_j/T)_{,j} dV \geq 0 \quad . \quad (A16)$$

Now define

$$T_L \equiv \frac{1}{V_L} \int_{V_L} T dV \quad , \quad (A17)$$

and

$$\dot{s}_L \equiv \frac{1}{T_L V_L} \int_{V_L} \dot{s} T dV \quad , \quad (A18)$$

so that substitution of definitions (A11), (A17) and (A18) into (A16) will result in

$$\dot{s}_L T_L - r_L + \frac{1}{V_L} \int_{V_L} T (q_j/T)_{,j} dV \geq 0 \quad . \quad (A19)$$

Now note that the last term in (A19) may be written as follows using the product rule:

$$\frac{1}{V_L} \int_{V_L} T (q_j/T)_{,j} dV = \frac{1}{V_L} \int_{V_L} q_{j,j} dV - \frac{1}{V_L} \int_{V_L} (q_j g_j/T) dV \quad . \quad (A20)$$

Define now

$$T_{L,j} \equiv \frac{1}{V_L} \int_{S_1} T n_j dS \quad . \quad (A21)$$

Thus, for the case when T is a linear function of coordinates in V_L , definitions (A10) and (A21) may be substituted into (A20) and this result into (A19) to obtain

$$\dot{s}_I - \frac{r_L}{T_L} + \left(\frac{q_L}{T_L} \right)_{,j} \geq \dot{s}_c \geq 0, \quad (A22)$$

where

$$\dot{s}_c \equiv (1/T_L V_L) \int_{V_L} (q_j g_j / T) dV - (1/T_L^2 V_L^2) \int_{V_L} q_j dV : \frac{1}{V_L} \int_{V_L} g_j dV. \quad (A23)$$

\dot{s}_c can be shown to be strictly nonnegative with the assumption that T is everywhere nonnegative, along with equation (9).

We now assume that the local volume is small enough compared to B that the standard procedure may be utilized to obtain the linear conservation of momentum equations [39]

$$\sigma_{Lji,j} = 0, \quad (A24)$$

similar to pointwise equations (2), and the conservation of angular momentum may also be obtained

$$\sigma_{Lij} = \sigma_{Lji}, \quad (A25)$$

similar to equations (3). Thus, it is assumed that no body moments are introduced via material inhomogeneity or other sources. This assumption must be relaxed when the model is utilized for interply delamination, since in this case the local volume element goes through the entire laminate thickness.

Equations (A24), (A25), (A15), (A22), (A14), (A18), (A5), (A7), and (A6) are rewritten as equations (12) through (20), respectively, in the main text.

APPENDIX 6.3

unclassified

SECURITY CLASSIFICATION OF THIS PAGE

REPORT DOCUMENTATION PAGE

1a. REPORT SECURITY CLASSIFICATION Unclassified			1b. RESTRICTIVE MARKINGS		
2a. SECURITY CLASSIFICATION AUTHORITY			3. DISTRIBUTION/AVAILABILITY OF REPORT Unlimited		
2b. DECLASSIFICATION/DOWNGRADING SCHEDULE					
4. PERFORMING ORGANIZATION REPORT NUMBER(S)			5. MONITORING ORGANIZATION REPORT NUMBER(S)		
6a. NAME OF PERFORMING ORGANIZATION Aerospace Engineering Dept.		6b. OFFICE SYMBOL (If applicable)	7a. NAME OF MONITORING ORGANIZATION Air Force Office of Scientific Research		
6c. ADDRESS (City, State and ZIP Code) Texas A&M University College Station, TX 77843			7b. ADDRESS (City, State and ZIP Code) Bolling AFB Washington, D.C. 20332		
8a. NAME OF FUNDING/SPONSORING ORGANIZATION AFOSR		8b. OFFICE SYMBOL (If applicable)	9. PROCUREMENT INSTRUMENT IDENTIFICATION NUMBER Grant No. AFOSR-84-0067		
8c. ADDRESS (City, State and ZIP Code) same			10. SOURCE OF FUNDING NOS.		
			PROGRAM ELEMENT NO.	PROJECT NO.	TASK NO.
11. TITLE (Include Security Classification) A Thermomechanical Constitutive Theory for....			WORK UNIT NO.		
12. PERSONAL AUTHOR(S) D.H. Allen, C.E. Harris, and S.E. Groves					
13a. TYPE OF REPORT Interim		13b. TIME COVERED FROM _____ TO _____		14. DATE OF REPORT (Yr., Mo., Day) October 1985	
15. PAGE COUNT 38					
16. SUPPLEMENTARY NOTATION					
17. COSATI CODES			18. SUBJECT TERMS (Continue on reverse if necessary and identify by block number)		
FIELD	GROUP	SUB. GR.	composites		
			internal state variables		
			damage		
			continuum mechanics		
			laminate analysis		
19. ABSTRACT (Continue on reverse if necessary and identify by block number) A continuum mechanics approach is utilized herein to develop a model for predicting the thermomechanical constitution of initially elastic composites subjected to both monotonic and cyclic fatigue loading. In this model the damage is characterized by a set of second order tensor valued internal state variables representing locally averaged measures of specific damage states such as matrix cracks, fiber-matrix debonding, interlaminar cracking, or any other damage state. Locally averaged history dependent constitutive equations are constructed utilizing constraints imposed from thermodynamics with internal state variables. In Part I the thermodynamics with internal state variables was constructed and it was shown that suitable definitions of the locally averaged field variables led to useful thermodynamic constraints on a local scale containing statistically homogeneous damage. Based on this result the Helmholtz free energy was then expanded in a Taylor series in terms of strain, temperature, and the internal state variables to obtain the stress-strain relation for composites with damage. In Part II, the three dimensional tensor equations					
20. DISTRIBUTION/AVAILABILITY OF ABSTRACT UNCLASSIFIED/UNLIMITED <input checked="" type="checkbox"/> SAME AS RPT. <input type="checkbox"/> DTIC USERS <input type="checkbox"/>			21. ABSTRACT SECURITY CLASSIFICATION Unclassified		
22a. NAME OF RESPONSIBLE INDIVIDUAL Anthony K. Amos			22b. TELEPHONE NUMBER (Include Area Code) (202) 767-4937		22c. OFFICE SYMBOL

A THERMOMECHANICAL CONSTITUTIVE THEORY FOR ELASTIC
COMPOSITES WITH DISTRIBUTED DAMAGE

PART II: Application to Matrix Cracking
in Laminated Composites

by

D.H. Allen

C.E. Harris

and

S.E. Groves

Aerospace Engineering Department
Texas A&M University
College Station, Texas 77843

AD-A175 017

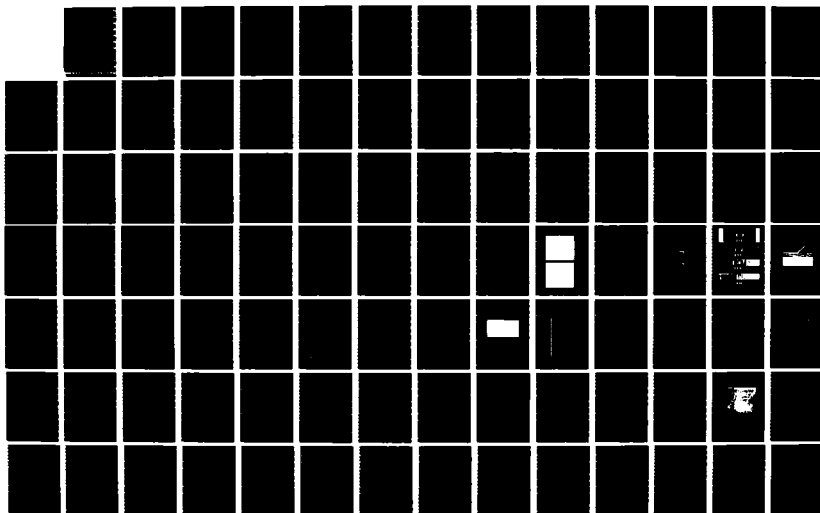
RESEARCH ON DAMAGE MODELS FOR CONTINUOUS FIBER
COMPOSITES(U) TEXAS A AND M UNIV COLLEGE STATION
MECHANICS AND MATERIALS CE D H ALLEN ET AL FEB 86

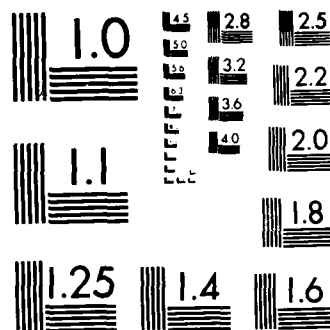
3/4

UNCLASSIFIED

MM-5023-86-5 AFOSR-TR-86-2077 AFOSR-84-0067 F/G 11/4

NL





MICROCOPY RESOLUTION TEST CHART
NATIONAL BUREAU OF STANDARDS-1963-A

A THERMOMECHANICAL CONSTITUTIVE THEORY FOR ELASTIC COMPOSITES WITH DISTRIBUTED DAMAGE

PART II: Application to Matrix Cracking in Laminated Composites

by

D.H. Allen
C.E. Harris
S.E. Groves

ABSTRACT

A continuum mechanics approach is utilized herein to develop a model for predicting the thermomechanical constitution of initially elastic composites subjected to both monotonic and cyclic fatigue loading. In this model the damage is characterized by a set of second order tensor valued internal state variables representing locally averaged measures of specific damage states such as matrix cracks, fiber-matrix debonding, interlaminar cracking, or any other damage state. Locally averaged history dependent constitutive equations are constructed utilizing constraints imposed from thermodynamics with internal state variables. In Part I the thermodynamics with internal state variables was constructed and it was shown that suitable definitions of the locally averaged field variables led to useful thermodynamic constraints on a local scale containing statistically homogeneous damage. Based on this result the Helmholtz free energy was then expanded in a Taylor series in terms of strain, temperature, and the internal state variables to obtain the stress-strain relation for composites with damage. In Part II, the three dimensional tensor equations from Part I [1] are simplified using symmetry constraints. After introducing engineering notation and expressing the constitutive equations in the standard laminate coordinate system, a specialized constitutive model is developed for the case of matrix cracks only. The potential of the model to predict degradation of effective stiffness components is demonstrated by solving the problem of transverse matrix cracks in the 90° layer of several crossply laminates.

To solve the example problems, the undamaged moduli are determined from experimental data. The internal state variable for matrix cracking is then related to the strain energy release rate due to cracking by utilizing linear elastic fracture mechanics. These values are then utilized as input to a modified laminate analysis scheme to predict effective stiffnesses in a variety of crossply laminates. The values of effective (damage degraded) stiffnesses predicted by the constitutive model are in agreement with experimental results. The agreement obtained in these example problems, while limited to transverse matrix cracks only, demonstrates the potential of the constitutive model to predict degraded stiffnesses.

INTRODUCTION

In Part I it was hypothesized that damage can be modeled in continuous fiber composites by a set of second order tensor valued internal state variables which represent locally averaged measures of matrix cracking, interlaminar delamination, and other damage mechanisms on a scale which is assumed to be small compared to the scale of the boundary value problem of interest. Continuum mechanics with internal state variables [1] was then utilized to construct stress-strain relations in which all components of the degraded modulus tensor can be determined for a given damage state.

The purpose of this paper (Part II) is to demonstrate how the model may be utilized to predict the reduced stiffness of laminates which are subjected to known damage states. This procedure is illustrated via specific examples in which there is a single damage mode consisting of matrix cracking. It is shown that the properties of a single lamina with known damage can be utilized as given properties to obtain favorable comparisons to experimental results for specific laminates.

The model application is accomplished by first imposing symmetry constraints, reducing to generalized plane stress, and finally performing the laminate integration.

SIMPLIFICATION OF THE MODEL

We now consider the stress-strain relation described in equations (42) through (45) of Part I (see Appendix A). For the examples to be considered herein, it is assumed that all residual stress components are zero ($\sigma_{Lij}^R=0$), and that there are no temperature changes ($\Delta T_L=0$).

Reduction to Single-Index Notation

By incorporating the symmetry of the stress and strain tensors, the quadratic dependence of the Helmholtz free energy on strain, and the Voigt single index notation [2], the constitutive equations reduce to (see Appendix A)

$$\sigma_i = C_{ij} \epsilon_j + I \eta_k^{\eta} \alpha_k^{\eta} \quad . \quad (1)$$

Although we have dropped the subscript L, all quantities in equations (1) represent locally averaged measures. The subscripts i and j range from 1 to 6, the subscript k ranges from 1 to 9, and the superscript η ranges from 1 to N, the number of damage modes.

At this point, further reductions can be made to the number of unknown constants in equations (1) only by specifying the material symmetry and specific damage modes of interest.

Material Symmetry Constraints

Material symmetries may now be utilized to further simplify the constitutive equations. The material in question is assumed to be initially transversely isotropic in the undamaged state on the local scale, where the plane of isotropy is the $x_2 - x_3$ plane shown in Fig. 2. In the undamaged state the modulus tensor C_{ij} is given by [3]

$$[C] = \begin{bmatrix} C_{11} & C_{12} & C_{12} & 0 & 0 & 0 \\ C_{12} & C_{22} & C_{23} & 0 & 0 & 0 \\ C_{12} & C_{23} & C_{22} & 0 & 0 & 0 \\ 0 & 0 & 0 & C_{44} & 0 & 0 \\ 0 & 0 & 0 & 0 & C_{55} & 0 \\ 0 & 0 & 0 & 0 & 0 & C_{55} \end{bmatrix}, \quad (2)$$

where $C_{44} = 2(S_{22} - S_{23})$, and S_{22} and S_{23} are the associated compliance terms.

It is assumed that the crack induces orthotropy in three planes: the plane of the crack, the plane in which the crack opening displacement \vec{u}^c and crack normal \vec{n}^c lie, and a third plane which is orthogonal to the first two. Therefore, the damage tensor I_{ik}^1 is an orthotropic tensor containing 15 unknown constants in the coordinates described by the crack geometry (see Appendix B), given by

$$[I^1] = \begin{bmatrix} I_{11}^1 & I_{12}^1 & I_{13}^1 & 0 & 0 & 0 & 0 & 0 & 0 \\ I_{21}^1 & I_{22}^1 & I_{23}^1 & 0 & 0 & 0 & 0 & 0 & 0 \\ I_{31}^1 & I_{32}^1 & I_{33}^1 & 0 & 0 & 0 & 0 & 0 & 0 \\ 0 & 0 & 0 & I_{44}^1 & I_{45}^1 & 0 & 0 & 0 & 0 \\ 0 & 0 & 0 & 0 & 0 & I_{56}^1 & I_{57}^1 & 0 & 0 \\ 0 & 0 & 0 & 0 & 0 & 0 & 0 & I_{68}^1 & I_{69}^1 \end{bmatrix}, \quad (3)$$

Thus, the complete constitutive equations (1) (assuming the damage growth law is known) require the determination of 5 independent material constants for the undamaged modulus tensor C_{Lij} , and 15 independent constants for the damage tensor, I_{ik}^1 . It should be noted, however, that the planes of these symmetries will not coincide unless the crack

displacement \vec{u}^c is oriented parallel to the x_1 , x_2 , or x_3 axis in ply coordinates.

Application to Matrix Cracking in Continuous Fiber Laminates

As discussed in the introduction, the capability of the constitutive model will be demonstrated by considering the case of matrix cracking in continuous fiber laminated composites. An example of this damage state is shown schematically in Fig. 1. In order to apply the proposed constitutive model to this system we first examine the response of a single ply subjected to transverse matrix cracking, as shown in Fig. 2. Assuming that the crack geometry is symmetric about normals to each of the ply coordinates, the internal state variable associated with matrix cracking is represented in ply coordinates by

$$[\alpha_k^1] = [0 \quad \alpha_2^1 \quad 0 \quad 0 \quad \alpha_5^1 \quad 0 \quad 0 \quad \alpha_8^1 \quad 0] \quad , \quad (4)$$

where the single subscripted notation is defined by equations (7a). This implies that the crack normal \vec{n}^c in a single ply is parallel to the local x_2 coordinate. Furthermore, the crack-opening displacement, \vec{u}^c , may contain three components.

Note that a second order tensor representation of the internal state variable may be insufficient if the crack displacement \vec{u}^c or normal \vec{n}^c rotates during the load history. In this case a higher order tensor may be required [4]. However, since the crack is matrix dominated and constrained by fibers, time dependent rotation is assumed to be negligible and the second order tensorial representation is considered adequate in the current model. Recent experimental evidence [5] indicates that cracks do indeed change planes sometimes in multi-ply laminates with several adjacent crossplies at the same orientation. However, the crack plane is essentially straight in each ply, the level at which the local volume is constructed for matrix cracks.

For the single damage mode of matrix cracking described in Fig. 1, equations (1) reduce to

$$\sigma_i = C_{ij} \epsilon_j + I_{12}^1 \alpha_2^1 + I_{15}^1 \alpha_5^1 + I_{18}^1 \alpha_8^1 \quad . \quad (5)$$

For relatively thin laminates it is useful to apply the conditions of generalized plane stress where the out-of-plane shear stresses σ_4 and σ_5 are neglected. Applying these conditions to equations (5), imposing the symmetry constraints described in equations (2) and (3), and using matrix notation results in

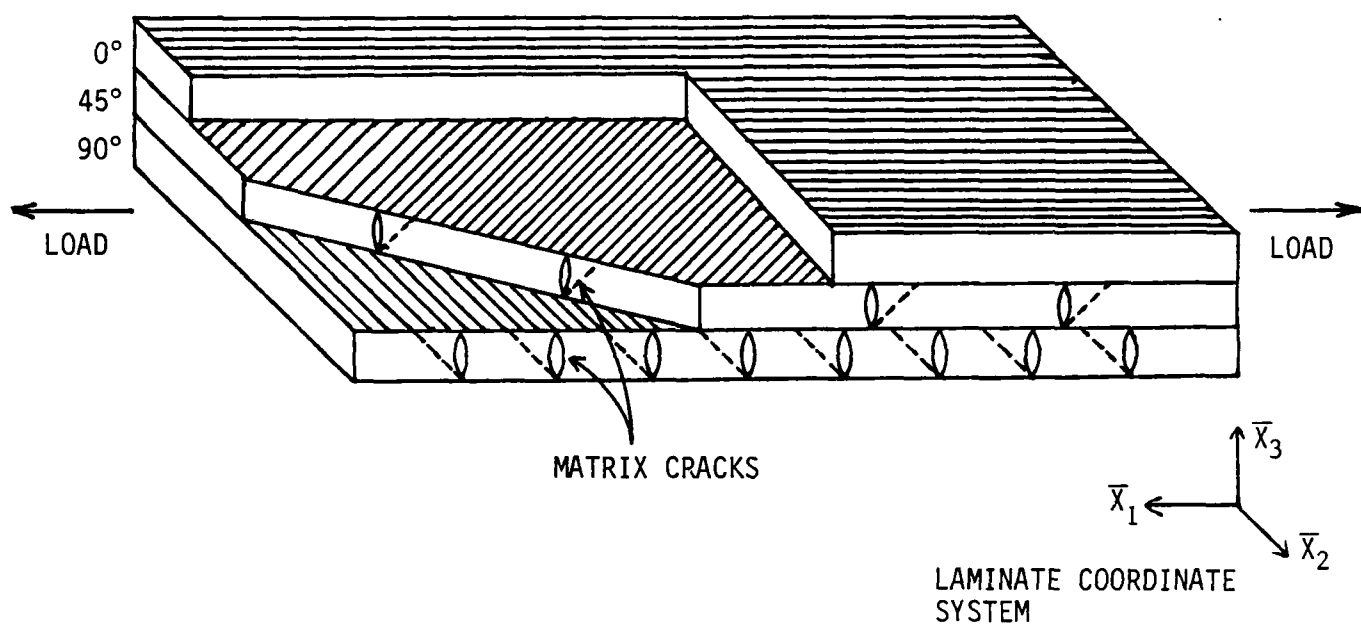


Fig. 1. Matrix Cracking in a Laminated Continuous Fiber Composite

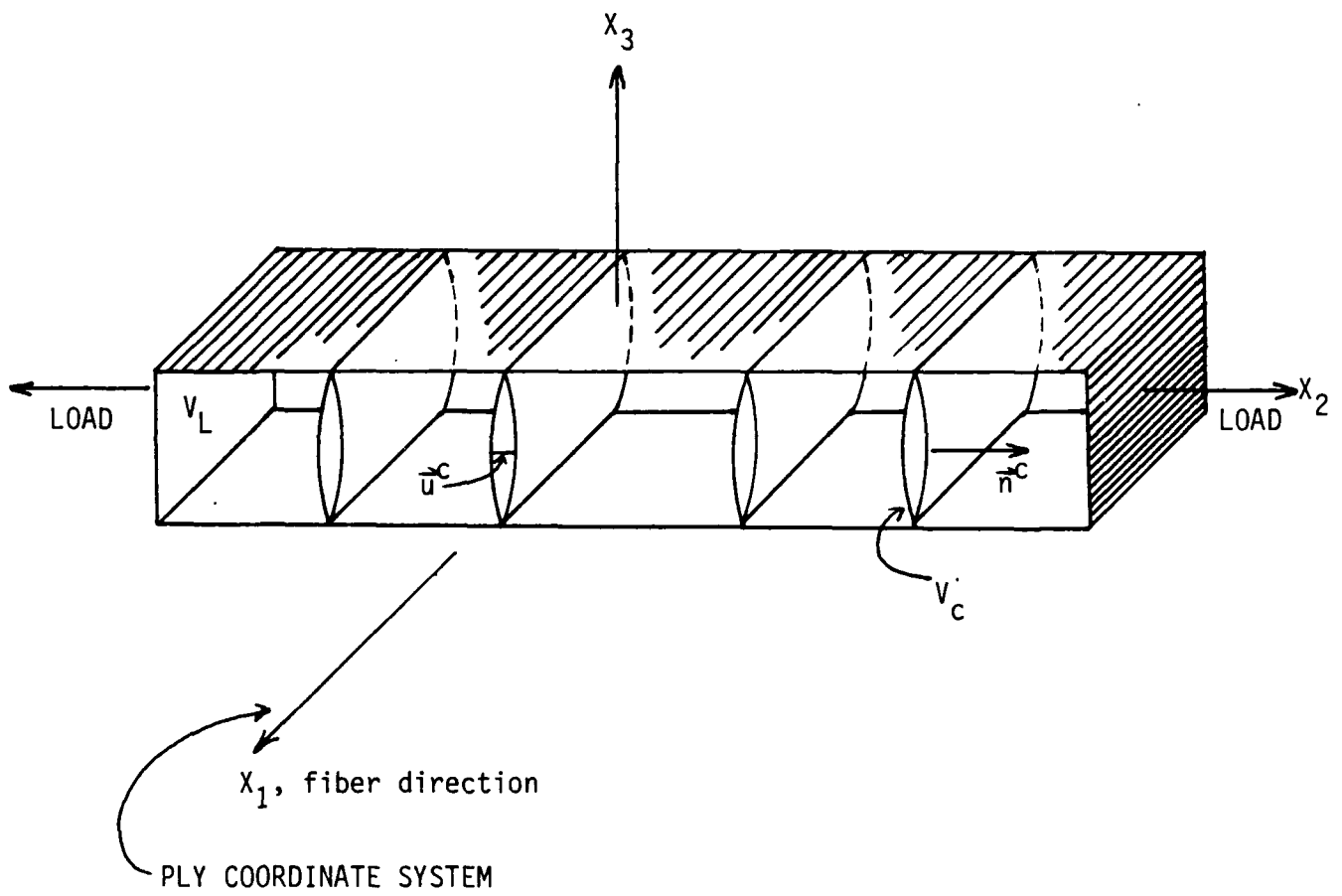


Fig. 2. Transverse Matrix Cracking in a Single Ply

$$\begin{Bmatrix} \sigma_1 \\ \sigma_2 \\ \sigma_3 \\ \sigma_6 \end{Bmatrix} = \begin{bmatrix} C_{11} & C_{12} & C_{12} & 0 \\ C_{12} & C_{22} & C_{23} & 0 \\ C_{12} & C_{23} & C_{33} & 0 \\ 0 & 0 & 0 & C_{66} \end{bmatrix} \begin{Bmatrix} \varepsilon_1 \\ \varepsilon_2 \\ \varepsilon_3 \\ \varepsilon_6 \end{Bmatrix} + [I^1] \{\alpha^1\} \quad , (6)$$

where

$$[I^1] = \begin{bmatrix} 0 & I_{12}^1 & 0 & 0 & 0 & 0 & 0 & 0 & 0 \\ 0 & I_{22}^1 & 0 & 0 & 0 & 0 & 0 & 0 & 0 \\ 0 & I_{32}^1 & 0 & 0 & 0 & 0 & 0 & 0 & 0 \\ 0 & 0 & 0 & 0 & 0 & 0 & 0 & I_{68}^1 & 0 \end{bmatrix} \quad . (7)$$

Note that the fifth column of the coefficient matrix in equations (5) is zero due to the fact that α_5 does not contribute to the in-plane stresses in the generalized plane stress reduction. Furthermore, note that I_{12}^1 , I_{22}^1 and I_{32}^1 are the coefficients of the effect of loss of stiffness on the normal stresses σ_1 , σ_2 and σ_3 , respectively. Finally, note that I_{68}^1 is the coefficient determining the influence of stiffness loss on the in-plane shear stress σ_6 . It is apparent from the above equations that for generalized plane stress conditions there are ten unknown material constants to be determined for the case of matrix cracking.

Determination of the I Matrix

Theoretically it is possible to determine the I matrix directly from experimental data. This may be accomplished by subjecting test coupons to prescribed deformation histories, removing the deformations, and nondestructively evaluating the damage state. The residual stresses will determine the I matrix. However, in graphite/epoxy laminates this procedure breaks down due to the fact that although the crack surfaces may be determined nondestructively using x-rays and edge replicas, the crack opening displacements cannot be accurately determined experimentally. Therefore, an alternative approach is used herein to evaluate the I matrix.

As described in Appendix C, for the case considered in this paper, at least to a first approximation, it can be shown that

$$\begin{aligned} I_{12}^1 &= -C_{12} & I_{22}^1 &= -C_{22} \\ I_{32}^1 &= -C_{23} & I_{68}^1 &= -C_{66} \end{aligned} \quad . (8)$$

Therefore, the number of unknown material constants is reduced to a total of six for the case considered herein.

Laminate Equations

In order to utilize single lamina equations to characterize the response of multilayered laminates, it is necessary to globally average the local ply constitutive equations. This is accomplished herein by imposing the Kirchhoff hypothesis for thin plates [5]. However, higher order plate or shell theories could be utilized also. Generalized plane strain conditions are imposed rather than plane strain because this is consistent with the stress state in equations (6) (A detailed description of the global averaging is given in Appendix D). The resulting equations are as follows:

$$\{N\} = [A]\{\epsilon^0\} + \{D\} \quad , \quad (9)$$

or

$$\{\epsilon^0\} = [A^{-1}](\{N\} - \{D\}) \quad , \quad (10)$$

where

$$A_{ij} \equiv \sum_{k=1}^n (\bar{C}_{ij})_k t_k \quad , \quad (11)$$

and

$$\{D\} \equiv \sum_{k=1}^n ([\bar{I}^1]_k (z_k - z_{k-1}) \{\bar{\alpha}^1\}_k \quad , \quad (12)$$

$[\bar{I}^1]_k$ and $\{\bar{\alpha}^1\}_k$ are in laminate coordinates as defined in Appendix E, and $\{\epsilon^0\}$ contains the laminate midplane strains. Furthermore, k specifies the ply and t_k is the ply thickness. For convenience, we have assumed that no moments are produced by the damage (in the absence of curvature), which is assumed to hold for symmetric laminates.

In order to determine the effective stiffness for any damage state, we evaluate the rate of change of $\{N\}$ with respect to the midsurface strains $\{\epsilon^0\}$ during unloading, that is,

$$S'_{im} = \partial N_i / \partial \epsilon_m^0 = A_{ij} + \sum_{k=1}^n \sum_{j=1}^9 (\bar{I}_{ij})_k (z_k - z_{k-1}) (\partial \bar{\alpha}_j / \partial \epsilon_m^0)_k \quad , \quad (13)$$

where S'_{im} is defined to be the effective stiffness. Experimental work on graphite/epoxy laminates has shown that S'_{11} is very nearly a constant during unloading, implying that, at least as a first approximation for crossply laminates,

$$(\partial \bar{\alpha}_1 / \partial \epsilon_1^0)_k \approx \text{constant} \quad k=1, \dots, n \quad (14)$$

THE INTERNAL STATE VARIABLE FOR MATRIX CRACK DAMAGE

Equation (41) in Part I [1] gave the second order Taylor series expansion of the local energy per unit volume due to cracking, u_L^C , in terms of strain, ϵ_{Lij} , temperature, ΔT , and the internal state variable (ISV), α_{Lij} . For demonstration purposes, the predictions of this paper are being confined to symmetric cross-ply laminates loaded in uniaxial tension. For this case, α_2^1 is the only component of the ISV of interest and is defined (in the ply coordinate system) as

$$\alpha_2^1 = \frac{1}{V_L} \int_{S_2} u_2 dS \quad (15)$$

where u_2 is the crack-opening displacement, V_L is the local element volume and S_2 is the surface area of matrix cracks. Furthermore, we will consider only the case of load-up in the fixed grip mode where matrix crack extension occurs at constant strain. Therefore, if the higher order terms in the Taylor series expansion are neglected, the local energy due to cracking reduces to

$$u_L^C = (A + I_{22}^1 \epsilon_2) \alpha_2^1 \quad (16)$$

where A is a constant. Since equation (16) applies to load-up in the fixed grip mode, α_2^1 can be related to the strain energy release rate, G_m , for matrix cracking by noting that u_L^C is related to G_m as follows:

$$u_L^C(t) = -\frac{1}{V_L} \int_0^{S_2(t)} G_m dS \quad (17)$$

where it is assumed that the initial matrix crack surface area is zero and $S_2(t)$ is the surface area at time t . If we make the assumption that the energy stored due to residual damage is negligible, then the constant A in equation (16) is zero, and equating (16) and (17) yields

$$I_{22}^1 \epsilon_2^1 \alpha_2^1 = -\frac{1}{V_L} \int_0^{S_2(t)} G_m dS \quad , \quad (18)$$

for stable crack growth. In order to properly account for crack interaction an expression for G_m will be determined experimentally.

Using the standard definition of strain energy release rate

$$G_m = -\frac{1}{B} \frac{\partial U}{\partial a} \quad , \quad (19)$$

and noting that matrix crack surface area is defined as

$$S = 2Ba \quad , \quad (20)$$

the strain energy release rate can be expressed in terms of matrix crack surface area as follows

$$G_m = -2 \frac{\partial U}{\partial S} \quad . \quad (21)$$

Furthermore, the strain energy in a 90° layer is defined by

$$U = \frac{1}{2} E_{22} \epsilon_2^2 \quad , \quad (22)$$

for a uniform applied strain, ϵ_2 , in an elastic material. Assuming the applied strain is constant, substituting (22) into (21) results in

$$G_m = -V_L \epsilon_2^2 \frac{\partial E_{22}}{\partial S} \quad . \quad (23)$$

It is noted that Equation (23) is similar to the expression for strain energy release rate written in terms of test specimen compliance.

The rule of mixtures yields the following expression for the loading direction modulus of a cross-ply laminate:

$$E_x = \frac{pE_{11} + qE_{22}}{p+q} \quad , \quad (24)$$

where p is the number of 0° plies and q is the number of 90° plies. Assuming that matrix cracks are confined to the 90° plies,

$$\frac{\partial E_x}{\partial S} = \frac{q}{p+q} \frac{\partial E_{22}}{\partial S} \quad . \quad (25)$$

Substituting (25) into (23) gives

$$G_m = -V_L \epsilon_2^2 \frac{p+q}{q} \frac{\partial E_x}{\partial S} \quad . \quad (26)$$

If the right hand side of equation (26) is determined experimentally from a laminate that has a 90° layer that is a single ply thick, the resulting strain energy release rate can be utilized for other layups by observing that the strain energy release rate for a ply in a layer that is n plies thick is given by (See Appendix F.)

$$(G_m)_1 = -n V_L \epsilon_2^2 \left(\frac{p+q}{q} \right) \left[\frac{\partial E_x}{\partial S} \right]_{1 \text{ ply layer}} \quad , \quad (27)$$

where V_L is the volume of a single ply. Equation (27) can now be substituted into equation (18) to obtain the expression for the ISV of a single 90° ply for matrix crack extension during load-up. The resulting equation is

$$a_2^1 = \epsilon_2 \frac{n(p+q)}{I_{22}^1 q} \int_0^{S_2(t)} \frac{\partial E_x}{\partial S} dS \quad . \quad (28)$$

The integral term in equation (28) can be evaluated as follows:

$$\int_0^{S_2(t)} \frac{\partial E_x}{\partial S} dS = \int_{E_{x0}}^{E_{x1}} dE_{x1} = E_{x1} - E_{x0} \quad , \quad (29)$$

where E_{x0} is the undamaged elastic modulus and E_{x1} is the degraded modulus corresponding to damage state $S_2(t_1)$. Substituting (29) into (28) and rearranging, the ISV for load-up

is expressed as

$$\alpha_2^1 \Big|_{\substack{\text{load-up} \\ \text{at } S_2(t_1)}} = \varepsilon_2 \cdot n \frac{(p+q)}{q} \frac{E_{x0}}{I_{22}} \left(\frac{E_{x1}}{E_{x0}} \Big|_{S_2(t_1)} - 1 \right) \quad . \quad (30)$$

Although it is possible for matrix crack surface area to increase during unloading, in the current development this effect is assumed to be negligible. Therefore, on unloading α_2^1 depends only on the crack-closure displacement, u_2 in equation (15), and would go to zero on complete crack closure. Assuming that the crack-closure displacement is linear with strain and the matrix crack surface area is constant, equation (15) can be rewritten as

$$\alpha_2^1 \Big|_{\text{unloading}} = c \varepsilon_2 \quad , \quad (31)$$

where c is a constant of proportionality.

The constants in equations (30) and (31) must be determined from experimental data. Considering a tensile test with a load and unloading cycle, at the instant of load reversal the expressions for the ISV for load-up and unloading must be equal. Therefore, setting equation (30) equal to (31) and rearranging, gives the following relationship

$$c \Big|_{S_2(t_1)} = n \frac{(p+q)}{q} \frac{E_{x0}}{I_{22}} \left(\frac{E_{x1}}{E_{x0}} \Big|_{S_2(t_1)} - 1 \right) \quad . \quad (32)$$

It should be noted that all matrix cracking information is contained in the term E_{x1}/E_{x0} . Since equation (32) applies only to a single 90° ply, E_{x1} was determined from the experimental results of the $[0/90/0]_S$ laminate. The following expression was obtained from a least squares curve fit to the experimental values of E_{x1}/E_{x0} versus S_1 :

$$E_{x1}/E_{x0} = 0.9969 - 0.061607 \cdot S_2(t_1) + 0.046230 \cdot S_2(t_1)^2 \quad . \quad (33)$$

Recalling equation (13), it is seen that the effective stiffness of a laminate can be obtained by specifying $\partial \alpha_2^1 / \partial \varepsilon_2$. On unloading this is given by equation (31) to be

$$\partial \alpha_2^1 / \partial \varepsilon_2 = c \quad . \quad (34)$$

Therefore, equations (32) and (33) are used with laminate equations (13) to predict the effective stiffness of any laminate.

MODEL COMPARISON TO EXPERIMENT

The model has been utilized to predict the damage dependent reduced stiffness of several crossply laminates. This has been accomplished by utilizing the laminate stiffness equations (13), in conjunction with the damage evaluation procedure described in the previous section. The reduced stiffnesses predicted by the model have been compared to experimental results obtained from graphite/epoxy coupons composed of Hercules AS4/3502.

The coupons were obtained from laminates fabricated from prepreg tape using a hot press technique in the Mechanics and Materials Center at Texas A&M University. Quasi-static tensile tests were conducted on an Instron 1128 screw driven uniaxial testing machine. Matrix crack damage states were evaluated by x-ray radiography and edge replication. Further details of these procedures are contained in reference [5]. Initial undamaged lamina properties are given in Table 1. These properties were obtained experimentally from $[0]_8$, $[90]_8$ and $\pm[45]_{2s}$ laminates. Energy release rates were obtained from $[0,90,0]$ control coupons. Experimental results for stiffness loss as a function of surface area of matrix cracks are given in Fig. 3.

The lamina properties and strain energy release rate described above were used as input to the model to produce the predicted results for the $[0,90]_s$, $[0,90_2]_s$, $[0,90,0]_s$, and $[0,90_3]_s$ laminates shown in Figs. 4 through 7. As shown in the figures, the comparisons to the experimentally determined values of reduced stiffness are quite good in all cases.

SUMMARY AND CONCLUSIONS

A model for predicting the stiffness loss in laminated composites as a function of microstructural damage has been proposed in this two part paper. In part I the general theoretical framework was constructed for elastic composites with damage. In part II the model has been specialized for the case of matrix cracks in crossply laminates. In this process the following key developments have been reported:

- 1) material symmetry constraints have been imposed on the damage constant tensor I_{ijkl} ;
- 2) the damage tensor α_{ij} has been reduced for the case of plane stress;
- 3) an approximate procedure has been proposed for obtaining the damage constant tensor;
- 4) damage dependent laminate equations have been constructed; and
- 5) the internal state for any crossply layup has been found to be derivable from energy release rates experimentally obtained from a single layup.

The model has been demonstrated to be accurate in predicting the damage dependent reduced stiffness of several graphite/epoxy crossply laminates with matrix cracks.

Current and future development of the model will deal with the following issues:

1) application of the model to laminates with both matrix cracks and interply delaminations;

2) application of the model to layups more complex than crossply laminates; and

3) development of internal state variable growth laws for matrix cracking and interply delamination.

Table 1. Material Properties for Hercules AS4/3502

Lamina Properties

Longitudinal Modulus	E_{11}	$21.0 \times 10^6 \pm 2.0\% \text{ psi}$
Transverse Modulus	E_{22}	$1.39 \times 10^6 \pm 2.1\% \text{ psi}$
Shear Modulus	G_{12}	$0.694 \times 10^6 \text{ psi}$
Poisson's Ratio	ν_{12}	$0.310 \pm 3.7\%$
Longitudinal Strength	F_{tu1}	$326,000 \pm 3.5\% \text{ psi}$
Transverse Strength	F_{tu2}	$11,085 \pm 9.8\% \text{ psi}$
Long. Failure Strain	ϵ_{tu1}	$0.0144 \pm 4.6\% \text{ in/in}$
Tran. Failure Strain	ϵ_{tu2}	$0.00773 \pm 6.7\% \text{ in/in}$

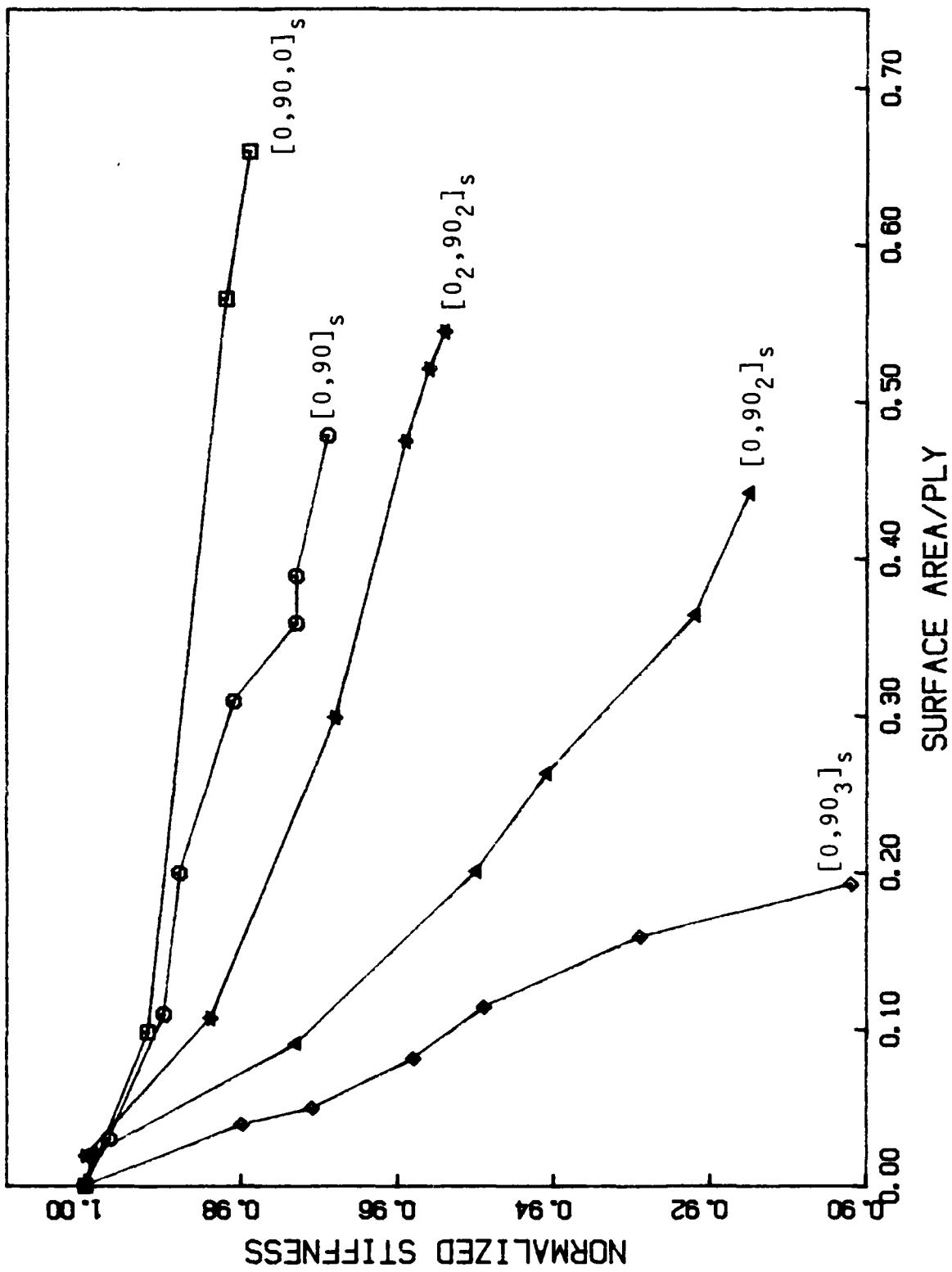


Fig. 3. Experimental Results for Stiffness Loss vs. Crack Area for Several Crossply Laminates

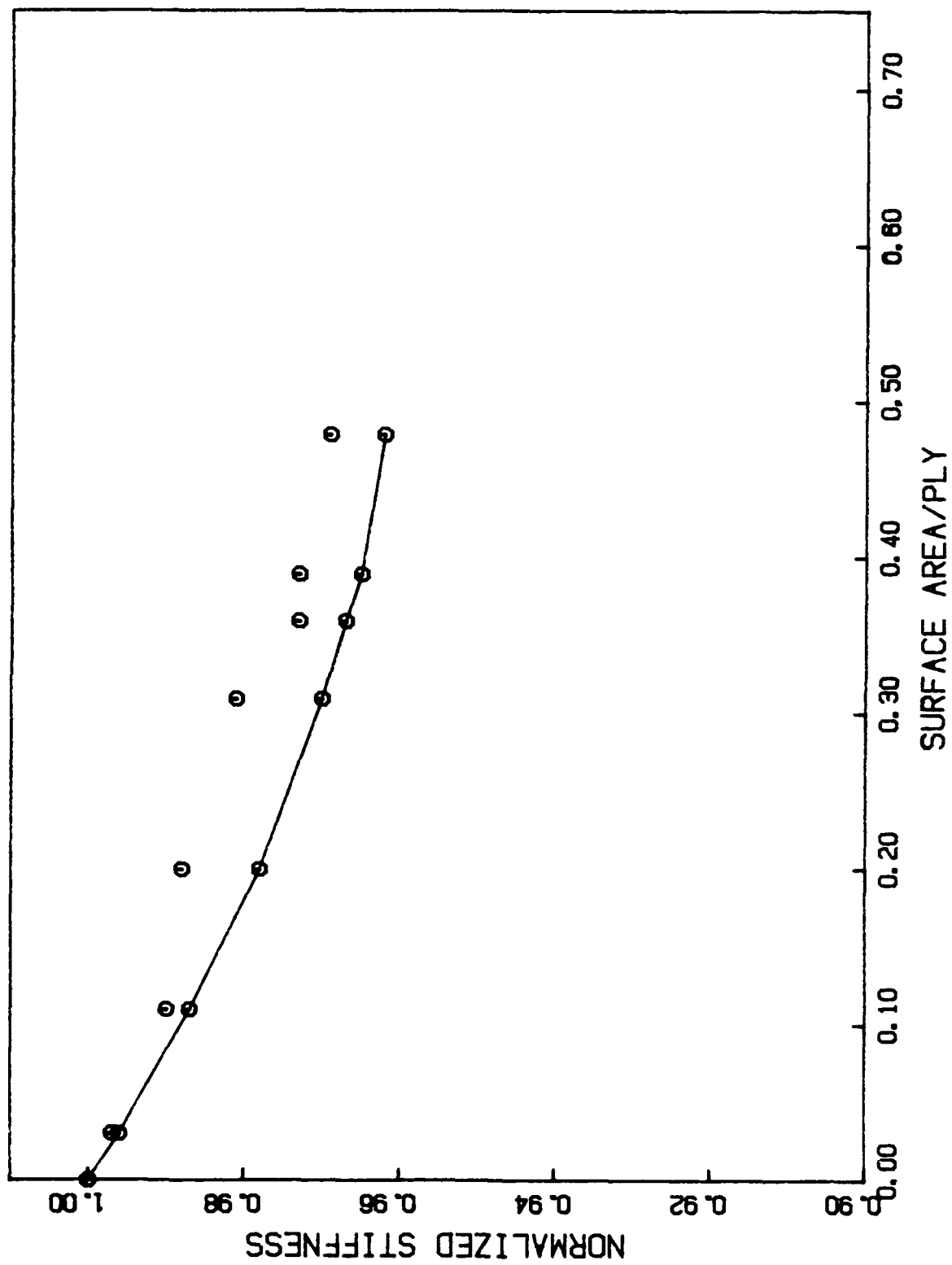


Fig. 4. Model vs. Experiment for $[0,90]_s$ Laminate

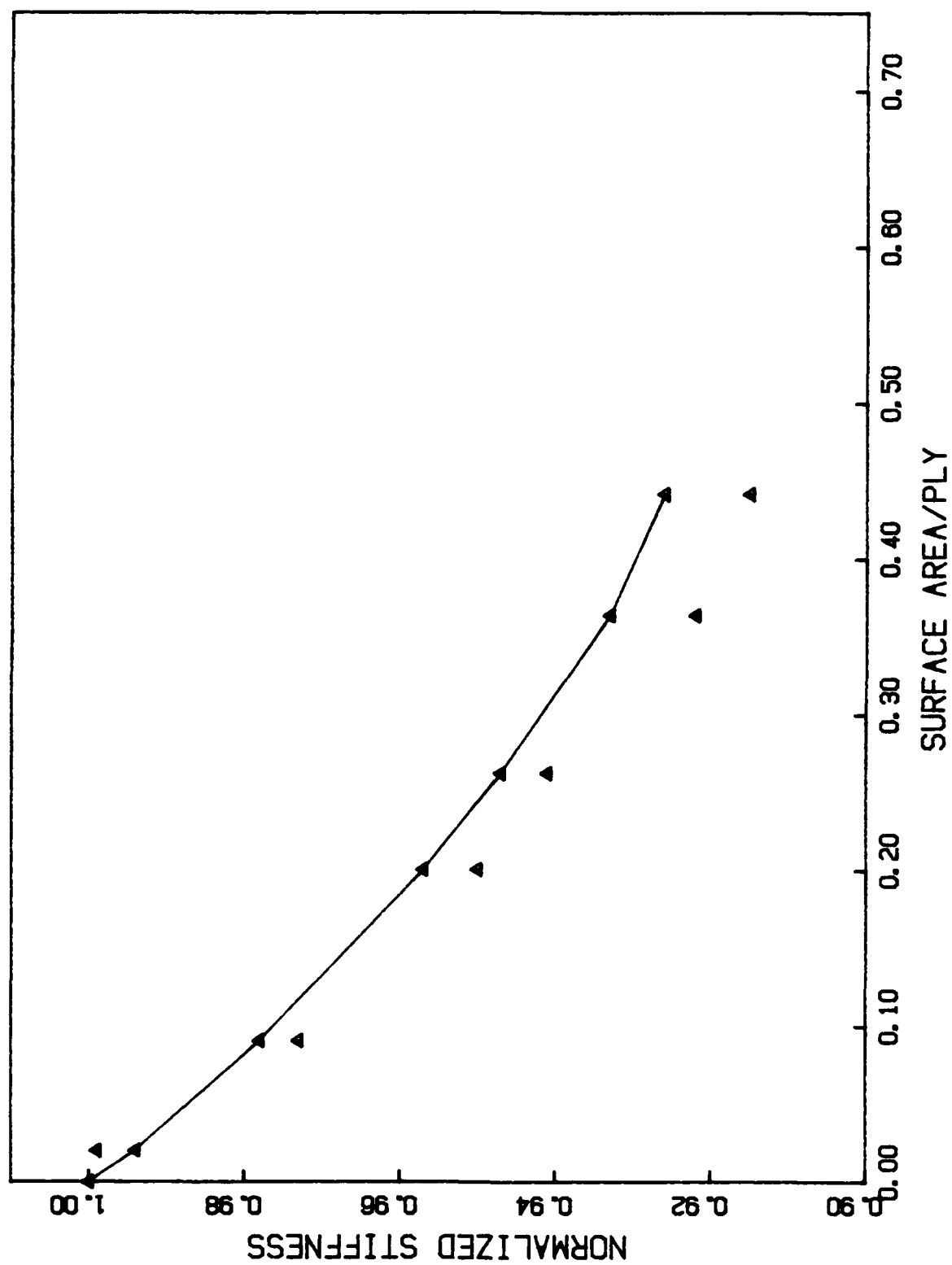


Fig. 5. Model vs. Experiment for $[0,90_2]_s$ Laminate

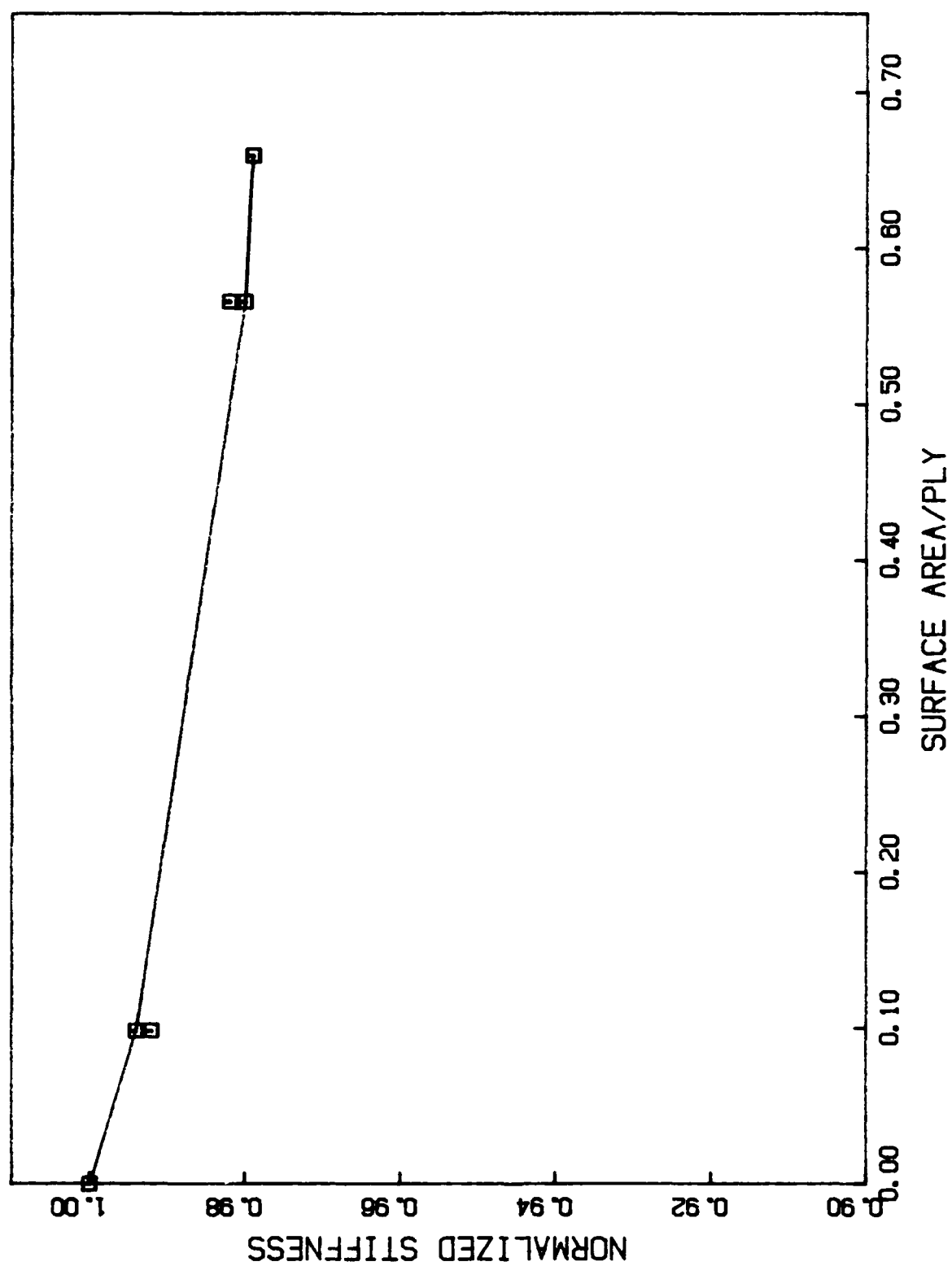


Fig. 6. Model vs. Experiment for $[0,90,0]_s$ Laminate

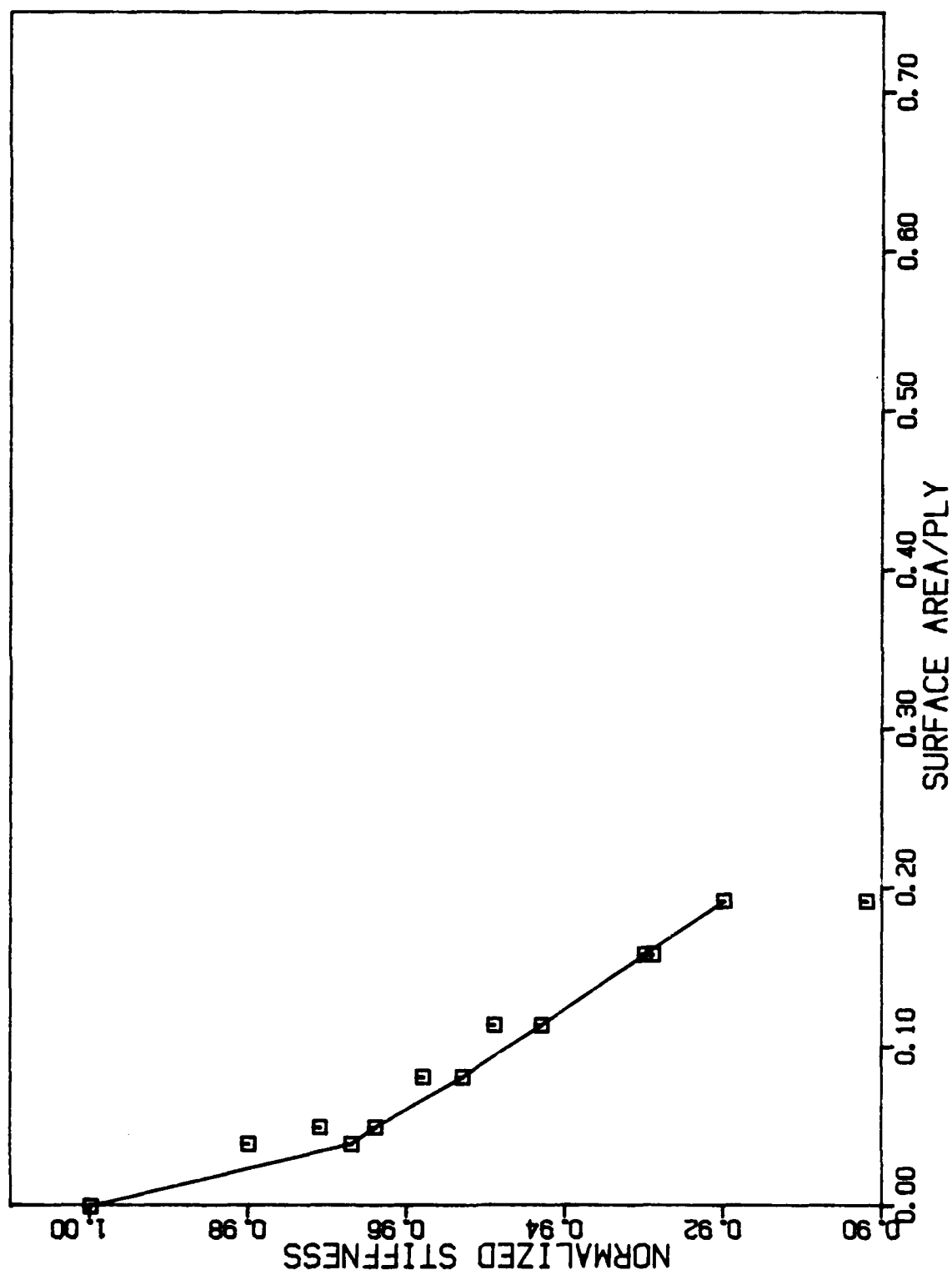


Fig. 7. Model vs. Experiment for $[0,90_3]_5$ Laminate

ACKNOWLEDGEMENT

The authors would like to acknowledge the financial support provided by a grant from the Air Force Office of Scientific Research, grant no. AFOSR-84-0067. Also, the authors would like to acknowledge the helpful discussions with Professor Richard A. Schapery, of the Civil Engineering Department at Texas A&M University.

REFERENCES

1. Allen, D.H., Groves, S.E., Schapery, R.A., and Harris, C.E., "A Thermomechanical Constitutive Theory for Elastic Composites with Distributed Damage - Part I: Theoretical Development," Texas A&M University Mechanics and Materials Center, MM-5023-85-17, October, 1985.
2. Frederick, D. and Chang, T.S., Continuum Mechanics, Scientific Publishers, Inc., Cambridge, Mass., 1972.
3. Jones, R.M., Mechanics of Composite Materials, McGraw-Hill, 1975.
4. Krajcinovic, D., "Constitutive Equations for Damaging Materials," Journal of Applied Mechanics, Transactions of the ASME, 83-APM-12, June, 1983.
5. Norvell, R.G., "An Investigation of Damage Accumulation in Graphite/Epoxy Laminates," Texas A&M University Thesis, August, 1985.

APPENDIX A: APPLICATION OF SYMMETRY CONSTRAINTS

The damage-dependent constitutive model (equations (42) through (45) of Part I [1]) is defined as follows:

$$\sigma_{ij} = \sigma_{ij}^R + C_{ijkl}(\epsilon_{kl} - \epsilon_{kl}^T) + I_{ijkl}^{\eta} \alpha_{kl}^{\eta} \quad , \quad (1a)$$

where σ_{ij} is the local stress tensor, ϵ_{kl} is the local strain tensor, σ_{ij}^R is the residual stress in the absence of strain and temperature change, C_{ijkl} is the undamaged modulus tensor, ϵ_{kl}^T is the thermal strain tensor, α_{kl}^{η} is the internal state variable tensor, and I_{ijkl}^{η} is the damage modulus tensor. Furthermore, we have dropped the subscript L (denoting locally averaged quantities) for convenience.

For demonstration purposes, the residual stress tensor and the temperature change are assumed to be negligible, resulting in

$$\sigma_{ij} = C_{ijkl} \epsilon_{kl} + I_{ijkl}^{\eta} \alpha_{kl}^{\eta} \quad , \quad (2a)$$

Note that I_{ijkl}^{η} is a fourth order tensor with 81 coefficients for each value of η . It is assumed here that the constitutive equations given by (2a) are statistically homogeneous. Therefore, the conditions of stress and strain symmetry as well as the existence of an elastic potential can be applied to equations (2a) to obtain

$$C_{ijkl} = C_{jikl}, \quad C_{ijkl} = C_{ijlk}, \quad C_{ijkl} = C_{klij} \quad , \quad (3a)$$

and

$$I_{ijkl}^{\eta} = I_{jikl}^{\eta} \quad , \quad (4a)$$

It is most convenient at this point to reindex the constitutive tensors using the Voigt notation [2] where

$$\begin{aligned} \sigma_1 &\equiv \sigma_{11} & \sigma_4 &\equiv \sigma_{23} = \sigma_{32} \\ \sigma_2 &\equiv \sigma_{22} & \sigma_5 &\equiv \sigma_{13} = \sigma_{31} \\ \sigma_3 &\equiv \sigma_{33} & \sigma_6 &\equiv \sigma_{12} = \sigma_{21} \end{aligned} \quad , \quad (5a)$$

and

$$\begin{aligned}
\epsilon_1 &\equiv \epsilon_{11} & \epsilon_4 &\equiv 2\epsilon_{23} = 2\epsilon_{32} \\
\epsilon_2 &\equiv \epsilon_{22} & \epsilon_5 &\equiv 2\epsilon_{13} = 2\epsilon_{31} \\
\epsilon_3 &\equiv \epsilon_{33} & \epsilon_6 &\equiv 2\epsilon_{12} = 2\epsilon_{21}
\end{aligned}
\tag{6a}$$

Furthermore, for all values of n

$$\begin{aligned}
\alpha_1 &\equiv \alpha_{11} & \alpha_4 &\equiv \alpha_{23} & \alpha_7 &\equiv \alpha_{31} \\
\alpha_2 &\equiv \alpha_{22} & \alpha_5 &\equiv \alpha_{32} & \alpha_8 &\equiv \alpha_{12} \\
\alpha_3 &\equiv \alpha_{33} & \alpha_6 &\equiv \alpha_{13} & \alpha_9 &\equiv \alpha_{21}
\end{aligned}
\tag{7a}$$

Using the contracted notation, equations (2a) can be written as

$$\sigma_i = C_{ij} \epsilon_j + I_{ik}^n \alpha_k^n \tag{8a}$$

where i and j range from 1 to 6, k ranges from 1 to 9, and n ranges from 1 to N , where N is the number of damage modes.

APPENDIX B: SYMMETRY CONSTRAINTS ON THE DAMAGE MODULUS TENSOR

Consider the following component of internal energy due to cracking:

$$u_I^C \equiv I_{ijkl}^1 \epsilon_{ij} \alpha_{kl}^1 \quad . \quad (1b)$$

Since the strain tensor is symmetric

$$I_{ijkl}^1 = I_{jikl}^1 \quad . \quad (2b)$$

Therefore, there are 54 independent constants in the damage modulus tensor I_{ijkl}^1 . Expanding out equation (1b) thus gives

$$\begin{aligned} u_I^C = & I_{1111}^1 \epsilon_{11} \alpha_{11}^1 + I_{1122}^1 \epsilon_{11} \alpha_{22}^1 + I_{1133}^1 \epsilon_{11} \alpha_{33}^1 + I_{1123}^1 \epsilon_{11} \alpha_{23}^1 \\ & + I_{1132}^1 \epsilon_{11} \alpha_{32}^1 + I_{1113}^1 \epsilon_{11} \alpha_{13}^1 + I_{1131}^1 \epsilon_{11} \alpha_{31}^1 + I_{1112}^1 \epsilon_{11} \alpha_{12}^1 \\ & + I_{1121}^1 \epsilon_{11} \alpha_{21}^1 + I_{2211}^1 \epsilon_{22} \alpha_{11}^1 + I_{2222}^1 \epsilon_{22} \alpha_{22}^1 + I_{2233}^1 \epsilon_{22} \alpha_{33}^1 \\ & + I_{2223}^1 \epsilon_{22} \alpha_{23}^1 + I_{2232}^1 \epsilon_{22} \alpha_{32}^1 + I_{2213}^1 \epsilon_{22} \alpha_{13}^1 + I_{2231}^1 \epsilon_{22} \alpha_{31}^1 \\ & + I_{2212}^1 \epsilon_{22} \alpha_{12}^1 + I_{2221}^1 \epsilon_{22} \alpha_{21}^1 + I_{3311}^1 \epsilon_{33} \alpha_{11}^1 + I_{3322}^1 \epsilon_{33} \alpha_{22}^1 \\ & + I_{3333}^1 \epsilon_{33} \alpha_{33}^1 + I_{3323}^1 \epsilon_{33} \alpha_{23}^1 + I_{3332}^1 \epsilon_{33} \alpha_{32}^1 + I_{3313}^1 \epsilon_{33} \alpha_{13}^1 \\ & + I_{3331}^1 \epsilon_{33} \alpha_{31}^1 + I_{3312}^1 \epsilon_{33} \alpha_{12}^1 + I_{3321}^1 \epsilon_{33} \alpha_{21}^1 + I_{2311}^1 \epsilon_{23} \alpha_{11}^1 \\ & + I_{2322}^1 \epsilon_{23} \alpha_{22}^1 + I_{2333}^1 \epsilon_{23} \alpha_{33}^1 + I_{2323}^1 \epsilon_{23} \alpha_{23}^1 + I_{2332}^1 \epsilon_{23} \alpha_{32}^1 \\ & + I_{2313}^1 \epsilon_{23} \alpha_{13}^1 + I_{2331}^1 \epsilon_{23} \alpha_{31}^1 + I_{2312}^1 \epsilon_{23} \alpha_{12}^1 + I_{2321}^1 \epsilon_{23} \alpha_{21}^1 \\ & + I_{1311}^1 \epsilon_{13} \alpha_{11}^1 + I_{1322}^1 \epsilon_{13} \alpha_{22}^1 + I_{1333}^1 \epsilon_{13} \alpha_{33}^1 + I_{1323}^1 \epsilon_{13} \alpha_{23}^1 \\ & + I_{1332}^1 \epsilon_{13} \alpha_{32}^1 + I_{1313}^1 \epsilon_{13} \alpha_{13}^1 + I_{1331}^1 \epsilon_{13} \alpha_{31}^1 + I_{1312}^1 \epsilon_{13} \alpha_{12}^1 \\ & + I_{1321}^1 \epsilon_{13} \alpha_{21}^1 + I_{1211}^1 \epsilon_{12} \alpha_{11}^1 + I_{1222}^1 \epsilon_{12} \alpha_{22}^1 + I_{1233}^1 \epsilon_{12} \alpha_{33}^1 \\ & + I_{1223}^1 \epsilon_{12} \alpha_{23}^1 + I_{1232}^1 \epsilon_{12} \alpha_{32}^1 + I_{1213}^1 \epsilon_{12} \alpha_{13}^1 + I_{1231}^1 \epsilon_{12} \alpha_{31}^1 \\ & + I_{1212}^1 \epsilon_{12} \alpha_{12}^1 + I_{1221}^1 \epsilon_{12} \alpha_{21}^1 \quad . \quad (3b) \end{aligned}$$

We now wish to impose orthotropic symmetry. In order to do this, first rotate 180° about the x_3 axis [2]. The direction cosines for this transformation are

$$[a_{ik'}] = \begin{bmatrix} -1 & 0 & 0 \\ 0 & -1 & 0 \\ 0 & 0 & 1 \end{bmatrix} \quad . \quad (4b)$$

Therefore, since ϵ_{ij} is a second order tensor,

$$\epsilon_{k'1'} = \epsilon_{ij} a_{ik'} a_{j1'} \quad , \quad (5b)$$

it follows that

$$[\epsilon_{k'1'}] = \begin{bmatrix} \epsilon_{11} & \epsilon_{12} & -\epsilon_{13} \\ \epsilon_{12} & \epsilon_{22} & -\epsilon_{23} \\ -\epsilon_{13} & -\epsilon_{23} & \epsilon_{33} \end{bmatrix} \quad . \quad (6b)$$

Furthermore,

$$[a_{k'1'}^1] = \begin{bmatrix} a_{11}^1 & a_{12}^1 & -a_{13}^1 \\ a_{21}^1 & a_{22}^1 & -a_{23}^1 \\ -a_{31}^1 & -a_{32}^1 & a_{33}^1 \end{bmatrix} \quad . \quad (7b)$$

Since u_i^C must be independent of coordinate system

$$u_1^C = I_{p'q'r's'}^1 \epsilon_{p'q'} a_{r's'}^1 \quad . \quad (8b)$$

Substituting (6b) and (7b) into (8b) and comparing this result to (3b) will result in

$$\begin{aligned} I_{1123}^1 &= I_{1132}^1 = I_{1113}^1 = I_{1131}^1 = I_{2223}^1 = I_{2232}^1 = 0 \\ I_{2213}^1 &= I_{2231}^1 = I_{3323}^1 = I_{3332}^1 = I_{3313}^1 = I_{3331}^1 = 0 \\ I_{2311}^1 &= I_{2322}^1 = I_{2333}^1 = I_{2312}^1 = I_{2321}^1 = I_{1311}^1 = 0 \\ I_{1322}^1 &= I_{1333}^1 = I_{1312}^1 = I_{1321}^1 = I_{1223}^1 = I_{1232}^1 = 0 \\ I_{1213}^1 &= I_{1231}^1 = 0 \end{aligned} \quad . \quad (9b)$$

Rotating 180° about the x_2 axis gives

$$[a_{ik}] = \begin{bmatrix} -1 & 0 & 0 \\ 0 & 1 & 0 \\ 0 & 0 & -1 \end{bmatrix} \quad . \quad (10b)$$

Therefore,

$$[\epsilon_{k'1}] = \begin{bmatrix} \epsilon_{11} & -\epsilon_{12} & \epsilon_{13} \\ -\epsilon_{12} & \epsilon_{22} & -\epsilon_{23} \\ \epsilon_{13} & -\epsilon_{23} & \epsilon_{33} \end{bmatrix} \quad . \quad (11b)$$

Furthermore,

$$[\alpha_{k'1}^1] = \begin{bmatrix} \alpha_{11}^1 & -\alpha_{12}^1 & \alpha_{13}^1 \\ -\alpha_{21}^1 & \alpha_{22}^1 & -\alpha_{23}^1 \\ \alpha_{31}^1 & -\alpha_{32}^1 & \alpha_{33}^1 \end{bmatrix} \quad . \quad (12b)$$

Substituting (11b) and (12b) into (8b) and comparing to (3b) results in

$$\begin{aligned} I_{1112}^1 &= I_{1121}^1 = I_{2212}^1 = I_{2221}^1 = I_{3312}^1 = I_{3321}^1 = 0 \\ I_{2313}^1 &= I_{2331}^1 = I_{1323}^1 = I_{1332}^1 = I_{1211}^1 = I_{1222}^1 = I_{1233}^1 = 0 \end{aligned} \quad . \quad (13b)$$

Rotating 180° about the x_1 axis yields no additional constraints. Therefore, imposition of orthotropic symmetry on I_{ijk}^1 reduces the number of constants to 15. These are

$$\begin{aligned} I_{11}^1 &= I_{1111}^1 & I_{12}^1 &= I_{1122}^1 & I_{21}^1 &= I_{2211}^1 \\ I_{22}^1 &= I_{2222}^1 & I_{13}^1 &= I_{1133}^1 & I_{31}^1 &= I_{3311}^1 \\ I_{33}^1 &= I_{3333}^1 & I_{23}^1 &= I_{2233}^1 & I_{32}^1 &= I_{3322}^1 \\ I_{44}^1 &= I_{2323}^1 & I_{45}^1 &= I_{2332}^1 & I_{56}^1 &= I_{1313}^1 \\ I_{57}^1 &= I_{1331}^1 & I_{68}^1 &= I_{1212}^1 & I_{69}^1 &= I_{2121}^1 \end{aligned} \quad . \quad (14b)$$

Therefore, the orthotropic damage modulus matrix is given by

$$[I^1] = \begin{bmatrix} I_{11}^1 & I_{12}^1 & I_{13}^1 & 0 & 0 & 0 & 0 & 0 & 0 \\ I_{21}^1 & I_{22}^1 & I_{23}^1 & 0 & 0 & 0 & 0 & 0 & 0 \\ I_{31}^1 & I_{32}^1 & I_{33}^1 & 0 & 0 & 0 & 0 & 0 & 0 \\ 0 & 0 & 0 & I_{44}^1 & I_{45}^1 & 0 & 0 & 0 & 0 \\ 0 & 0 & 0 & 0 & 0 & I_{56}^1 & I_{57}^1 & 0 & 0 \\ 0 & 0 & 0 & 0 & 0 & 0 & 0 & I_{68}^1 & I_{69}^1 \end{bmatrix} \quad . \quad (15b)$$

For the case where

$$[\alpha^1] = [0 \quad \alpha_2^1 \quad 0 \quad 0 \quad \alpha_5^1 \quad 0 \quad 0 \quad \alpha_8^1 \quad 0] \quad , \quad (16b)$$

equation (15b) reduces to

$$[I^1] = \begin{bmatrix} 0 & I_{12}^1 & 0 & 0 & 0 & 0 & 0 & 0 & 0 \\ 0 & I_{22}^1 & 0 & 0 & 0 & 0 & 0 & 0 & 0 \\ 0 & I_{23}^1 & 0 & 0 & 0 & 0 & 0 & 0 & 0 \\ 0 & 0 & 0 & 0 & I_{45}^1 & 0 & 0 & 0 & 0 \\ 0 & 0 & 0 & 0 & 0 & 0 & 0 & 0 & 0 \\ 0 & 0 & 0 & 0 & 0 & 0 & 0 & I_{68}^1 & 0 \end{bmatrix} \quad . \quad (17b)$$

APPENDIX C: DETERMINATION OF THE I MATRIX

At a material point in V_L the stress-strain relation in the absence of temperature change is

$$\sigma_{ij} = C_{ijkl} \epsilon_{kl} \quad . \quad (1c)$$

Integrating over the local volume (excluding cracks) gives

$$\sigma'_{ij} = \frac{1}{V_L} \int_{V_L - V_C} \sigma_{ij} dV = \frac{1}{V_L} \int_{V_L - V_C} C_{ijkl} \epsilon_{kl} dV \quad , \quad (2c)$$

where σ'_{ij} is the average stress outside the damage zones. In this section this value of the stress tensor is assumed to be identical to the average stress σ_{Lij} , which includes the average of the stress in the damage zones. Assuming that C_{ijkl} is spatially homogeneous in V_L , the above may be written

$$\sigma'_{ij} = \frac{C_{ijkl}}{V_L} \int_{V_L - V_C} \epsilon_{kl} dV = \frac{C_{ijkl}}{V_L} \int_{V_L - V_C} \frac{1}{2} (u_{k,l} + u_{l,k}) dV \quad . \quad (3c)$$

Using the divergence theorem on the last term gives

$$\sigma'_{ij} = C_{ijkl} \left[\frac{1}{V_L} \int_{S_1} \frac{1}{2} (u_k n_l + u_l n_k) dS + \frac{1}{V_L} \int_{S_2} \frac{1}{2} (u_k n_l + u_l n_k) dS \right] \quad . \quad (4c)$$

Or, equivalently,

$$\sigma'_{ij} = C_{ijkl} \left(\epsilon_{Lkl} - \frac{1}{2} \alpha_{kl} - \frac{1}{2} \alpha_{lk} \right) \quad . \quad (5c)$$

However, the Taylor series expansion has already given (for isothermal conditions)

$$\sigma'_{ij} = C_{ijkl} \epsilon_{kl} + I_{ijkl} \alpha_{kl} \quad . \quad (6c)$$

Therefore, equating like terms in equations (5c) and (6c) gives

$$I_{ijkl} = -C_{ijkl}$$

$$k=1$$

$$I_{ijkl} = -\frac{1}{2}(C_{ijkl} + C_{ijlk})$$

$$k \neq 1$$

. (7c)

APPENDIX D: LAMINATE EQUATIONS

The values of generalized plane strain are given by

$$\begin{Bmatrix} \epsilon_x \\ \epsilon_y \\ \epsilon_z \\ \epsilon_{xy} \end{Bmatrix} = \begin{Bmatrix} \epsilon_x^0 \\ \epsilon_y^0 \\ \epsilon_z^0 \\ \epsilon_{xy}^0 \end{Bmatrix} + z \begin{Bmatrix} \kappa_x \\ \kappa_y \\ 0 \\ \kappa_{xy} \end{Bmatrix} \quad , \quad (1d)$$

where the superscript o denotes the midsurface strains and the κ matrix denotes the midsurface curvatures. Under the condition of generalized plane strain there is no warping allowed out-of-plane, which implies that $\kappa_z=0$.

It is now assumed that no moments or curvatures are imposed and that all laminates studied are symmetric through the thickness (including damage). Therefore, in order to determine the resultant forces, it is necessary only to integrate the given stress state over the laminate thickness to obtain

$$\begin{Bmatrix} N_x \\ N_y \\ N_z \\ N_{xy} \end{Bmatrix} = \int_{-t/2}^{t/2} \begin{Bmatrix} \sigma_x \\ \sigma_y \\ \sigma_z \\ \sigma_{xy} \end{Bmatrix} dz \quad , \quad (2d)$$

where t is the total thickness of the laminate.

Substituting equations (8a) and (1d) into (2d) for the case where there are no rotations results in

$$\{N\} = \int_{-t/2}^{t/2} ([\bar{C}]\{\epsilon^0\} + [\bar{I}^1]\{\bar{\alpha}^1\}) dz \quad , \quad (3d)$$

where $\{N\}$ denotes the force resultants, overbars denote that these quantities are transformed to global coordinates, and $\{\epsilon^0\}$ represents the mid-surface strains. Note that since transverse cracks are assumed to go completely through the thickness of the cracked plies the stiffness and damage are assumed to be spatially constant through the thickness of a single ply. Therefore, equation (3d) can be written as

$$\{N\} = \sum_{k=1}^n ([\bar{C}]_k (z_k - z_{k-1}) \{\epsilon^0\} + [\bar{I}^1]_k (z_k - z_{k-1}) \{\bar{\alpha}^1\}_k) \quad , \quad (4d)$$

where k specifies the ply and $z_k - z_{k-1}$ is the thickness of each ply. One can define

$$A_{ij} \equiv \sum_{k=1}^n (\bar{C}_{ij})_k (z_k - z_{k-1}) \quad , \quad (5d)$$

and

$$\{D\} \equiv \begin{Bmatrix} D_1^1 \\ D_2^1 \\ D_3^1 \\ D_4^1 \end{Bmatrix} = \sum_{k=1}^n ([\bar{I}^1]_k (z_k - z_{k-1}) \{\bar{\alpha}^1\}_k) \quad , \quad (6d)$$

where A_{ij} represents the laminate averaged stiffness matrix and $\{D\}$ is the laminate averaged damage term. Thus, the laminate averaged constitutive equations become

$$\{N\} = [A] \{\epsilon^0\} + \{D\} \quad . \quad (7d)$$

Experimental testing is often conducted on uniaxial testing machines in which the applied force resultants are input and the strains are experimentally determined output. Therefore, at times, it is more convenient to express the strains in terms of the applied force resultants as follows:

$$\{\epsilon^0\} = [A]^{-1} (\{N\} - \{D\}) \quad . \quad (8d)$$

Note also that moments will be produced even in the absence of strain if the damage state is not symmetric through the thickness. However, for the case considered herein, it will be assumed that all damage states are symmetric, and moments are therefore not considered.

APPENDIX E: TRANSFORMATION EQUATIONS FOR THE DAMAGE TENSOR AND THE DAMAGE MODULUS TENSOR

Consider a coordinate rotation θ in the laminate plane (x_1 - x_2 plane) measured clockwise from the ply coordinate system to the laminate coordinate system. For this case the direction cosines are

$$[a_{ik}] = \begin{bmatrix} \cos\theta & -\sin\theta & 0 \\ \sin\theta & \cos\theta & 0 \\ 0 & 0 & 1 \end{bmatrix} \quad . \quad (1e)$$

Recall that since a_{ij}^1 is a second order tensor

$$\bar{a}_{k'1'}^1 = a_{ij}^1 a_{ik'} a_{j1'} \quad . \quad (2e)$$

Substituting (1e) into (2e) thus gives

$$\{\bar{a}^1\} = \left\{ \begin{array}{cccc} a_{12}^1 \cos\theta \sin\theta + a_{22}^1 \sin^2\theta & + & 0 & \\ -a_{12}^1 \sin\theta \cos\theta + a_{22}^1 \cos^2\theta & + & 0 & \\ 0 & + & 0 & + 0 \\ 0 & + & 0 & + 0 \\ 0 & + & 0 & + a_{32}^1 \cos\theta \\ 0 & + & 0 & + 0 \\ 0 & + & 0 & + a_{32}^1 \sin\theta \\ a_{12}^1 \cos^2\theta & + & a_{22}^1 \sin\theta \cos\theta & + 0 \\ -a_{12}^1 \sin^2\theta & + & a_{22}^1 \sin\theta \cos\theta & + 0 \end{array} \right\} \quad . \quad (3e)$$

Furthermore, $\bar{I}_{p'q'r's'}^1$ is given by

$$\bar{I}_{p'q'r's'}^1 = I_{ijkl}^1 a_{ip'} a_{jq'} a_{kr'} a_{ls'} \quad . \quad (4e)$$

Substituting the nonzero components from equation (17b) into (4e) gives

$$\begin{aligned} \bar{I}_{p,q,r,s}^1 = & I_{12}^1 a_{1p} a_{1q} a_{2r} a_{2s} + I_{22}^1 a_{2p} a_{2q} a_{2r} a_{2s} \\ & + I_{32}^1 a_{2p} a_{2q} a_{3r} a_{3s} + I_{68}^1 a_{2p} a_{1q} a_{1r} a_{2s} \quad . \quad (5e) \end{aligned}$$

APPENDIX F: DIMENSIONAL ANALYSIS OF STRAIN ENERGY RELEASE RATES

Consider the cracked 90° layer shown in Fig. F1. The total strain energy in the region surrounding the crack that includes the strain energy available to be released during crack extension is given by

$$U = U_A + U_B \quad , (1f)$$

where U_A is the strain energy ahead of the advancing crack, and U_B is the strain energy behind the advancing crack.

In terms of strain energy density, U_0 , equation (1f) becomes

$$U = (U_0)_A [t(w-a)l_E] + (U_0)_B [tal_E] \quad , (2f)$$

where l_E is the effective length of the material from which strain energy will be released by the advancing crack. The effective length is a function of both the crack spacing, S , and the thickness of the 90° layer. Therefore, l_E can be expressed as

$$l_E = ct \quad , (3f)$$

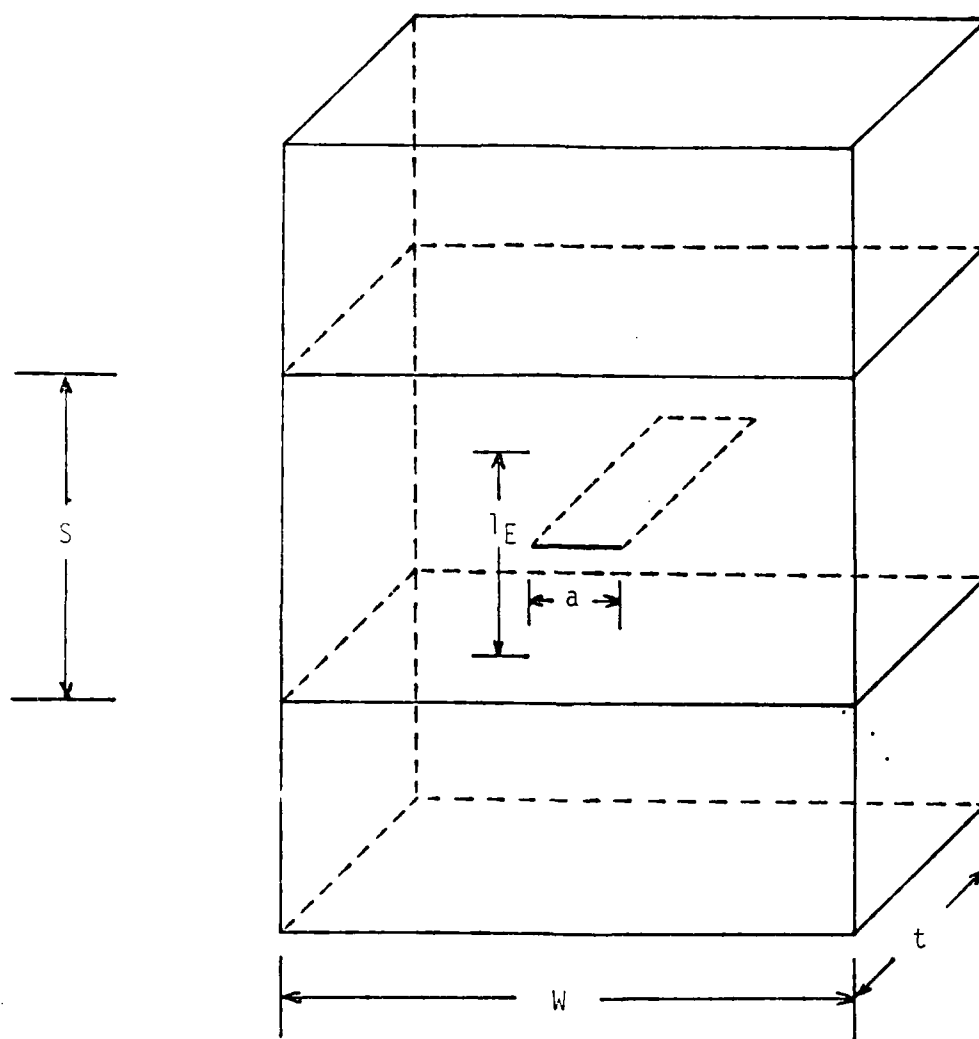
where c is a nondimensional function of the crack spacing and the 90° layer thickness. In addition, the strain energy density ahead of the crack and behind the crack can be expressed as functions of the strain energy density in the 90° layer in the absence of cracks multiplied by some dimensionless constant that depends on the existing matrix crack spacing and the thickness of the 90° layer. Written symbolically, then

$$(U_0)_A = U_0 f_A \quad , (4f)$$

and

$$(U_0)_B = U_0 f_B \quad , (5f)$$

where U_0 is the strain energy density in the 90° layer in the absence of cracks, and f_A and f_B are functions of the crack spacing, S , and time, t . Substituting (3f), (4f) and (5f) into (2f) yields



l_E = effective length of material in which strain energy is released during crack extension

S = spacing between two adjacent fully developed matrix cracks

Fig. F1 Crack Geometry in 90° Layer

$$\begin{aligned}
 U &= U_0 f_A [ct^2(w-a)] + U_0 f_B [ct^2 a] \\
 &= U_0 ct^2 [f_A w + a(f_B - f_A)]
 \end{aligned}
 \quad . (6f)$$

Strain energy release rate at each crack tip is defined as follows

$$G = \frac{1}{2t} \frac{\partial U}{\partial a} \quad . (7f)$$

Substituting (6f) into (7f) thus gives

$$G = \frac{1}{2} U_0 ct (f_A - f_B) \quad . (8f)$$

Notice that c , f_A and f_B are all functions of the layer thickness and existing matrix crack spacing. Therefore, define a new function f such that

$$f(S,t) = c(f_A - f_B) \quad . (9f)$$

Since the function $f(S,t)$ is a dimensionless function, it must be a function of S/t . Therefore,

$$c(f_A - f_B) = f(S/t) \quad . (10f)$$

Substituting (10f) into (8f) yields the following expression for the available strain energy release rate for matrix cracks

$$G = \frac{1}{2} t [U_0 f(S/t)] \quad . (11f)$$

Therefore, the available strain energy release rate due to matrix cracks in a 90° layer is linearly proportional to the thickness of the 90° layer. The quantity in the brackets in equation (11f) is related to the properties of the composite material system and the laminate stacking sequence. This quantity can be determined from experimental data.

If it is assumed that cracking occurs when the available strain energy release rate is equal to the critical strain energy release rate which is constant for all matrix cracking, then

$$G = G_{CR} \quad . (12f)$$

Furthermore, for a linear elastic material with rigid fibers, the

strain energy density is given by

$$U_0 = \frac{1}{2} E_{22} \epsilon_{22}^2 \quad . \quad (13f)$$

Substituting (11f) and (13f) into (12f) and solving for strain results in the following expression for the strain in the 90° layer at which matrix crack extension occurs:

$$\epsilon_{22} = \left[\frac{G_{cR}}{t E_{22} f(S/t)} \right]^{1/2} \quad . \quad (14f)$$

Rearranging gives

$$\frac{4G_{cR}}{t E_{22} \epsilon_{22}^2} = f(S/t) \quad . \quad (15f)$$

Finally, the thickness of the 90° layer is given by

$$t = n t_1 \quad , \quad (16f)$$

where t_1 is the thickness of one ply and n is the number of consecutive 90° plies. Substituting equation (16f) into (15f) results in

$$\frac{4G_{cR}}{t_1 E_{22}} \left[\frac{1}{n \epsilon_{22}^2} \right] = f(S/t) \quad . \quad (17f)$$

If the influence function, $f(S/t)$, is constant for all laminate stacking sequences, then the left hand side of equation (15f) will be a function of matrix crack surface area only.

The terms in parentheses on the left and right hand sides of equation (17f) are laminate specific while all other terms are constants. The function $f(S/t)$ is constant for all laminates then a plot of $n \epsilon_{22}^2$ versus t/S should be the same for all laminates. The experimental data is plotted in Fig. F2 and as can be seen the data for all laminates follow the same trend curve. Therefore, it can be seen that the available strain energy release rate is a function of the 90° layer thickness and the matrix crack surface area. All other laminate parameters such as the number of consecutive 0° plies results in second order effects on the energy release rate.

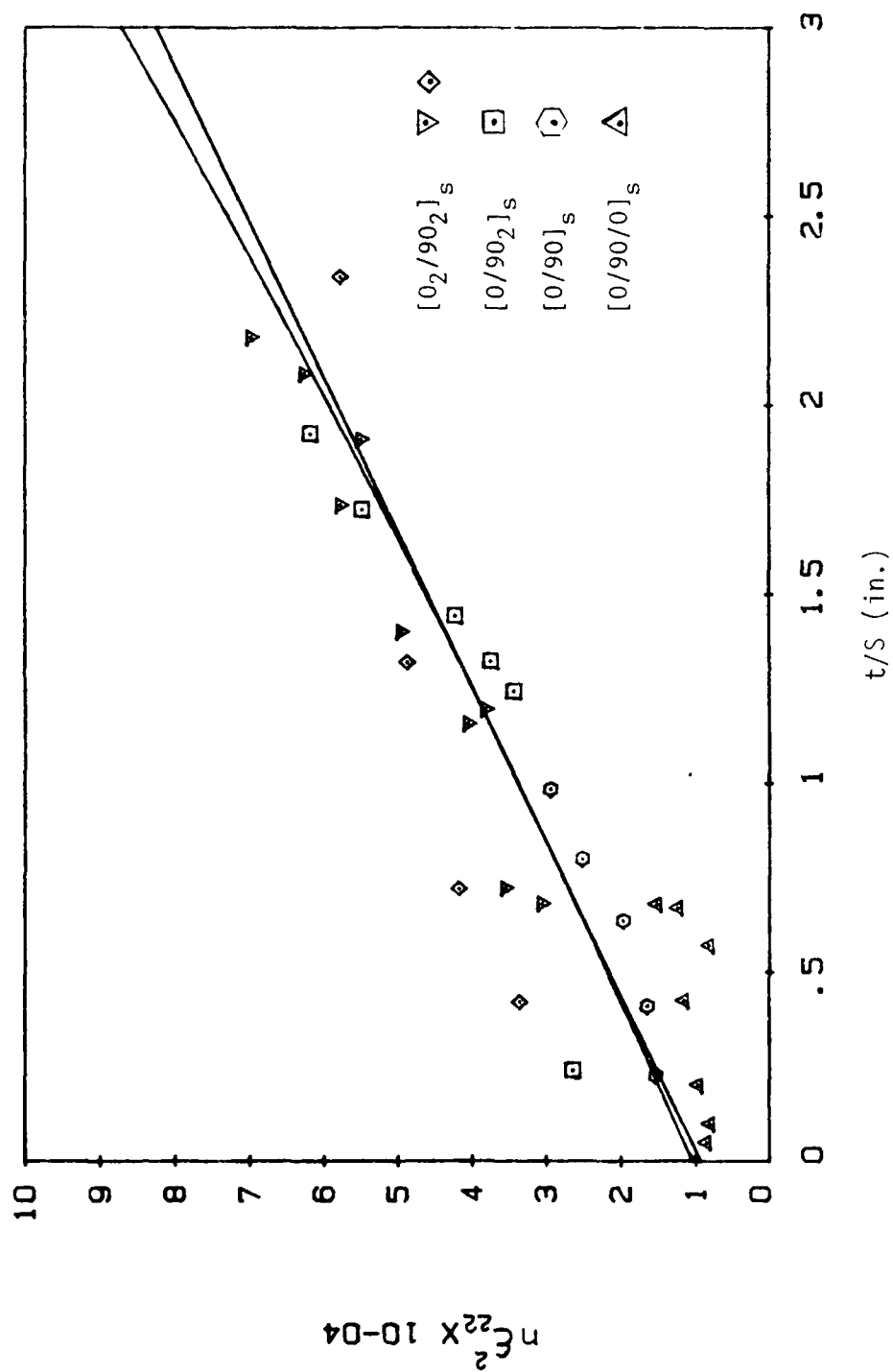


Fig. F2 Experimental strain energy release rate results for a variety of cross-ply laminates. (The solid lines are a straight line and quadratic least squares curve fit).

APPENDIX 6.4

REPORT DOCUMENTATION PAGE

1a. REPORT SECURITY CLASSIFICATION Unclassified		1b. RESTRICTIVE MARKINGS	
2a. SECURITY CLASSIFICATION AUTHORITY		3. DISTRIBUTION/AVAILABILITY OF REPORT	
2b. DECLASSIFICATION/DOWNGRADING SCHEDULE			
4. PERFORMING ORGANIZATION REPORT NUMBER(S) MM - 5023 - 85 - 23		5. MONITORING ORGANIZATION REPORT NUMBER(S)	
6a. NAME OF PERFORMING ORGANIZATION Aerospace Engineering Dept. Texas A&M University		6b. OFFICE SYMBOL (If applicable)	
7a. NAME OF MONITORING ORGANIZATION Air Force Office of Scientific Research		7b. ADDRESS (City, State and ZIP Code) Bolling AFB Washington, D.C. 20332	
8a. NAME OF FUNDING/SPONSORING ORGANIZATION AFOSR		8b. OFFICE SYMBOL (If applicable)	
9. PROCUREMENT INSTRUMENT IDENTIFICATION NUMBER		10. SOURCE OF FUNDING NOS.	
11. TITLE (Include Security Classification) An Experimental And Analytical Treatment Of The Mechanics Of Damage In Laminated Composites		PROGRAM ELEMENT NO.	PROJECT NO.
12. PERSONAL AUTHOR(S) Scott E. Groves, David H. Allen, C.E. Harris, A.L. Highsmith		TASK NO.	WORK UNIT NO.
13a. TYPE OF REPORT Interim		13b. TIME COVERED FROM 6-85 TO 11-85	
14. DATE OF REPORT (Yr., Mo., Day) November 1, 1985		15. PAGE COUNT 34	
16. SUPPLEMENTARY NOTATION			
17. COSATI CODES		18. SUBJECT TERMS (Continue on reverse if necessary and identify by block number)	
FIELD	GROUP	SUB. GR.	
19. ABSTRACT (Continue on reverse if necessary and identify by block number) See Attachment			
20. DISTRIBUTION/AVAILABILITY OF ABSTRACT UNCLASSIFIED/UNLIMITED <input checked="" type="checkbox"/> SAME AS RPT <input type="checkbox"/> DTIC USERS <input type="checkbox"/>		21. ABSTRACT SECURITY CLASSIFICATION	
22a. NAME OF RESPONSIBLE INDIVIDUAL		22b. TELEPHONE NUMBER (Include Area Code)	22c. OFFICE SYMBOL

AN EXPERIMENTAL AND ANALYTICAL TREATMENT OF THE MECHANICS OF DAMAGE
IN LAMINATED COMPOSITES

BY

S.E. GROVES

D.H. ALLEN

C.E. HARRIS

A.L. HIGHSMITH

R.G. NORVELL

AEROSPACE ENGINEERING DEPARTMENT

TEXAS A & M UNIVERSITY

COLLEGE STATION, TEXAS 77843

ABSTRACT

The development of damage in cross-ply Hercules AS4/3502 graphite/epoxy laminates has been investigated. Specific endeavors were to identify the mechanisms for initiation and growth of matrix cracks and to determine the effect of matrix cracking on the stiffness loss in cross-ply laminates. Two types of matrix cracks were identified. These include both "straight" and "angle" type cracks. While straight cracks have been the subject of extensive research efforts, a treatment of the angle cracks does not appear in the literature. The growth mechanisms of the angle cracks were found to be distinctly different from those of the straight cracks, which are essentially driven by shear lag. The experimental study of matrix crack damage revealed that the angle cracks formed after the straight cracks and followed a repeatable pattern of location and orientation relative to the straight cracks. Therefore, it was postulated that the growth mechanism for angle cracks is driven by the stress state resulting from the formation of the straight cracks. This phenomenon was analytically investigated by a finite element model of straight cracks in a cross-ply laminate. The finite element results substantiate the postulated growth mechanism. Growth mechanisms for both types of cracks were experimentally related to the number of consecutive 90° plies, the ratio of 0° to 90° plies, and the applied stress level. Finally, experimental results indicate that as much as a 10 percent degradation in axial stiffness due to matrix cracking in cross-ply laminates such as a $[0,90_3]_s$.

INTRODUCTION

Damage accumulation in composite laminates has become an extremely important design criterion in modern aerospace structures. To make more efficient use of composite laminates in the design and construction of aircraft and large space structures, the scale of acceptable damage must be increased. Consequently, the composite designer must be aware of the effect on structural behavior of damage modes such as matrix cracking, interlaminar delamination, and fiber breakage. Also, he must be able to characterize the constitution of the composite laminate throughout its load history. In spite of the considerable research that has occurred, a complete understanding and formulation of the mechanics of damage in composite materials is not available.

Most of the previous work may be classified as experimental, emphasizing the various types of damage and their possible causes [1-8]. This has been supported by extensive analytical investigations which describe the stress and deformation fields in the damaged regions. Methods used to analyze the damage regions are finite elements [9-16], finite differences [3,8,15], shear lag [16], modified classical lamination theory [4,6,10], and general analytical techniques ranging from classical fracture mechanics [17-24], nonlinear viscoelastic theories [25], to general boundary value problem solutions for special crack geometries [18,26]. Only recently has significant attention been given to the development of cumulative damage models capable of predicting the resulting damage from a specified load history. These models proceed from three basically different paths; 1) fracture mechanics [14,27-31], 2) empirical [32-39], and 3) internal state

variable theories which are based on thermodynamics [40-49].

The primary objective of the research program, for which the results reported herein have been obtained, is the development of a damage dependent constitutive model for predicting the stiffness loss in composite laminates. This model has been developed from a continuum mechanics approach utilizing thermodynamic constraints wherein the damage is characterized by a set of second order tensor valued internal state variables [48,49]. To characterize these internal state variables, the mechanics of damage must be studied experimentally and described analytically. The subject of this paper is the experimental and analytical correlation of matrix crack damage in continuous fiber graphite/epoxy laminates.

After a brief description of the damage-dependent constitutive model, the paper will focus attention on the following research objectives:

1. Experimental study of the mechanisms of initiation of matrix cracks in graphite/epoxy laminates.
2. Correlation of experimental observations of cracks with finite element analysis results.
3. Identification of the effects of matrix cracking on the axial stiffness loss in cross-ply laminates.

DAMAGE MODEL

A continuum mechanics approach has been utilized by the author, for predicting the stiffness of continuous fiber composites subjected to both monotonic and cyclic fatigue loading in the presence of damage [48,49]. In this model, each specific damage mode is characterized by a second order tensor valued internal state variable representing locally averaged measures of damage. Utilizing thermodynamics, the constitutive equations have been developed as follows:

$$\sigma_{Lij} = \sigma_{Lij}^R + C_{Lijkl} \epsilon_{Lkl} + D_{Lijkl}^n \alpha_{Lkl}^n, \quad (1)$$

where σ_{Lij} is the stress tensor, σ_{Lij}^R represents the residual stress tensor, ϵ_{Lkl} is the strain tensor, C_{Lijkl} is the undamaged elastic modulus tensor, D_{Lijkl}^n represents the damage modulus tensor, and α_{Lkl}^n represents the internal state variables. The subscript L denotes locally average properties with all other subscripts ranging from one to three and the superscript n ranges from one to the number of damage modes.

The internal state variable is represented by a diadic product between the crack opening displacement vector, u_k^c , and its corresponding unit normal vector, n_1^c , integrated over the local volume element as follows:

$$\alpha_{Lkl}^n = \frac{1}{V_L} \int_{S_2^n} u_k^c n_1^c dS, \quad (2)$$

where V_L is the local volume and S_2^n is the crack surface area of each

damage mode. One of the major goals of the research is to establish a direct dependence of α_{Lk1}^n on S_2^n , since S_2^n can be measured experimentally. Complete characterization of the constitutive equations will require development of the growth laws for the internal state variables of the general form

$$\dot{\alpha}_{Lk1}^n = \Omega_{k1}^n(\epsilon_{Lk1}, \dot{\epsilon}_{Lk1}, T_L, \alpha_{Lk1}^n) \quad (3)$$

In order to develop accurate growth laws, one must have a thorough understanding of the microphysics of the damage process. The remainder of this paper will be devoted to a discussion of the damage mechanisms associated with the first fundamental damage mode of matrix cracking.

EXPERIMENTAL PROGRAM

The purpose of the experimental program was twofold. One objective was to make as many physical observations as possible concerning the development of matrix cracking in order to identify the mechanisms of initiation and growth. The second objective was to identify the effect of matrix cracking on axial stiffness in a variety of angle-ply laminates. To isolate this specific damage state cross-ply laminates consisting of 0° and 90° plies were studied (see Table 1). This array of laminates was selected in order to examine the effect of the number of successive 90° plies, as well as the percentage of 90° plies to the 0° constraining plies. Another reason for choosing the $0^\circ/90^\circ$ cross-ply laminate was that it minimizes the development of other damage modes, especially edge delamination. The material system was Hercules AS4/3502 graphite/epoxy. The unidirectional properties are given in Table 2.

In order to identify the various aspects of matrix cracking one must nondestructively evaluate the damage in each laminate. This was accomplished by using edge replication [50] and X-ray radiography. These methods have become quite common for detecting damage in composite laminates. Since graphite/epoxy is relatively transparent to x-rays, zinc iodide [51] was introduced into the damaged laminate to produce enhanced radiographs of the damage.

A typical edge replica showing damage in a cross-ply $[0,90_3]_s$ laminate is shown in Fig 1. In this figure one can see two distinctly different types of matrix cracks: straight cracks and angle cracks. The mechanisms for each crack will be discussed in the next section. An

TYPE	LAY-UP	SUCCESSIVE 90° PLIES	PERCENTAGE 90° PLIES
A	$[0/90_4]_s$	8	80
B	$[0/90_3]_s$	6	75
C	$[0/90_2]_s$	4	66
D	$[0/90]_s$	2	50
E	$[0_2/90_2]_s$	4	50
F	$[0/90/0]_s$	1	33
G	$[0/90/0/90]_s$	2/1	50

Table 1. Laminates Types Tested.

LAMINA PROPERTIES

LONGITUDINAL MODULUS, E_{11}	144.78 ± 2.0 % GPa (21.0 MSI)
TRANSVERSE MODULUS, E_{22}	9.58 ± 2.1 % GPa (1.39 MSI)
SHEAR MODULUS, G_{12} ¹	4.785 GPa (0.694 MSI)
POISSON'S RATIO, ν_{12}	0.310 ± 3.7 %
LONGITUDINAL STRENGTH, F_{1u}	2.247 ± 3.5 % GPa (326 KSI)
TRANSVERSE STRENGTH, F_{tu}	0.0764 ± 9.8 % GPa (11.1 KSI)
LONG. FAILURE STRAIN, ϵ_{1u}	0.0144 ± 4.6 %
TRAN. FAILURE STRAIN, ϵ_{tu}	0.00773 ± 6.7 %

PREPREG PROPERTIES

FIBER AREAL WEIGHT ²	164 G/M ²
FIBER VOLUME FRACTION ²	$0.58 \pm .03$
RESIN CONTENT, % BY WEIGHT ²	35 ± 3

1 ANALYTICALLY CALCULATED FROM A $[\pm 45]_s$ LAMINATE

2 HERCULES INC. SPECIFICATIONS

Table 2. Material Properties for Hercules AS4/3502.

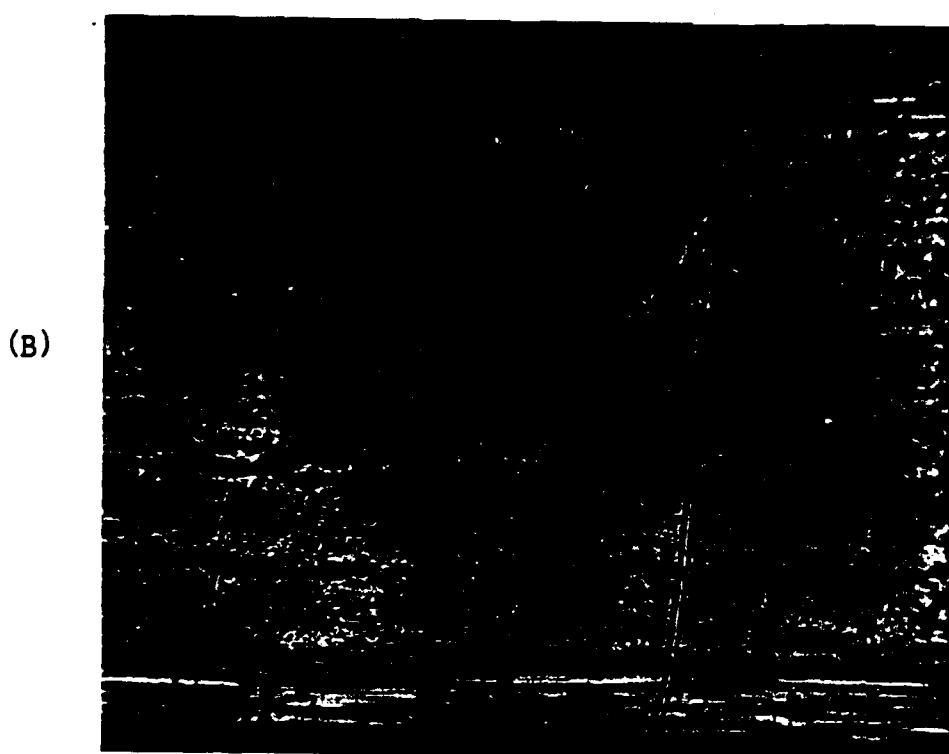
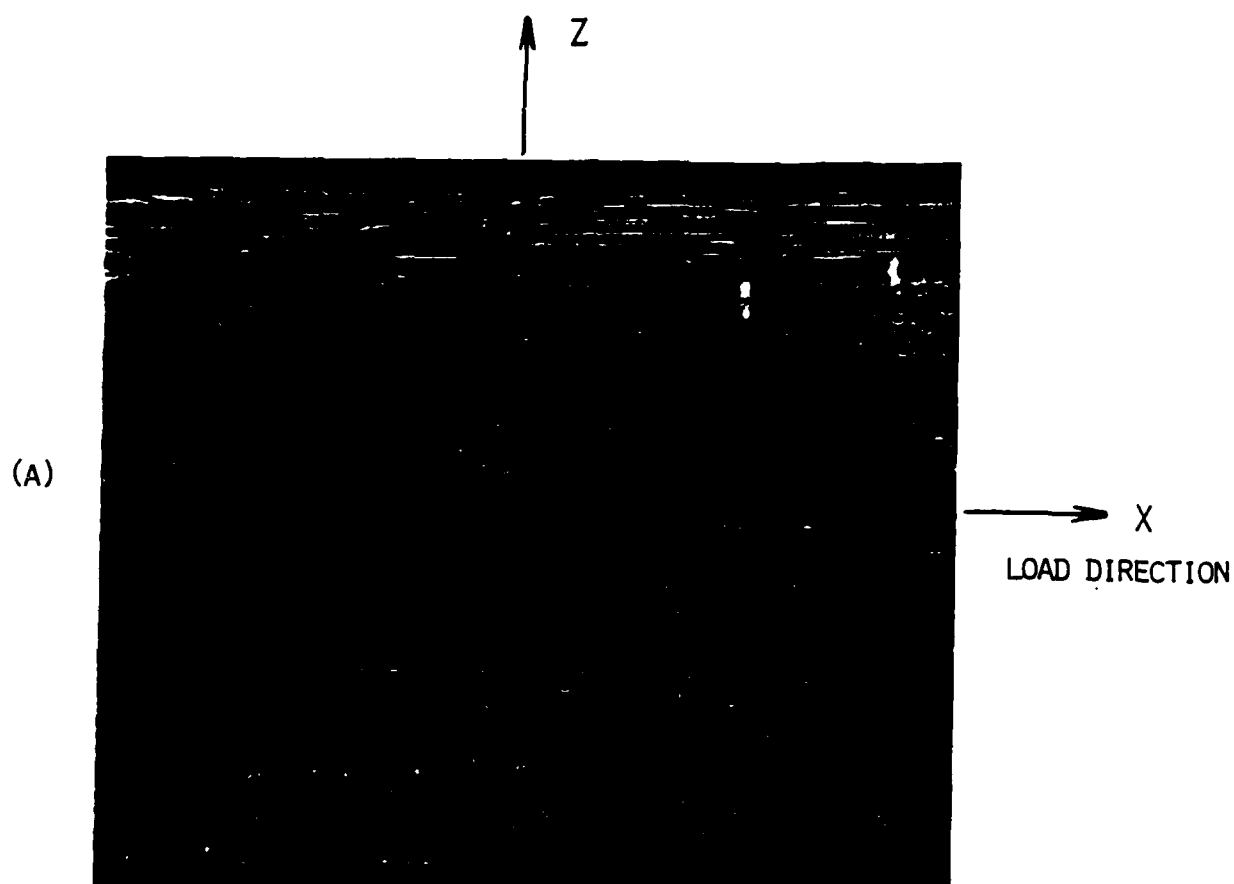


Fig. 1. EDGE REPLICAS OF MATRIX CRACKS;
A) PARTIAL CRACKS, B) CURVED CRACKS

x-ray radiograph of this same damage mode is shown in Fig 2. It is very easy to distinguish an angle crack from a straight crack. A straight crack appears as a sharp narrow band while an angle crack appears as a wider, fuzzy band.

The mechanical testing was conducted using an Instron 1125 universal testing system. All tests were conducted under monotonic loading at a constant cross-head displacement rate of 0.05 in/min following ASTM standard 3039-76. The axial strain was measured using a one inch MTS extensometer(632.11B-20). The data were recorded with a digital data acquisition system (at 35KHz) using a Digital 1123 Plus computer. The loading was interrupted periodically to measure the axial stiffness and to document the damage state by edge replication and x-ray radiography. A typical progression of damage development is shown in Fig. 3. Other damage modes, including interlaminar delaminations and axial splitting, are visible in these radiographs. Interlaminar delaminations were observed to develop at the intersection of straight and angle cracks with the 0° interface (see Fig. 4) as well as at the intersection of axial splits and transverse matrix cracks. (A detailed description of the experimental methods and results is given in reference [52].) The remaining portion of the paper will be concerned only with matrix cracking. Therefore, all mechanical test were terminated when damage modes other than matrix cracking initiated.

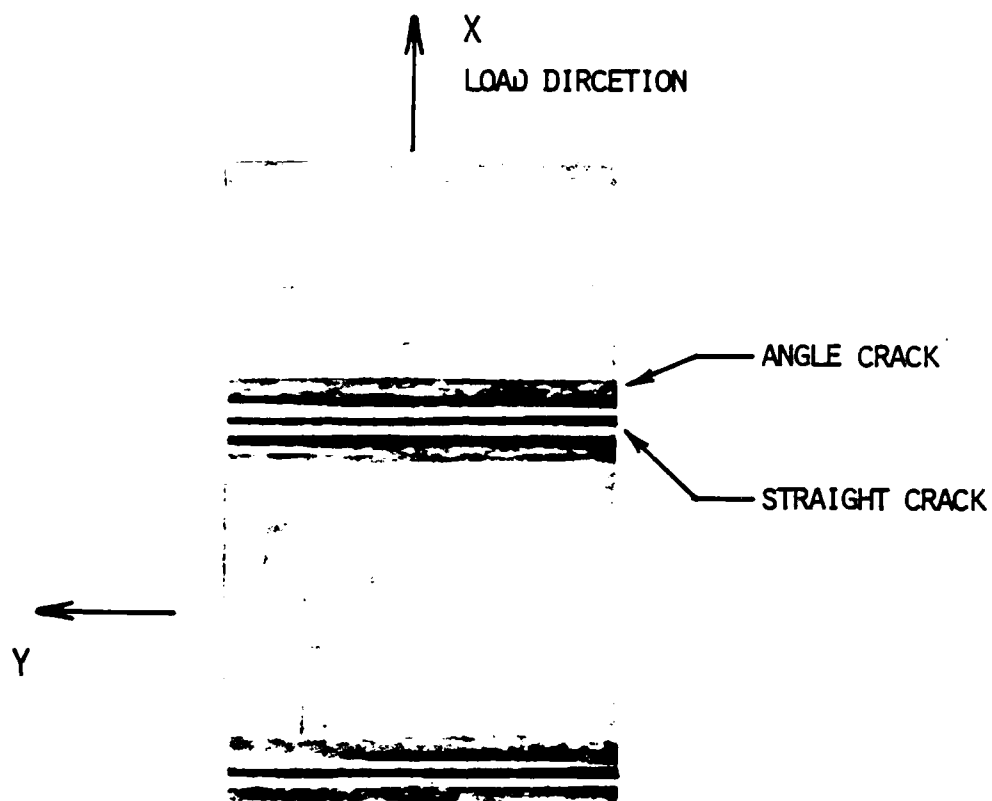


FIG. 2. DETAIL OF X-RAY RADIOGRAPH SHOWING DIFFERENCE BETWEEN STRAIGHT AND ANGLE CRACKS

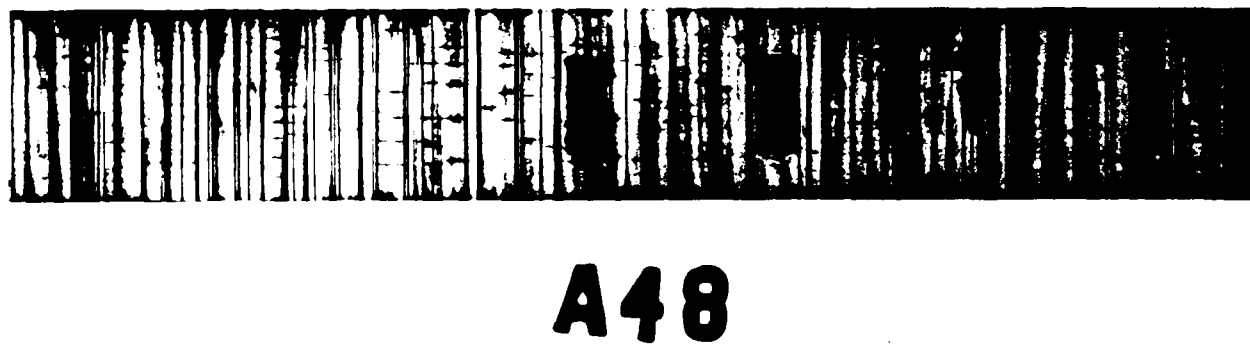
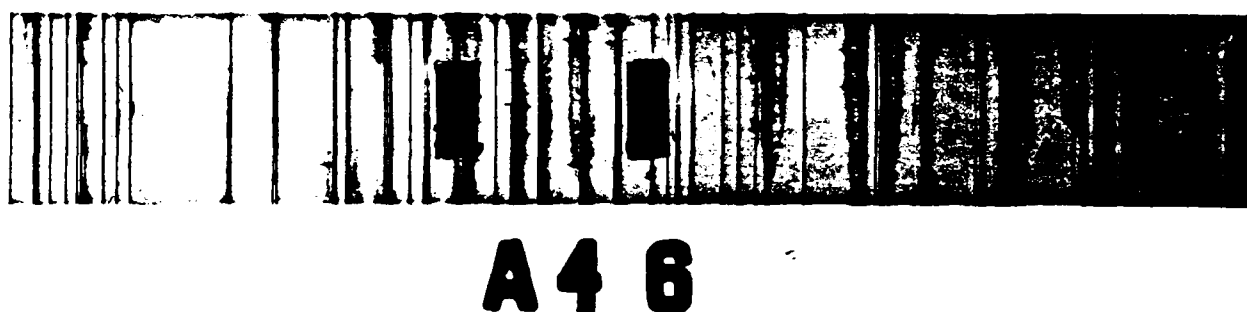
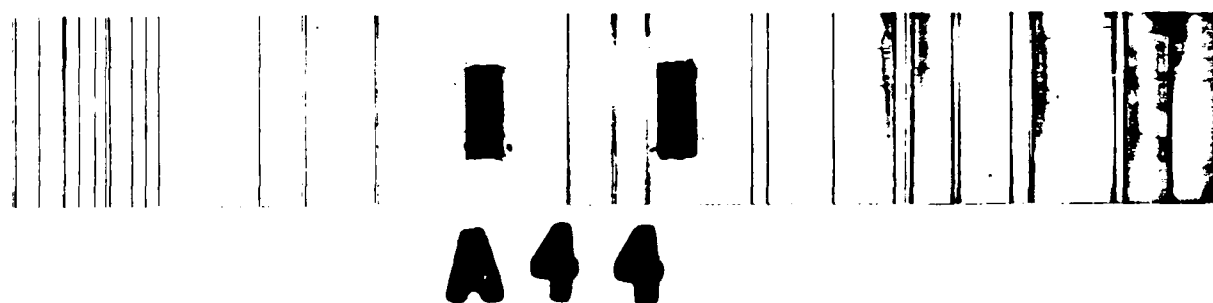
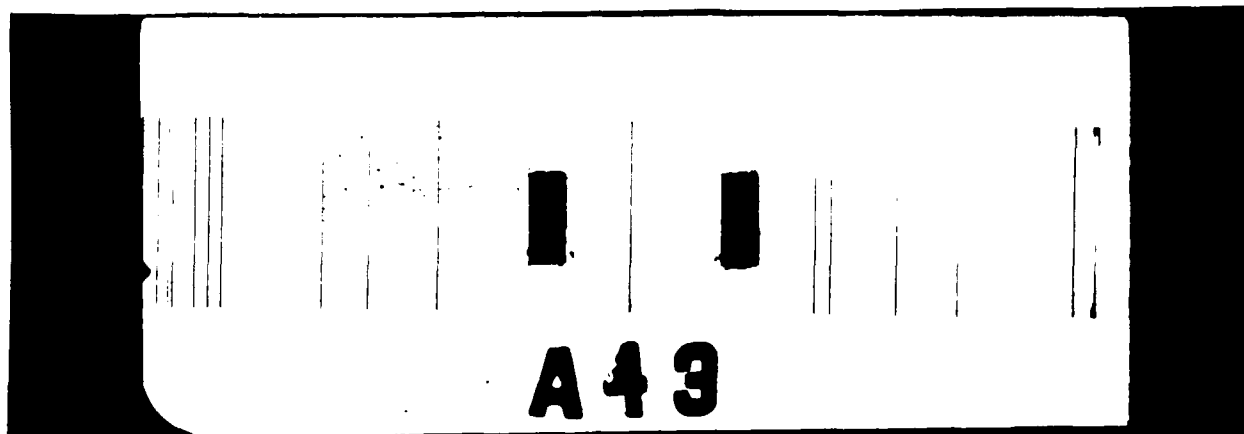


FIG. 3. X-RAY RADIOGRAPH OF DAMAGE IN A $[0/90_4]_s$ LAMINATE



FIG. 4. MICROGRAPH OF DELAMINATION PROPAGATING FROM AN
ANGLE CRACK AT THE $0^{\circ}/90^{\circ}$ INTERFACE OF A $[0/90_3]_s$
LAMINATE

EXPERIMENTAL RESULTS

IDENTIFICATION OF MATRIX CRACK MECHANISMS

We observed in Fig. 1, two distinct types of matrix cracks, straight cracks and angle cracks, each having its own unique growth mechanism. A schematic diagram of a well defined crack system for a $[0,90_n]_s$ laminate, where n is greater than 1, is shown in Fig. 5. A straight crack is defined to be a matrix crack extending completely through the off-axis ply oriented normal to the laminate (x,y) plane. This type of crack grows very suddenly and probably emanates from a preexisting microscopic flaw. This behavior is generally accepted as a form of brittle fracture and can be described by fracture mechanics concepts. It is widely accepted that the density (number of cracks per inch) of straight cracks is driven by shear lag [3] between the off-axis plies and the constraining plies.

An angle crack is a matrix crack extending partially from the $0^\circ/90^\circ$ interface oriented at an angle to the laminate plane. Angle cracks are always located near a straight crack and always grow toward the straight crack. This type of matrix cracking, though probably encountered by others, has yet to be reported in the literature. Sequential edge replicas indicate that the growth of the angle crack is much slower than that of the straight cracks, suggesting a ductile mode of fracture. Hence, this would represent a fracture process which is different from that for straight cracks. The angle cracks can be seen to extend only partially across the ply thickness. Angle cracks at opposite $0^\circ/90^\circ$ interfaces almost always coalesce to form a single curved crack, as shown in Figs. 1 and 5. Furthermore, there are even occurrences of two

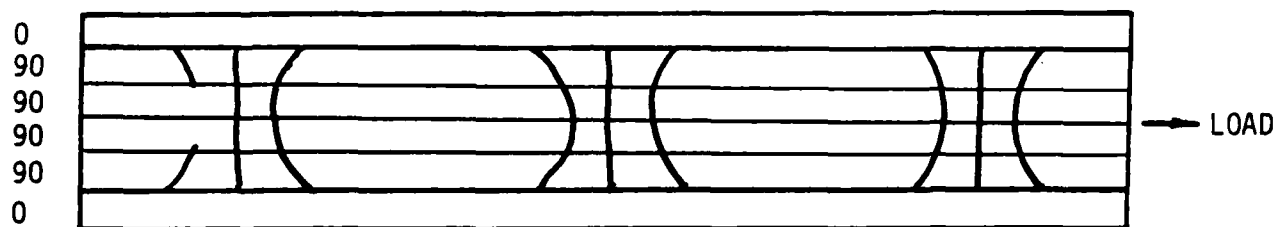


Fig. 5. Matrix Cracking in a $[0,90_2]_s$ Laminate.

curved cracks located on one side of a straight crack. It is hypothesized that the orientation and location of the curved crack is related to the orientation of the principal stresses in the vicinity of a straight crack. This hypothesis has been investigated analytically and will be discussed in a later section.

The experimental results showed a correlation between the number of curved cracks and changes in the local stress field associated with the straight cracks. There are several factors that influence the local stress field surrounding the straight cracks. One factor directly affecting this stress field is the number of consecutive 90° plies in the laminate. Figure 6 shows the relation between straight cracks and curved cracks for an increasing number of 90° plies in a $[0,90_n]_s$ laminate. For $n=1$ there are no curved cracks because most of the stress is carried by the 0° ply. As n increases the amount of stress carried by the 90° plies increases, thus resulting in a corresponding increase in the number of curved cracks. It is interesting to note that for n greater than 2 there are more curved cracks than straight cracks, however the total number of cracks for all three laminates is 48,52,and 50 respectively, which appears to be fairly constant.

INCREASE IN CURVED CRACKS AS NUMBER
OF CONSECUTIVE 90° PLIES INCREASES

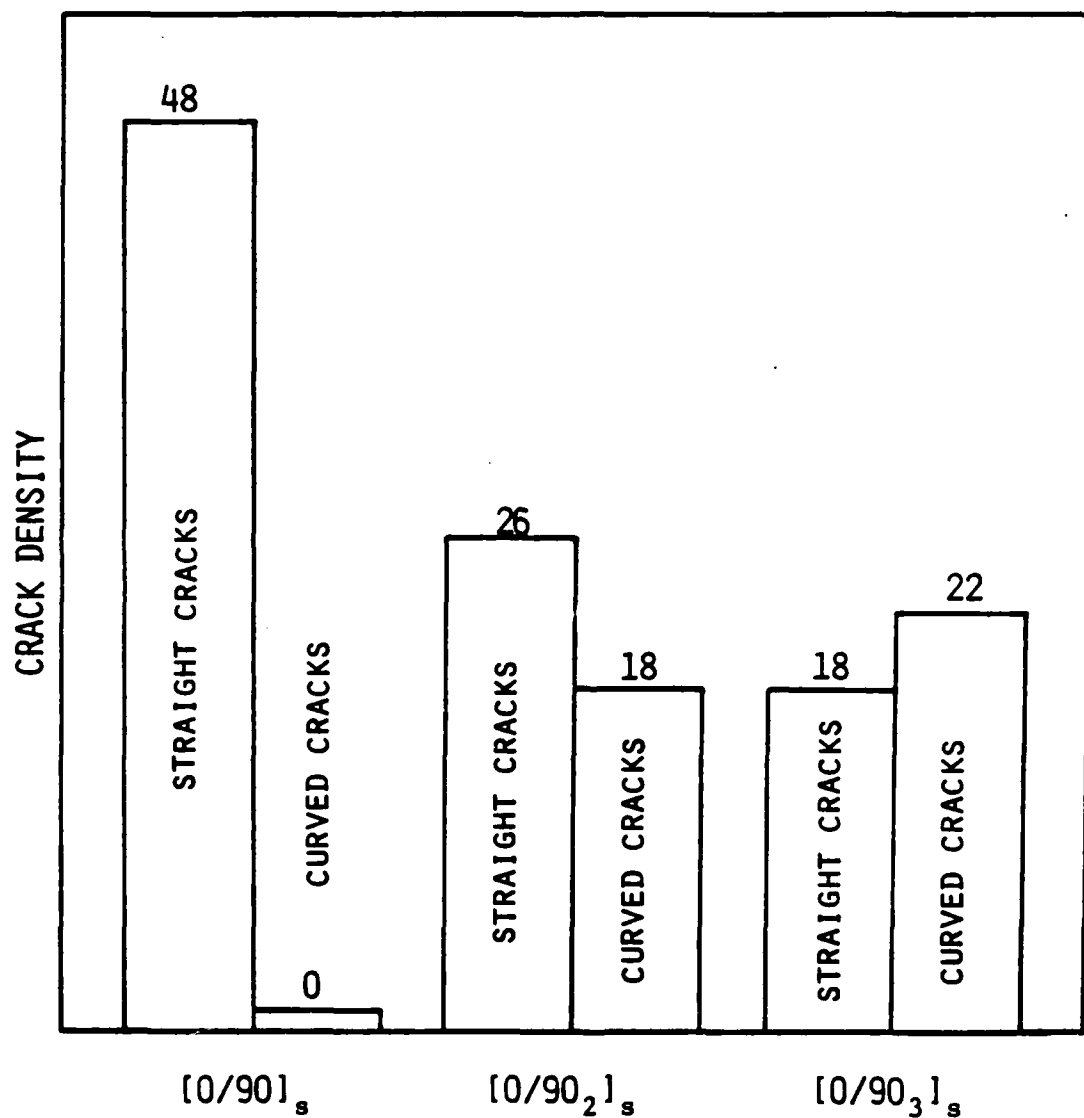


Fig. 6. Increase in Curved Cracks as Number of Consecutive 90° Plies Increases.

EFFECT OF MATRIX CRACKING ON AXIAL STIFFNESS LOSS

The axial stiffness loss due to matrix cracking in five laminates was monitored during step-wise monotonic loadings. The stiffness was measured only on the unloading portion of the axial stress-strain curves. Thus, stiffness was used to indicate the degree of damage development during any monotonic loading step. The stiffness results are shown in Fig. 7. All curves represent an average of two or more separate specimen results. The stiffness values are normalized to the undamaged stiffness and compared to the total crack density, which is the total number of straight cracks and curved cracks per unit length of specimen.

One can see that for $[0,90_n]_s$ laminates, where $n=1/2, 1, 2$, and 3 , stiffness loss increases with increasing n . This is explained by the fact that for increasing n more load is carried by the 90° plies. Hence, for the same crack density (damage), the laminate with more 90° plies will lose more stiffness. This same trend can be explained by ply discount, however, the ply discount method over estimates the total stiffness loss. It is noted here that the last data points for the $[0,90,0]_s$ and $[0,90]_s$ were taken after application of 95 percent of the ultimate load, whereas the last data points for the remaining laminates correspond to the test termination loads when other damage modes began to occur.

For laminates with identical $0^\circ/90^\circ$ ratios such as the $[0,90]_s$ and $[0_2,90_2]_s$, the laminate with the higher consecutive number of 90° plies shows greater stiffness loss. This is due to the fact that the laminate with the higher consecutive number of 90's has more crack surface area

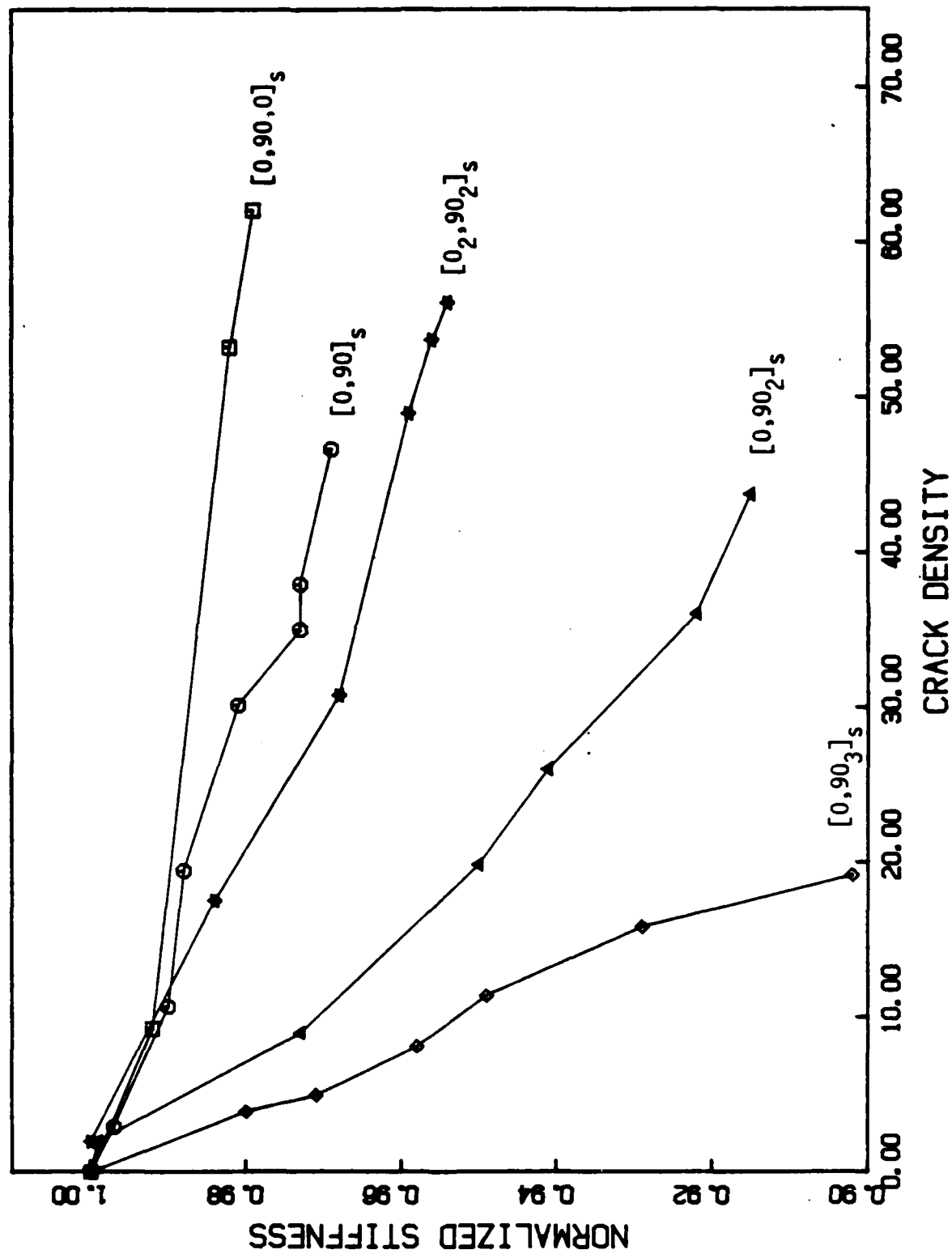


Fig. 7. Axial Stiffness Loss in Cross-Ply Laminates for Matrix Cracking Only.

for a given crack density resulting in a larger crack opening displacement. This implies that the internal state variable α_{Lk1}^n in the constitutive model is larger for increasing values of consecutive 90° plies.

A final trend in the data can be observed by combining Figs. 6 and 7. The stiffness loss increases as the ratio of curved cracks to straight cracks increases. This result suggests that the curved cracks cannot be considered by the model to be simply additional straight cracks.

CORRELATION OF CURVED CRACKS WITH FINITE ELEMENT RESULTS

A finite element model utilizing constant strain triangular elements (CST) incorporating internal boundary generation was developed for analyzing the stress and strain fields in the vicinity of a straight matrix crack. The ply level material constitution was assumed to be transversely isotropic elastic. The objective was to analytically correlate the observed location and orientation of the angle crack and to investigate the influence of existing straight cracks on angle crack formation.

The $[0,90_2]_s$ laminate was used for the correlation between the experimental and analytical results. A typical crack family for this laminate is shown in Fig. 8. The mean experimental distance from the straight crack to the nearest curved crack at the ply interface (based on 25 separate crack measurements) was found to be 9.8 mils (0.2489 mm), and the standard deviation was found to be 2.08 mils (0.05283 mm). The minimum distance was 7.0 mils (0.1778 mm). The mean angle between the curved cracks and the normal to the interface was found to be 30° . The analytical distance measured from the z-axis was determined by the location of the maximum principal stress relative to the straight crack. The basic finite element mesh used to model the $[0,90_2]_s$ laminate with a straight matrix crack is shown in Fig. 9. The squares shown in the figure actually correspond to two "CST" elements. The broad dark line shown between the 0/90 interface represents the resin rich region where there are actually four rows of "CST" elements. More elements were used in the interior 90° ply to increase the accuracy of the solution. In all plies, the aspect ratio per element was kept below 5. The crack

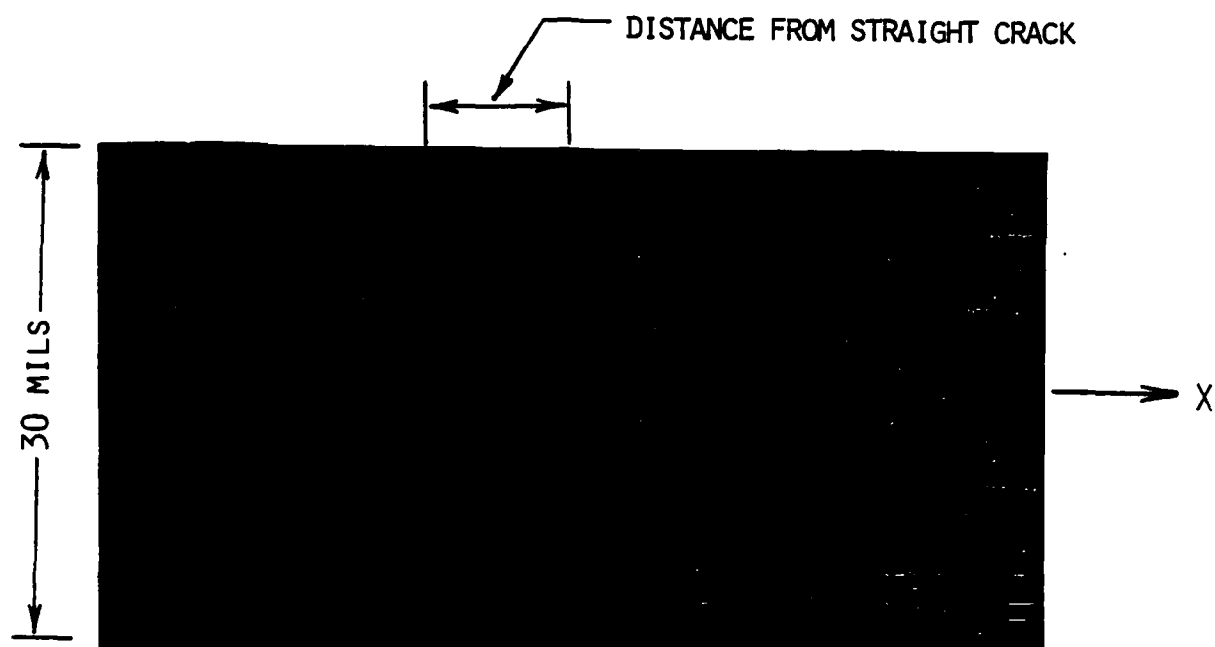


FIG. 8. TYPICAL CRACK FAMILY IN A $[0/90_2]_s$ LAMINATE

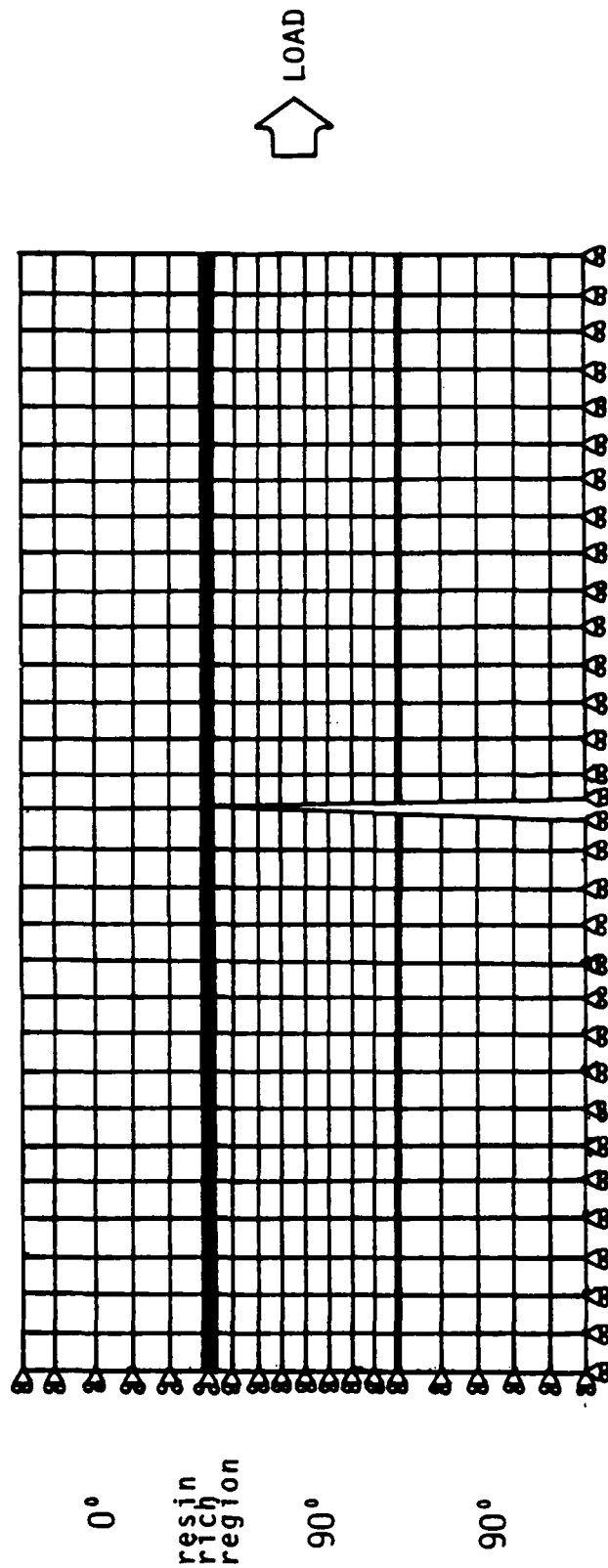


Fig. 9. FINITE ELEMENT MODEL OF A $[0/90_2]_s$
LAMINATE WITH A RESIN RICH REGION

density was varied by changing the length of the overall mesh. The actual mesh used corresponds to 40 cracks per inch. The stress field was produced by applying a uniform end displacement corresponding to a net axial strain of one percent.

The orientation and magnitude of the principal stress in the 90° ply is significantly influenced by the properties of the resin rich region since the majority of the load transferred between the 0/90 plies occurs in this region. The actual properties of the resin rich region were unknown (partially due to the unavailability of neat resin properties), and consequently the thickness and stiffness properties of this region had to be assumed. The effects of these assumed properties were parametrically evaluated. The initial thickness of the resin rich region was chosen to be 1/10 the ply thickness, where one ply thickness was 0.005 inches (0.127 mm). The constitutive behavior was assumed to be isotropic in the resin rich region, with $E = 0.5 \times 10^6$ PSI (3.4475 GPa) and $\nu = 0.3$.

The analytical results for the above properties are shown in Fig. 10. The magnitude of the principal stress for the first three rows of elements below the resin rich region are shown. For comparison, Fig. 10 also shows the experimental locations of the curved cracks. Again, it was hypothesized that the analytically determined location of the curved crack corresponds to the peak in the principal stress. Thus, it is found for this case that the peaks do not fall within the experimental range. The peaks in the principal stress can be shifted closer to the experimental range by doubling the thickness of the resin rich region or by decreasing the stiffness of the resin rich region. However, the peak in row 1 does not fall within an acceptable distance of the mean experimental distance using reasonable engineering properties. Matrix

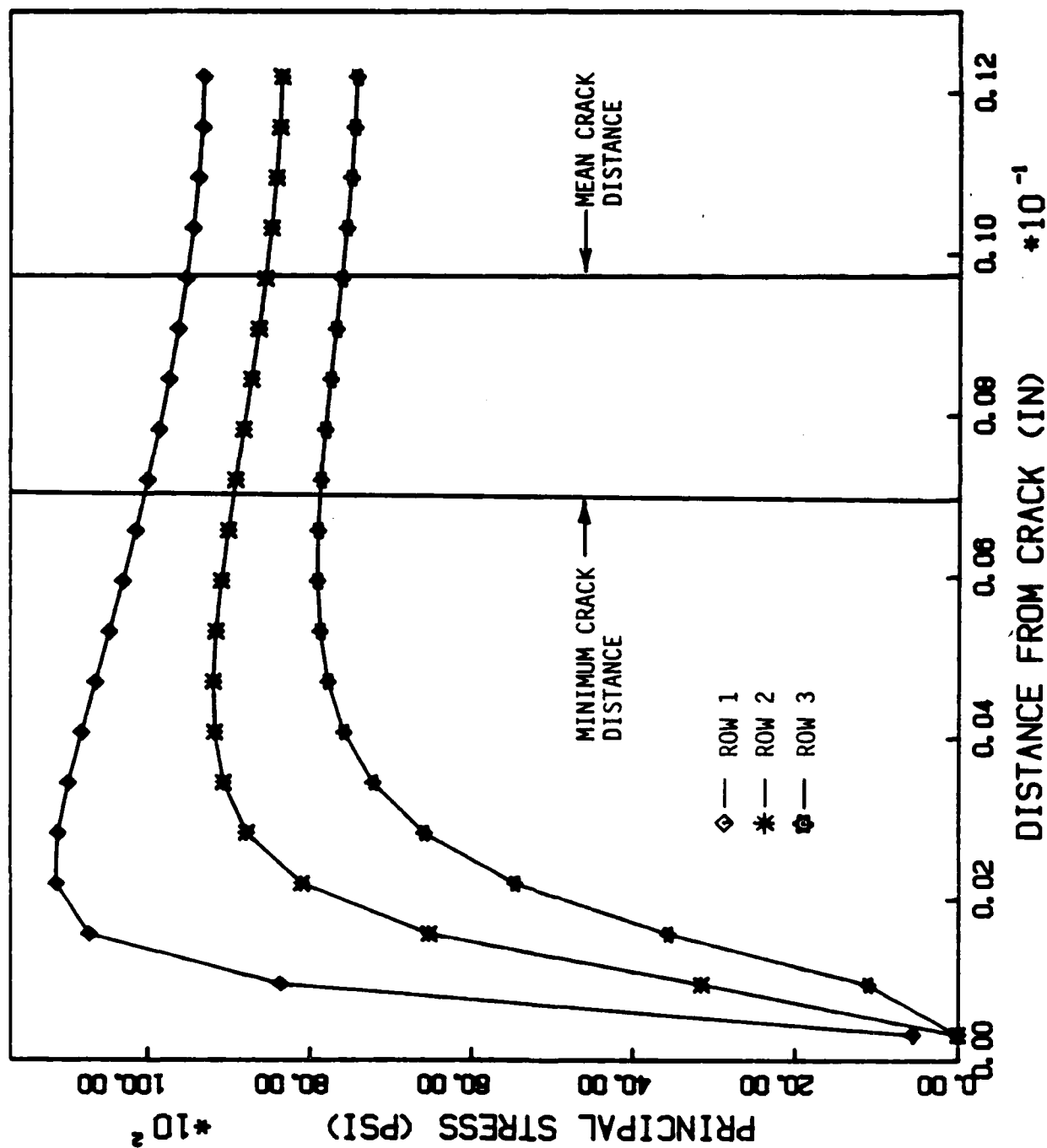


Fig. 10. Variation of Principal Stress Near the $0^\circ/90^\circ$ Interface.

yielding in the resin rich area is another factor that may affect the stress distribution. The shear stress in the resin rich area near the straight crack is much larger than the shear strength of the in-situ matrix. By assuming failure in those elements where the stress exceeds the shear strength, the peak in the principal stress can be shifted toward the experimental results. Finally, the inherent numerical difficulties associated with the solution of this problem cannot be ignored. Thousands of "CST" elements are required to adequately model the straight crack problem. Furthermore, the "CST" element does not model large gradients in shear stress very accurately, and cannot account for the large singularities in the stress field near the crack tip.

The variation in the principal stress angle near the 0/90 interface is shown in Fig. 11. The experimental results are also shown in Fig. 11. The results indicate a maximum angle of about 40° decreasing towards 0° . The principal stress angles corresponding to the peak principal stresses are between 30° and 40° . This is in close agreement with the experimental results. The complete trajectory (profile) of angle cracks which have coalesced to form "curved cracks" can be estimated by examining the principal stress angle throughout the 90° plies at a given distance from the straight crack. The estimated profile at a distance of 0.004 inches (0.1076 mm) shown in Fig. 12, has the same profile as the curved cracks observed experimentally. While it is recognized that this stress state will be altered locally once the angle crack forms, it will nonetheless establish the general direction of crack growth.

For completeness, it is noted that similar results have been obtained for the analytical location and orientation of the angle crack

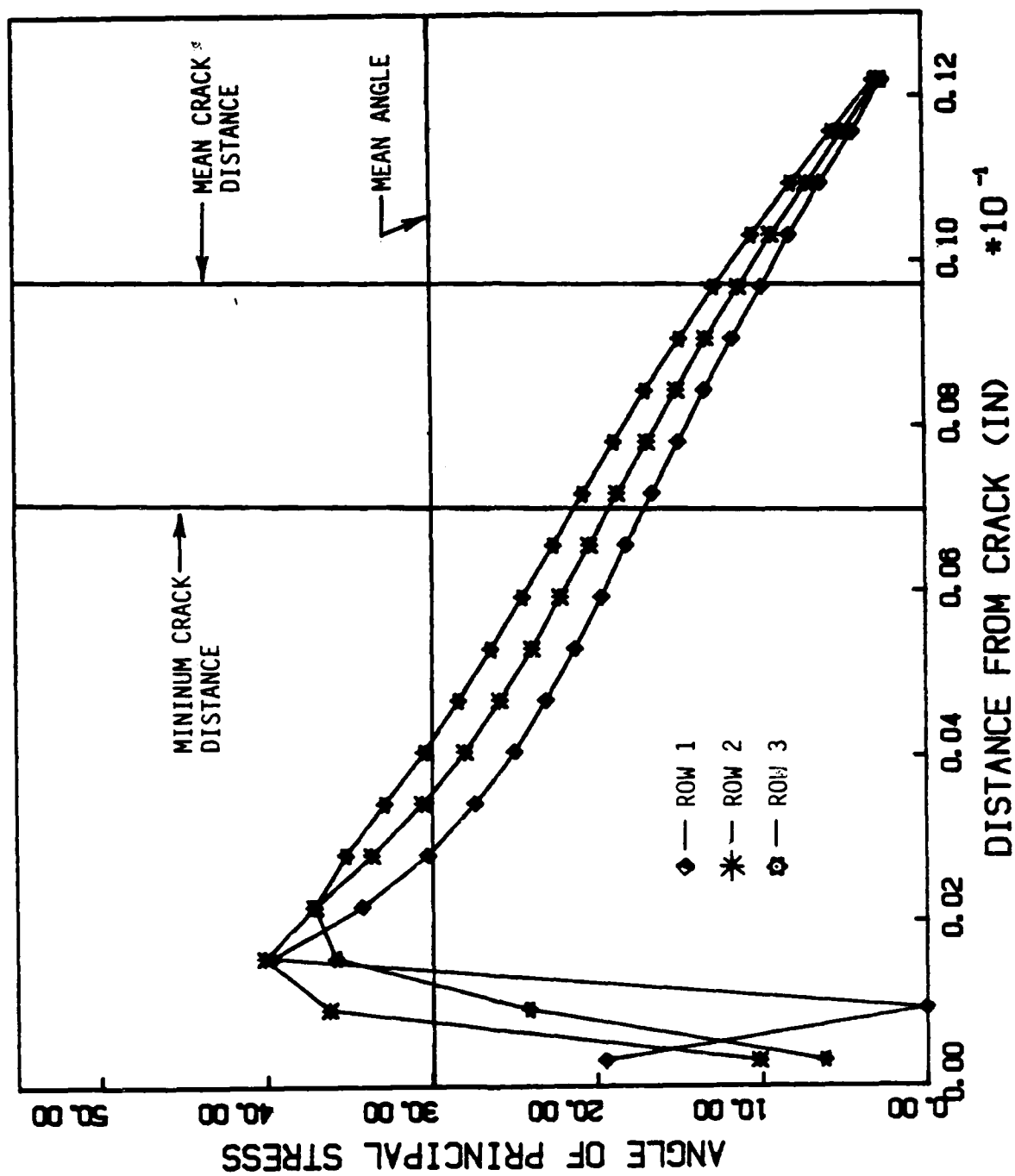


Fig. 11. Variation in the Principal Stress Angle Near the $0^{\circ}/90^{\circ}$ Interface.

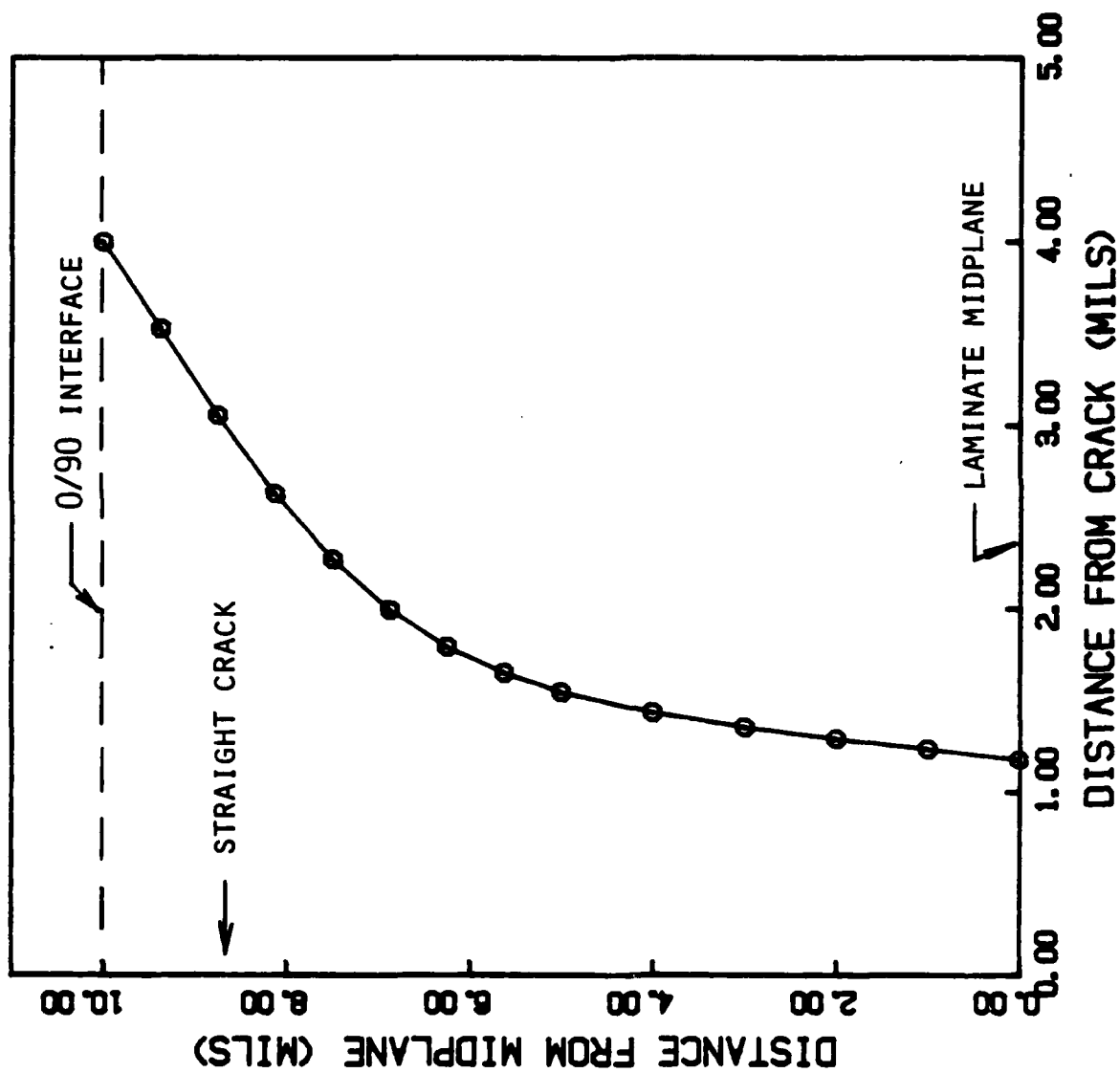


FIG. 12. ESTIMATED CRACK PROFILE FOR $[0,90_2]_s$.

using the following quantities: principal strain, octahedral shear stress, and the strain energy density.

CONCLUSION

It is essential to the development of a physically sound constitutive model for the mechanics of damage to be fully understood. A complete understanding of damage mechanics requires analytical investigations including finite element analysis, fracture mechanics, and analytical solutions as well as experimental observations. However, the end model should contain as few constants as possible and be characterized from experimental results only.

This paper has described the mechanics of matrix crack damage in cross-ply laminates. Two types of matrix cracks have been identified: straight cracks and angle cracks. The straight cracks exhibit a brittle fracture behavior and form before the angle cracks. The localized stress state resulting after the formation of the straight cracks dictate the location and orientation of the angle cracks which exhibit slow stable crack growth behavior. The formations of both the straight and angle cracks are related to the number of consecutive 90° plies, the ratio of 0° to 90° plies, the applied stress level, and the orientation of the principal stress.

Finally, an extensive data base for continued development of the damage-dependent constitutive model has been obtained. A significant reduction in stiffness was found to occur as a result of both the straight and angle cracks.

ACKNOWLEDGEMENT

The authors wish to acknowledge the funding for this research provided by a grant from the Air Force Office of Scientific Research.

REFERENCES

1. Jamison, R.D. and Reifsnider, K.L., "Advanced Fatigue Damage Development in Graphite Epoxy Laminates," AFWAL TR-82-3103, December 1982.
2. Reifsnider, K.L., Henneke, E.G., Stinchcomb, W.W., and Duke, J.C., "Damage Mechanics and NDE of Composite Laminates," MECHANICS OF COMPOSITE MATERIALS, 1982, pp. 399-420.
3. Highsmith, A.L., Stinchcomb, W.W., and Reifsnider, K.L., "Stiffness Reduction Resulting From Transverse Cracking in Fiber-Reinforced Composite Laminates," VPI-E-81.33, Virginia Polytechnic Institute, November, 1981.
4. O'Brien, T.K., Johnston, N.J., Morris, D.H., and Simonds, R.H., "A Simple Test for the Interlaminar Fracture Toughness of Composites," SAMPE JOURNAL, July/August 1982, pp. 8-15.
5. Wang, S.S. and Wang, H.T., "Interlaminar Crack Growth in Fiber Reinforced Composites During Fatigue," JOURNAL OF ENGINEERING MATERIALS AND TECHNOLOGY, Vol. 101, January 1979, pp. 34-41.
6. O'Brien, T.K., "The Effect of Delamination on the Tensile Strength of Unnotched Quasi-Isotropic, Graphite/Epoxy Laminates," Proc. 1982 JOINT CONFERENCE ON EXPERIMENTAL MECHANICS, SESA and JSME, May 23-28 pp. 236-243.
7. Wang, A.S.D. and Crossman, F.W., "Some New Results on Edge Effects in Symmetric Composites Laminates," JOURNAL OF COMPOSITE MATERIALS, Vol. 11, January 1977, pp. 92-106.
8. Altus, E., Rotem, A., and Shmveli, M., "Free Edge Effect in Angle Ply Laminates-A New Three Dimensional Finite Difference Solution," JOURNAL OF COMPOSITE MATERIALS, Vol. 14, January 1980, pp. 21-30.
9. Rybicki, E.F., Schmueser, D.W., and Fox, J., "An Energy Release Rate Approach for Stable Crack Growth in the Free-Edge Delamination Problem," J. COMPOSITE MATERIALS, Vol. 11, October 1977, pp. 470-87
10. Arenburg, R.T., "Analysis of the Effect of Matrix Degradation on Fatigue Behavior of a Graphite/Epoxy Laminate," Thesis, Texas A&M University, May 1982.
11. Rybicki, E.F. and Kanninen, M.F., "A Finite Element Calculation of Stress Intensity Factors by a Modified Crack Closure Integral," ENGINEERING FRACTURE MECHANICS, Vol. 9, 1977, pp. 931-938.
12. Melosh, H.J. and Raetsky, A., "A Simple and Efficient Method for Introducing Faults into Finite Element Computations," BULLETIN OF THE SEISMOLOGICAL SOCIETY OF AMERICA, Vol. 71, October 1981.
13. Kobayashi, A.S., "Hybrid Experimental-Numerical Stress Analysis," UWA/DME/TR-83/47, ONR, April 1983.

14. Chou, P.C., Wang, A.S.D., and Miller, H., "Cumulative Damage Model for Advanced Composite Materials," AFWAL-TR-82-4083, Air Force Wright Aeronautical Laboratories, April 1982.
15. Talug, A., "Analysis of Stress Fields in Composite Laminates With Interior Cracks," Thesis, Doctor of Philosophy, College of Eng., Virginia Polytechnic Institute, September 1978.
16. Reifsnider, K.L., "Some Fundamental Aspects of the Fatigue and Fracture Response of Composite Materials," PROC. 14th ANNUAL SOCIETY OF ENG. SCI. MEETING, Lehigh University, Nov. 14-16, 1979.
17. Liebowitz, H., Subramonian, N., and Lee, J.D., "Mechanics of Fracture - Fundamentals and Some Recent Developments," ISRAEL J. OF TECHNOLOGY, Vol. 17, 1979, pp. 273-294.
18. Erdogan, F. and Gupta, G.D., "Layered Composites With an Interface Flaw," INT. J. SOLIDS STRUCTURES, Vol. 7, 1971, pp. 1089-1107.
19. Rice, J.R., "A Path Independent Integral and the Approximate Analysis of Strain Concentration by Notches and Cracks," JOURNAL OF APPLIED MECHANICS, June 1968, pp. 379-389.
20. Badaliance, R. and Sih, G.C., "An Approximate Three-Dimensional Theory of Layered Plates Containing Through Thickness Cracks," ENG. FRACTURE MECHANICS, 1975, Vol. 7, pp. 1-22.
21. Tada, H., Paris, P.C., and Irwin, G.R., "THE STRESS ANALYSIS OF CRACKS HANDBOOK, Del Research Corporation, Hellertown, Penn. 1973.
22. Altus, E. and Rotem A., "A 3-D Fracture Mechanics Approach to the Strength of Composite Materials," ENG. FRACTURE MECHANICS, Vol. 14, pp. 637-644.
23. Chen, E.P. and Sih, G.C., "Stress Intensity Factor for a Three-Layered Plate With a Crack in the Center Layer," ENG. FRACTURE MECHANICS, Vol. 14, pp. 195-214.
24. Sih, G.C., Hilton, P.D., Badaliance, R., Shenberger, P.S., and Villarreal, G., "Fracture Mechanics for Fibrous Composites," ANALYSIS OF THE TEST METHODS FOR HIGH MODULUS FIBERS AND COMPOSITES ASTM STP 521, 1973.
25. Schapery, R.A., "Correspondence Principles and a Generalized J-Integral for Deformation and Fracture Analysis of Nonlinear Viscoelastic Media," MM-3724-80-16, Air Force Office of Scientific Research, November 1980.
26. Wang, S.S. and Choi, I., "The Interface Crack Between Dissimilar Anisotropic Composite Materials," J. APPLIED MECHANICS, 83-APM-6, Transactions of the ASME, June 1983.
27. Chou, P.C. and Wang, A.S.D., "Cumulative Damage Model for Advanced Composite Materials," Interim Tech Report 4, Contract No. F33615-80-C-5039, Air Force Wright Aeronautical Labs., February 1983.

28. Backlund, J., "Fracture Analysis of Notched Composites," COMPUTERS AND STRUCTURES, Vol. 13, pp. 145-154.
29. Schapery, R.A., "On Viscoelastic Deformation and Failure Behavior of Composite Materials With Distributed Flaws," ADVANCES IN AEROSPACE STRUCTURES AND MATERIALS, AD-01, 1981, pp. 5020.
30. Schapery, R.A., "Models for Damage Growth and Fracture in Nonlinear Viscoelastic Particulate Composites," MM-3168-82-5, Mechanics and Materials Center, Texas A&M University, August 1982.
31. Schapery, R.A., "Continuum Aspects of Crack Growth in Time Dependent Materials," MM-4665-83-2, Texas A&M University, February 1983.
32. Chou, P.C. and Croman, R., "Residual Strength in Fatigue Based on the Strength-Life Equal Rank Assumption," J. COMPOSITE MATERIALS, Vol. 12, April 1978, pp. 177-194.
33. Hahn, H.T. and Kim, R.Y., "Proof Testing of Composite Materials," J. COMPOSITE MATERIALS, Vol. 9, July 1975, pp. 297-311.
34. Hashin, Z. and Rotem, A., "A Cumulative Damage Theory of Fatigue Failure," AFOSR 76-3015, TAU-SOE/395-77, February 1977.
35. Hashin, Z. and Laird, C., "Cumulative Damage Under Two Level Cycling: Some Theoretical Predictions and Test Data," N00014-78-C-0544, TR-3, August 1979.
36. Gottesman, T., Hashin, Z., and Brull, M.A., "Effective Elastic Properties of Cracked Materials," N00014-78-C-0544, TR-6, ONR, May 1981.
37. Hashin, Z., "Failure Criteria for Unidirectional Fiber Composites," J. APPLIED MECHANICS, Vol. 47, June 1980, pp. 329-334.
38. Hashin, Z., "A Reinterpretation of the Palmgren-Miner Rule for Fatigue Life Prediction," J. APPLIED MECHANICS, Vol. 47, June 1980, pp. 324-329.
39. Hashin, Z., "Static and Fatigue Failure Criteria for Unidirectional Fiber Composites," N00014-78-0544, ONR, Tel Aviv University, 1982.
40. Talreja, R., "Fatigue of Composite Materials: Damage Mechanisms and Fatigue-Life Diagrams," PROC. ROYAL SOCIETY OF LONDON, A 378, pp. 461-475, 1981, Printed in Great Britain.
41. Talreja, R., "A Continuum Mechanics Characterization of Damage in Composite Materials," PROC. R. SOC. LONDON, Vol. 399A, 1985, pp. 195-216.
42. Coleman, B.D. and Noll, W., "The Thermodynamics of Elastic Materials With Heat Conduction and Viscosity," ARCHIVES OF RATIONAL MECH. AND ANALYSIS, Vol. 13, 1963, pp. 167-178.

43. Coleman, B.D. and Gurtin, M.E., "Thermodynamics With Internal State Variables," J. CHEM. PHYS., Vol. 47, No. 2, 1967, pp. 597-613.
44. Truesdell, C. and Toupin, R.A., "The Classical Field Theories," ENCYCLOPEDIA OF PHYSICS, ed. S. Flugge, Vol. 3/1, Springer-Verlag, Berlin, 1960, pp. 226-793.
45. Krajcinovic, D. and Fonseka, G.U., "The Continuous Damage Theory of Brittle Materials, Part 1: General Theory," J. APPLIED MECHANICS, Vol. 48, 1981, pp. 809-815.
46. Fonseka, G.U. and Krajcinovic, D., "The Continuous Damage Theory of Brittle Materials, Part 2: Uniaxial and Plane Response Modes," J. APPLIED MECHANICS, Vol. 48, 1981, pp. 816-824.
47. Krajcinovic, D., "Constitutive Equations for Damaging Materials," J. APPLIED MECHANICS, Transactions of the ASME, 83-APM-12, Houston, 1983.
48. Allen, D.H., Groves, S.E., and Schapery, R.A., "A Thermomechanical Constitutive Theory for Elastic Composites with Distributed Damage, Part I: Theoretical Development," MM-5023-85-14, Texas A&M Univ., October 1985.
49. Allen, D.H., Harris, C.E., Groves, S.E., and Schapery, R.A., "A Thermomechanical Constitutive Theory for Elastic Composites with Distributed Damage, Part II: Application to Matrix Cracking in Laminated Composites," MM-5023-85-15, Texas A&M Univ, Oct. 1985.
50. Stalnaker, D.O. and Stinchcomb, W.W., "Load History-Edge Damage Studies in Two Quasi-Isotropic Graphite/Epoxy Laminates," ASTM STP-674, 1980, p. 620.
51. Rummel, W.D., Tedrow, T., and Brinkerhof, H.D., "Enhanced X-ray Stereoscopic NDE of Composite Materials," Martin/Aerospace Denver, Air Force Wright Aeronautical Labs, AFWAL-TR-80-3053, 1980.
52. Norvell, R.G., "An Investigation of Damage Accumulation in Graphite/Epoxy Laminates," Texas A&M University M.S. Thesis, August 1985.

APPENDIX 6.5

CHARACTERIZATION OF STIFFNESS LOSS IN CROSSPLY
LAMINATES WITH CURVED MATRIX CRACKS

by

D.H. Allen
C.E. Harris
S.E. Groves

Aerospace Engineering Department
Texas A&M University
College Station, TX 77843

to be presented at the

Japan - United States Conference
Composite Materials
June 23-25, 1986
Tokyo, Japan

DRAFT

CHARACTERIZATION OF STIFFNESS LOSS IN CROSSPLY
LAMINATES WITH CURVED MATRIX CRACKS

by

D.H. Allen
C.E. Harris
S.E. Groves

Aerospace Engineering Department
Texas A&M University
College Station, TX 77843, U.S.A.

ABSTRACT

Experimental evidence has shown that in crossply laminates numerous matrix cracks often become curved with respect to the plane normal to the laminate plane when three or more 90° plies are stacked in succession. This phenomenon produces damage dependent stiffness losses in the out-of-plane direction. The authors have constructed a general model for predicting stiffness loss as a function of damage in composite laminates, and the current paper seeks to model this out-of-plane stiffness loss. The model predictions are compared to finite element results, and it is shown that the model is accurate in predicting this stiffness loss due to curved cracks.

NOMENCLATURE

σ_j - ply averaged stress in Voigt notation

ϵ_i - ply averaged strain in Voigt notation

a_{ij}^n - nth internal state variable in tensor notation

a_j^n - nth internal state variable in extended Voigt notation

V_L - local volume element over which properties are averaged

S_2^n - surface area of cracks in nth damage mode in V_L

u_i - crack opening displacement vector

n_j - crack face unit normal vector

C_{ij} - elastic modulus tensor in Voigt notation

S_{im} - damage dependent laminate stiffness component

n - number of plies in laminate

t_k - thickness of nth ply

ϵ_j^0 - midsurface strain components of laminate

INTRODUCTION

The authors have previously developed a model for predicting stiffness loss as a function of damage in composite media [1]. The model utilizes a set of second order tensor valued internal state variables (ISV's) to describe internal damage. These ISV's are defined by

$$\alpha_{ij}^n = \frac{1}{V_L} \int_{S_2^n} u_i n_j dS \quad . \quad (1)$$

Thermodynamic concepts have been utilized to construct stress-strain relations of the form

$$\sigma_i = C_{ij} \epsilon_j + I_{ij}^n \alpha_j^n \quad , \quad (2)$$

where the above equations are in ply coordinates and are interpreted to apply at the ply level. Furthermore, α^n is contracted to single index notation using the following extended Voigt notation [2]:

$$\begin{array}{lll} \alpha_1^n \equiv \alpha_{11}^n & \alpha_4^n \equiv \alpha_{23}^n & \alpha_7^n \equiv \alpha_{31}^n \\ \alpha_2^n \equiv \alpha_{22}^n & \alpha_5^n \equiv \alpha_{32}^n & \alpha_8^n \equiv \alpha_{12}^n \\ \alpha_3^n \equiv \alpha_{33}^n & \alpha_6^n \equiv \alpha_{13}^n & \alpha_9^n \equiv \alpha_{21}^n \end{array} \quad . \quad (3)$$

The model described briefly above has been utilized to predict axial stiffness loss as a function of matrix crack damage in several graphite/epoxy crossply laminates [2]. Comparison to experiment was quite good. The model has also been utilized to perform a preliminary study of stiffness loss in a chopped fiber metal-matrix composite [3].

In the current paper, out-of-plane stiffness loss is modelled for crossply laminates with curved cracks of the type shown in Fig. 1. Since it is not possible to obtain accurate experimental measurements of this component of stiffness loss, the model is compared to finite element results in order to determine model accuracy.

MODEL FORMULATION

In reference 2 it was shown that equations (2) may be implemented to a laminate analysis scheme to produce damage dependent stiffness components in global laminate coordinates. The resulting stiffness equations are

$$S_{im} = \sum_{k=1}^n (\bar{C}_{ij})_k t_k - \sum_{k=1}^n \sum_{j=1}^9 (\bar{C}_{ij})_k t_k (\partial \alpha_j^n / \partial \epsilon_m^0)_k \quad , \quad (4)$$

where the overbars indicate that the quantities are in the laminate coordinates shown in Fig. 2. Therefore, the stiffness predictions require that C_{ij} and α_j be transformed from local ply coordinates to global laminate coordinates.

The last term in equations (4), wherein the gradient of damage is taken with respect to midsurface strain, applies only to unloading conditions. Experimental evidence indicates that for AS4/3502 graphite/epoxy laminates at room temperature $\partial \alpha_j / \partial \epsilon^0$ are to a first order approximation constant during unloading [4]. Furthermore, in a [0,90,0] laminate all components of $\partial \alpha_j / \partial \epsilon^0$ in ply coordinates are negligible except $\partial \alpha_2 / \partial \epsilon_2^0$. This term may be obtained for a general layup by utilizing experimentally determined energy release rates from a single [0,90,0] coupon [2]. The next section details the transformation of this quantity from the coordinates of the crack to laminate coordinates.

COORDINATE TRANSFORMATIONS FOR CURVED CRACKS

Consider now a local volume element with n_c cracks as shown in Fig. 3. Equations (1) may be written in the following form:

$$\alpha_{ij}^1 = \frac{1}{twL} \sum_{k=1}^{n_c} \int_{S_{2k}^1} u_i n_j dS \quad , \quad (5)$$

where matrix cracking is designated by the superscript 1. Now define

$$\alpha_{ij}^{1k} = \frac{1}{twL} \int_{S_{2k}^1} u_i n_j dS \quad , \quad (6)$$

so that equation (5) may be written

$$\alpha_{ij}^1 = \sum_{k=1}^{n_c} \alpha_{ij}^{1k} \quad . \quad (7)$$

Now, since α_{ij}^1 is a second order tensor,

$$\alpha_{ij}^1 = \sum_{k=1}^{n_c} a_{ip}^k a_{jq}^k \alpha_{p'q'}^{1k} \quad , \quad (8)$$

where a_{ip}^k are the direction cosines relating the coordinates of the k th crack to the laminate coordinates. Differentiating (8) with respect to the midplane strain components gives

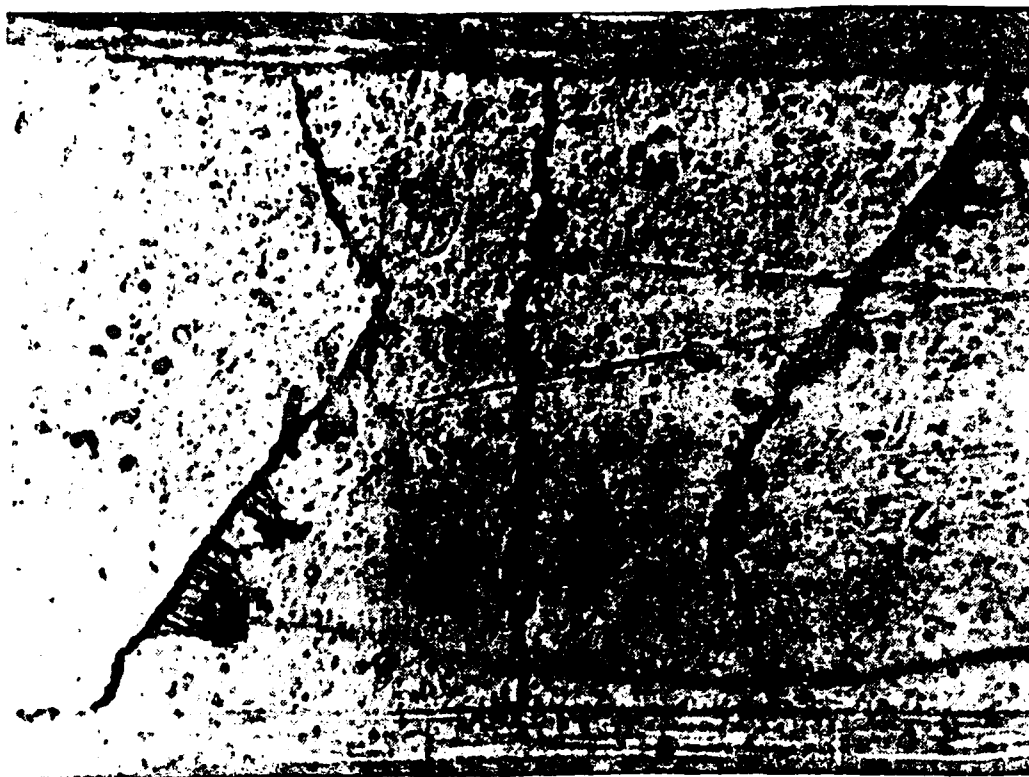


Fig. 1. Edge Replica of Curved Matrix Cracks in
[0/90₄]_s Laminate

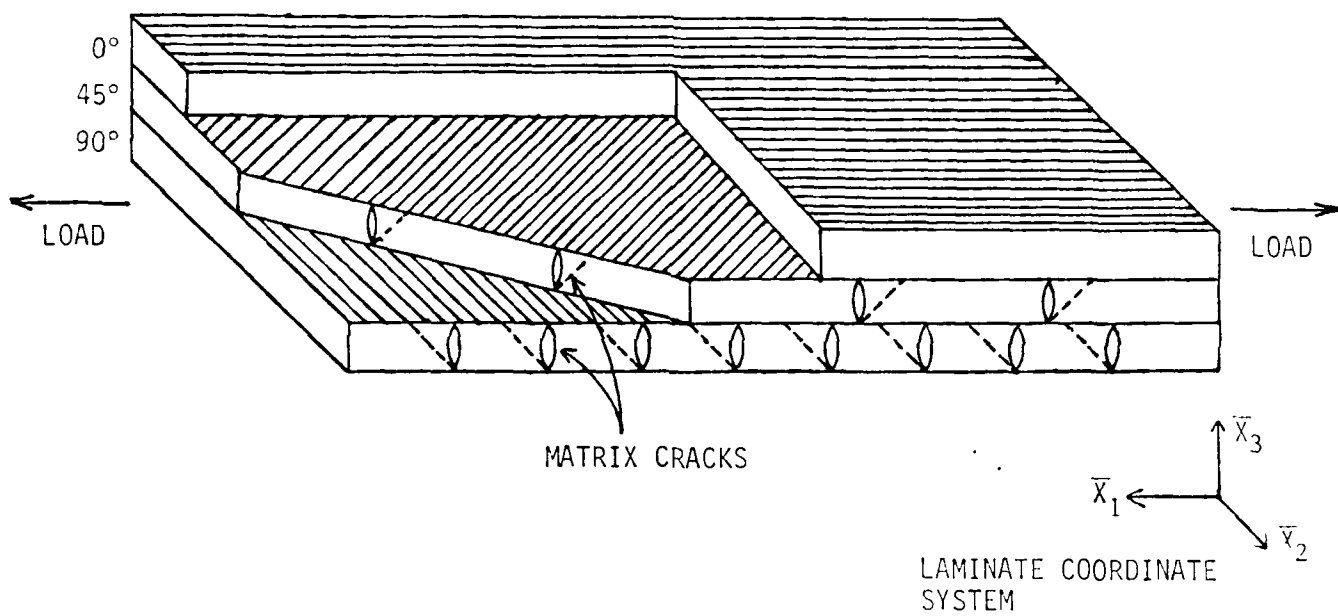


Fig. 2. Matrix Cracking in a Laminated Continuous Fiber Composite

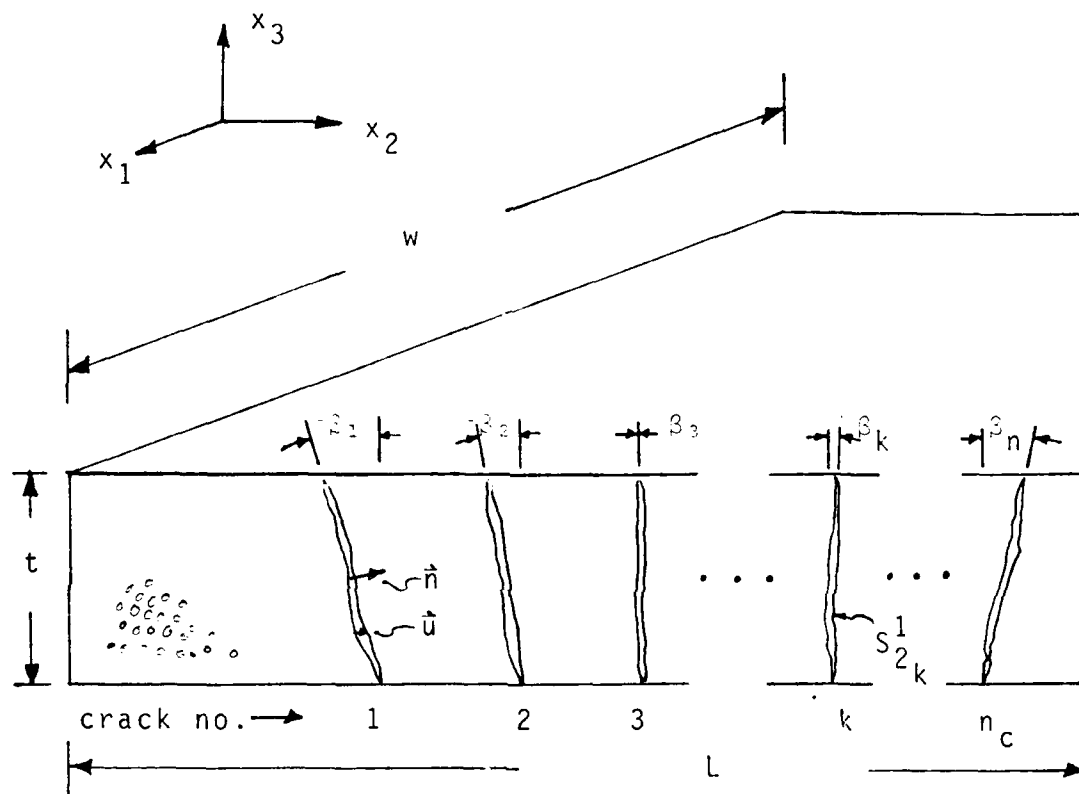


Fig. 3. Description of Curved Crack Geometry in a Single Crossply

$$\frac{\partial \alpha_{ij}^{-1}}{\partial \epsilon_{mn}} = \sum_{k=1}^{n_c} a_{ip}^k a_{jq}^k \frac{\partial \alpha_{p,q}^{1k}}{\partial \epsilon_{mn}} \quad (9)$$

Transforming to the coordinates of the crack gives

$$\begin{aligned} \frac{\partial \alpha_{ij}^{-1}}{\partial \epsilon_{mn}} &= \sum_{k=1}^{n_c} a_{ip}^k a_{jq}^k \frac{\partial \alpha_{p,q}^{1k}}{\partial \epsilon_{r',s'}} \frac{\partial \epsilon_{r',s'}^k}{\partial \epsilon_{mn}} \\ &= \sum_{k=1}^{n_c} a_{ip}^k a_{jq}^k a_{mn}^k a_{ns}^k \frac{\partial \alpha_{p,q}^{1k}}{\partial \epsilon_{r',s'}^k} \end{aligned} \quad (10)$$

However, since it is assumed that $\partial \alpha_{22}^1 / \partial \epsilon_{22}$ is the only non-zero component, the above reduces to

$$\frac{\partial \alpha_{ij}^{-1}}{\partial \epsilon_{mn}} = \sum_{k=1}^{n_c} a_{i2}^k a_{j2}^k a_{m2}^k a_{n2}^k \frac{\partial \alpha_{2,2}^1}{\partial \epsilon_{2,2}^1} \quad (11)$$

The above equations may be utilized to obtain the last term in reduced stiffness equations (4), where it is assumed that $\partial \alpha_{2,2}^1 / \partial \epsilon_{2,2}^1$ is independent of crack orientation and is obtained from [0,90,0] experimental data [2].

REFERENCES

- (1) Allen, D. H., Groves, S.E., Schapery, R.A., and Harris, C.E., "A Thermomechanical Constitutive Theory for Elastic Composites with Distributed Damage - Part I: Theoretical Development," Texas A&M University Mechanics and Materials Center, MM-5023-85-17, October, 1985.
- (2) Allen, D. H., Harris, C.E., Groves, S.E., and Schapery, R.A., "A Thermomechanical Constitutive Theory for Elastic Composites with Distributed Damage - Part II: Application to Matrix Cracking in Laminated Composites," Texas A&M Mechanics and Materials Center, MM-5023-85-15, October 1985.
- (3) Jones, R.M., Mechanics of Composite Materials, McGraw-Hill, 1975.
- (4) Norvell, R.G., "An Investigation of Damage Accumulation in Graphite/Epoxy Laminates," Texas A&M University, Thesis, August, 1985.

APPENDIX 6.6

A DAMAGE MODEL FOR CONTINUOUS FIBER COMPOSITE LAMINATES
WITH MATRIX CRACKS AND INTERLAMINAR DELAMINATIONS

by

S.E. Groves

D.H. Allen

C.E. Harris

and

I. Georgiou

DRAFT

ABSTRACT

A continuum mechanics approach has been utilized by the authors to develop a model for predicting the stiffness loss of continuous fiber composites subjected to both monotonic and cyclic fatigue loading in the presence of matrix cracking and interlaminar delaminations. In this model, each specific damage mode is characterized by a second order tensor valued internal state variable representing locally averaged measures of both matrix cracks and interlaminar delaminations. The resulting constitutive equations are reduced to laminate theory by globally averaging the stress field over the laminate thickness. In this paper the internal state variables are defined and related to their respective surface area of damage. For simplicity only crossply laminates $[0,90,0]_s$, $[0,90_2]_s$, $[0,90]_s$ and $[0_2,90_2]_s$ are studied. It is assumed for these laminates that only a mode I fracture process need be modelled by the internal state variable.

INTRODUCTION

Two common forms of damage in continuous fiber composites are matrix cracks and interlaminar delaminations. Matrix cracks generally form parallel to the fibers in the off-axis plies with the plane of the crack extending through the thickness of ply [5, 51]. However, the growth through each ply is not necessarily self similar and may, in fact, form complex patterns such as curved cracks [50]. Interlaminar delaminations usually initiate at the intersection of a matrix crack with the ply interface. These delaminations result from the interlaminar stresses which develop due to the interaction of the matrix crack with the ply interface. A small but significant reduction in the stiffness of laminates will occur due to these damage modes. The stiffness loss is an important parameter because it has been related to life predictions [5].

In order to fully utilize the potential of composites one must be able to characterize the constitution throughout its complete load history. With regard to characterizing the constitution of composites with damage, there has been a considerable amount of work. This characterization has followed three basically different paths; 1) fracture mechanics [16,29-33]; 2) empirical (34-41); and 3) internal state variable theories which are based on thermodynamics [1,2, 42-49].

In this paper the internal state variable theory of Allen, et al. [1,2], is utilized. To characterize the internal state variables, the mechanics of damage must be studied experimentally and describe analytically. The subject of this paper is to characterize the damage model and compare its predictions to experimentally determined stiffness loss in crossply laminates with both matrix cracks and interlaminar delaminations.

DAMAGE MODEL

The thermomechanical constitutive equations with distributed damage as developed by Allen, et al. [1], are given by

$$\sigma_{Lij} = \sigma_{Lij}^R + E_{Lij} \Delta T_L + C_{Lijk} \epsilon_{Lke} + I_{ijk}^? \alpha_{Lke}^? \quad (1)$$

where n ranges from one to two for each damage mode, σ_{Lij}^R are the residual stresses, ϵ_{Lkl} are the strains, ΔT_L represents the temperature change from the reference state, tensors E, C , and I^n are material constants, and α_{Lkl}^n are the locally averaged internal state variables. The subscript "L" is used to denote locally averaged field variables and material constants and for notational simplicity will be omitted. All other subscripts range from one to three. In this research all experimental tests will be conducted at constant temperature. Furthermore, it will be assumed that the change in stress due to each damage mode is uncoupled, thus allowing one to omit the cross terms on n . It will also be assumed that the residual stresses are negligible on unloading. Under the above assumptions the constitutive equations simplify to

$$\sigma_{ij} = C_{ijkl} \epsilon_{kl} + I_{ijkl}^m \alpha_{kl}^m + I_{ijkl}^D \alpha_{kl}^D, \quad (2)$$

where for notational simplicity the superscript "1" on I has been replaced by "m" to denote matrix cracking and the superscript "2" on I has been replaced by "D" to denote interlaminar delamination. It is noted that equations (2) represents the locally averaged constitutive equations and a different local volume must be used for each damage mode. Equations (2) are reduced to single index notation by incorporating the symmetry of the stress and strain, the quadratic dependence of the Helmholtz free energy on strain, and the Voigt single index notation [52]. The resulting equations are

$$\sigma_i = C_{ij} \epsilon_j + I_{ik}^m \alpha_k^m + I_{ik}^D \alpha_k^D, \quad (3)$$

where i and j range from one to six and k ranges from one to nine because α_{kl}^n is an asymmetric tensor

The constitutive equations can be simplified further by imposing material symmetry constraints. The material in question is assumed to be initially transversely isotropic in the undamaged state. It is assumed that both damage modes introduce orthotropy into the material system. Therefore, the damage tensor I_{ik}^n is essentially an orthotropic tensor.

In order to complete the description of the model it is necessary to characterize the internal state variables, average them over their respective local volumes, and then introduce the constitutive equations into the laminate theory.

Characterization of Internal State Variables

The locally averaged internal state variable as given in Reference [1] is defined as follows:

$$\alpha_{Lkl}^n = \frac{1}{V_L} \int_{S_2^n} u_k^c n_l^c dS, \quad (4)$$

where V_L is the local volume, S_2^n is the crack surface area of each damage mode, u_k^c is the crack opening displacement vector, and n_l^c represents the unit normal vector associated with the crack orientation.

In Reference [2] it was shown that for predicting the axial stiffness loss in crossply laminates due to matrix cracking that the only ISV for matrix cracking of interest is α_2^m . Note that the ply coordinate system used here is identical to that used in Reference [53]. The local volume for this damage mode is a single ply. Therefore, all terms associated with matrix cracking are averaged over each ply before introduction into the laminate analysis scheme.

For interlaminar delaminations there are only three non zero components of the tensor valued internal state variable, α_6^D , α_4^D , and α_3^D [54]. Since only the axial stiffness loss is predicted herein only α_3^D is of interest. Furthermore, since interlaminar delaminations form at the ply interface, a different local volume must be used. In this case the entire laminate is treated as the local volume.

Note that it can be shown using thermodynamics that $I_{ijk1} = -C_{ijk1}$ [2]. Therefore, introducing the non zero internal state variables into equation (3) will reduce to

$$\sigma_i = C_{ij} \epsilon_j - C_{i2}^m \alpha_2^m - C_{i3}^D \alpha_3^D \quad (5)$$

Development of Laminate Equations

In order to utilize single lamina equations to characterize the response of multilayered laminates, it is necessary to globally average the local ply constitutive equations. This is accomplished herein by imposing the Kirchhoff hypothesis for plates [53]. It is noted that only symmetric layups are considered and that only the resultant forces are desired. The resulting equations are as follows:

$$\{N\} = [A]\{\epsilon\} + \{N^m\} + \{N^D\} \quad (6)$$

where $[A]$ represents the conventional undamaged extensional stiffness, given by $A_{ij} = \sum_k (C_{ij})_k t_k$, $\{\epsilon\}$ are the midplane strains, $\{N^m\}$ represents the resultant forces due to matrix cracking, and $\{N^D\}$ represents the resultant forces due to interlaminar delamination. It should be recalled that there are two different local volumes used for averaging the properties for each damage mode. For matrix cracking

$$N_i^m = - \sum_{k=1}^n (C_{i2})_k t_k (\alpha_2^m)_k \quad (7)$$

where t_k is the local ply thickness and $(\alpha)_k^m$ represents the locally averaged measure of the ISV per ply. Note, equation (7) is still in local ply coordinates. For interlaminar delamination the local volume is the laminate, therefore, the locally averaged properties are given by the respective laminate properties. Thus, the resultant forces are given by

$$N_i^D = \left[- \sum_{k=1}^n (C_{i3})_k t_k \right] \alpha_3^D \quad (8)$$

In final form the laminate equations are thus given by

$$\{N\} = [A]\{\epsilon\} - \sum_{K=1}^n \left\{ \bar{C}_{12} \right\}_K t_K (\alpha_2^m)_K - \{A_{13}\} \alpha_3^0 \quad (10)$$

The stiffness in the axial direction is defined by

$$S'_x = \frac{\partial N_x}{\partial \epsilon_x} \quad (11)$$

Substituting equation (10) into (11) gives

$$S'_x = A_{11} - \sum_{K=1}^n (\bar{C}_{11})_K t_K \left(\frac{\partial \alpha_2^m}{\partial \epsilon_x} \right)_K - A_{13} \frac{\partial \alpha_3^0}{\partial \epsilon_x} \quad (12)$$

For crossply laminates with matrix cracking in only the off-axis plies, equation (12) reduces to

$$S'_x = 2t_K \left[pC_{11} + qC_{22} - qC_{22} \left(\frac{\partial \alpha_2^m}{\partial \epsilon_x} \right)_K - (pC_{13} + qC_{23}) \frac{\partial \alpha_3^0}{\partial \epsilon_x} \right] \quad (13)$$

where p denotes the number of 0° plies and q denotes the number of 90° plies. Note, this equation assume the same damage state in each ply and also assumes all plies the same thickness. The axial modulus is thus given by

$$E'_x = \frac{S'_x}{2(p+q)t_K} \quad (14)$$

Relation of Internal State Variable to Surface Area

The internal state variables can be related to the surface area of damage using fracture mechanics and thermodynamics. Utilizing thermodynamic constraints it was shown in Allen, et al. [1,2], that the free energy due to damage reduces to

$$u^c = \sum_{i,j,k,l} I_{ijkl}^? \epsilon_{ij} \alpha_{kl}^? \quad (15)$$

or in single index notation

$$u^c = \sum_{i,k} I_{ik}^? \epsilon_i \alpha_k^? \quad (16)$$

From fracture mechanics the free energy due to damage is related to the strain energy release rate as follows

$$u^c = -\frac{1}{V_c} \int_0^{S_2^*(t)} G_2 dS \quad (17)$$

where S_2^2 is the surface area of damage for each mode. It is assumed here that the energy release rate is uncoupled for each damage mode. For matrix cracking, then,

$$u^c = -\frac{1}{V_L^m} \int_0^{S_2^m(t)} G_m dS \quad (18)$$

and for interlaminar delamination,

$$\bar{u}^c = -\frac{h}{V_L^0} \int_0^{S_2^0(t)} G_0 dS \quad (19)$$

where the bar over u^c denotes a laminate free energy. Equating equations (16), (18), and (19) and noting the respective local volumes, the internal state variables are related to the surface area as follows

$$\alpha_2^m = \frac{-1}{V_L C_{22} \epsilon_x} \int_0^{S_2^m} G_m dS \quad (20)$$

and

$$\alpha_3^0 = \frac{-h}{V_L A_{13} \epsilon_x} \int_0^{S_2^0} G_0 dS \quad (21)$$

The energy release rate for each damage mode can be defined in terms of surface area by

$$G_m = -2 \frac{\partial U}{\partial S^m} \quad (22)$$

and

$$G_0 = -2 \frac{\partial U}{\partial S^0} \quad (23)$$

where the conversion $S=2Ba$ for damage surface area is employed. Furthermore the strain energy in the body is given by

$$U = \frac{1}{2} V E_{xx} \epsilon_x^2 \quad (24)$$

Substituting equation (24) into equations (22) and (23) yields

$$G_m = -V \epsilon_x^2 \frac{\partial \epsilon_x}{\partial S^m} \quad (25)$$

and

$$G_0 = -V \epsilon_x^2 \frac{\partial \epsilon_x}{\partial S^0} \quad (26)$$

Therefore,

$$\alpha_2^m = \frac{E_x}{C_{22}} \int_0^{S_2^m(t)} \frac{\partial E_x}{\partial S^m} dS \quad (27)$$

and

$$\alpha_3^0 = \frac{E_x h}{A_{13}} \int_0^{S_2^0(t)} \frac{\partial E_x}{\partial S^0} dS. \quad (28)$$

Application of Internal State Variables

The constants in equations (27) and (28) must be determined experimentally. In Reference [2] it was shown that for equation (27) one could relate the strain energy release rate in multiple 90° plies to the energy release rate in one 90° ply. Thus, one needed only to conduct experimental test on one laminate, to fully characterize equation (27) for any multiple stacking sequence of 90° plies.

In work to date it has been found that for equation (28) $\partial E_x / \partial S^D$ for any crossply laminate is directly related to the number of constraining 0° plies and only indirectly related by the number of consecutive 90° plies. Further investigations are underway to analyze the dependence of fracture energy for delamination on the laminate sequence.

Model Results

At this time no experimental data have been obtained for the crossply laminates with matrix cracks and interlaminar delaminations. However, both damage modes have been incorporated into a (plane strain) finite element program with results given in Fig. 1. Values of $\partial E_x / \partial S^D$ were obtained from the finite element results and are given below

Laminate	$E_x / S^D \times 10^6$
$[0,90_2]_s$	-.296125
$[0,90]_s$	-.309375
$[0_2,90_2]_s$	-.228125

the finite element results shown in Fig. 1 are produced using the above values.

REFERENCES

1. Allen, D.H., Groves, S.E., and Schapery, R.A., "A Thermomechanical Constitutive Theory for Elastic Composites with Distributed Damage, Part I: Theoretical Development," MM-5023-85-14, Texas A&M University, October 1985.

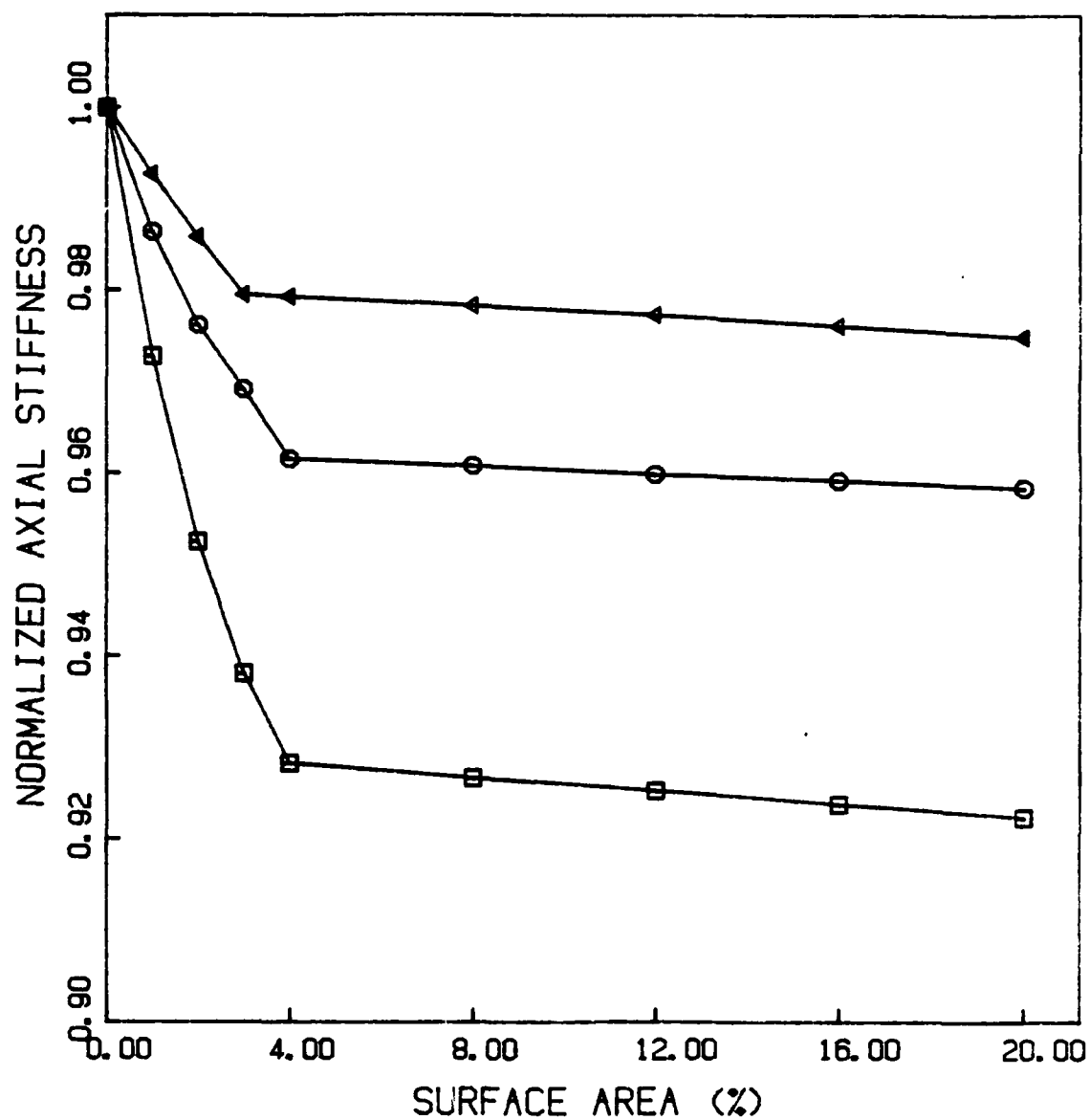


Fig. 1. Finite Element Predictions of the stiffness loss in a $[0,90_2]$ laminate with matrix cracks and interlaminar delaminations.

2. Allen, D.H., Harris, C.E., Groves, S.E., and Schapery, R.A., "A Thermomechanical Constitutive Theory for Elastic Composites with Distributed Damage, Part II: Application to Matrix Cracking in Laminated Composites," MM-5023-85-15, Texas A&M University, October 1985.
3. Jamison, R.D. and Reifsnider, K.L., "Advanced Fatigue Damage Development in Graphite Epoxy Laminates," AFWAL TR-82-3103, December 1982.
4. Reifsnider, K.L., Henneke, E.G., Stinchcomb, W.W., and Duke, J.C., "Damage Mechanics and NDE of Composite Laminates," MECHANICS OF COMPOSITE MATERIALS, 1982, pp. 399-420.
5. Highsmith, A.L., Stinchcomb, W.W., and Reifsnider, K.L., "Stiffness Reduction Resulting From Transverse Cracking in Fiber-Reinforced Composite Laminates," VPI-E-81.33, Virginia Polytechnic Institute, November, 1981.
6. O'Brien, T.K., Johnston, N.J., Morris, D.H., and Simonds, R.H., "A Simple Test for the Interlaminar Fracture Toughness of Composites," SAMPE JOURNAL, July/August 1982, pp. 8-15.
7. Wang, S.S. and Wang, H.T., "Interlaminar Crack Growth in Fiber Reinforced Composites During Fatigue," JOURNAL OF ENGINEERING MATERIALS AND TECHNOLOGY, Vol. 101, January 1979, pp. 34-41.
8. O'Brien, T.K., "The Effect of Delamination on the Tensile Strength of Unnotched Quasi-Isotropic Graphite/Epoxy Laminates," Proc. 1982 JOINT CONFERENCE ON EXPERIMENTAL MECHANICS, SESA AND JSME, May 23-28 pp. 236-243.
9. Wang, A.S.D. and Crossman, F.W., "Some New Results on Edge Effects in Symmetric Composites Laminates," JOURNAL OF COMPOSITE MATERIALS, Vol. 11, January 1977, pp. 92-106.
10. Altus, E., Rotem, A., and Shmueli, M., "Free Edge Effect in Angle Ply Laminates - A New Three Dimensional Finite Difference Solution," JOURNAL OF COMPOSITE MATERIALS, Vol. 14, January 1980, pp. 21-30.
11. Rybicki, E.F., Schmueser, D.W., and Fox, J., "An Energy Release Rate Approach for Stable Crack Growth in the Free-Edge Delamination Problem," J. COMPOSITE MATERIALS, Vol. 11, October 1977, pp. 470-487.
12. Arenburg, R.T., "Analysis of the Effect of Matrix Degradation on Fatigue Behavior of a Graphite/Epoxy Laminate," Thesis, Texas A&M University, May 1982.
13. Rybicki, E.F. and Kanninen, M.F., "A Finite Element Calculation of Stress Intensity Factors by a Modified Crack Closure Integral," ENGINEERING FRACTURE MECHANICS, Vol. 9, 1977, pp. 931-938.

14. Melosh, H.J. and Raetsky, A., "A Simple and Efficient Method for Introducing Faults into Finite Element Computations," BULLETIN OF THE SEISMOLOGICAL SOCIETY OF AMERICA, Vol. 71, October 1981.
15. Kobayashi, A.S., "Hybrid Experimental-Numerical Stress Analysis," UWA/DME/TR-83/47, ONR, April 1983.
16. Chou, P.C., Wang, A.S.D., and Miller, H., "Cumulative Damage Model for Advanced Composite Materials," AFWAL-TR-82-4083, Air Force Wright Aeronautical Laboratories, April 1982.
17. Talug, A., "Analysis of Stress Fields in Composite Laminates with Interior Cracks," Thesis, Doctor of Philosophy, College of Engineering, Virginia Polytechnic Institute, September 1978.
18. Reifsnider, K.L., "Some Fundamental Aspects of the Fatigue and Fracture Response of Composite Materials," PROC. 14th ANNUAL SOCIETY OF ENG. SCI. MEETING, Lehigh University, Nov. 14-16, 1979.
19. Liebowitz, H., Subramonian, N., and Lee, J.D., "Mechanics of Fracture - Fundamentals and Some Recent Developments," ISRAEL J. OF TECHNOLOGY, Vol. 17, 1979, pp. 273-294.
20. Erdogan, F. and Gupta, G.D., "Layered Composites with an Interface Flaw," INT. J. SOLIDS STRUCTURES, Vol. 7, 1971, pp. 1089-1107.
21. Rice, J.R., "A Path Independent Integral and the Approximate Analysis of Strain Concentration by Notches and Cracks," JOURNAL OF APPLIED MECHANICS, June 1968, pp. 379-389.
22. Badaliance, R., and Sin, G.C., "An Approximate Three-Dimensional Theory of Layered Plates Containing Through Thickness Cracks," ENG. FRACTURE MECHANICS, 1975, Vol. 7, 1-22.
23. Tada, H., Paris, P.C., and Irwin, G.R., "THE STRESS ANALYSIS OF CRACKS HANDBOOK, Del Research Corporation, Hellertown, Penn. 1973.
24. Altus, E. and Rotem A., "A 3-D Fracture Mechanics Approach to the Strength of Composite Materials," ENG. FRACTURE MECHANICS, Vol. 14, pp. 637-644.
25. Chen, E.P. and Sih, G.C., "Stress Intensity Factor for A Three -Layered Plate with a Crack in the Center Layer," ENG. FRACTURE MECHANICS, Vol. 14, 195-214.
26. Sih, G.C., Hilton, P.D., Badaliance, R., Shenberger, P.S., and Villarreal, G., "Fracture Mechanics for Fibrous Composites," ANALYSIS OF THE TEST METHODS FOR HIGH MODULUS FIBERS AND COMPOSITE ASTM STP 521, 1973.
27. Schapery, R.A., "Correspondence Principles and a Generalized J. Integral for Deformation and Fracture Analysis of Nonlinear Viscoelastic Media," MM-3724-80-16, Air Force Office of Scientific Research, November 1980.

28. Wang, S.S. and Choi, I., "The Interface Crack Between Dissimilar Anisotropic Composite Materials," J. APPLIED MECHANICS, 83-APM-6, Transactions of the ASME, June 1983.
29. Chou, P.C. and Wang, A.S.D., "Cumulative Damage Model for Advanced Composite Materials," Interim Tech Report 4, Contract No. F33615-80-C-5039, Air Force Wright Aeronautical Labs., February 1983.
30. Backlund, J., "Fracture Analysis of Notched Composites," COMPUTERS AND STRUCTURES, Vol. 13, pp. 145-154.
31. Schapery, R.A., "On Viscoelastic Deformation and Failure Behavior of Composite Materials with Distributed Flaws," ADVANCES IN AEROSPACE STRUCTURES AND MATERIALS, AD-01, 1981, pp. 5020.
32. Schapery, R.A., "Models for Damage Growth and Fracture in Nonlinear Viscoelastic Particulate Composites," MM-3168-82-5, Mechanics and Materials Center, Texas A&M University, August 1982.
33. Schapery, R.A., "Continuum Aspects of Crack Growth in Time Dependent Materials," MM-4665-83-2, Texas A&M University, February 1983.
34. Chou, P.C. and Croman, R., "Residual Strength in Fatigue Based on the Strength-Life Equal Rank Assumption," J. COMPOSITE MATERIALS, Vol. 12, April 1978, pp. 177-194.
35. Hahn, H.T. and Kim, R.Y., "Proof Testing of Composite Materials," J. COMPOSITE MATERIALS, Vol. 9, July 1975, pp. 297-311.
36. Hashin, Z. and Rotem, A., "A Cumulative Damage Theory of Fatigue Failure," AFOSR 76-3015, TAU-SOE/395-77 February 1977.
37. Hashin, Z. and Laird, C., "Cumulative Damage Under Two Level Cycling: Some Theoretical Predictions and Test Data," N00014-78-C-0544, TR-3, August 1979.
38. Gottesman, T., Hashin, Z., and Brull, M.A., "Effective Elastic Properties of Cracked Materials," N00014-78-C-0544, TR-6, ONR, May 1981.
39. Hashin, Z., "Failure Criteria for Unidirectional Fiber Composites," J. APPLIED MECHANICS, Vol. 47, June 1980, pp. 329-334.
40. Hashin, Z., "A Reinterpretation of the Palmgren-Miner Rule for Fatigue Life Prediction," J. APPLIED MECHANICS, Vol. 47, June 1980, pp. 324-329.
41. Hashin, Z., "Static and Fatigue Failure Criteria for Unidirectional Fiber Composites," N00014-78-0544, ONR, Tel Aviv University, 1982.
42. Talreja, R., "Fatigue of Composite Materials: Damage Mechanisms and Fatigue-Life Diagrams," PROC. ROYAL SOCIETY OF LONDON, A 378, pp. 461-475, 1981, Printed in Great Britain.

AD-A175 817

RESEARCH ON DAMAGE MODELS FOR CONTINUOUS FIBER
COMPOSITES(U) TEXAS A AND M UNIV COLLEGE STATION
MECHANICS AND MATERIALS CE D H ALLEN ET AL FEB 86

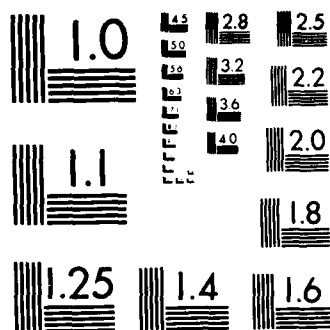
4/4

UNCLASSIFIED

AA-5823-86-5 AFOSR-TR-86-2877 AFOSR-84-8867 F/G 11/4

NL





MICROCOPY RESOLUTION TEST CHART
NATIONAL BUREAU OF STANDARDS 1963 A

43. Talreja, R., "A Continuum Mechanics Characterization of Damage in Composite Materials," PROC. R. SOC. LONDON, Vol. 399A, 1985, pp. 195-216.
44. Coleman, B.D. and Noll, W., "The Thermodynamics of Elastic Materials with Heat Conduction and Viscosity," ARCHIVES OF RATIONAL MECH. AND ANALYSIS, Vol. 13, 1963, pp. 167-178.
45. Coleman, B.D. and Gurtin, M.E., "Thermodynamics with Internal State Variables," J. CHEM. PHYS., Vol. 47, No. 2, 1967, pp. 597-613.
46. Truesdell, R. and Toupin, R.A., "The Classical Field Theories," ENCYCLOPEDIA OF PHYSICS, ed. S. Flugge, Vol. 3/1, Springer-Verlag, Berlin, 1960, pp. 226-793.
47. Krajcinovic, D. and Fonseka, G.U., "The Continuous Damage Theory of Brittle Materials, Part 1: General Theory," J. APPLIED MECHANICS, Vol. 48, 1981, pp. 809-815.
48. Fonseka, G.U. and Krajcinovic, D., "The Continuous Damage Theory of Brittle Materials, Part 2: Uniaxial and Plane Response Modes," J. APPLIED MECHANICS, Vol. 48, 1981, pp. 816-824.
49. Krajcinovic, D., "Constitutive Equations for Damaging Materials," J. APPLIED MECHANICS, Transactions of the ASME, 83-APM-12, Houston, 1983.
50. Groves, S.E., Allen, D.H., Harris, C.E., Highsmith, A.L., and Norvell, R.G., "An Experimental and Analytical Treatment of the Mechanics of Damage in Laminated Composites, presented at SES, Oct. 1985.
51. Norvell, R.G., "An Investigation of Damage Accumulation in Graphite/Epoxy Laminates," Thesis, Texas A&M University, 1985.
52. Frederick, D. and Chang, T.S., Continuum Mechanics, Scientific Publishers, Inc., Cambridge, Mass., 1972.
53. Jones, R.M. Mechanics of Composite Materials, McGraw-Hill, 1975.
54. Groves, S.E., "A Cumulative Damage Model for Continuous Fiber Composite Laminates with Matrix Cracking and Interlaminar Delaminations," Dissertation, Texas A&M University, 1986.

END

1-87

DTIC